Design of Functional Polyesters for Electronic and Biological Applications

Ashley M. Nelson

Dissertation submitted to the faculty of the Virginia Polytechnic Institute and State University in partial fulfillment of the requirements for the degree of

Doctor of Philosophy
In
Chemistry

Timothy E. Long, Chair
Robert B. Moore
S. Richard Turner
Maren Roman

June 22, 2015
Blacksburg, VA

Keywords: polyester, melt polymerization, renewable, gene delivery, liquid crystalline

Design of Functional Polyesters for Electronic and Biological Applications

Ashley M. Nelson

Abstract

Melt polymerization and novel monomers enabled the synthesis of polyesters for electronic and biological applications. Inspiration from nature and a passion for environmental preservation instigated an emphasis on the incorporation of renewable resources into polymeric materials. Critical analysis of current research surrounding bisphenol-A replacements and ion-containing segmented polyurethanes aided in identifying benchmark polymers, including limitations, challenges, and future needs. Structure-property-morphology relationships were investigated to evaluate the polymers for success in the proposed applications as well as to improve understanding of polyester compositions to further design and develop sophisticated polymers for emerging applications.

Aiming to utilize the reported [2 + 2] cycloaddition of the known mesogen 4,4'-dimethyl-*trans*-stilbene dicarboxylate (SDE) to overcome ultraviolet (UV) induced degradation issues in electronic encasings, the synthesis of copolyesters containing SDE ensued. 1,6-Hexanediol (HD) and 1,4-butanediol comonomers in varying weight ratios readily copolymerized with SDE under melt transesterification conditions to afford a systematic series of copolyesters. Differential scanning calorimetry revealed all copolyesters exhibited liquid crystalline transitions and melting temperatures ranged from 196 °C – 317 °C. Additionally, melt rheology displayed shear thinning to facilitate melt processing. Compression molded films exhibited high storage moduli, a glassy plateau until the onset of flow, and tensile testing revealed a Young's

modulus of ~900 MPa for poly(SDE-HD). These properties enable a wide range of working temperatures and environments for electronic applications.

Adding complexity to linear liquid crystalline copolyesters, copolymerization with oligomeric hydroxyl-functionalized polyethers afforded segmented liquid crystalline copolyesters. 4,4'-Biphenyl dicarboxylate (BDE), commercially available diols containing 4, 5, 6, 8, or 10 methylene units, and introducing poly(tetramethylene oxide) or a Pluronic® triblock oligoethers in varying weight % were used to synthesize multiple series of segmented copolyesters. Comparing melting transitions as a function of methylene spacer length elucidated the expected even-odd effect and melting temperatures ranged from 150 °C to 300 °C. Furthermore, incorporating the flexible soft segment did not prevent formation of a liquid crystalline morphology. Complementary findings between differential scanning calorimetry and small-angle X-ray scattering confirmed a microphase-separated morphology. Thermomechanical analysis revealed tunable plateau moduli and temperature windows based on both soft segment content and methylene spacer length, and tensile testing showed the strain at break doubled from 75 weight % to 50 weight % hard segment content. The same compositions Young's moduli decreased from 107 ± 12 MPa at 75 weight % hard segment to 19 ± 1 MPa with 50 weight % hard segment, demonstrating the mechanical trade-off and range of properties possible with small compositional changes. These segmented copolyesters could find use in high-performance applications including electronic and aerospace industries.

A two-step synthesis transformed caffeine into a novel caffeine-containing methacrylate (CMA). Conventional free radical copolymerization with a comonomer known to provide a low glass transition temperature (T_g), 2-ethylhexyl methacrylate (EHMA), allowed the investigation of the effect of small amounts of pendant caffeine on polymer properties. Thermal and

thermomechanical testing indicated CMA incorporation dramatically increased the storage modulus, however, a microphase-separated morphology was not attained. Association of the pendant caffeine groups through non-covalent π-π stacking could present opportunities for novel thermoplastics and it is proposed that placing the pendant group further from the backbone, and potentially increasing the concentration, could aid in promoting microphase-separation.

Alkenes are reactive sites for placing functional groups, particularly those required for polyester synthesis. Methyl 9-decenoate (9-DAME), a plant-based fatty acid, provided a platform for novel biodegradable, renewable, polyesters. A formic acid hydration reaction generated an isomeric mixture of AB hydroxyester or AB hydroxyacid monomers for melt polymerization. Thermal analysis elucidated the plant-based polyesters exhibited a single transition, a T_g of about -60 °C. Aliphatic polyesters commonly crystallize, thus the isomeric mixture of secondary alcohols seemed to introduce enough irregularity to prevent crystallization. These polyesters offer an amorphous, biodegradable, sustainable replacement for applications currently using semi-crystalline poly(ε-caprolactone), which is not obtained from renewable monomers and also exhibits a -60 °C T_g. Additional applications requiring low-T_g polymers such as pressure sensitive adhesives or thermoplastic elastomers could also benefit from these novel polyesters. 9-DAME also was transformed into an ABB' monomer after an epoxidation and subsequent hydrolysis. Successful gelation under melt transesterification conditions provided evidence that the multifunctional monomer could perform as a renewable, biodegradable, branching and/or crosslinking agent.

Novel copolyesters comprised of a bromomethyl imidazolium diol and adipic acid demonstrated potential as non-viral gene delivery vectors. Melt polycondensation produced water dispersible polyesters which bound deoxyribonucleic acid at low N/P ratios. The

polyplexes showed stability in water over 24 h and no cytotoxic effect on human cervical cancer cells (HeLa). A luciferase transfection assay revealed the copolyesters successfully underwent endocytosis and released the nucleic acid better than controls. The copolyesters with pendant imidazolium functionality also provided tunable T_gs, -41 °C to 40 °C, and the ability to electrospin into fibers upon blending with poly(ethylene oxide). These additional properties furthered potential applications to include pressure sensitive adhesives and biocompatible antibacterial bandages.

To my grandma and best friend,

Joyce A. Sunderman.

Whom without her love, encouragement, confidence, and undying support

this would have been a mere dream.

Acknowledgements

I would like to start by thanking my advisor and mentor, Dr. Timothy E. Long. His passion for science, starting at the fundamentals and building up to functional polymeric materials mimics how he runs his research group. When I arrived at Virginia Tech my eagerness to learn was embraced with appropriate challenges to instill the fundamentals of not only how to conduct research but of polymer science. Structure-property is probably the most typed word in this dissertation, and rightly so. Eventually, as the fundamentals engrained in my head I was able to share my creativity and passion and bring my own scientific personality to the Long Group which was both welcomed and challenged for further growth. I would also like to thank my committee members Dr. Robert B. Moore, Dr. S. Richard Turner, and Dr. Maren Roman for your time, support, collaboration, and challenging questions. I appreciate the commitment from you to help mold my graduate career when I know each of you have demanding positions and your own students to advise. Some of my favorite memories are during committee meetings when everyone chimed in with a different point of view based on the diverse backgrounds; I think that displays our field and how it advances at its finest. I am so grateful for having Valerie Owens, Naya Sou, Brent Bowden, and Laurie Good to help throughout my years here at Virginia Tech. I would also like to thank the various funding sources and collaborators including the MCOE, Solvay, Sabic, and Elevance Renewable Sciences. Thank you to all my past teachers, especially the math and chemistry professors at the University of Evansville. My undergraduate education prepared me immensely well for the transition to graduate school

and the support, assistance, and opportunities obtained while at UE allowed me to find and pursue my passion(s).

The Long Group is a special group of people – alumni, current students, and future students. The friendships made alongside a few powerpoint slides or late-night reaction watching are some that I know will never be rivaled. From the time I started until now I've worked with or alongside 30 graduate students and post-docs – each of you had a hand in my path and I thank for your time, support, and friendship. To my graduate mentor, Dr. Nancy Zhang – thank you for teaching me the polyester ropes, for challenging me to think differently than the norm, for sharing your scientific creativity, for being a fantastic cheerleader from the West coast, and for sharing the horticulture garden getaway spot. I'm so thankful we've remained friends; see you in CA soon! To Dr. Stephen June, you are one of my very best friends and I cannot thank you enough for your support and confidence when I needed it most (and a big thanks for keeping Frances company, too)! Evan, I will miss our monthly dinners and hearing about all your crazy fantastically creative ideas. You inspire me daily! Dr. Matthew Hunley – thank you for your friendship, advice, and never letting me miss a Hokie game! Thank you to the alumni who reached out for career advice even though we only met in passing, Dr. Scott Trenor and Dr. John Layman, this speaks volumes about the kind of people Long Group members are. Thank you to Dr. Sean Hemp, Dr. Michael Allen, Dr. Matthew Green, Dr. Adam Smith, and Dr. Asem Abdulahad for being fantastic role models who each took time to teach me new syntheses, techniques, and/or lend a listening ear. I would also like to thank the undergraduate students I mentored, Richard (Nick) Carmean, Jessica Chau, and Neil Forsythe, for your time and patience as we learned and worked together. I hope you learned as much as I did. To my fellow polyester folks: Joseph Dennis, Ryan Mondschein, and Katherine Valentine –

keep the melt reactors hot, you are all doing fantastic things and I can't wait to read your papers! Alexandra Fersner and Allison Pekkanen, thank you for being not only great scientists to bounce ideas off of and work with, but for being great friends.

I would like to thank my mother, Julie M. Nelson, for instilling in me the benefits of hard work and perseverance. For being there when the times got tough and never ever doubting I would succeed. Thank you to my grandparents, Joyce A. Sunderman and James J. Sunderman; you are my rocks. To my aunts, Janine R. Hartmann and Jodi A. Noble and their families, you all bring so much joy to my life and your constant support is more than I could ever ask for. To my godchildren, Grady Noble and Lillian Hartmann, I hope you know that you too can and will achieve great things. I love you all from the bottom of my heart! Finally, a huge heartfelt thank you (and high five) to James C. Dustin – you've taught me so much about life and love and I'm looking forward to the future.

Attributions

Dr. Timothy E. Long is a professor in chemistry and the director of the Macromolecules and Interfaces Institute. He is the author's research advisor and mentor, generating research ideas and obtaining funding, allowing the author to conduct research in his laboratory, and discussing and evaluating the author's research and performance.

Dr. Robert B. Moore is a professor in chemistry, the director of the MACR degree program, and a member of the author's PhD committee. Small angle X-ray scattering (SAXS) and wide-angle X-ray scattering (WAXD) experiments were performed in his laboratory on the segmented liquid crystalline copolyesters. Numerous helpful discussions about the results enabled a well-rounded manuscript for publication, which is currently under review in Macromolecular Chemistry and Physics, and Dr. Moore is included as a coauthor (chapter 4).

Gregory B. Fahs is a chemistry PhD graduate student working under Dr. Robert B. Moore. Greg performed SAXS and WAXD analysis on the author's segmented liquid crystalline copolyesters, taking the time to fit the data and partake in helpful discussions. He is a coauthor on the manuscript that is currently under review for publication in Macromolecular Chemistry and Physics (chapter 4).

Dr. Sean T. Hemp obtained his PhD under the direction of Dr. Timothy E. Long at Virginia Tech and now works at Michelin. While he was a graduate student Sean taught the author lab techniques, was always available to discuss and answer questions, and was an excellent role model for conducting research. While the author was away on an internship Sean worked out the conditions for copolymerization and precipitation of caffeine methacrylate with 2-ethylhexylmethacrylate and is a coauthor on a manuscript which is undergoing major revisions for publication in the Journal of Polymer Science Part A: Polymer Chemistry (chapter 5).

Richard N. Carmean is currently a graduate student at the University of Florida working under Dr. Brent Sumerlin. Nick attended Virginia Tech for undergraduate education and performed undergraduate research in the Long group. The author mentored Nick for about 3 months and he aided in the synthesis and isolation of caffeine methacrylate (chapter 5). Nick also synthesized some stilbene-containing liquid crystalline copolyesters (chapter 3).

Jessica Chau obtained her undergraduate degree from Virginia Tech and is currently working at Pfizer Consumer Healthcare in Richmond, VA. The author mentored Jessica for 1.5 years of undergraduate research while she was a student at Virginia Tech. Jessica aided in multiple projects including isolation of caffeine methacrylate, which is currently undergoing major revisions for publication in the Journal of Polymer Science Part A: Polymer Chemistry, and she is a coauthor (chapter 5). Other projects she assisted with include the synthesis, compression molding, and thermomechanical analysis of liquid crystalline copolyesters containing stilbene and isosorbide as well as the synthesis of oligoesters for 3D printing.

Dr. Michael H. Allen Jr. obtained his PhD under the direction of Dr. Timothy E. Long at Virginia Tech and now works at Adhesives Research. Mike taught the author conventional free radical polymerization, a technique the author used for the caffeine methacrylate project (chapter 5).

Keren Zhang is a PhD candidate in chemistry advised by Dr. Timothy E. Long. The author and Keren collaborated on project(s) funded by Elevance Renewable Sciences, Inc. Keren synthesized the ABB' dihydroxyester plant-based monomer discussed and polymerized in chapter 6. She would be a coauthor if this work was to be submitted for publication.

Allison M. Pekkanen is a biomedical engineering graduate student co-advised between Dr. M. Nichole Rylander and Dr. Timothy E. Long. Allison performed the cytotoxicity and transfection

studies for the imidazolium copolyester non-viral gene delivery project (chapter 8) and participated in numerous insightful discussions. Allison is included as a coauthor on the manuscript in preparation.

Neil L. Forsythe is an undergraduate at Pomona College who participated in a summer undergraduate research program at Virginia Tech. While here, Neil joined the Long group and the author was his mentor. He synthesized the novel bromobutyl imidazolium diol and electrospun the imidazolium homopolyester. Neil is included as a coauthor on a manuscript that is currently in preparation to submit to Biomacromolecules (chapter 8).

John H. Herlihy is a graduate student at Virginia Tech who spent time as a member of the Long research group; however, is now a PhD student in plant physiology. While in the Long group John taught the author how to perform gel binding assays and did initial cytotoxicity and transfection assays with the imidazolium-containing copolyesters (chapter 8). John is included as a coauthor on the manuscript in preparation.

Dr. Musan Zhang obtained her PhD in chemistry under the direction of Dr. Timothy E. Long and was the author's graduate mentor. Nancy taught the author how to synthesize polyesters and research-based discussions were crucial to the development of the author as a graduate student and scientist. Nancy developed the synthesis of the bromomethyl imidazolium diol used in chapter 8 and is a coauthor on the manuscript in preparation.

Dr. M. Nichole Rylander is currently an associate professor in the mechanical engineering department at The University of Texas at Austin, however, she was a joint assistant professor in the mechanical and biomedical engineering departments at Virginia Tech until 2014. Dr. Rylander provided funding for Allison Pekkanen and resources for the cell experiments performed in chapter 8.

Table of Contents

Chapter 1: Introduction 1
1.1 Dissertation Overview 1
1.2 References 4
Chapter 2: A Perspective on Emerging Polymer Technologies for Bisphenol-A Replacement 5
2.1 Abstract 5
2.2 Introduction: Health Concerns and Bisphenol-A Properties 6
2.3 Polycarbonates 10
2.4 Polyesters 13
2.5 Epoxies 16
2.6 Polyimides 19
2.7 Summary and Future Directions for Bisphenol-A Replacement 22
2.8 Acknowledgements 23
2.9 References 24
Chapter 3: Stilbene-Containing Thermotropic Liquid Crystalline (Co)polyesters for Electronic and Aerospace Applications 28
3.1 Abstract 28
3.2 Introduction 29
3.3 Experimental 32
3.3.1 Materials 32
3.3.2 Analytical Methods 32
3.3.3 Polymer Synthesis 33
3.4 Results and Discussion 33
3.4.1 Molecular Weight Characterization and Solid-Stating Strategies 33
3.4.2 Thermal Characterization and Liquid Crystallinity 37
3.4.3 Thermomechanical, Tensile, and Rheological Characterization 41
3.5 Conclusions 44
3.6 Acknowledgements 45

3.7 References 46
Chapter 4: High-Performance Segmented Liquid Crystalline Copolyesters 48
4.1 Abstract 48
4.2 Introduction 49
4.3 Experimental 52
4.3.1 Materials 52
4.3.2 Analytical Methods 52
4.3.3 Polymer Synthesis 54
4.4 Results and Discussion 55
4.4.1 Synthesis and Structural Confirmation 55
4.4.2 Thermal and Morphological Characterization 57
4.4.3 Thermomechanical Characterization and Tensile Testing 69
4.5 Conclusions 73
4.6 Acknowledgements 74
4.7 References 75
4.8 Supporting Information 76
Chapter 5: Free Radical Polymerization of Caffeine-Containing Methacrylate Monomers 82
5.1 Abstract 82
5.2 Introduction 83
5.3 Experimental 86
5.3.1 Materials 86
5.3.2 Analytical Methods 86
5.4 Results and Discussions 91
5.4.1 Synthesis and Copolymerization of Caffeine-containing Methacrylate 91
5.4.2 Structural Confirmation and Molecular Weight Analysis of Poly($EHMA_x$-*co*-CMA_y) 94
5.4.3 Thermal, Thermomechanical, and Rheological Characterization of Caffeine-containing Copolymers 99
5.5 Conclusions 106
5.6 Acknowledgements 107

5.7 References 108
5.8 Supporting Information 110
Chapter 6: Synthesis of Novel Amorphous Copolyesters and Crosslinking Additives from Plant-Based Monomers 112
6.1 Abstract 112
6.2 Introduction 113
6.3 Experimental 116
6.3.1 Materials 116
6.3.2 Analytical Methods 116
6.3.3 Monomer and Polymer Synthesis 117
6.4 Results and Discussion 120
6.4.1 Synthesis and Polymerization of AB Plant-based Monomer 120
6.4.2 Thermal Analysis of Plant-based Polyesters 132
6.4.3 Synthesis and Crosslinking of ABB' Plant-based Monomer 134
6.4.4 Thermal Characterization of Crosslinked Networks 138
6.5 Conclusions 140
6.6 Acknowledgements 141
6.7 References 142
6.8 Supporting Information 144
Chapter 7: Synthesis, Properties and Applications of Ion-Containing Polyurethane Segmented Copolymers 147
7.1 Abstract 147
7.2 Introduction 148
7.3 Synthesis of Ion-Containing Segmented Polyurethanes 150
7.4 Ion-Containing Biobased Polyols and Waterborne Polyurethane Dispersions 155
7.5 Effect of Ion-Incorporation on Segmented Polyurethane Properties 161
7.6 Applications of Ion-Containing Segmented Polyurethanes 168
7.7 Conclusions 177
7.8 Acknowledgements 177
7.9 References 179

Chapter 8: Melt-Stable Imidazolium-Containing Copolyesters as Potential Non-viral Gene Delivery Vehicles 183
8.1 Abstract 183
8.2 Introduction 184
8.3 Experimental 188
8.3.1 Materials 188
8.3.2 Analytical Methods 188
8.3.3 Synthesis of Imidazolium-containing Diols 189
8.3.4 Neutral Control Polyester Synthesis 190
8.3.5 Imidazolium-Containing (Co)polyesters Synthesis 190
8.3.6 Gel Electrophoresis 191
8.3.7 Polyplex Stability Study 192
8.3.8 Cell Culture 192
8.3.9 Cytotoxicity Protocol 192
8.3.10 Transfection Assay 193
8.3.11 Electrospinning 194
8.4 Results and Discussion 194
8.4.1 Synthesis of Imidazolium-containing (Co)polyesters 194
8.4.2 Thermal and Sorption Analysis of Imidazolium Polyesters 201
8.4.3 Imidazolium (Co)polyesters as Non-viral Gene Delivery Vectors 205
8.4.4 Electrospinning and Other Potential Applications 214
8.5 Conclusions 215
8.6 Acknowledgements 216
8.7 References 217
8.8 Supporting Information 219
Chapter 9: Overall Conclusions 221
Chapter 10: Suggested Future Work 224
10.1 Segmented Liquid Crystalline Copolyesters 224
10.2 Incorporating Caffeine into Polyesters 226
10.3 Novel Step Growth Monomers 228

10.4 Further Improving the Impact and Breadth of the Imidazolium Diol 230
10.5 Photocrosslinkable Polyesters and Monomers for Additive Manufacturing..... 232
10.6 References 234

List of Figures

Figure 2.1. Three-dimensional representation of the chemical structures of estrogen (a) and BPA (b). 7
Figure 2.2. DMA of BPA-PC exhibiting the β-transition. Reproduced by permission of [23]. 9
Figure 2.3. Two BPA-PC chains with different conformations due to the rotation of the carbonate bonds denoted with asterisks. Adapted figure from [24]. 9
Figure 2.4. DMA of PCHC. Reproduced by permission from [23] 12
Figure 2.5. The repeating unit of isosorbide PC.[34] 12
Figure 2.6. The repeating unit of commercial BPA fumarate polyesters.[39] 14
Figure 2.7. The crystal structure of *cis* CBDO. Reproduced by permission of [51]. 15
Figure 2.8. The repeating unit of a CBDO copolyester of DMT and EG.[53] 16
Figure 2.9. The repeating unit of BPA-containing poly(ether imide) commercially known as Ultem®.[81] 19
Figure 2.10. The chemical structure of TMC.[89] 21
Figure 2.11. The repeating unit of a generic BMI resin.[79] 21
Figure 3.1. UV-induced photo-Fries rearrangement 30
Figure 3.2. ^{1}H NMR confirms structure of poly(SDE-HD) 35
Figure 3.3. Complex viscosity of poly(SDE-HD) obtained at 263 °C before and after SSP 37
Figure 3.4. Thermal degradation profile of poly(SDE-HD) 38
Figure 3.5. DSC trace of poly(SDE-HD) exhibiting both a melting and isotropic transition 39
Figure 3.6. The effect of alkyl spacer length on the thermal transitions and liquid crystallinity of SDE-containing polyesters 41
Figure 3.7. DMA and tan delta curves for poly(SDE-HD) (solid line) and poly(SDE-HD)$_{90}$-*co*-poly(SDE-BD)$_{10}$ (dotted line) 42
Figure 3.8. Melt rheology of poly(SDE-HD) elucidating shear thinning 44
Figure 4.1. ^{1}H NMR spectra of BB$_6$P10R5$_{50}$ 57
Figure 4.2. Thermal degradation profiles of BB$_6$P10R5$_y$ with soft segment (SS) and hard segment (HS) homopolymer controls showing increased thermal stability with increasing HS content 58

Figure 4.3. The effect of methylene spacer length on the HS melting temperature of the BB_xPTMO_y series at varying weight percent HS 59
Figure 4.4. DSC analysis of BB_6P10R5_y series showing independent thermal transitions for the hard and soft segments suggesting a microphase-separated morphology 61
Figure 4.5. SAXS profiles for BB_6P10R5_y series (vertically shifted) which coupled with DSC further supports a microphase-separated morphology 62
Figure 4.6. Quench cooling curves revealing a T_m and T_i for the complete BB_6P10R5_y series .. 65
Figure 4.7. WAXD profiles of the BB_6P10R5_y series highlighting the highly crystalline hard segment and appearance of polymorphs upon soft segment incorporation 68
Figure 4.8. Overlaid DMA curves for BB_6PTMO_{50}, BB_8PTMO_{50}, BB_6PTMO_{25}, and BB_8PTMO_{25} (a) and thermomechanical analysis of the BB_6P10R5_y series (b)..... 70
Figure 4.9. First heat and cooling DMA curves (a) and overlaid first heat, cool, and second heat traces (b) showing thermomechanical hysteresis of BB_6P10R5_{25} 71
Figure 4.10. Representative tensile curves for BB_6P10R5_{50} and BB_6P10R5_{25}..... 72
Figure 4.11. First heat and quench cooling cycle DSC thermogram of BB_6 homopolymer..... 76
Figure 4.12. The quench cooling and second heat DSC curve for the liquid crystalline BB_5PTMO_{25} exhibiting a T_m and T_i for the hard segment and T_m for the soft segment 77
Figure 5.1. Chemical structures of caffeine (with atoms numbered for reference), theophylline, and theobromine..... 84
Figure 5.2. Chemical structures of adenosine, caffeine, and adenine (with atoms numbered for reference) 85
Figure 5.3. Photoreaction kinetics of caffeine with various alcohols as a function of time, determined using ^1H NMR spectroscopy, with primary (methanol), secondary (ethanol), and tertiary (isopropanol) radicals showing the independence of radical intermediate stability 93
Figure 5.4. Structural confirmation of poly($EHMA_{95}$-co-CMA_5) using ^1H NMR spectroscopy 95
Figure 5.5. Normalized absorbance spectra for CMA-containing copolymers, including a caffeine control in dioxane showing a distinct red shift when caffeine is bound to the polymer backbone 96
Figure 5.6. Light scattering SEC chromatograms of poly(EHMA) control and caffeine-containing copolymers 97

Figure 5.7. Two-step thermal degradation profile of caffeine-containing copolymers 100
Figure 5.8. Proposed thermal degradation route of caffeine-containing copolymers resulting in the loss of free caffeine. Adapted with permission.[45] 101
Figure 5.9. DSC shows broad T_g's for the copolymers, trending upward with increasing CMA content 103
Figure 5.10. Melt rheology exhibits higher moduli with increasing CMA content 104
Figure 5.11. Complex viscosity of poly(EHMA) and caffeine-containing copolymers at 30 °C 105
Figure 5.12. Thermomechanical analysis of 5 mol % CMA copolymer, showing an increased and extended glassy modulus compared to poly(EHMA) control 106
Figure 5.13. ^{1}H NMR spectroscopy confirms structure of novel caffeine methacrylate 110
Figure 5.14. Particle size with respect to mean volume % (a) and mean intensity % (b) for the (co)polymers in THF 111
Figure 6.1. Repeating units of PLA (a) and PP (b) 114
Figure 6.2. ^{1}H NMR spectroscopy of isomeric mixture of AB hydroxyester monomer confirms isomeric mixture and shows evidence of dimer 123
Figure 6.3. Zoomed in ^{1}H NMR spectra reveals evidence of AB hydroxyester dimer (top) and unreacted 9-DAME (bottom) 124
Figure 6.4. ^{1}H NMR spectroscopy confirms bio-based polyester structure and shows expected disappearance of methyl ester from monomer 127
Figure 6.5. Advanced polymer chromatography (APC) provides excellent separation of low molecular weight species, allowing for monitoring molecular weight as the reaction proceeds 129
Figure 6.6. ^{1}H NMR spectra of AB hydroxyacid monomer (bottom) exhibiting presence of dimer and polymer (top) revealing the disappearance of the carboxylic acid upon polymerization 131
Figure 6.7. Thermal degradation profiles of bio-based AB monomers and resulting polyesters after different reaction procedures 133
Figure 6.8. Isomeric mixture of bio-based monomers affords low T_g amorphous copolyesters 134
Figure 6.9. Thermal degradation profiles of novel MDHD-based polyester networks 139
Figure 6.10. Thermal analysis of bio-based polyester networks 140

Figure 6.11. ^{1}H NMR spectroscopy of as-received 9-DAME 144
Figure 6.12. ^{1}H NMR spectroscopy of 9,10-epoxydecanoate 145
Figure 6.13. ^{1}H NMR spectroscopy confirms structure of MDHD ABB' monomer 146
Figure 7.1. Hydrogen bonding, shown with dashed lines, between the hydrogen and carbonyl oxygen in urethane bonds. 149
Figure 7.2. Prepolymer route to segmented polyurethanes. 151
Figure 7.3. Some polyurethane monomers which place ionic groups in HS.[26-28,33,34] 153
Figure 7.4. Polyols used in the synthesis of segmented polyurethanes.[27,42,43] 155
Figure 7.5. The chemical structures of glycerol and castor oil. 156
Figure 7.6. Modulus as a function of temperature for polycarbonate-based PUD films with varying ionic content. Reproduced with permission from ref.[66] 164
Figure 7.7. Tensile curves of the uncharged, TEP and TBP polyurethanes with 75 weight percent HS content. Reproduced with permission from ref.[26] 167
Figure 7.8. The PUD (a), representative film (b) and foam (c) of the PUD/PVA/glass nanoparticle composites, and SEM image of the foam containing 10 % bioactive glass nanoparticle. Adapted with permission from ref.[70] 169
Figure 7.9. A model demonstrating the rearrangement of zwitterion-containing polyurethanes with different M_n's in water, based on contact angle analysis, and the resultant effect on protein adsorption. Adapted with permission from ref.[31] 171
Figure 7.10. The chemical structure of the zwitterionic phospholipid endcapping agent and protein adsorption results for zwitterionic-containing segmented polyurethanes with various SS polyol components. Adapted with permission from ref.[86] 172
Figure 7.11. DMA curves (a) and conductivity (b) of imidazolium-containing polyurethanes with varying amounts of IL. Adapted with permission from ref.[33] 175
Figure 7.12. Cartoon showing proposed ionic aggregation and IL intercalation providing enhanced thermomechanical strength and ionic conductivity. Reproduced with permission from ref.[33] 175
Figure 8.1. ^{1}H NMR spectroscopy confirms structure of bromomethyl imidazolium diol 196
Figure 8.2. ^{1}H NMR spectroscopy confirms structure of melt stable imidazolium homopolyester, PImA 199

Figure 8.3. 12 h TGA isotherm of BrBuIm diol at 180 °C and proposed Hofmann elimination arrow-moving mechanism (inset) 201
Figure 8.4. Water sorption analysis demonstrating increased hydrophilicity of PImA (red) compared to PNA (blue) 202
Figure 8.5. Degradation profiles of imidazolium-containing (co)polyesters and neutral control. Char residue scales with imidazolium content..... 203
Figure 8.6. Fox equation plot demonstrating increasing glass transition temperature (T_g) with increasing ionic content 205
Figure 8.7. DNA gel binding assay shows imidazolium-containing (co)polyesters completely bind DNA at N/P ratios of 4 (P(NA_{50}-*co*-ImA_{50}) and P(NA_{25}-*co*-ImA_{75})) and 5 (PImA) 207
Figure 8.8. Hydrodynamic diameter of polyplexes from dynamic light scattering showing stability over 24 h in water..... 208
Figure 8.9. Cytotoxicity assay demonstrating insignificant toxicity in HeLa cells and confirming biocompatibility of imidazolium-containing (co)polyesters (error bars are the standard deviation from the average of n=5 samples)..... 210
Figure 8.10. Charged polyesters transfected significantly better than controls at low N/P ratios in serum-free media 212
Figure 8.11. SEM images of electrospun fibers from blends of PImA and 300,000 g/mol poly(ethylene oxide) for potential antimicrobial and adhesive applications. 18 mm collector distance, left: +/-15 kV, right: +10 kV –15 kV..... 215
Figure 8.12. ^{1}H NMR spectroscopy confirms structure of bromo-containing intermediate diol 219
Figure 8.13. ^{1}H NMR spectroscopy confirms structure of novel bromobutyl imidazolium diol 220
Figure 10.1. Commercially available trifunctional diblock polyether..... 226
Figure 10.2. Commercially available diacrylates 233

List of Tables

Table 3.1. Thermal transitions of various stilbene-containing (co)polyesters. N.D. = not detected 39

Table 3.2. Tensile data obtained for poly(SDE-HD) 43

Table 4.1. Scattering vector maxima and calculated Bragg spacing from the SAXS profiles of the BB_6P10R5_y series 63

Table 4.2. Thermal transitions from the quench cooling traces for the liquid crystalline BB_6P10R5_y series 66

Table 4.3. Melting and isotropic transitions determined from DSC quench cooling curves for various liquid crystalline BB_xPTMO_y segmented copolyesters (*shoulder) 67

Table 4.4. Thermal transitions from DSC for the neat 2K P10R5 SS oligomer 77

Table 4.5. BB_6P10R5_{65} WAXD peaks and corresponding Bragg spacing 78

Table 4.6. BB_6P10R5_{50} WAXD peaks and corresponding Bragg spacing 79

Table 4.7. BB_6P10R5_{25} WAXD peaks and corresponding Bragg spacing 80

Table 4.8. BB_6 WAXD peaks and corresponding Bragg spacing 81

Table 5.1. Molecular weight and thermal degradation of caffeine-containing copolymers 99

Table 6.1. Relative molecular weights of hydroxyester polymerization as a function of reaction time 130

Table 6.2. Synthetic procedures and thermal analysis of ABB' polyester crosslinked networks 138

Table 7.1. Thermal transitions of segmented polyurethanes with sulfonate groups in the hard and soft segments. Reproduced with permission from ref.[27] 165

List of Schemes

Scheme 2.1. The synthesis of BPA-PC from BPA and diphenyl carbonate.[16, 25] 10
Scheme 2.2. Synthesis and repeating unit of CBDO-PC.[36] 12
Scheme 2.3. The common synthetic route for the production of BPA-containing epoxy resins.[16, 62] 17
Scheme 2.4. The synthetic route to the 1,3,4-oxadiazole containing diol precursor.[78] 19
Scheme 3.1. Synthesis of poly(SDE-HD)$_x$-*co*-poly(SDE-BD)$_y$ using melt transesterification ... 35
Scheme 4.1. Synthesis of poly(BB-HD)$_x$-*ran*-poly(BB-P10R5$_{2K}$)$_y$ (BB$_6$P10R5$_y$ series) using melt transesterification 56
Scheme 5.1. Synthesis of hydroxyl-functionalized caffeine using a peroxide-initiated photoreaction 92
Scheme 5.2. Synthesis of caffeine methacrylate (CMA) monomer 94
Scheme 5.3. Synthesis of caffeine-containing copolymers using conventional free radical polymerization 94
Scheme 6.1. Synthesis of isomeric mixture of AB hydroxyester or hydroxyacid monomers for step-growth polymerization 121
Scheme 6.2. Melt polymerization of bio-based AB monomers readily achieves polyesters, eliminating solvents and excess purification 125
Scheme 6.3. Two step synthesis of ABB' hydroxyester step-growth monomer and/or crosslinking additive. (a) Epoxidation of 9-DAME (b) Hydrolysis of epoxidized 9-DAME yields MDHD 135
Scheme 6.4. Melt transesterification of MDHD ABB' monomer affords crosslinked networks 137
Scheme 7.1. Synthesis of a zwitterionic diol.[30,31] 152
Scheme 7.2. PUD synthesis via the solution process.[65] 159
Scheme 7.3. Isocyanate-free route to the 5-membered cyclic carbonate and the subsequent ring opening reaction with a primary amine, revealing the hydroxy-urethane chemistry.[82] 161
Scheme 7.4. Functionalization reaction of isocyanate-endcapped polyurethanes with UV-active HEMA. 176

Scheme 8.1. Substitution reaction affords alkyl imidazolium diols 195
Scheme 8.2. Synthesis of noncharged polyester, poly(neopentylene adipate) (PNA)..... 197
Scheme 8.3. Catalyst-free melt polycondensation affords imidazolium-containing (co)polyesters 198
Scheme 10.1. Synthesis of ion-containing segmented liquid crystalline copolyesters..... 225
Scheme 10.2. Copolymerizing with a trifunctional polyol to obtain branched segmented liquid crystalline copolyesters..... 226
Scheme 10.3. Proposed synthesis of caffeine endcapped oligoesters..... 228
Scheme 10.4. Substitution reaction to generate a caffeine diol 228
Scheme 10.5. Ring-opening functionalized cyclic carbonates to obtain multifunctional monomers..... 229
Scheme 10.6. 3-step synthesis to a trifluorosulfonimide-containing diester 230
Scheme 10.7. Synthesis of segmented imidazolium-containing copolyesters for improved transfection..... 231
Scheme 10.8. Polyurethanes containing pendant imidazolium groups..... 232
Scheme 10.9. Proposed route to novel photocrosslinkable polyester ionomers 233

Chapter 1: Introduction

1.1 *Dissertation Overview*

Wallace Carothers' discovered and synthesized the first polyester about 85 years ago, and the possibilities and applications remain seemingly endless today.[1,2] The use of aliphatic, aromatic, cycloaliphatic, ionic, and any combination thereof provides an ever-growing versatile library of monomers to continually develop novel polyesters for emerging applications.[2-4] The ability to change the structure of the polyester backbone as well as pendant groups offers intricate design parameters for sophisticated, functional polymeric materials.[5] Although many polymerization techniques afford polyesters, melt polymerization, the reaction of a diacid or diester and diol at high temperatures in the presence of an appropriate catalyst, is a common industrially employed method.[2,6,7] This technique does not require any solvent or post-polymerization workup and catalysts enable short reaction times.[2] One challenging requirement, especially when designing and synthesizing novel polyester monomers, is that the monomers must remain stable at elevated temperatures. The following describes some of the inspiration for various research projects in which melt polymerization afforded polyesters to address challenges and elucidate structure-property-morphology relationships.

Liquid crystalline polymers offer unique optical properties due to anisotropic alignment of the polymer chains.[8] Main-chain thermotropic liquid crystalline polyesters are a distinct class of polymers that contain the rigid, anisotropic segments, along the backbone and the anisotropy is temperature-dependent. When prepared for applications desiring high working temperatures and mechanical integrity, these rigid-rod polyesters are often highly crystalline, exhibit high moduli, low dielectric constants, and shear thinning for melt processability.[9] Wholly aromatic

thermotropic liquid crystalline polyesters are commercially used to encase electronics. Unfortunately, ultraviolet (UV) light can induce a degradative side reaction known as the Photo-Fries rearrangement on aromatic esters.[10,11] This reaction generates a phenol, which causes undesirable coloring, and kinks the rigid backbone of the polyester, ultimately diminishing the mechanical integrity and performance.[10,12] High-performance polymer replacements are desired which do not degrade under taxing UV and high temperature environments.

A thrust toward sustainable polymeric materials is increasingly relevant and encouraged.[13,14] Plant-based compounds offer chemical functionality, or a facile derivatization can incorporate the desired functionality, for polyester synthesis.[15] Often new, pure, bio-based chemicals rely on enhanced industrial refinement and isolation processes.[16] Elevance Renewable Sciences, Inc. established a process to obtain a plant-based acid-alkene in high purity and involved assistance in developing renewable polyesters with properties rivaling current petroleum-based polymers. Ideally the novel polyesters would also exploit the hydrolytically unstable ester linkages to provide sustainable, degradable polyesters.[17,18] This degradation pathway reduces environmental waste and also offers a triggerable, degradable linkage when designing polyesters.[19] Utilizing the inherent degradation and biocompatibility, designing melt-stable ion-containing polyesters for non-viral gene delivery applications was also of interest to aid in understanding the structural and ionic effects of the polymer on efficient transfection.[20-22]

The following dissertation investigates structure-property-morphology relationships of liquid crystalline copolyesters, segmented liquid crystalline copolyesters, imidazolium-containing copolyesters, and both polyesters and methacrylate copolymers containing renewable resources. Transesterification, direct esterification, free radical copolymerization, small-molecule synthesis techniques, and an array of polymer characterization tools enabled the

synthesis and evaluation of polyesters for the desired applications. The specific challenges addressed include UV and heat stable electronic coatings, increasing sustainability without sacrificing polymer properties, and non-viral gene delivery vehicles. After gaining further insight into the specific polyesters and resulting physical properties, potential applications broadened to include pressure sensitive adhesives, antibacterial bandages, aerospace coatings, thermoplastic elastomers, thermosets, and hyperbranched polymeric additives. Additionally, two timely reviews, focusing on high-performance polymers for bisphenol-A replacement and ion-containing segmented polyurethanes, are included.

1.2 *References*

(1) Carothers, W. H.; Dorough, G. L.; Natta, F. J. v. *Journal of the American Chemical Society* **1932**, *54*, 761.
(2) Rogers, M. E.; Long, T. E. *Synthetic methods in step-growth polymers*; Wiley-Interscience: Hoboken, N.J., 2003.
(3) Lin, Q.; Pasatta, J.; Wang, Z.-H.; Ratta, V.; Wilkes, G. L.; Long, T. E. *Polymer International* **2002**, *51*, 540.
(4) Zhang, M.; Zhang, M.; Moore, R. B.; Long, T. E. *Polymer* **2013**, *54*, 3521.
(5) Burgess, S. K.; Leisen, J. E.; Kraftschik, B. E.; Mubarak, C. R.; Kriegel, R. M.; Koros, W. J. *Macromolecules* **2014**, *47*, 1383.
(6) Unal, S.; Long, T. E. *Macromolecules* **2006**, *39*, 2788.
(7) Liu, C.; Liu, F.; Cai, J.; Xie, W.; Long, T. E.; Turner, S. R.; Lyons, A.; Gross, R. A. *Biomacromolecules* **2011**, *12*, 3291.
(8) Donald, A.; Windle, A.; Hanna, S. *Liquid Crystalline Polymers*; 2nd ed.; Cambridge University Press, 2006.
(9) Economy, J.; Goranov, K.; Hergenrother, P., Ed.; Springer Berlin / Heidelberg: 1994; Vol. 117, p 221.
(10) Belluč, D.; Hrdlovič, P. *Chemical Reviews* **1967**, *67*, 599.
(11) Coppinger, G. M.; Bell, E. R. *The Journal of Physical Chemistry* **1966**, *70*, 3479.
(12) Bangee, O. D.; Wilson, V. H.; East, G. C.; Holme, I. *Polymer Degradation and Stability* **1995**, *50*, 313.
(13) Singh, S. P.; Ekanem, E.; Wakefield Jr, T.; Comer, S. *International Food and Agribusiness Management Review* **2003**, *5*, 14.
(14) Gandini, A. *Macromolecules* **2008**, *41*, 9491.
(15) Mooney, Brian P. *Biochemical journal*, *418*, 219.
(16) Gandini, A.; Lacerda, T. M. *Progress in Polymer Science*.
(17) Li, S. *Journal of Biomedical Materials Research* **1999**, *48*, 342.
(18) Hakkarainen, M. In *Degradable Aliphatic Polyesters*; Springer Berlin Heidelberg: 2002; Vol. 157, p 113.
(19) Xu, P.; Li, S.-Y.; Li, Q.; Ren, J.; Van Kirk, E. A.; Murdoch, W. J.; Radosz, M.; Shen, Y. *Biotechnology and Bioengineering* **2006**, *95*, 893.
(20) Hemp, S. T.; Allen, M. H.; Green, M. D.; Long, T. E. *Biomacromolecules* **2012**, *13*, 231.
(21) Hemp, S. T.; Smith, A. E.; Bryson, J. M.; Allen, M. H.; Long, T. E. *Biomacromolecules* **2012**, *13*, 2439.
(22) Allen, M. H.; Green, M. D.; Getaneh, H. K.; Miller, K. M.; Long, T. E. *Biomacromolecules* **2011**, *12*, 2243.

Chapter 2: A Perspective on Emerging Polymer Technologies for Bisphenol-A Replacement

(Published in *Polymer International* **2012**, *61*, 1485.)

Ashley M. Nelson and Timothy E. Long

Department of Chemistry, Macromolecules and Interfaces Institute
Virginia Tech, Blacksubrg, VA 24061-0212

2.1 *Abstract*

Recent attention surrounds bisphenol-A (BPA) due to potential estrogen mimicry and human health hazards. The public's negative reactions to these concerns threaten the commercial use of BPA requiring the global polymer community to investigate suitable replacements for commercial products that demand high thermal and mechanical properties from BPA. This review highlights four classes of polymers which often utilize BPA for enhancing specific properties: polycarbonates, polyesters, epoxies, and polyimides. A compilation of recent efforts involving the design of BPA-free polymers is provided. Alternate monomers include 2,2,4,4-tetramethyl-1,3-cyclobutanediol (CBDO) and isosorbide, and emerging polymers that exhibit acceptable thermal and mechanical properties are discussed.

2.2 *Introduction: Health Concerns and Bisphenol-A Properties*

Bisphenol-A (BPA) is classified as an endocrine-disrupting chemical (EDC) due to validated reports of its ability to mimic estrogen binding both *in vivo* and *in vitro*.[1-3] The potential health hazards of EDCs include various cancers, brain and behavioral changes in fetuses or infants, and female reproductive issues.[4, 5] **Figure 1** suggests the chemical similarities between estrogen and BPA, as both amphiphilic compounds contain hydrocarbon rings and two hydroxyl groups.[6, 7] A variety of potential BPA-containing commercial products for food or beverage packaging include reusable plastic bottles, baby bottles, can liners, and dental sealants.[3, 8, 9] The hydrolytic degradation of BPA polycarbonate (PC) yields the BPA monomer, and as expected, degradation rates depend on use conditions.[10, 11] Despite the increasingly negative public opinion, the U.S. Food and Drug Administration (FDA) regulates and deems products containing BPA safe for use.[12] A copious amount of earlier research on the safety of BPA also indicated that the amount of BPA exposure and ingestion of the average human does not induce adverse health effects.[13-15] Upon ingestion, the human body metabolizes BPA into monoglucoronide.[13] Monoglucoronide, unlike BPA, does not perform as an EDC, and the body excretes the metabolite without causing harm.

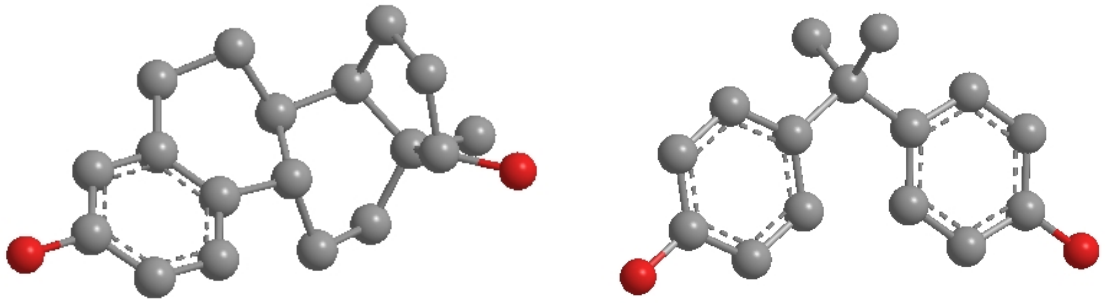

a b

Figure 2.1. Three-dimensional representation of the chemical structures of estrogen (a) and BPA (b).

BPA is an aromatic, bulky diol which affords excellent thermal, mechanical, optical, and electrical properties upon incorporation into a polymer.[16, 17] A main factor that influences the toughness of a polymer at room temperature is the glass transition temperature (T_g).[18] T_g is the temperature marking the onset of segmental motion and depends on rigidity of the backbone, steric hindrance of pendant groups, molecular symmetry, and intermolecular and intramolecular interactions. Rubbers display high impact properties and sub-ambient T_g's whereas plastics exhibit high T_g's, often causing brittleness. Secondary transitions, often classified as β- and γ-transitions, are present in the dynamic mechanical thermal analysis for many polymers, and the transitions characteristically occur in polymers with high impact properties.[18, 19] These transitions always occur at temperatures below the T_g and result from the onset of motion of side-chains or groups and/or conformational changes. BPA-PC serves as a benchmark for impact properties and to ascertain the influence of BPA on mechanical polyesters.[20-22]

BPA-PC exhibits a T_g of approximately 150 °C, a melting temperature (T_m) of 267 °C, and a β-transition at -100 °C in the amorphous state and -30 °C in the semi-crystalline state.[18] **Figure 2** shows the dynamic mechanical analysis (DMA) curve for BPA-PC.[23] The β-transition

correlates to the lowest temperature peak in the tan δ trace, and the high T_g and T_m of BPA-PC provides outstanding thermal properties. Investigation of both the T_g and β-transition found that the β-transition imparted exceptional toughness, and many researchers have attempted to attribute molecular conformational changes to the β-transition.[22] Locati et al.[20] reported that the β-transition included motion of both the carbonate and phenyl groups, and the movement of the phenyl groups below the T_g contributed to the improved mechanical properties. The movement of the phenyl and carbonate groups occurs due to a large amount of free volume. This free volume allows for conformational rotations as well as movement of the two pendant methyl groups in each repeating unit, allowing the polymer to absorb energy at temperatures below the T_g.[18, 20] **Figure 3** shows two segments of BPA-PC chains, and bond rotation of the carbonate groups causes the adjacent phenyl rings to undergo a ring-flip motion in the polymer backbone.[24] The superior mechanical properties of BPA serve as benchmarks for the comparison to various engineering thermoplastics. Developing a fundamental understanding of these properties will facilitate the discovery of replacement monomers for BPA.

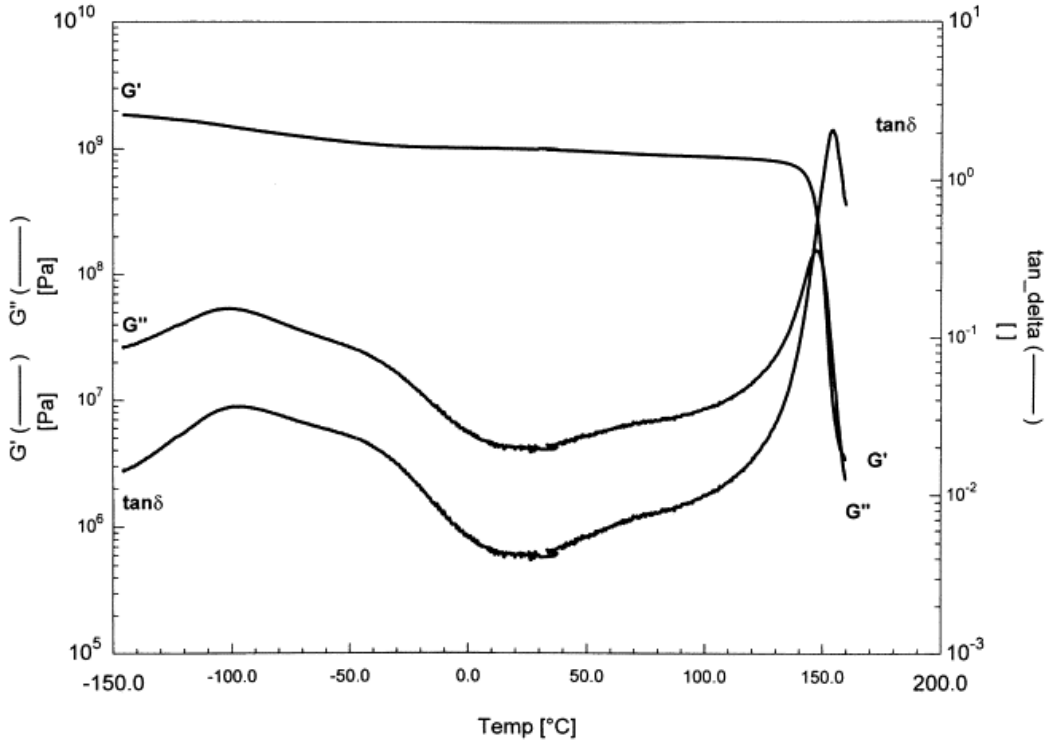

Figure 2.2. DMA of BPA-PC exhibiting the β-transition. Reproduced by permission of [23].

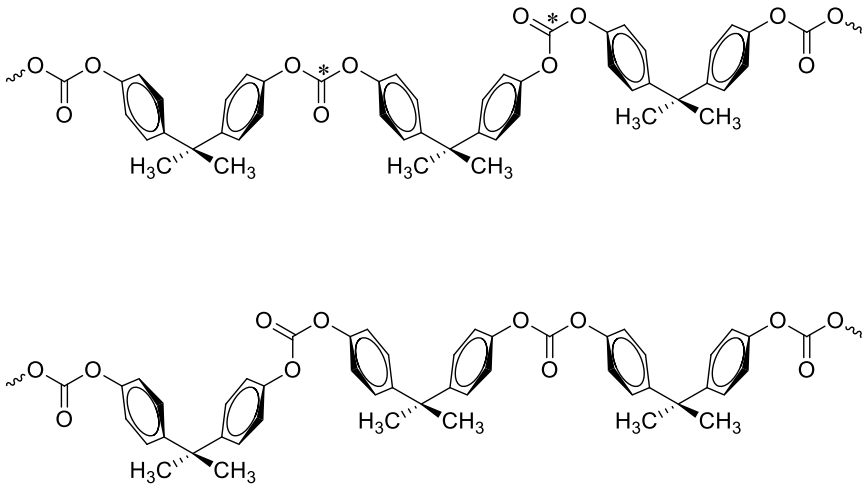

Figure 2.3. Two BPA-PC chains with different conformations due to the rotation of the carbonate bonds denoted with asterisks. Adapted figure from [24].

2.3 *Polycarbonates*

A common industrial method to synthesize BPA-PC is the transesterification of BPA and diphenyl carbonate as depicted in **Scheme 1**.[16, 25] BPA-PC demonstrates utility in a variety of applications ranging from plastic bottles to compact disks to electrical connectors due to the aforementioned properties. In particular, the optical clarity and low birefringence of BPA-PC broaden the commercial use of this polymer.[26, 27] In addition to BPA-PC in commercial applications, many researchers employed BPA to impart BPA-like properties or to understand existing BPA-PC resins. Antiplasticizers function as polymer additives that increase both modulus and tensile strength.[28, 29] Ueda[17] blended *meta*-terphenyl with BPA-PC for antiplasticization, which improved BPA-PC properties for compact disks. Kricheldorf et al.[30] investigated various catalysts for the polycondensation of BPA with diphosgene and determined that formation of molecular weight limiting cyclics was an unavoidable side reaction. Conversely, Brunelle and Shannon[31] prepared cyclic oligomers as monomers to form high molecular weight BPA-PC.

Scheme 2.1. The synthesis of BPA-PC from BPA and diphenyl carbonate.[16, 25]

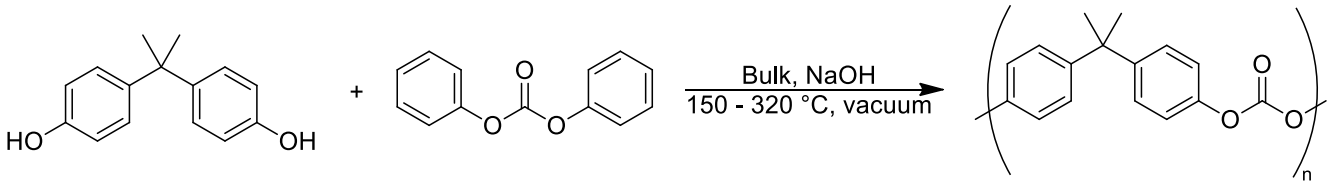

An abundance of literature focuses on BPA-containing PCs; however, many researchers explore the removal of BPA in next generation materials. **Figure 4** shows the ring opening polymerization of cyclohexene oxide in the presence of carbon dioxide (CO_2) and DMA of the resulting PC.[23] Despite the presence of a β-transition, the properties of poly(cyclohexane

carbonate) (PCHC) are not equivalent to BPA-PC, but the elimination of BPA and replacement of phosgene with CO_2 offers a viable PC for lower temperature and impact applications. More sustainable PCs utilize isosorbide, a renewable resource derived from glucose.[32] Isosorbide contains two fused 5-membered rings with *trans* hydroxyl groups. The incorporation of isosorbide into PCs afforded thermally stable polymers.[33-35] Isosorbide PCs and copolycarbonates resulted from various polymerization methods including interfacial, melt, and solution polycondensation.[34] **Figure 5** depicts the repeating unit of isosorbide PC. Isosorbide PC exhibits a T_g of 144 °C and, regardless of the comonomer(s) chosen, PCs with T_g's greater than 120 °C resulted.[34, 35] Although the authors did not address the mechanical properties of the isosorbide PCs, the thermal properties and overall polymer structure suggest possible candidates for potential BPA-PC replacements. Brunelle et al.[36] also investigated the use of 2,2,4,4-tetramethyl-1,3-cyclobutanediol (CBDO). A combination of melt transesterification and solid state polymerization yielded weatherable polycarbonates. **Scheme 2** shows the synthesis and repeating unit of CBDO-PC. CBDO is a common monomer used in the synthesis of BPA-replacement polymers and is further discussed in the polyester section of this review.

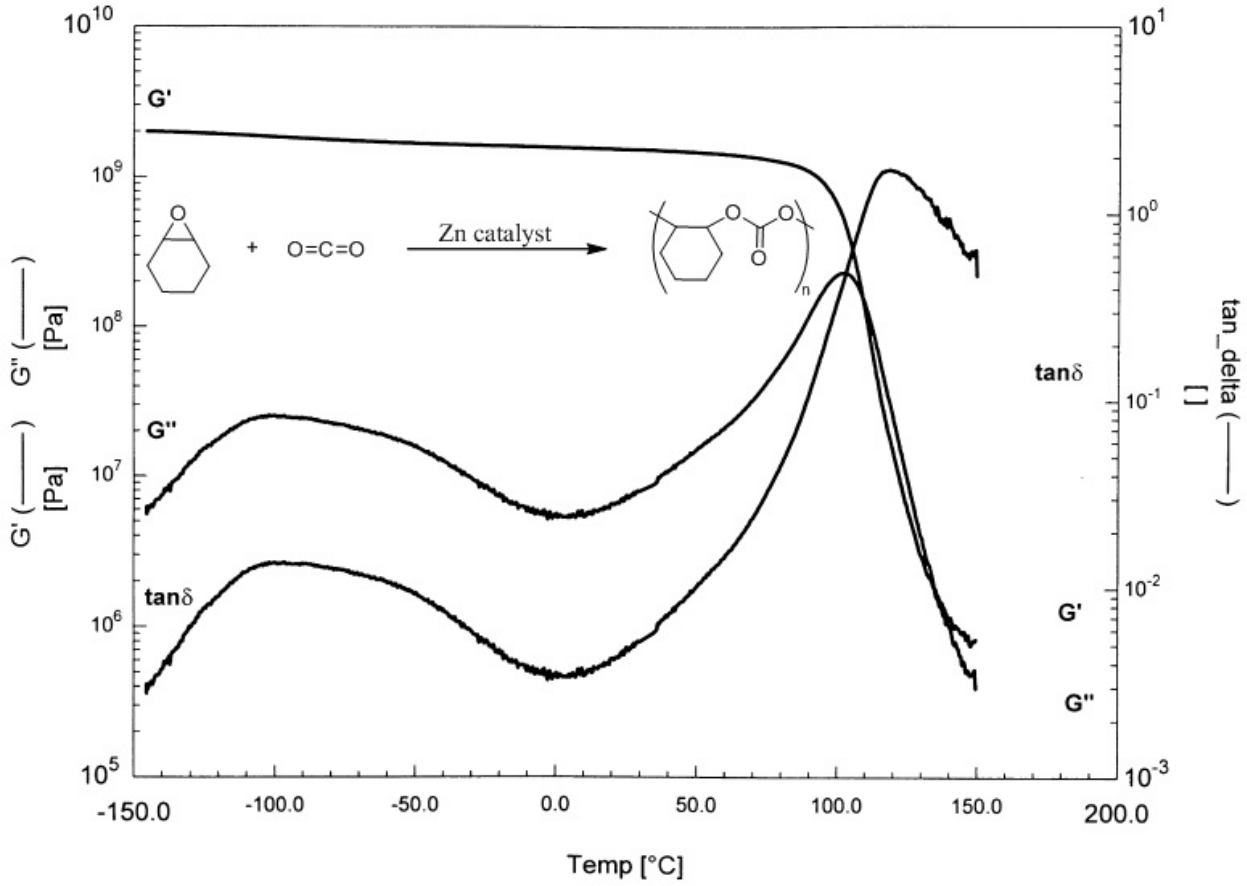

Figure 2.4. DMA of PCHC. Reproduced by permission from [23].

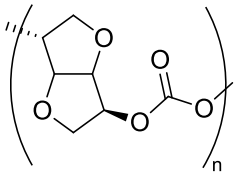

Figure 2.5. The repeating unit of isosorbide PC.[34]

Scheme 2.2. Synthesis and repeating unit of CBDO-PC.[36]

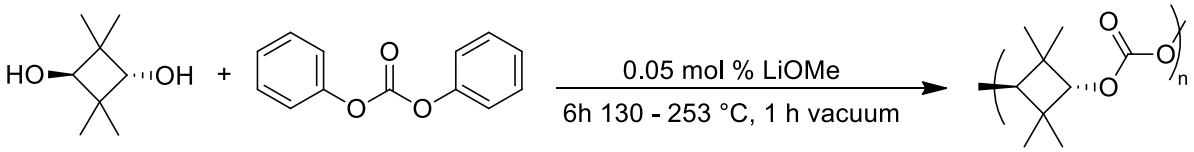

Segmented block copolymers consist of rigid and flexible blocks that microphase separate affording elastomeric properties.[16, 37] The synthesis of PC block copolymers with BPA-

free hard segments may provide mechanical properties that exceed BPA-PC due to elastomeric behavior without the necessity of any secondary transitions.[16, 38] For example, Memon and Williams[38] reported the synthesis of a segmented block copolymer with phenolphthalein as the hard segment. This polymer exhibited a T_g of 244 °C and a Young's modulus of 3.2 MPa, whereas, the BPA version exhibited a T_g of 142 °C and a Young's modulus of 617 kPa. Currently, the most commercially successful replacement for BPA-PC is Eastman's Tritan™ copolyester, highlighted in the subsequent polyester section of this review.

2.4 *Polyesters*

Commercialization of BPA-containing high performance polyesters is not as prevalent as PCs, epoxies, or polyimides due to high processing temperatures, decreasing reactivity of phenols, and an overall absence of mechanical toughness in products.[39, 40] Poly(BPA-terephthalate)-*co*-poly(BPA-isophthalate), is a fully aromatic polyester with commercial success.[41] These copolymers demonstrated thermal stability, optical clarity, toughness, and UV stability. Unsaturated polyarylates are another class of BPA-containing polyesters with commercial importance due to exceptional chemical and hydrolytic resistance.[39] The production of two families of BPA-containing unsaturated polyarylates occurs on the industrial scale. The unsaturation results from the incorporation of either maleic anhydride or fumaric acid, and **Figure 6** depicts the repeating unit of typical BPA fumarate polyesters.

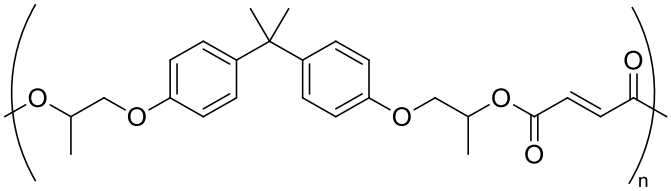

Figure 2.6. The repeating unit of commercial BPA fumarate polyesters.[39]

Aromatic polyesters lack high performance polymer properties because of poor solubility, which has prompted recent laboratory research. Wadgaonkar et al.[42] found the copolymerization of BPA-containing polyarylates with a compound containing a flexible pendant group improved room temperature solubility in organic solvents without sacrificing other properties. Patel et al.[43] reported similar results upon copolymerization with *s*-triazine rings. Copolymerization with oligomeric siloxanes also proved as a suitable route for soluble polyarylates.[44] Chen et al.[45] found that the copolymerization of BPA, 1,6-hexanediol, terephthaloyl chloride, and oligolactide yielded high molecular weight biodegradable polyesters. These copolyesters are under investigation for use in tissue engineering applications. Preliminary cell work suggested potential biocompatibility despite the incorporation of BPA. The syntheses of these copolyesters occurred in the absence of solvent, and the polymers demonstrated thermal stability to ~370 °C with T_g's ranging from 52 – 90 °C depending on composition.

The number of commercial BPA-containing polyesters is not significant compared to other polymer classes; however, the replacement of BPA-containing high performance polymers with novel polyesters is proving successful. Perhaps the most recent commercially significant polymer is Eastman's Tritan™ copolyester, which was launched in 2007. Tritan™ is touted as the first polymer which replaced BPA-PC in many applications, most importantly those applications in which human exposure is a concern.[46-48] Copolyesters consisting of *cis*/*trans*

CBDO demonstrate properties approaching BPA-PC.[49] The pendant methyl groups and presence of a β-transition in polymers containing CBDO are noteworthy and help explain the increased mechanical properties.[50] **Figure 7** shows the crystal structure of the *cis* isomer of CBDO.[51] Natarajan et al.[52] compared the effect of *cis* and *trans* cyclohexane vs. CBDO in the backbone of polyesters. An increase in *trans* cyclobutane rings results in a higher degree of rigidity.

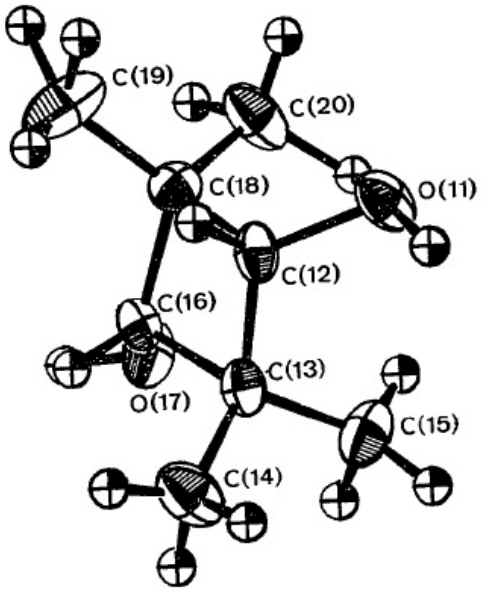

Figure 2.7. The crystal structure of *cis* CBDO. Reproduced by permission of [51].

Since the discovery of the desirable polymer properties that result upon CBDO incorporation, the laboratory investigation of this monomer is abundant.[53-55] Kelsey et al.[53] synthesized copolyesters of CBDO, dimethyl terephthalate (DMT), and various aliphatic diols. **Figure 8** depicts these copolyesters with ethylene glycol (EG). The copolyesters were amorphous, tough, injection moldable, exhibited high T_g's, and demonstrated UV stability greater than BPA-containing polycarbonates. The solubility of the resulting copolymers depended on the *cis/trans* ratio of the CBDO monomer, offering a facile route to tune properties for specific applications.

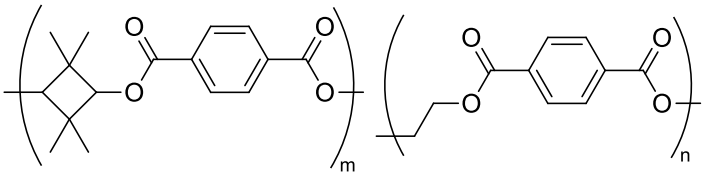

Figure 2.8. The repeating unit of a CBDO copolyester of DMT and EG.[53]

As discussed above as a BPA replacement in PCs, the incorporation of isosorbide to improve polyester properties is also under investigation.[56-58] Incorporating isosorbide into poly(butylene terephthalate) (PBT) increased the T_g from ~45 °C to 92 °C with 42 mol % isosorbide incorporation.[57] The T_m's of the copolyesters decreased from 226 °C to 155 °C with 30 mol % isosorbide. Above 30 mol % incorporation, the polyesters were amorphous. The incorporation of isosorbide broadened the range of applications for this thermoplastic polyester. Other high molecular weight copolymers of a similar structure demonstrated efficient thermal properties and are capable of industrial scale production.[56] The use of environmentally friendly monomers in polyester synthesis is expanding, particularly the incorporation of isosorbide into liquid-crystalline polyesters.[58-60]

2.5 *Epoxies*

The commercial production of epoxy resins involving the reaction of BPA with epichlorohydrin in the presence of a base, e.g. sodium hydroxide (NaOH), originated in the 1940s.[16, 61, 62] **Scheme 3** depicts epoxy resin synthesis. Epoxy resins account for ~20 % of BPA's commercial use, falling second only to polycarbonates.[63] Commercial epoxy resins offer many of the characteristic properties that BPA provides; however, overall toughness decreases due to the necessary crosslinking reaction.[64] The curing process of epoxies involves the addition of a crosslinking agent. Different crosslinking agents follow different mechanistic paths and the

nature of the crosslinking agent dictates the properties of the resulting system.[16, 61, 62] When curing an epoxy resin, both the temperature at which curing occurs and the curing time affect the properties. The ideal combination of time and temperature differs for each epoxy system and depends on the T_g of the uncured epoxy resin, the T_g of the gel point of the epoxy resin, and the T_g of the fully cured epoxy resin.[65] In an attempt to improve the impact properties of commercial epoxy resins, Unnikrishnan and Thachil[66] physically blended phenol- and cardanol-based resol resins with commercial BPA-containing epoxy resins. The blending reduced moduli; however, tensile strength, elongation at break, energy absorbed, compressive break, hardness shore, and water absorption properties improved.

Scheme 2.3. The common synthetic route for the production of BPA-containing epoxy resins.[16, 62]

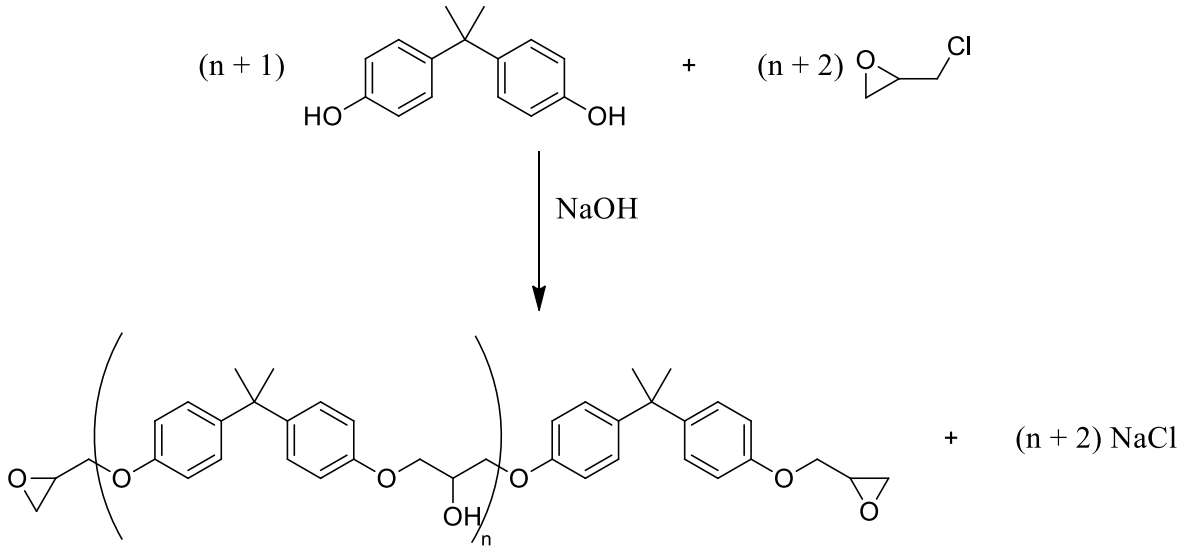

Determining novel approaches for decreasing the environmental impact of polymers and polymer systems motivates researchers. Recently, natural oils and varying weight percents of epoxy resins cured with recycled PET partially replaced BPA.[67-69] Incorporation of these green components into epoxy resins with a different crosslinking agent allowed for the targeting of

specific properties. In an effort to synthesize water soluble epoxies, Motawie et al.[70] replaced BPA with poly(ethylene glycol) (PEG). Despite a successful synthetic strategy, upon curing, the PEG-based epoxies failed to compete with the hardness and adhesive properties of BPA-containing epoxies, and found better use as optional plasticizers.

A common monomer explored for BPA replacement, isosorbide-containing epoxy resins are under investigation.[71, 72] Lukaszczyk et al.[72] prepared isosorbide epoxy resins identical to the BPA-containing epoxy resins described above using epichlorohydrin and NaOH. The curing of the isosorbide resins occurred with four different curing agents: phthalic anhydride, tetrahydrophthalic anhydride, triethylenetetramine, and isophorone diamine. The resulting mechanical properties, such as flexural modulus and impact strength, remained higher than BPA-containing resins. The novel epoxies also demonstrated decreased chemical resistance to acids and bases compared to the commercial BPA epoxy benchmark.

An abundance of research on the incorporation of block copolymers into BPA-containing epoxy resins has ensued.[73-75] Gibbs and coworkers[76] investigated the effect of incorporating poly(methyl acrylate-*co*-glycidyl methacrylate-*b*-polyisoprene) into BPA-free epoxy resins. Improved phase separation resulted compared to a BPA-containing epoxy resin with the same block copolymer modification. The effect of more defined microphase separation on the toughness of the epoxy resins has yet to undergo investigation. Wang et al.[77] synthesized another BPA-free epoxy resin containing dicyclopentadiene which demonstrated increased impact properties, but lacked other properties in relation to commercial BPA epoxy. Balamurugan and Kannan[78] synthesized liquid crystalline epoxy resins with 1,3,4-oxadiazole units. **Scheme 4** depicts the synthesis of the 1,3,4-oxadiazole containing diol precursor. Curing

of the liquid crystalline resins occurred in both the liquid crystalline and isotropic state, and the resulting properties depended on the state of curing. Comparison of these resins to commercial BPA epoxy resins showed increased thermal stability and fracture toughness. The resins most capable of commercially replacing high performance BPA-containing epoxies are bismaleimides (BMIs) and this review discusses these resins in detail in the polyimide section below.[79]

Scheme 2.4. The synthetic route to the 1,3,4-oxadiazole containing diol precursor.[78]

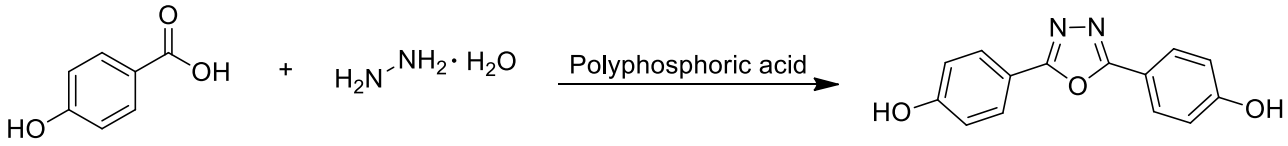

2.6 *Polyimides*

The synthesis of high molecular weight aromatic polyimides often requires two steps, first the production of a soluble poly(amic acid) intermediate and subsequent dehydration to form the polyimide.[16, 80] The insolubility and high melting temperature of aromatic polyimides cause difficulties in processing. General Electric commercialized the production of a melt processable aromatic poly(ether imide), Ultem®.[81] Ultem® is a BPA-containing polyimide with a T_g of 217 °C. **Figure 9** depicts the repeating unit. Ultem® exhibits high thermal stability, chemical resistance, toughness, transparency, and electrical stability.

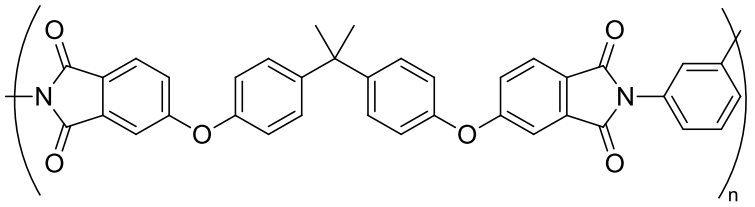

Figure 2.9. The repeating unit of BPA-containing poly(ether imide) commercially known as Ultem®.[81]

BMI resins, another class of commercially important BPA-containing polyimides, function in applications similar to epoxies.[79, 82, 83] Initially the rationale for the synthesis of BMI resins was to avoid processing issues of the commonly insoluble and thermally stable aromatic polyimides.[84] In an attempt to increase toughness of BPA-containing BMIs, Heiden et al.[85] investigated the effect of adding hyperbranched polyesters. This addition increased the fracture toughness of the resins 79 – 138 %. The higher degree of branching led to more improvement, yet a negative impact on the thermal properties resulted. As the amount of branching increased, a decrease in the T_g of 15 – 40 °C occurred. Exploring the same concept, Mather et al.[86] reported increased toughness without compromising thermal properties using hyperbranched polyimides. Despite many challenges, research focusing on the synthesis of processable polyimides still proceeds and recently novel BPA based diamine monomers proved successful.[87] Bruma and colleagues[88] synthesized a series of BPA-based poly(ether imides) with the potential application as gas separation membranes.

Finding replacements for BPA in polyimides is under investigation in many laboratories. Penczek et al.[89] replaced BPA with (*R*,*S*)-1,1-bis(4-hydroxyphenyl)-3,3,5-trimethylcyclohexane (TMC) in polyimide resins with applications in varnishes and coatings and found the polymer exhibited an increased resistance to abrasion. **Figure 10** portrays the chemical structure of TMC. The resulting polyimides, however, were insoluble in methylcyclohexanol, and a 20 °C increase in the Boëtius "melting point" relative to BPA-containing polyimides occurred. In an effort to expand the use of polyimides and make them competitive with commercial thermoplastic elastomers, Kricheldorf et al.[90, 91] synthesized BPA-free polyimide elastomers with flexible poly(ethylene oxide) (PEO) or poly(tetramethylene oxide) PTMO units. They reported good mechanical and thermal properties; however, the injection molding of these systems was not

feasible. The synthesis of liquid crystalline polyimides containing isosorbide also occurred and interesting textures resulted.[92, 93]

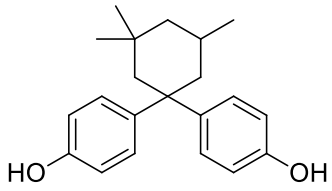

Figure 2.10. The chemical structure of TMC.[89]

The final class of BPA-free polyimides with increasing commercial importance are BMI resins. BMIs allow for a wider temperature range and better moisture stability than commercialized epoxy resins.[79] Most epoxies require the addition of BPA to afford the mechanical and thermal properties necessary. A plethora of rigid aromatic monomers are available for BMI synthesis because imides provide enhanced thermal properties, and mechanical enhancement remains a concern. A highly investigated avenue to obtain the desired properties combines both epoxies and BMIs, analogous to the use of copolymers. Similar synthesis and curing processes for both epoxies and BMIs ease the industrial translation from the production of one system to another. **Figure 11** depicts a BMI resin where R is a functional group of choice and Ar is an aromatic monomer. The chain ends of the BMI resins contain maleimide functionality for the curing process in the same manner the ends of epoxy resins exhibit epoxide functionality.[16]

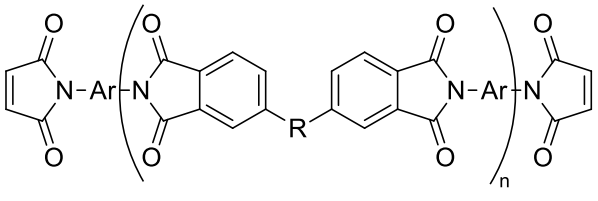

Figure 2.11. The repeating unit of a generic BMI resin.[79]

2.7 *Summary and Future Directions for Bisphenol-A Replacement*

Commercialized PCs, polyesters, epoxies, and polyimides all contain the highly debated monomer BPA.[16, 39, 61, 62, 81] In an effort to answer the ever-prevalent need for the replacement of BPA-containing polymers, an abundance of research is currently underway. Segmented block copolycarbonates, isosorbide-containing PCs, and Eastman's Tritan™ copolyester are promising replacements for BPA-containing PCs.[34, 35, 38, 46-48] Copolymerization and isosorbide incorporation proved as successful routes for improving the thermal and mechanical properties of polyesters.[56-58, 94, 95] Bismaleimide resins, 1,3,4-oxadiazole resins, and isosorbide resins are viable replacements for BPA-containing epoxies.[72, 78, 79] BPA-containing polyimides are finding replacements in TMC and, upon further development, the incorporation of flexible PEO and PTMO units.[89-91]

Isosorbide and CBDO, two highly investigated monomers, demonstrate properties similar to BPA upon incorporation into various polymers. Both BPA and CBDO impart a rigid backbone and each result in polymers which display β-transitions.[18, 20, 22, 50] Isosorbide also introduces the necessary rigidity into a polymer backbone for increased mechanical properties. Unlike BPA and CBDO, isosorbide does not contain any pendant groups and the presence of a β-transition is not characteristic of isosorbide-containing polymers. Isosorbide does, however, impart chirality which potentially introduces helical polymer chain conformations.[57, 96] Further investigation of the effect of chirality on high performance polymers would give insight into the enhanced thermal and mechanical properties achieved using isosorbide.

Copolymerization is a viable route for replacing BPA in various polymer systems because it allows for the tuning of properties based on the desired monomers and/or polymer

structure. In a similar fashion, blending various property enhancing additives into commercially produced BPA-free polymers or polymers which could easily translate into commercial production would potentially afford a facile route to replace already existing polymers. From the information obtained upon investigating CBDO and isosorbide, compounds capable of replicating the properties obtained upon BPA addition should exhibit high thermal stability, incorporate rigidity into the polymer backbone, and display β-transitions and/or incorporate chirality in the polymer backbone. Further investigations and an improved understanding of the various monomers will lead to a more concrete list of criteria for screening BPA replacements.

2.8 *Acknowledgements*

The authors would like to thank the U.S. Army Research Laboratory and the U.S. Army Research Office under the Army Materials Center of Excellence Program, contract W911NF-06-2-0014 for financial support.

2.9 *References*

1. Kunz N, Camm EJ, Somm E, Lodygensky G, Darbre S, Aubert ML, et al., *Int J Dev Neurosci* **29**:37-43 (2011).
2. Kuruto-Niwa R, Nozawa R, Miyakoshi T, Shiozawa T, Terao Y, *Environ Toxicol Pharmacol* **19**:121-30 (2005).
3. Kim Y-J, Yun H-J, Ryu J-C, *BioChip J* **5**:86-94 (2011).
4. Hengstler JG, Foth H, Gebel T, Kramer PJ, Lilienblum W, Schweinfurth H, et al., *Crit Rev Toxicol* **41**:263-91 (2011).
5. Borrell B, *Nature (London, U K)* **464**:1122-4 (2010).
6. Michael E B, *Biochemical Pharmacology* **82**:1-8 (2011).
7. Ogawa T, Ohta K, Iijima T, Suzuki T, Ohta S, Endo Y, *Bioorganic & Medicinal Chemistry* **17**:1109-17 (2009).
8. Kubwabo C, Kosarac I, Stewart B, Gauthier BR, Lalonde K, Lalonde PJ, *Food Addit Contam, Part A* **26**:928-37 (2009).
9. Kobayashi K, Miyagawa M, Wang R-S, Sekiguchi S, Suda M, Honma T, *Ind Health* **40**:375-81 (2002).
10. Grause G, Tsukada N, Hall WJ, Kameda T, Williams PT, Yoshioka T, *Polym J* **42**:438-42 (2010).
11. Bair HE, Falcone DR, Hellman MY, Johnson GE, Kelleher PG, *J Appl Polym Sci* **26**:1777-86 (1981).
12. Vandenberg LN, Chahoud I, Padmanabhan V, Paumgartten FJR, Schoenfelder G, *Environ Health Perspect* **118**:1051-4 (2010).
13. Pritchett JJ, Kuester RK, Sipes IG, *Drug Metabolism and Disposition* **30**:1180-5 (2002).
14. Völkel W, Colnot T, Csanády GA, Filser JG, Dekant W, *Chemical Research in Toxicology* **15**:1281-7 (2002).
15. Tsai W-T, *J Environ Sci Health, Part C: Environ Carcinog Ecotoxicol Rev* **24**:225-55 (2006).
16. Odian G, Principles of Polymerization, Fourth Edition, John Wiley & Sons, Inc., Hoboken, NJ, (2004).
17. Ueda M, *Polym Eng Sci* **44**:1877-84 (2004).
18. Nielsen LE, Mechanical Properties of Polymers, Reinhold Publishing Corporation, US, (1962).
19. Crompton TR. Polymer Reference Book. Smithers Rapra Technology; 2006.
20. Locati G, Tobolsky AV, *Advances in Molecular Relaxation Processes* **1**:375-408 (1970).
21. Poliks MD, Gullion T, Schaefer J, *Macromolecules* **23**:2678-81 (1990).
22. Mercier JP, Aklonis JJ, Litt M, Tobolsky AV, *Journal of Applied Polymer Science* **9**:447-59 (1965).
23. Koning C, Wildeson J, Parton R, Plum B, Steeman P, Darensbourg DJ, *Polymer* **42**:3995-4004 (2001).
24. Jones AA, *Macromolecules* **18**:902-6 (1985).
25. Allen G, Bevington JC, Comprehensive polymer science : the synthesis, characterization, reactions & applications of polymers, Pergamon Press, Oxford, England; New York, (1989).

26. Agnès R, *Polymer Degradation and Stability* **49**:163-79 (1995).
27. Mason JP, Newcome JM, Tennant JM, Compositions Having Low Birefringence. United States 08/640,300 (2001).
28. Jackson WJ, Caldwell JR, *Journal of Applied Polymer Science* **11**:211-26 (1967).
29. Jackson WJ, Caldwell JR, *Journal of Applied Polymer Science* **11**:227-44 (1967).
30. Kricheldorf HR, Schwarz G, Bohme S, Schultz C-L, *J Polym Sci, Part A: Polym Chem* **41**:890-904 (2003).
31. Brunelle DJ, Shannon TG, *Macromolecules* **24**:3035-44 (1991).
32. Feng X, East AJ, Hammond WB, Zhang Y, Jaffe M, *Polymers for Advanced Technologies* **22**:139-50 (2011).
33. Chatti S, Schwarz G, Kricheldorf HR, *Macromolecules* **39**:9064-70 (2006).
34. Kricheldorf HR, Sun S-J, Gerken A, Chang T-C, *Macromolecules* **29**:8077-82 (1996).
35. Sun S-J, Schwarz G, Kricheldorf HR, Chang T-C, *J Polym Sci, Part A: Polym Chem* **37**:1125-33 (1999).
36. Acar AE, Brunelle Daniel J. Synthesis and Physical Properties of Tetramethylcyclobutanediol Polycarbonates. Advances in Polycarbonates: American Chemical Society; 2005. p. 216-28.
37. Baltá-Calleja FJ, Roslaniec Z, Block copolymers, Marcel Dekker, New York, (2000).
38. Memon NA, Williams HL, *Journal of Applied Polymer Science* **17**:1361-76 (1973).
39. Schweitzer PA, Corrosion engineering handbook. Corrosion of polymers and elastomers, CRC Press, Boca Raton, (2007).
40. G B, *Polymer* **15**:527-35 (1974).
41. Bristow JF, Kalika DS, *Macromolecules* **27**:1808-13 (1994).
42. More AS, Naik PV, Kumbhar KP, Wadgaonkar PP, *Polym Int* **59**:1408-14 (2010).
43. Asundaria ST, Patel PR, Patel KC, *Int J Polym Mater* **58**:692-705 (2009).
44. Waghmare PB, Idage SB, Menon SK, Idage BB, *J Appl Polym Sci* **100**:3222-8 (2006).
45. Chen Y, Yang Y, Su J, Tan L, Wang Y, *Reactive and Functional Polymers* **67**:396-407 (2007).
46. Issues for Debate in Environmental Management: Selections from CQ Researcher, SAGE Publications, Inc., Thousand Oaks, (2010).
47. Davies J, Sullivan DG, Drink Containers. United States 12/357,114 (2010).
48. Malotky DL, Kainz B, Diehl CF, Lindenmuth D, Young TJ, Argyropoulos JN, Coating Compositions and Articles Made Therefrom. United States 13/039,145 (2011).
49. Crawford ED, McWilliams DS, Porter DS, Connell GW, Film(s) and/or Sheet(s) Made From Polyester Compositions Containing Cyclobutanediol and Articles Made Therefrom. United States 0270569 A1 (2007).
50. Geiger CC, Davies JD, Daly WH, *Journal of Polymer Science Part A: Polymer Chemistry* **33**:2317-27 (1995).
51. Shirrell CD, Williams DE, *Acta Crystallogr, Sect B* **B32**:1867-70 (1976).
52. Sulatha MS, Purushotham S, Natarajan U, *Polymer* **43**:6295-305 (2002).
53. Kelsey DR, Scardino BM, Grebowicz JS, Chuah HH, *Macromolecules* **33**:5810-8 (2000).
54. Hoppens NC, Hudnall TW, Foster A, Booth CJ, *J Polym Sci, Part A: Polym Chem* **42**:3473-8 (2004).
55. Booth CJ, Kindinger M, McKenzie HR, Handcock J, Bray AV, Beall GW, *Polymer* **47**:6398-405 (2006).

56. Khanarian G, Charbonneau LF, Witteler HB, Polyesters Including Isosorbide as a Comonomer Blended with Other Thermoplastic Polymers. United States 6,359,070 B1 (2002).
57. Kricheldorf HR, Behnken G, Sell M, *Journal of Macromolecular Science, Part A* **44**:679-84 (2007).
58. Kricheldorf HR, Wulff DF, *Polymer* **39**:6145-51 (1998).
59. Lin Q, Pasatta J, Long TE, *Journal of Polymer Science Part A: Polymer Chemistry* **41**:2512-20 (2003).
60. Liu C, Liu F, Cai J, Xie W, Long TE, Turner SR, et al., *Biomacromolecules* **12**:3291-8 (2011).
61. Dearborn EC, Fuoss RM, MacKenzie AK, Shepherd RG, *Industrial & Engineering Chemistry* **45**:2715-21 (1953).
62. Ellis B, Chemistry and technology of epoxy resins, Blackie Academic & Professional, London; New York, (1993).
63. Ritter SK. Debating BPA's Toxicity. Chemical & Engineering News. 2011 June 6, 2011.
64. Park S-J, Jin F-L, Shin J-S, *Materials Science and Engineering: A* **390**:240-5 (2005).
65. Enns JB, Gillham JK, *Journal of Applied Polymer Science* **28**:2831-46 (1983).
66. Unnikrishnan KP, Thachil ET, *International Journal of Polymeric Materials* **55**:323-38 (2006).
67. Czub P, *Polym Adv Technol* **20**:194-208 (2009).
68. Czub P, *Polym Adv Technol* **20**:183-93 (2009).
69. Das G, Karak N, *J Appl Polym Sci* **118**:128-34 (2010).
70. Motawie AM, Sherif MH, Badr MM, Amer AA, Shehat AS, *Aust J Basic Appl Sci* **4**:1376-82 (2010).
71. East A, Jaffe M, Zhang Y, Catalani LH, New Jersey Institute of Technology, USA . Thermoset epoxy polymers from renewable resources. United States Patent 0009599A1 (2008).
72. Łukaszczyk J, Janicki B, Kaczmarek M, *European Polymer Journal* **47**:1601-6 (2011).
73. Grubbs RB, Dean JM, Broz ME, Bates FS, *Macromolecules* **33**:9522-34 (2000).
74. Dean JM, Lipic PM, Grubbs RB, Cook RF, Bates FS, *Journal of Polymer Science Part B: Polymer Physics* **39**:2996-3010 (2001).
75. Dean JM, Grubbs RB, Saad W, Cook RF, Bates FS, *Journal of Polymer Science Part B: Polymer Physics* **41**:2444-56 (2003).
76. Guo Q, Dean JM, Grubbs RB, Bates FS, *Journal of Polymer Science Part B: Polymer Physics* **41**:1994-2003 (2003).
77. Hsuan Lin C, Chung Chiang J, Shan Wang C, *Journal of Applied Polymer Science* **88**:2607-13 (2003).
78. Balamurugan R, Kannan P, *High Performance Polymers* **21**:251-64 (2009).
79. Chandra R, Rajabi L, *Journal of Macromolecular Science, Part C: Polymer Reviews* **37**:61-96 (1997).
80. C.E S, *Progress in Polymer Science* **16**:561-694 (1991).
81. ULTEM(R) PEI Resin Product Guide. In: Thermoplastics GE, editor. Pittsfield2003.
82. Gaina V, Gaina C, *Polym-Plast Technol Eng* **48**:525-9 (2009).
83. Bhuvana S, Devi MS, *Polym Compos* **28**:372-80 (2007).
84. Gaina C, Gaina V, *e-Polym* No pp. given (2008).

85. Gopala A, Wu H, Xu J, Heiden P, *Journal of Applied Polymer Science* **71**:1809-17 (1999).
86. Qin H, Mather PT, Baek J-B, Tan L-S, *Polymer* **47**:2813-21 (2006).
87. Thiruvasagam P, Venkatesan D, *High Perform Polym* **22**:682-93 (2010).
88. Bruma M, Hamciuc E, Yampolskii YP, Alentiev AY, Ronova IA, Rojkov EM, *Mol Cryst Liq Cryst* **418**:11-9 (2004).
89. Wardzinska E, Penczek P, *J Appl Polym Sci* **100**:4066-73 (2006).
90. Kricheldorf H, Wollheim T, Altstadt V, Koning C, Buning G, *Journal of Macromolecular Science: Pure & Applied Chemistry* **38**:451 (2001).
91. Wollheim T, Kricheldorf HR, Altstädt V, Koning CE, Buning GHW, *High Performance Polymers* **13**:119-32 (2001).
92. Kricheldorf HR, Probst N, *Macromolecular Rapid Communications* **16**:231-7 (1995).
93. Kricheldorf HR, Probst N, Gurau M, Berghahn M, *Macromolecules* **28**:6565-70 (1995).
94. Jansen MAG, Goossens JGP, De WG, Bailly C, Koning CE, *Anal Chim Acta* **557**:19-30 (2006).
95. Jansen MAG, Wu LH, Goossens JGP, De WG, Bailly C, Koning CE, *J Polym Sci, Part A: Polym Chem* **45**:882-99 (2007).
96. Chirackal VE, Sreekumar K, *J Mater Sci* **45**:1912-20 (2010).

Chapter 3: Stilbene-Containing Thermotropic Liquid Crystalline (Co)polyesters for Electronic and Aerospace Applications

(Updated/adapted from a 2012 Invention Disclosure at Virginia Tech (VTIP) and 2013 Virginia Space Grant Consortium Graduate Research Fellowship Final Paper)

Ashley M. Nelson and Timothy E. Long

Department of Chemistry, Macromolecules and Interfaces Institute
Virginia Tech, Blacksburg, VA 24061-0212

3.1 *Abstract*

Materials used in both electronic applications and space travel must maintain thermal and dimensional stability in extreme conditions, while remaining melt processable for ease of industrial production. The rigid chemical structure of stilbene often correlates to polymers exhibiting a liquid crystalline morphology and the olefin bond undergoes a [2 + 2] cycloaddition in the presence of ultraviolet (UV) light. Based on the combined benefits of a non-destructive photocrosslinking reaction and liquid crystallinity, we propose the use of stilbene-containing (co)polyesters for various electronic and aerospace applications. The synthesis and characterization of (co)polyesters consisting of 4,4'-dimethyl-*trans*-stilbene dicarboxylate (SDE), 1,6-hexanediol (HD), and 1,4-butanediol (BD) was performed. These (co)polyesters demonstrated thermal stability of greater than 360 °C and liquid crystalline morphologies, with melting temperatures ranging from 196 – 253 °C. Dynamic mechanical analysis afforded moduli ~1000 MPa and tensile data resulted in a Young's modulus of the same magnitude. Additionally, melt rheology elucidated the characteristic shear thinning expected of liquid crystalline polyesters. Polymerization with longer alkyl spacers investigated the effect of comonomer

composition on the thermal transitions and liquid crystallinity. Further testing includes UV and heat aging studies to ascertain the effect of an aliphatic comonomer to successfully eliminate the potential phenolic degradation and confirm the ability of these (co)polyesters to function in thermally taxing UV light conditions.

3.2 *Introduction*

Thermotropic liquid crystalline polyesters are a unique class of high performance polymers that exhibit order during melt processing above the crystalline melting point.[1] Mesogenic units, extended aromatic sequences, within the main chain promote the formation of this ordered morphology, often resulting in anisotropic, high modulus structures. These mesogenic units are typically either present in the backbone of the polymer or as pendant groups resulting in main-chain and side-chain liquid crystalline polymers respectively. Liquid crystalline polymers demonstrate outstanding dimensional stability at high temperatures, resistance to chemicals and corrosion, exhibit low dielectric constants, and high moduli over a wide temperature window.[2] Liquid crystalline polymers also exhibit shear thinning during melt processing, which facilitates melt extrusion and injection molding for product formation.[3] Based on these synergistic attributes, liquid crystalline polymers offer versatility for aerospace coatings, electronic materials, adhesives, and composites.

The ongoing sophistication of light-emitting diode (LED) technology is drastically increasing commercial appeal.[4] The broad array of applications, ranging in wavelength and power, require proper polymer encasings to ensure both productivity and safety. Exposure to ultraviolet (UV) light often results in polymer degradation and/or poor coloring due to side reactions, such as the photo-Fries rearrangement.[5,6] **Figure 1** depicts the photochemical-induced

photo-Fries rearrangement on the commercially produced liquid crystalline polyester, Xydar.[6] The phenol generated contributes to yellowing and the ketone formation kinks the rigid chain, disrupting the anisotropy.[7,8] Although this reaction does not physically degrade the polyester, it sacrifices the desired properties and functions. A limited number of commercial polymers exist which possess the necessary thermal, thermomechanical, and UV stability to overcome the environmental factors both the LED and aerospace industries require.

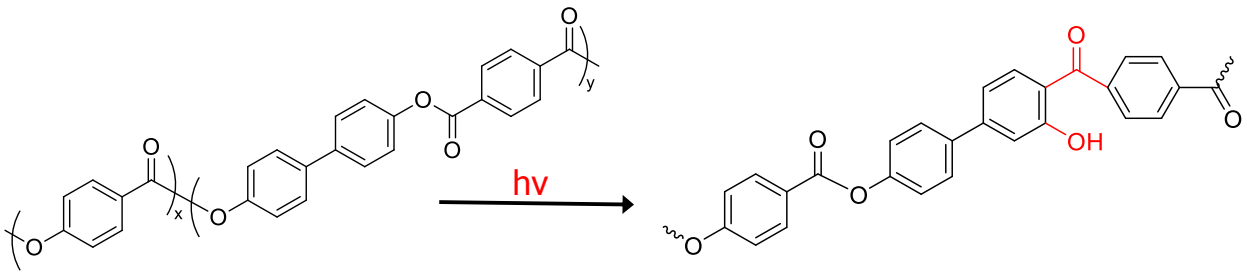

Figure 3.1. UV-induced photo-Fries rearrangement

Previous literature indicates that the incorporation of stilbene units into the polymer backbone results in liquid crystalline polymers, classifying stilbenes as mesogens.[9,10] Recently, Ravikrishnan et al.[11] synthesized poly(4,4'-stilbeneoxy) alkylarylphosphates, characterizing their liquid crystalline morphology and additional benefits such as flame resistance. Polarized optical microscopy (POM) allowed visual determination of the liquid crystalline nematic texture. In the 1980's, Eastman Kodak company obtained multiple patents on the (co)polymerization of 4,4'-dimethyl-*trans*-stilbene dicarboxylate (SDE) with aliphatic diols, including some of the aliphatic spacers of interest for these applications.[12-14] The well-established industrial synthesis provides an excellent basis for exploring these (co)polyesters for widespread applications.

Stilbenes are also known to undergo a [2 + 2] cycloaddition reaction in the presence of UV light.[11,15,16] This photo-induced crosslinking reaction forms a cyclobutane ring with two stilbene alkenes, a non-degradative process with the ability to provide enhanced

thermomechanical properties.[17] Copolyesters of 1.4-cyclohexanedimethanol, 1,4-cyclohexane dicarboxylate, and SDE efficiently crosslinked upon exposure to UV light.[15] Thermomechanical analysis exhibited tunable high temperature plateau moduli based on UV exposure, increased storage modulus with increasing UV. Somlai et al.[16] also demonstrated the photocrosslinking ability of stilbene-containing homopolymers through excitation of extremely thin films (ca. 50 – 100 nm achieved via spin coating), however, at long irradiation times stilbene degradation occurred. Although a slight concern and something to acknowledge, the suggested applications require non-transparent, and therefore, thicker films or polymer encasings/materials. With the highly crystalline visible-light scattering properties of these polyesters, the light should not penetrate all the way through the material, but solely crosslink on the surface.[9,18] If a surface degradation occurs as suggested above, the polymer layer underneath could then crosslink pending light penetration and alignment of the stilbene functional groups avoiding total material deformation/destruction. This beneficial crosslinking reaction utilizes the often degradative UV conditions to improve the material instead of causing deleterious effects as discussed above.

In the following, we describe the synthesis and characterization of high-performance photocrosslinkable liquid crystalline (co)polyesters containing stilbene for use in the harsh environments of both electronic and aerospace applications. Melt transesterification afforded a series of (co)polyesters containing varying ratios of 1,6-hexanediol (HD), and 1,4-butanediol (BD) aliphatic spacers copolymerized with SDE. Utilizing commercially available comonomers allowed for obtaining a wide-range of properties providing tailorable materials for application- or product-specified conditions. All copolyesters exhibited a liquid crystalline morphology and thermal, thermomechanical, and rheological characterization explored the effect of structure on the resulting polyester properties.

3.3 *Experimental*

3.3.1 Materials

1,6-Hexanediol (97%), 1,4-butanediol (99%), 1,5-pentanediol (97%), and 1,8-octanediol (98%), and 1,10-decanediol (98%) were obtained from Sigma Aldrich and used as received. 4,4'-Dimethyl-*trans*-stilbene dicarboxylate was generously supplied from Eastman Chemical Company and used as received. Titanium tetraisopropoxide ($Ti(OiPr)_4$) catalyst solution (0.01 g/mL in 1-butanol) was prepared according to previous literature.[19]

3.3.2 Analytical Methods

^1H NMR spectroscopy was obtained using a 400 MHz Varian Tecmag Apollo in a solvent mixture of pentafluorophenol and $CDCl_3$ at ambient temperature. A TA Instruments Hi-Res thermogravimetric analyzer (TGA) 2950 or Q500 provided polymer thermal weight loss in a N_2 atmosphere and a temperature ramp of 10 °C/min from 25 to 600 °C. Differential scanning calorimetry (DSC) was performed using a TA Instruments Q1000 or Q2000 heat/cool/heat method with a heating ramp of 10 °C/min and a cooling rate of 100 °C/min. Melt rheological studies were performed on a TA Instruments AR2000 rheometer using 25 mm parallel plate geometry. A strain sweep determined the linear viscoelastic regime and the experimental temperature range was sample dependent. Compression molding at 275 - 315 °C between Teflon® sheets produced free-standing polymer films ~0.3 mm thick. Dynamic mechanical analysis (TA Instruments Q800 DMA) provided thermomechanical properties of the polymer films under tension mode at a frequency of 1 Hz and a temperature ramp of 3 °C/min from 0 °C until the storage modulus reached less than 0.1 MPa. Tensile testing was performed on the

polymer films using an Instron 4411 with a crosshead speed of 0.5 mm/min. The tensile properties are represented as an average of five samples.

3.3.3 Polymer Synthesis

All polymers were synthesized using melt transesterification in a similar manner. The reaction setup consisted of a round-bottomed flask equipped with a mechanical stirrer, N_2 inlet, and distillation apparatus. The following procedure describes the synthesis of poly(4,4'-dimethyl-*trans*-stilbene dicarboxylate (SDE)-1,6-hexanediol (HD)). A dry 100 mL round bottom was charged with 8.4461 g (28.50 mmol) of SDE, 4.0401 g (34.19 mmol) of HD, and ~0.05 mL (40 ppm) titanium tetraisopropoxide. The reaction was purged with N_2 and degassed three times. The reaction, with a constant N_2 purge and stirring, was heated to 190 °C for 2 h. The temperature was then increased to 220 °C for 2 h and finally to 275 °C for 0.5 h. Vacuum was subsequently applied at 275 °C for 2 h. Isolation of the polymer occurred via breaking the round-bottomed flask and removing the solid polymer. To solid-state (SS) the polyester, small pieces of the polymer were placed in an identical setup as described above and heated to 130 °C with stirring and constant N_2 purge for about 25 h.

3.4 *Results and Discussion*

3.4.1 Molecular Weight Characterization and Solid-Stating Strategies

Polymerization proceeded using a melt transesterification strategy, an industrially relevant technique that eliminates solvent and allows direct isolation of the polyesters.[20,21] Both attributes of melt transesterification are critical principles of strategies for emerging green chemistry.[22] **Scheme 1** depicts the synthesis of a random copolyester containing SDE, HD, and

1,4-butanediol (BD). Varying monomer charge ratios provided a range of copolyesters enabling the exploration of structure-property-morphology relationships. As previously reported, the highly crystalline nature from the rigid, regular structure, resulted in limited solubility.[9,13,23] ^{1}H NMR performed in a mixture of pentafluorophenol and deuterated chloroform ($CDCl_3$) provided structural characterization. **Figure 2** displays the ^{1}H NMR spectra of poly(SDE-HD). All peaks are labeled accordingly and integrated as expected. The **d** peak exhibited a slightly larger value than the expected integration of 4 and is attributed to overlapping with the pentaflurophenol solvent peak. Mechanical strength and integrity often scale with molecular weight until a maximum or plateau occurs at high molecular weight.[24] This relationship allows a quantitative determination of molecular weight through the ability to obtain free-standing films.[25-27] Compression molding qualitatively showed melt transesterification produced polyesters of substantial molecular weight as insolubility in safe organic solvents impeded the use of size exclusion chromatography (SEC) for molecular weight characterization. Free-standing films formed with some compositions and mechanical testing ensued. Increasing BD concentration resulted in brittle films due to the melting temperatures of the SDE-BD segments being above the highest temperature reached during the polymerization. Intuitively, the success of melt transesterification depends on the polymer remaining in the melt and good mixing, therefore, when the melting temperature is above the final temperature reached in polymerization, high molecular weight is not always achieved.

Scheme 3.1. Synthesis of poly(SDE-HD)$_x$-*co*-poly(SDE-BD)$_y$ using melt transesterification

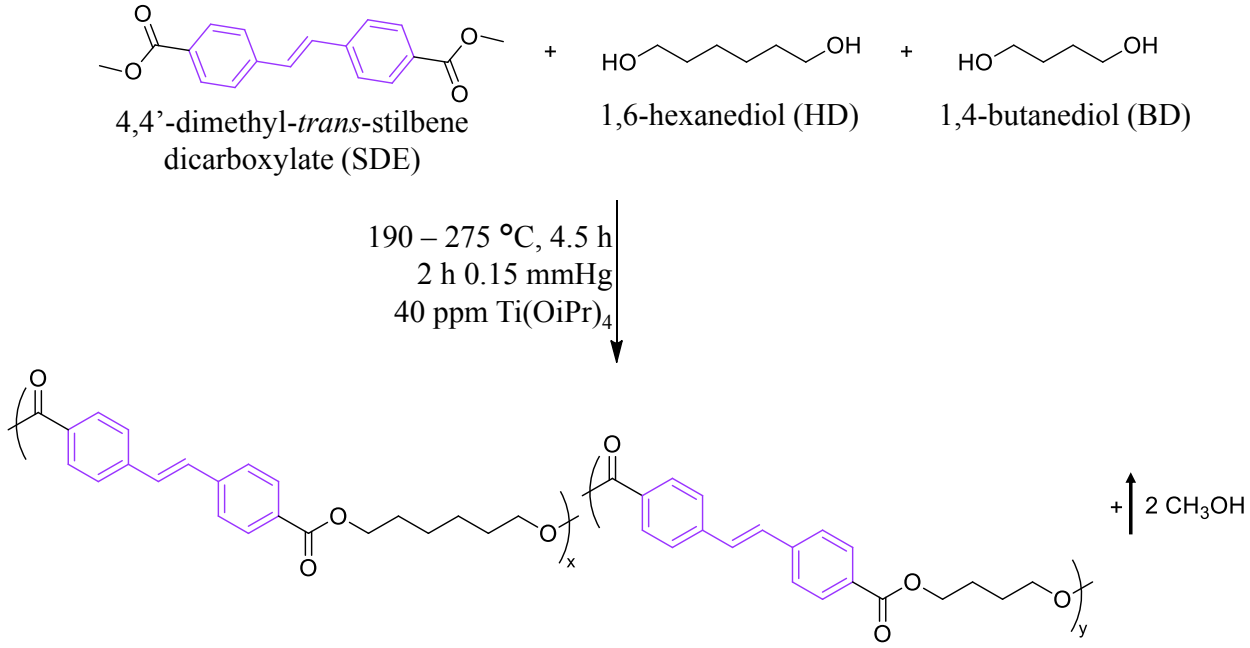

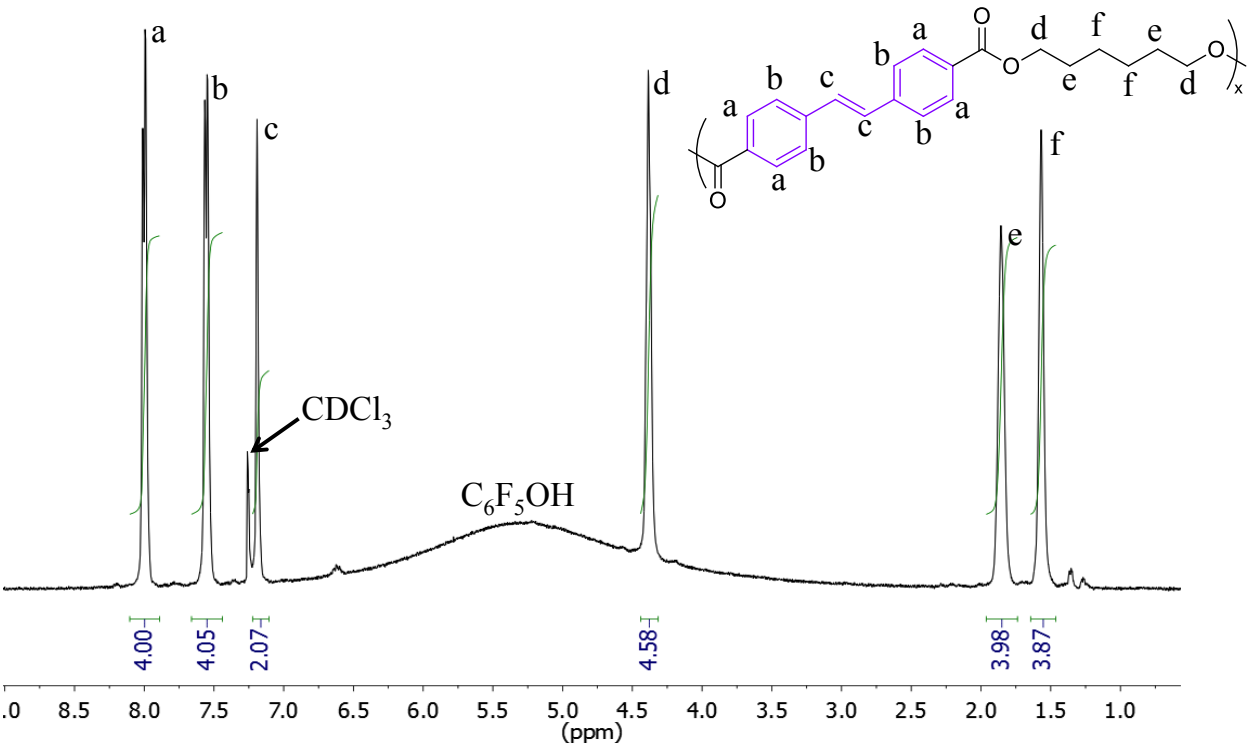

Figure 3.2. ^{1}H NMR confirms structure of poly(SDE-HD)

To overcome the aforementioned downfall when preparing high melting polymers, strategies such as solid-state polymerization (SSP) often follow.[14,28,29] In SSP, polymers are ground into small uniform particles, placed into a setup identical or similar to the reaction setup, and held at a temperature above the glass transition temperature (T_g) but below the melting temperature (T_m). The particles are then stirred and either wicked with N_2 or held under reduced pressure for an extended period of time. **Figure 3** shows the complex viscosity of poly(SDE-HD) before and after SSP. Zero-shear viscosity scales with molecular weight, thus providing a relative comparison of molecular weight between samples.[30,31] Similarly, comparison of the complex viscosity ($|\eta^*|$) obtained from frequency sweeps at the same low frequency of 0.1 Hz and temperature (263 °C) offered an indication of SSP success via relative molecular weight improvement. Before SS poly(SDE-HD) exhibited a complex viscosity of 12030 Pa·s at 0.1 Hz and after the value more than doubled to 25930 Pa·s, suggesting an increase in molecular weight upon SSP. It is important to note the SSP procedure used for this example did not provide uniform particle sizes, yet successfully demonstrated the capability to further enhance the molecular weight of these polyesters despite high T_m's.

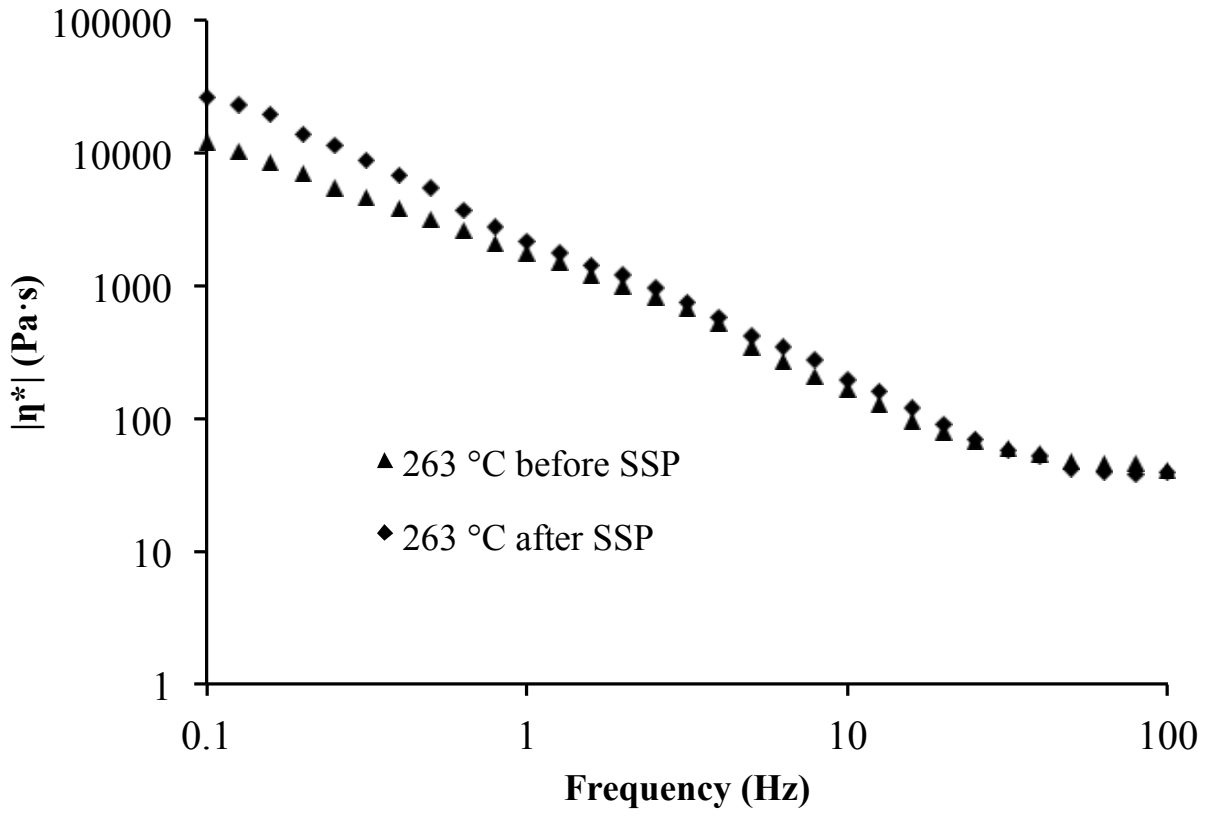

Figure 3.3. Complex viscosity of poly(SDE-HD) obtained at 263 °C before and after SSP

3.4.2 Thermal Characterization and Liquid Crystallinity

Understanding the thermal limitations of these (co)polymers is of utmost importance because the desired applications require diverse and potentially extreme temperatures. The TGA curve for poly(SDE-HD), seen in **Figure 4**, depicts a one-step degradation profile with an onset of weight loss at 384 °C. Copolyesters charged with 10, 25, 50, 75, 90, and 100 mol % BD also exhibited one-step degradations and thermal stability of greater than 360 °C. DSC determined the effect of (co)polymer composition on the thermal transitions. **Figure 5** depicts the DSC trace of poly(SDE-HD), which exhibited a T_m of 253 °C and an isotropic temperature (T_i) of 284 °C. As the incorporation of BD increased, the T_m depressed until the BD incorporation was greater

than HD, resulting in higher T_m's and T_i's than the HD-rich analogs. Some compositions also displayed a crystallization temperature (T_c). The lower T_m, while maintaining similar T_is, correlated to an increased mesophase stability ultimately lowering the required temperature for melt processing. **Table 1** summarizes the thermal transitions for the various (co)polyesters.

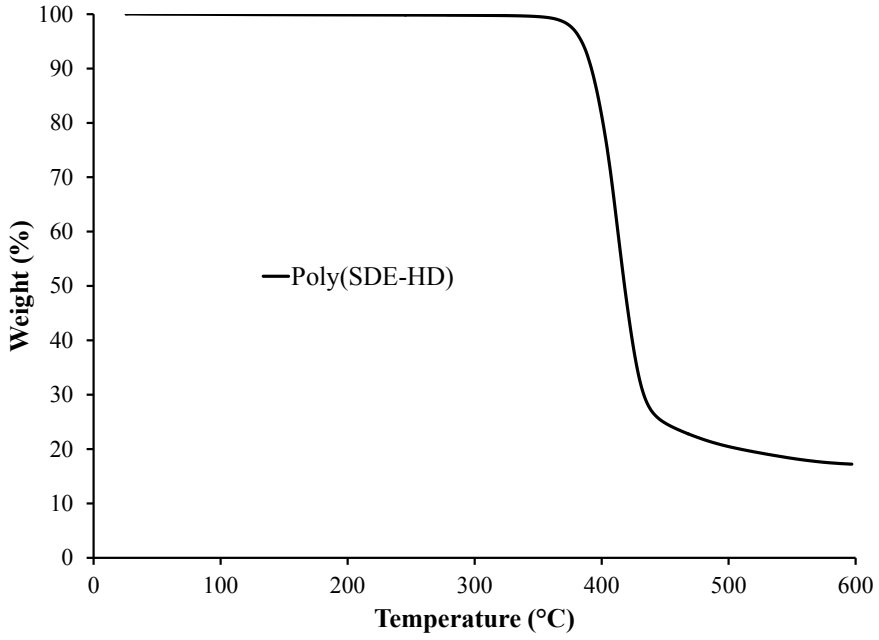

Figure 3.4. Thermal degradation profile of poly(SDE-HD)

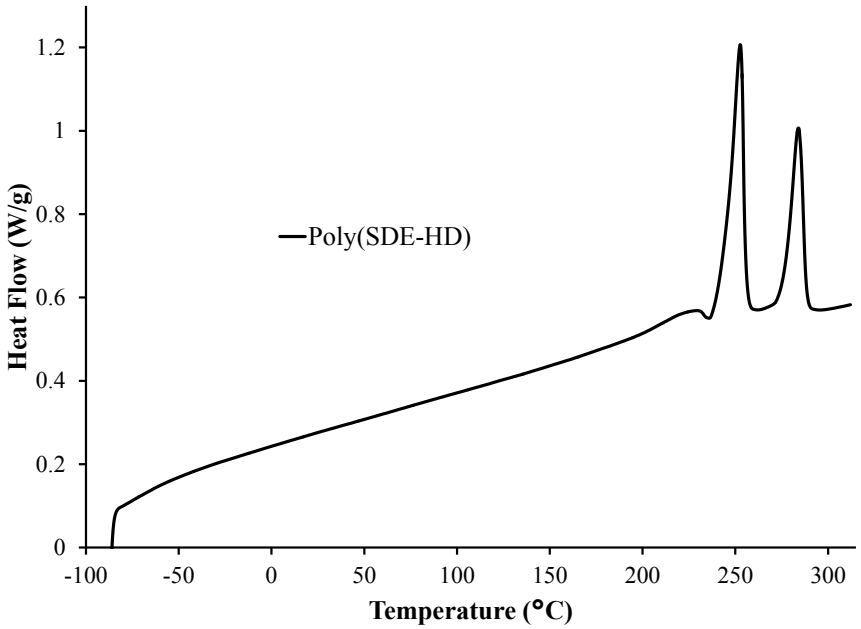

Figure 3.5. DSC trace of poly(SDE-HD) exhibiting both a melting and isotropic transition

Table 3.1. Thermal transitions of various stilbene-containing (co)polyesters. N.D. = not detected

Mol % HD	$T_{d,onset}$ (°C)	T_c (°C)	T_m (°C)	T_i (°C)
100	384	N.D	253	284
90	364	213	237	286
75	405	189	218	285
50	377	N.D	196	292
25	395	248	265	323
10	400	N.D	276	328
0	396	N.D	317	346

To further investigate the effect of the alkyl spacer length on the thermal transitions and liquid crystallinity, melt transesterification of SDE with 1,5-pentanediol (PD), 1,8-octanediol (OD), and 1,10-decanediol (DD) generated polyesters containing an odd diol (PD) and longer methylene spacers (OD and DD). As previously noted, poly(SDE-BD) showed an increased T_m and T_i compared to poly(SDE-HD). **Figure 6** shows the thermal transitions of SDE homopolymers containing PD, OD, and DD. Poly(SDE-PD) exhibited a lower T_m and T_i than both the BD and HD homopolymers. This is attributed to decreased crystallization and packing because of the odd spacer length.[32] Both poly(SDE-OD) and poly(SDE-DD) displayed solely T_ms in the heating curves, implying a lack of a liquid crystalline morphology. **Figure 6** displayed a common trend, the even-odd effect or stair-step relationship, between even and odd spacers in liquid crystalline polymers.[1,33] The shorter spacer, BD in this particular case, exhibited the highest T_m and T_i of 317 °C and 346°C, respectively. Upon changing the diol to a PD odd spacer evidence of both a T_m and T_i confirmed liquid crystallinity, however, the T_m (190 °C) and T_i (263 °C) severely decreased in comparison to the BD-analog. Despite the longer spacer of poly(SDE-HD), the T_m and T_i increased compared to poly(SDE-PD) since the symmetry and regularity of an even number of methylene units pack together more efficiently than an odd number. It is interesting to note even the long methylene spacers of poly(SDE-OD) and poly(SDE-DD) maintained higher T_m's than poly(SDE-PD), again highlighting the drastic effect of even-odd spacing on crystallization and ultimately thermal transitions.

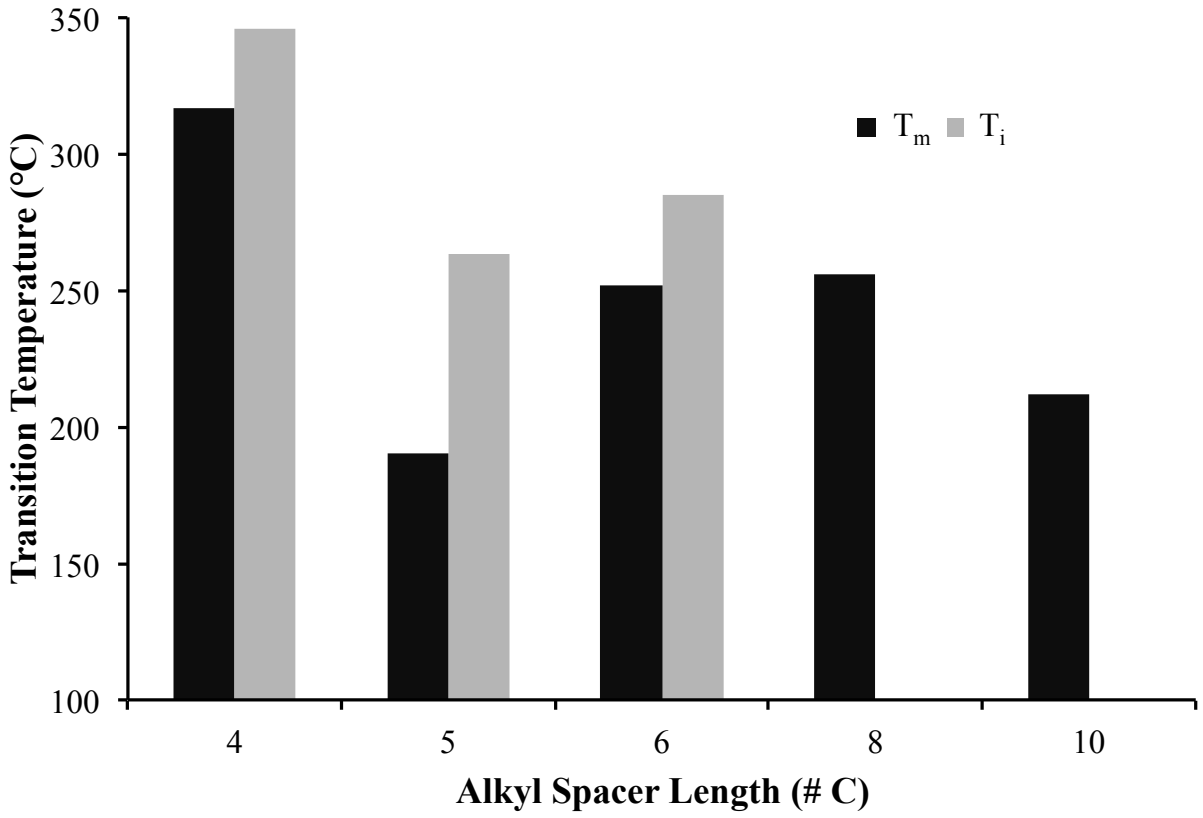

Figure 3.6. The effect of alkyl spacer length on the thermal transitions and liquid crystallinity of SDE-containing polyesters

3.4.3 Thermomechanical, Tensile, and Rheological Characterization

Dynamic mechanical analysis (DMA) afforded the moduli of the polyesters as a function of temperature. **Figure 7** displays the DMA and tan delta curves of poly(SDE-HD) and poly(SDE-HD)$_{90}$-*co*-poly(SDE-BD)$_{10}$. The polyesters both exhibited a small modulus drop at ~70 °C and maintained a glassy moduli until the onset of flow, 242 °C and 228 °C, for the homopolymer and copolymer respectively. The dimensional stability achieved over the wide temperature range is promising for these polyesters to function as protective coatings and encasings in the weatherable conditions of space travel.

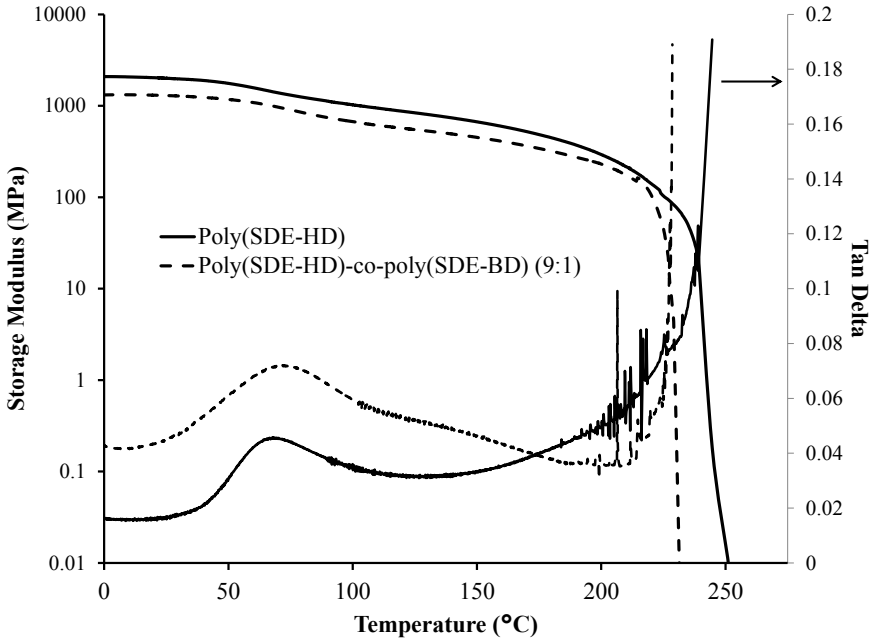

Figure 3.7. DMA and tan delta curves for poly(SDE-HD) (solid line) and poly(SDE-HD)$_{90}$-*co*-poly(SDE-BD)$_{10}$ (dotted line)

Tensile testing yielded another measure of polymer stiffness, the Young's modulus. **Table 2** contains the tensile data for poly(SDE-HD), which exhibited a Young's modulus of 890 ± 150 MPa, a stress at break of 30 ± 8 MPa, and a strain at break of 4 ± 2 %. Solvay's commercially produced liquid crystalline polymer Xydar® G-930 exhibits a tensile modulus of 15900 MPa, a tensile strength of 135 MPa and a tensile elongation at break of 1.6 % according to the technical data sheet.[34] Many factors affect tensile properties such as film/material preparation and history, molecular weight, and the test parameters. Additionally, an abundance of variations exist between commercial products and lab-synthesized polymers. Two particularly important parameters for mechanical testing include the difference in synthesis and processing optimization and standardized testing. These differences could contribute to the lower Young's modulus and stress at break of poly(SDE-HD).

Table 3.2. Tensile data obtained for poly(SDE-HD)

Mol % HD	Avg. Stress at Break (MPa)	Avg. Strain at Break (%)	Avg. Young's Modulus (MPa)
100	30 ± 8	4 ± 2	890 ± 150

Shear thinning, a characteristic rheological property of liquid crystalline polyesters, is an important measure to establish for predicting melt processability.[3] Shear thinning materials achieve lower viscosities as a function of shear rate, with liquid crystalline polymers often thinning at both low and high shear rates, which enables the production of smaller parts and also decreases the processing temperature these materials possessing characteristically high T_m's. Melt rheology afforded the flow properties of poly(SDE-HD). **Figure 8** depicts a frequency sweep of poly(SDE-HD) performed at various temperatures in the mesophase. The negative slope of the complex viscosity curve as a function of angular frequency, a dynamic shear experiment, illustrated the expected shear thinning of this liquid crystalline polyester.

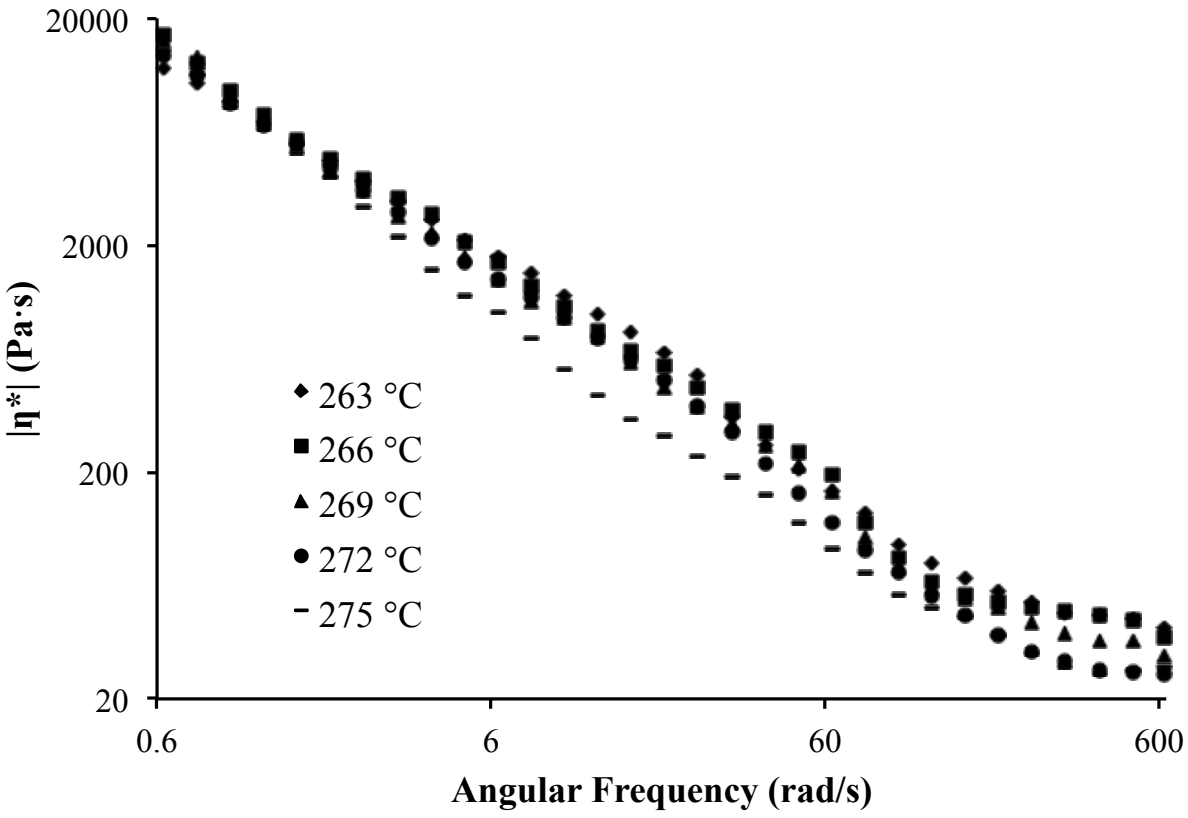

Figure 3.8. Melt rheology of poly(SDE-HD) elucidating shear thinning

3.5 *Conclusions*

We investigated (co)polyesters comprised of 4,4'-dimethyl-*trans*-stilbene dicarboxylate (SDE), 1,6-hexanediol (HD), and 1,4-butanediol (BD) for use in electronic and aerospace applications. ^{1}H NMR provided structural confirmation and the ability to melt press films quantitatively indicated melt transesterification afforded high molecular weight polyesters. Complex viscosity comparisons between a pre- and post-SSP polymer confirmed SSP as a successful route for increasing molecular weight. The series of stilbene-containing (co)polyesters demonstrated thermal stability of greater than 360 °C and liquid crystalline morphologies, with T_m's ranging from 196 °C – 253 °C. Dynamic mechanical analysis afforded

moduli ~1000 MPa and tensile testing resulted in a Young's modulus of a similar magnitude. Melt rheology elucidated the characteristic shear thinning expected of liquid crystalline polyesters. An investigation of alkyl spacer length and composition reinforced the importance of regularity and limited flexibility necessary to maintain a distinct liquid crystalline morphology. The library of compositions and material properties from the various characterization techniques provided structure-property-morphology relationships for future implementation to target specific parameters for an application. Further studies include UV heat and aging of these partially aromatic photocrosslinkable (co)polyesters alongside current commercial standards in the electronic and aerospace industries to test the hypothesis of enhanced stability in UV-rich and thermally diverse settings.

3.6 *Acknowledgements*

This material is based upon work supported in part by the U.S. Army Research Laboratory and the U.S. Army Research Office under the Army Materials Center of Excellence Program, contract W911NF-06-2-0014 and the Virginia Space Grant Consortium. The authors would like to thank Solvay for unrestricted financial support and Eastman Chemical Company for providing the SDE monomer. A special thanks to Maria Bertucci and Richard Carmean for relevant yet unreported data due to confidentiality.

3.7 *References*

(1) Donald, A.; Windle, A.; Hanna, S. *Liquid Crystalline Polymers*; 2nd ed.; Cambridge University Press, 2006.
(2) Economy, J.; Goranov, K. *Adv. Polym. Sci.* **1994**, *117*, 221.
(3) Ciferri, A. *Liquid Crystallinity in Polymers: Principles and Fundamental Properties*, 1991.
(4) Mottier, P. *LEDs for lighting applications*; John Wiley & Sons, 2009.
(5) Rusu, E.; Comanita, E.; Onciu, M. *Roum. Chem. Q. Rev.* **2000**, *7*, 241.
(6) Belluč, D.; Hrdlovič, P. *Chemical Reviews* **1967**, *67*, 599.
(7) Bangee, O. D.; Wilson, V. H.; East, G. C.; Holme, I. *Polymer Degradation and Stability* **1995**, *50*, 313.
(8) Allen, N. S.; Bullen, D. J.; McKellar, J. F. *Journal of Materials Science* **1978**, *13*, 2692.
(9) Jackson, W. J.; Morris, J. C. *Journal of Polymer Science Part A: Polymer Chemistry* **1988**, *26*, 835.
(10) Blumstein, A.; Sivaramakrishnan, K. N.; Blumstein, R. B.; Clough, S. B. *Polymer* **1982**, *23*, 47.
(11) Ravikrishnan, A.; Sudhakara, P.; Kannan, P. *Polymer Engineering & Science* **2011**, 598.
(12) Morris, J. C.; Jackson, W. J.; C08G63/54, C08G63/18, C08G63/54 ed. US, 1984; Vol. US4459402 (A).
(13) Morris, J. C.; Jackson, W. J.; C08G63/54, C08G63/52, C08G63/54 ed. US, 1988; Vol. US4739033 (A).
(14) Morris, J. C.; Jackson, W. J.; C08G63/54, C08G63/52, C08G63/54 ed. US, 1988; Vol. US4728717 (A).
(15) Montgomery, S. J.; Kannan, G.; Galperin, E.; Kim, S. D. *Macromolecules* **2010**, *43*, 5238.
(16) Somlai, A. P.; Cozad, R. A.; Page, K. A.; Williams, H. R.; Creed, D.; Hoyle, C. E. *Photochemical & Photobiological Sciences* **2008**, *7*, 578.
(17) Chun, B. C.; Cha, S. H.; Chung, Y.-C.; Cho, J. W. *Journal of Applied Polymer Science* **2002**, *83*, 27.
(18) Griffin, A. C.; Havens, S. J. *Journal of Polymer Science: Polymer Physics Edition* **1981**, *19*, 951.
(19) Kang, H.; Lin, Q.; Armentrout, R. S.; Long, T. E. *Macromolecules* **2002**, *35*, 8738.
(20) Zhang, M.; Zhang, M.; Moore, R. B.; Long, T. E. *Polymer* **2013**, *54*, 3521.
(21) Lin, Q.; Pasatta, J.; Long, T. E. *J. Polym. Sci., Part A: Polym. Chem.* **2003**, *41*, 2512.
(22) Anastas, P.; Eghbali, N. *Chemical Society Reviews* **2010**, *39*, 301.
(23) Meurisse, P.; Noel, C.; Monnerie, L.; Fayolle, B. *British Polymer Journal* **1981**, *13*, 55.
(24) Odian, G. *Principles of Polymerization, Fourth Edition*; John Wiley & Sons, Inc.: Hoboken, NJ, 2004.
(25) Arnold, F. E.; Van Deusen, R. L. *Macromolecules* **1969**, *2*, 497.
(26) Nunes, R. W.; Martin, J. R.; Johnson, J. F. *Polymer Engineering & Science* **1982**, *22*, 205.
(27) Yeh, J.-M.; Liou, S.-J.; Lai, C.-Y.; Wu, P.-C.; Tsai, T.-Y. *Chemistry of Materials* **2001**, *13*, 1131.

(28) Jansen, M. A. G.; Wu, L. H.; Goossens, J. G. P.; De, W. G.; Bailly, C.; Koning, C. E. *J. Polym. Sci., Part A: Polym. Chem.* **2007**, *45*, 882.
(29) Jansen, M. A. G.; Goossens, J. G. P.; De, W. G.; Bailly, C.; Koning, C. E. *Anal. Chim. Acta* **2006**, *557*, 19.
(30) Kim, S. S.; Han, C. D. *Macromolecules* **1993**, *26*, 6633.
(31) Romo-Uribe, A.; Windle, A. H. *Macromolecules* **1995**, *28*, 7085.
(32) Tokita, M.; Watanabe, J. *Polym. J. (Tokyo, Jpn.)* **2006**, *38*, 611.
(33) Roviello, A.; Sirigu, A. *Die Makromolekulare Chemie* **1982**, *183*, 895.
(34) Solvay *Xydar(R) G-930 Technical Data Sheet*; Solvay, 2014.

Chapter 4: High-Performance Segmented Liquid Crystalline Copolyesters

(Manuscript Just Accepted for Publication in Macromolecular Chemistry and Physics)

Ashley M. Nelson, Gregory B. Fahs, Robert B. Moore, and Timothy E. Long

Department of Chemistry, Macromolecules and Interfaces Institute
Virginia Tech, Blacksubrg, VA 24061-0212

4.1 *Abstract*

The ability of a multiphase copolymer to exhibit both the physical properties of liquid crystalline and elastomeric polymers enables a variety of emerging applications. Traditional synthetic methods often require many steps to achieve such diversity in a copolymer. This work describes the synthesis and characterization of biphenyl-containing segmented copolyesters in a single-step. A fundamental investigation of the thermal and thermomechanical properties as a function of methylene spacer length demonstrated a relationship between melting temperature and even/odd spacer lengths. DSC and SAXS analysis revealed microphase-separation in these randomly segmented copolyesters. The copolymers retained a liquid crystalline morphology despite the incorporation of a flexible oligomeric polyether, and melting and isotropic temperatures ranged from 77 °C to 167 °C and 117 °C to 217 °C, respectively. WAXD provided further insight into the effect of the soft segment on the highly crystalline nature of the segmented copolyesters. Thermomechanical analysis and tensile testing elucidated the effect of hard segment content and structure. Plateau moduli ranged from ca. 5 – 150 MPa, and increasing from 50 to 75 wt. % HS doubled tensile strain. This synergy will enable superior

fabrication and processing of intricate electronic devices that require high thermal properties and mechanical durability.

4.2 *Introduction*

Over the past three decades, liquid crystalline (LC) polyesters have undergone extensive research due to their ability to either maintain anisotropy over a temperature range above the crystalline melting temperature (thermotropic) or induce anisotropy with the addition of solvent (lyotropic).[1-3] For thermotropic LC polymers, this unique feature arises from rigidity present in the polymer backbone and/or pendant to the main polymer chain from symmetric rigid sequences classified as mesogens.[1,4,5] According to earlier theories, mesogens must possess a length to diameter ratio of at least 4 to provide the inherent stiffness necessary to result in a LC morphology.[1] Despite the characteristic high melting temperature, LC polyesters are often melt processable with enhanced shear thinning, resulting from anisotropy that reduces the viscosity of the melt at typical processing temperatures.[4,6] This feature renders LC polyesters excellent candidates for a variety of commercial applications, including but not limited to protective coatings, displays, electronic devices, composites, substrates, and flame-resistant structures.[4,6-8]

Aside from commercial development, research on LC polyesters also flourishes in academic laboratories.[9-11] Hu et al.[9] investigated the effect of modifying poly(diethylene glycol 4,4'-bibenzoate), a known LC polyester, with kinked isophthalate units as a means to study oxygen transport. Positron annihilation lifetime spectroscopy (PALS) aided in understanding the relationship between crystallinity, fractional free volume, and the oxygen barrier. Also utilizing the rigid chemical structure of 4,4'-biphenyldicarboxylate (BB), Lin and coworkers[10] copolymerized melt stable sugars (isosorbide and isomannide) with aliphatic diols to produce

thermotropic LC polyesters. These copolyesters exhibited melting temperatures reaching 268 °C, and both polarized optical microscopy (POM) and atomic force microscopy (AFM) displayed a chiral liquid crystalline morphology.

Many high performance LC polyesters are typically comprised of a wholly aromatic backbone, which maximizes stiffness but often results in polymers that degrade prior to melting.[12] As rigidity is key when attempting to synthesize a LC polyester, many researchers studied copolymerizing mesogens with various methylene spacers and the resulting effect on the LC morphology and physical properties.[4,13] For example, Roviello et al.[13,14] polymerized 4,4'-dihydroxy-alpha-methylstilbene with methylene spacers ranging in length from 6 to 12 carbons. As methylene spacer length increased, the melting temperature of the polymers decreased, with the symmetric, even numbered spacers exhibiting higher melting temperatures than the odd numbered spacers. These novel lower melting LC polyesters allowed for extensive characterization of physical properties and LC morphology, providing crucial insight into structure-property relationships of LC polyesters.[4,13] These homopolymers are sometimes referred to as "segmented" LC polyesters, in reference to the polymerization of hard, mesogenic monomers with methylene spacers, which provide flexibility to the polymer backbone.

A more common definition of the term segmented copolymer is a copolymer that contains both hard and soft segments, often randomly copolymerizing preformed functional oligomers with various monomers.[15] The potential advantages of engineering liquid crystallinity into a block or segmented copolymer are numerous, thus the synthesis of these structures remain of great interest.[2,7,16-20] Convenient soft segments for the copolymerization of mesogenic monomers to afford segmented copolyesters include commercially available oligosiloxanes and oligoethers.[18,19,21] Transesterification, the reversible reaction of an ester and alcohol, is

commonly employed to synthesize polyesters.[15] The high temperature reaction of monomeric dimethyl or diethyl esters and diols in an inert atmosphere efficiently removes the methanol or ethanol byproduct, driving the reaction to the right, and a final vacuum step facilitates achieving the necessary 99+ % conversion required for step-growth polymerization.

Thuillier et al.[21] used the aforementioned one-pot melt transesterification procedure to synthesize truly segmented mesogen-containing copolyesters. Rigid biphenyl and stilbene diesters functioned as main-chain mesogens copolymerized with a flexible 5- or 6-carbon methylene spacer and oligomeric poly(tetramethylene oxide) (PTMO) of 620 and 2030 g/mol in varying weight percents. Structural characterization confirmed the integrity of the polymerization, and thermal analysis elucidated the relationship between hard segment content and methylene spacer length on the ability to maintain liquid crystallinity. Differential scanning calorimetry (DSC) exhibited both melting and isotropic transitions, indicating a liquid crystalline morphology, for segmented copolyesters containing biphenyl and pentanediol. Similarly, biphenyl-hexanediol segmented copolyesters also displayed liquid crystalline behavior when the hard segment content exceeded 55 weight (wt.) %. To further the understanding of the structure-property relationships between both hard and soft segments, our current work includes unprecedented shorter 4-carbon spacers and longer 8-carbon spacers. Additionally, we describe a Pluronic® oligoether to construct the soft segment, resulting in a novel series of segmented liquid crystalline copolyesters.

In this report, we describe the synthesis and characterization of high-performance segmented (co)polyesters containing liquid crystalline hard segments and flexible polyether soft segments. Copolymerizing 4,4'-biphenyldicarboxylate (BB) with commercially available methylene diol spacers ranging from 4 to 8 carbons to construct the hard segments and

poly(tetramethylene oxide) (PTMO) and Pluronic® oligoethers as soft segments provided novel segmented polyesters. This synthetic platform allowed for a fundamental investigation of structure-property relationships as a function of chemical composition and relative weight ratios of the various hard and soft segments. We investigated the ability of these segmented copolyesters to maintain a liquid crystalline morphology and a broad range of composition dependent thermal and thermomechanical properties.

4.3 *Experimental*

4.3.1 Materials

Dimethyl biphenyl-4,4'-dicarboxylate (BB), 1,4-butanediol (BD), 1,5-pentanediol (PD), 1,6-hexanediol (HD), 1,8-octanediol (OD), poly(tetramethylene oxide) (Terathane®) with a number-average molecular weight (M_n) ~2000 g/mol, and poly(propylene glycol)-block-poly(ethylene glycol)-*block*-poly(propylene glycol) comprised of 50 wt. % PEG and an average M_n ~2000 g/mol (Pluronic® 10R5; $P10R5_{2K}$) were purchased from Sigma Aldrich and used as received. A catalyst containing 0.01 g/mL titanium tetraisopropoxide in 1-butanol was prepared according to previous literature.[22]

4.3.2 Analytical Methods

^{1}H NMR spectroscopy was obtained using a 400 MHz Varian Tecmag Apollo or Agilent U4-DD2 400 MHz in either a solvent mixture of pentafluorophenol and $CDCl_3$ or deuterated trifluoroacetic acid (TFA_d) at ambient temperature. Thermal transitions were determined using a TA Instruments Hi-Res thermogravimetric analyzer (TGA) 2950 or Q50 under an inert atmosphere and a temperature ramp of 10 °C/min from 25 to 600 °C and either a TA Instruments

Q1000 or Q2000 differential scanning calorimeter (DSC) heat/cool/heat method with a heating ramp of 10 °C/min and a cooling rate of either 10 or 100 °C/min. Compression molding the polymers between Teflon® sheets afforded free-standing polymer films, which were subsequently used for thermomechanical and tensile analysis. Thermomechanical properties were determined using a TA Instruments Q800 dynamic mechanical analyzer (DMA) at a frequency of 1 Hz and a temperature ramp of 3 °C/min from 0 °C until flow. An Instron 4411 was used to perform tensile experiments at a crosshead speed of 0.5 mm/min and results are reported as an average of five samples. Small angle X-ray scattering (SAXS) experiments were performed using a Rigaku S-Max 3000 3 pinhole SAXS system, equipped with a rotating anode emitting X-ray with a wavelength of 0.154 nm (Cu Kα). The sample-to-detector distance was 1604 mm, and q-range was calibrated using a silver behenate standard. Two-dimensional SAXS patterns were obtained using a fully integrated 2D multiwire, proportional counting, gas-filled detector, with an exposure time of 1 h. All SAXS data was analyzed using the SAXSGUI software package to obtain radially integrated SAXS intensity versus scattering vector q, where $q=(4\pi/\lambda)\sin(\theta)$, θ is one-half of the scattering angle and λ is the wavelength of X-ray. SAXS profiles were corrected for sample thickness and transmission. SAXS profiles were vertically shifted to facilitate a comparison of the peak positions. Wide angle X-ray Diffraction (WAXD) experiments were performed using a Rigaku S-Max 3000 3 pinhole SAXS system, equipped with a rotating anode emitting X-rays with a wavelength of 0.154 nm (Cu Kα). Scattering from a silver behenate standard was used to calibrate the sample-to-detector distance. For WAXD, the sample-to-detector distance was 80.0 mm. WAXD two-dimensional diffraction patterns were obtained using an image plate, with an exposure time of 2 hours. All WAXD data were analyzed using the SAXSGUI software package to obtain azimuthal averaged WAXD intensity versus 2θ

profiles, where θ is one half of the scattering angle. WAXD profiles were vertically shifted to facilitate a comparison of the peak positions.

4.3.3 Polymer Synthesis

All polymers were synthesized using a similar melt transesterification procedure.[10,23] For the various compositions the charged weight percent SS ranged from 24-25 %, 52-54 %, and 64-66 % referred to as 25, 50, and 65 wt. % throughout. For example, in preparation of poly(BB-HD)$_{47}$-*ran*-poly(BB-P10R5$_{2K}$)$_{53}$, where the subscript corresponds to the weight percent of each segment charged and is further referred to as the 50 wt. % SS composition, 4.16 g of BB, 2.18 g of HD, 5.01 g of P10R5$_{2K}$, and 40 ppm (0.04 mL) of titanium tetraisopropoxide catalyst were added to a dry 100-mL round-bottomed flask equipped with a nitrogen inlet, mechanical stirrer, and distillation apparatus. A slight excess of HD was charged relative to BB in the above reaction, 1.00 mol eq BB to 1.43 mol eq HD, to compensate for potential premature low molar mass monomer distillation. High molecular weight copolymers were produced despite an initial offset stoichiometry since the excess was removed in the high temperature vacuum step at the end of the polymerization. The reaction was purged with nitrogen and degassed three times to ensure complete removal of oxygen prior to the start of the reaction. The round-bottomed flask was then lowered into a metal bath at 190 °C and allowed to proceed with a nitrogen purge and stirring for 2 h. The reaction temperature was then raised to 220 °C for another 2 h, followed by an increase to 275 °C for 0.5 h. With stirring maintained, vacuum was then applied at 275 °C and the reaction was complete after 2 h. The round-bottomed flask was broken to retrieve the resulting solid opaque polymer which was used without further purification.

4.4 *Results and Discussion*

4.4.1 Synthesis and Structural Confirmation

Main chain mesogen-containing polymers are often plagued with insolubility as the symmetry and rigidity in the polymer backbone result in a high level of crystallinity.[6] These physical characteristics pose a challenge for synthesizing high molecular weight polymers. Melt transesterification allows for the successful synthesis of these polyester systems due to the absence of solvent and promptly affords polyesters without any required purification steps. **Scheme 1** depicts the synthesis of poly(BB-HD)$_x$-*ran*-poly(BB-P10R5$_{2K}$)$_y$, where biphenyl is the mesogen, HD is the methylene spacer for the hard segment, and P10R5$_{2K}$ is the soft segment (SS) oligoether; denoted BB$_6$P10R5$_y$ (mesogen$_{\text{methylene spacer length}}SS_{\text{approximate wt. \% SS}}$). While maintaining the same polymerization procedure, various methylene spacers and oligoethers provided a myriad of segmented polyesters; BB$_4$PTMO$_y$, BB$_5$PTMO$_y$, BB$_6$PTMO$_y$, BB$_8$PTMO$_y$. This route easily allowed for tailoring polymer composition based on the weight ratio of reagents, while the methanol byproduct and excess reagents distilled from the reactor under vacuum.

Scheme 4.1. Synthesis of poly(BB-HD)$_x$-*ran*-poly(BB-P10R5$_{2K}$)$_y$ (BB$_6$P10R5$_y$ series) using melt transesterification

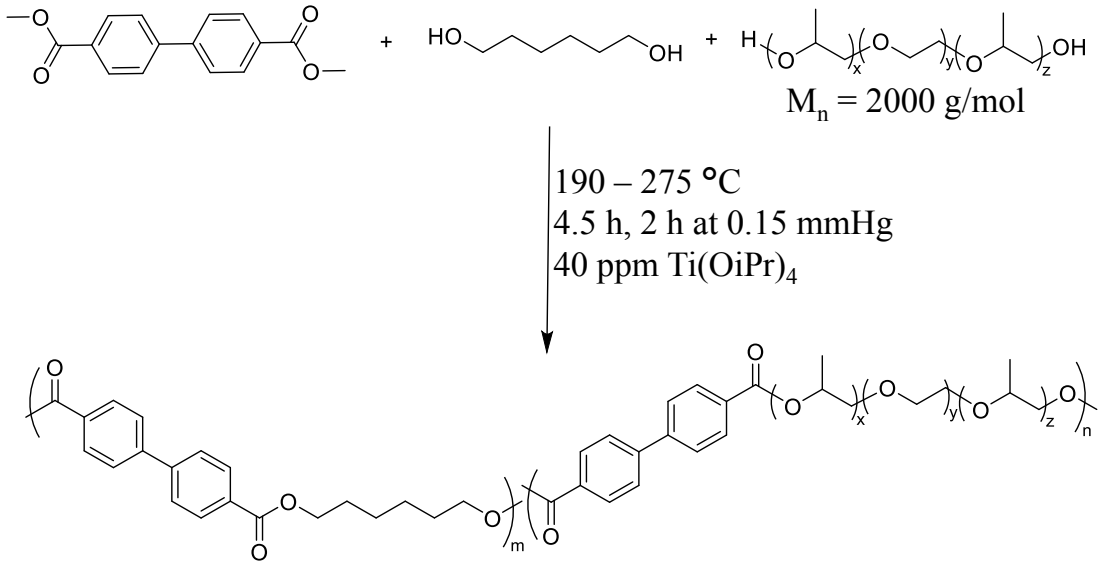

Previous literature reported solubility of biphenyl-containing liquid crystalline polyesters in trifluoroacetic acid (TFA) if quenched upon immediate removal from the melt to avoid the highly crystalline morphology.[23] For the BB$_6$P10R5$_y$ series, compositions with high soft segment content (65 and 50 wt. %) dissolved in TFA without quenching, allowing structural confirmation using ^{1}H NMR spectroscopy. **Figure 1** shows the ^{1}H NMR spectra and corresponding assignments for BB$_6$P10R5$_{50}$. Other series dissolved in a mixture of $CDCl_3$ and pentafluorophenol without quenching. To quantitatively assess the composition of the soluble BB$_6$P10R5$_y$ segmented copolymers, we evaluated the ratios of the integration of resonances g and c (Figure 1), which correspond to peaks specific to the soft segment and hard segment. A value of 0.10 for BB$_6$P10R5$_{65}$ and 0.17 for BB$_6$P10R5$_{50}$ corresponded well with the expected 15 wt. % difference in soft segment monomer feed between the two samples. GPC analysis and intrinsic viscosity measurements were not achieved due to limited solubility, but all BB$_6$P10R5$_y$ products formed films upon compression molding which is often indicative of high molecular weight polymers.[24-26]

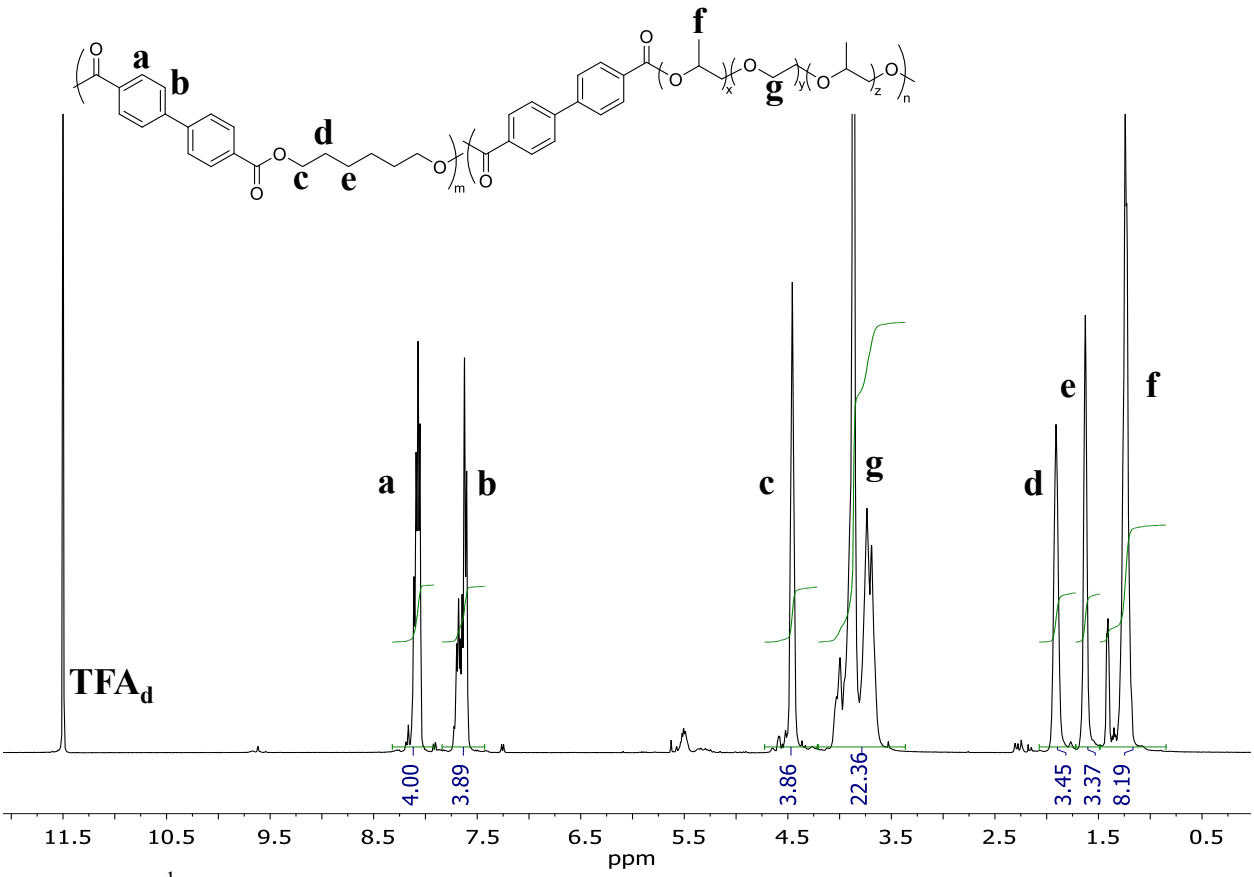

Figure 4.1. ^{1}H NMR spectra of BB_6P10R5_{50}

4.4.2 Thermal and Morphological Characterization

Thermotropic main chain liquid crystalline polyesters generally demonstrate excellent thermal stability, often possessing melting temperatures that exceed the polymer degradation temperature.[12] In contrast, low molecular weight polyether oligomers display limited thermal stability; the temperature for the onset of degradation for P10R5 (M_n ~2000 g/mol) is 228 °C. Upon copolymerization of the polyether oligomer, the resulting segmented polyesters possessed T_d values similar to the liquid crystalline homopolymer, BB_6. **Figure 2** depicts the thermal degradation profiles for the BB_6P10R5_y series. 2K P10R5 oligoether and BB_6P10R5_{65} both revealed a slight two-step degradation, which converts to a smooth, one step degradation profile

for BB_6P10R5_{50}, BB_6P10R5_{25}, and BB_6. Various BB_xPTMO_y compositions displayed one-step degradations that were less dependent on soft segment content, and the onset of degradation temperatures for the BB_4PTMO_y and BB_6PTMO_y were near 400 °C, whereas the BB_5PTMO_y and BB_8PTMO_y degraded closer to 360 °C.

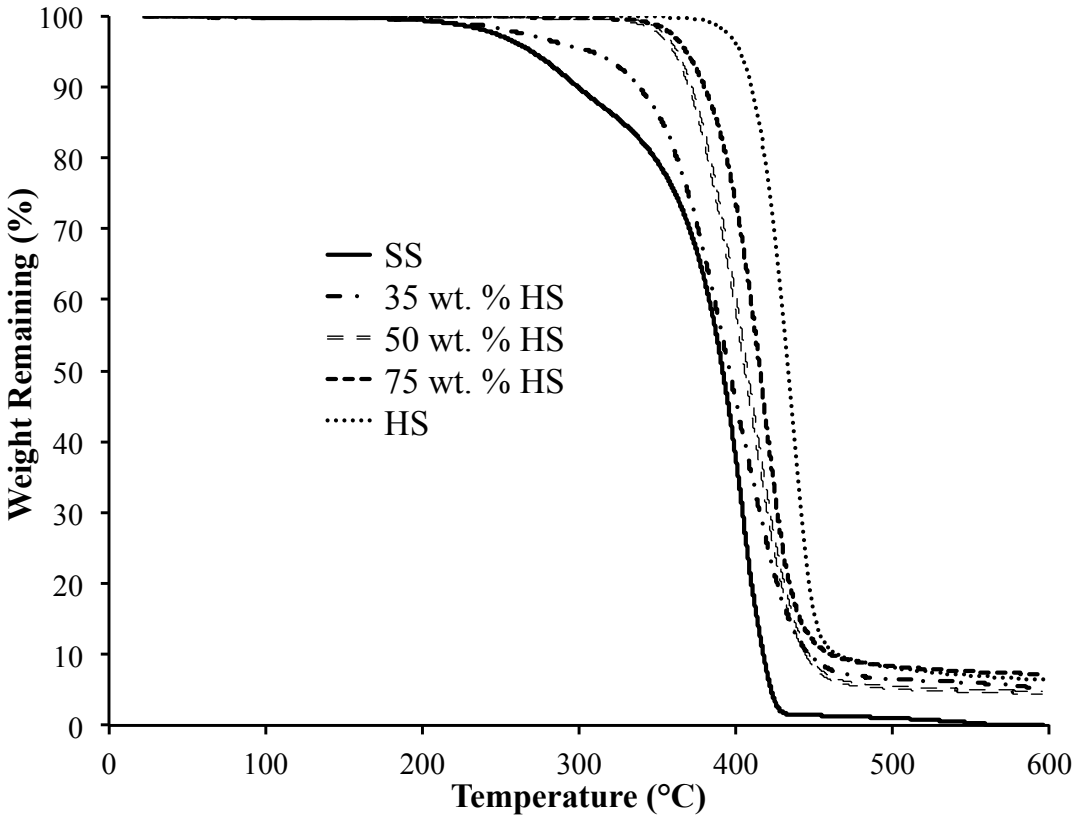

Figure 4.2. Thermal degradation profiles of BB_6P10R5_y with soft segment (SS) and hard segment (HS) homopolymer controls showing increased thermal stability with increasing HS content

The melting temperature (T_m) of a polymer directly correlates to the ability and propensity of the polymer chains to pack, thus a characteristic relationship between even and odd methylene spacers results in higher and lower T_m's respectively.[13] Longer methylene spacers also exhibit lower T_m's relative to the shorter even/odd spacers. This relationship between T_m and methylene spacer length was evident in the BB_xPTMO_y segmented copolymers, as shown in

Figure 3. Comparing the various methylene spacers at 75 wt. % HS, a 115 °C decrease occurred between the 4 and 5 methylene spacer, following a 36 °C increase to the 6 methylene spacer, and finally a 30 °C decrease for the 8 methylene spacer. Despite the drastic decrease in T_m from the 4 to 8 methylene spacer, the T_m for the 8 methylene spacer remained higher than the 5 methylene (odd) spacer; further demonstrating the packing ability of even and odd methylene units in the polymer chains.

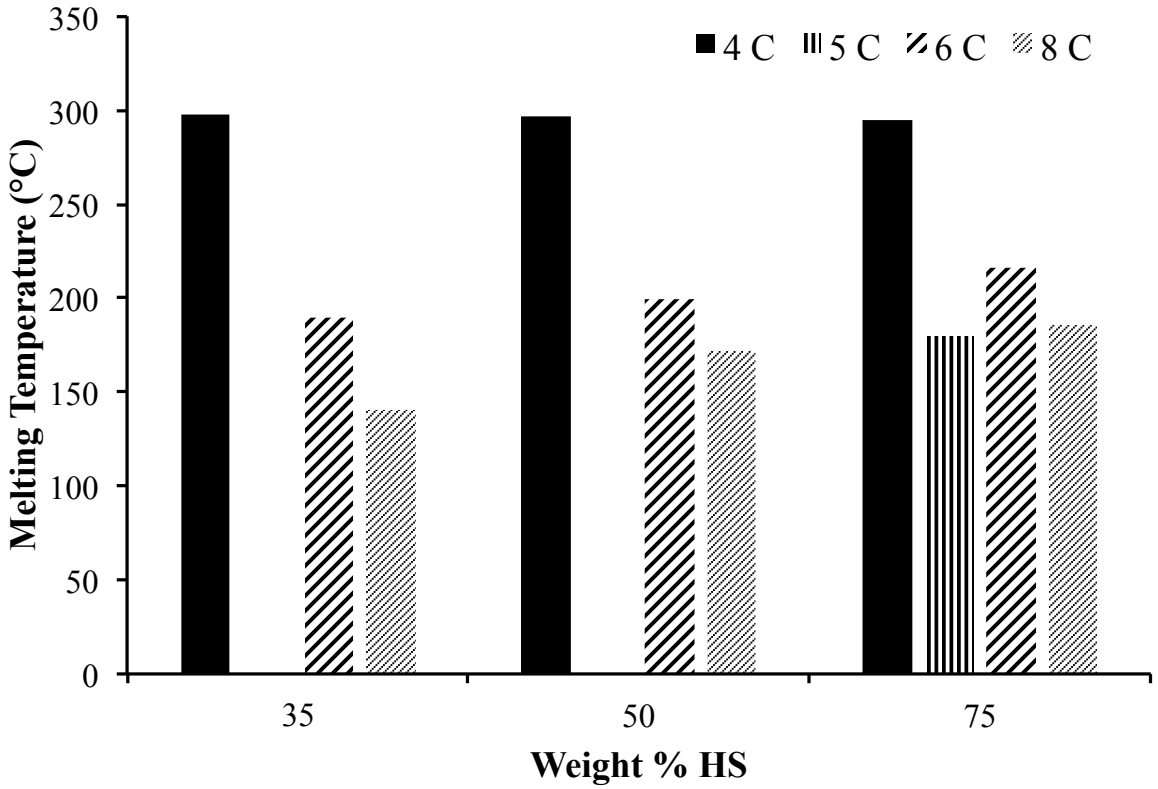

Figure 4.3. The effect of methylene spacer length on the HS melting temperature of the BB_xPTMO_y series at varying weight percent HS

The incorporation of a flexible oligomeric unit into the various segmented copolymers inherently affords a segmented copolymer microstructure similar to the microstructure of a thermoplastic elastomer.[27] A microphase-separated morphology often results from physical crosslinks and provides thermoplastic elastomers the tensile strength and elongation for many

applications. Segmented polyurethanes, a class of thermoplastic elastomers, commonly require a two-step synthesis to ensure a block copolymer with more control over the specific block lengths, and under most reaction conditions, each urethane bond is irreversible.[28,29] In contrast, all reactants under the high temperature procedure in this one-pot polymerization process readily undergo transesterification, thus we assume the length of each polyester segment is random. The transition temperatures obtained from the DSC thermograms provided insight into the bulk morphology of the materials.[30] In a microphase-separated network, each segment or block maintains the thermal transitions of the respective homopolymer as opposed to intermediate transitions arising from a phase-mixed morphology. The independence of the transition temperatures from weight % HS for the BB_xPTMO_y series depicted in **Figure 3** as well as in **Figure 4** for the BB_x10R5_y series suggests a microphase-separated morphology for these randomly segmented copolyesters.

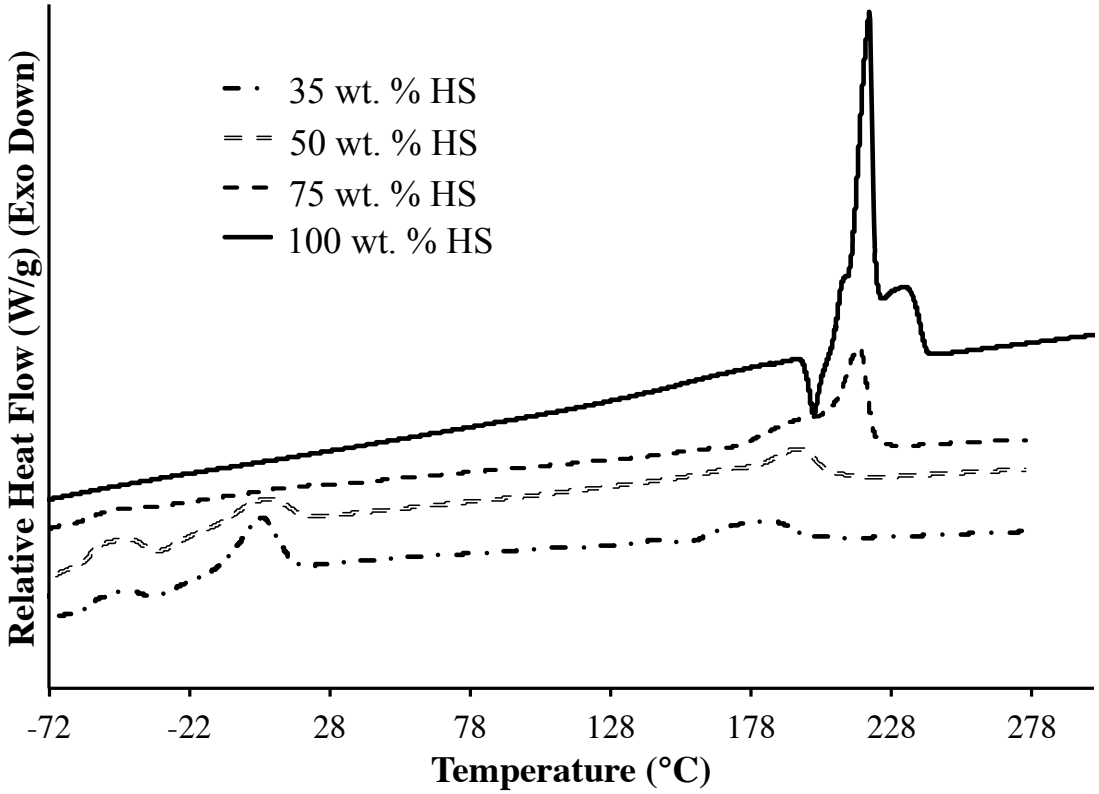

Figure 4.4. DSC analysis of BB_6P10R5_y series showing independent thermal transitions for the hard and soft segments suggesting a microphase-separated morphology

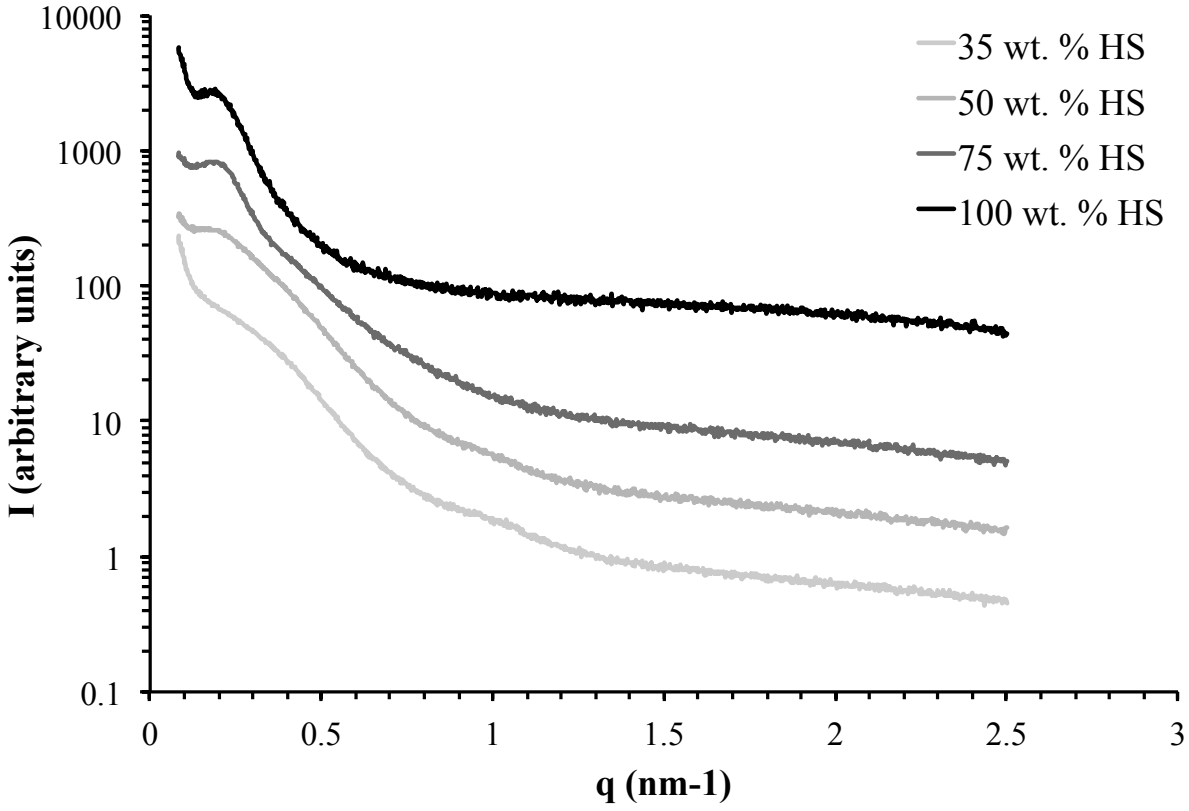

Figure 4.5. SAXS profiles for BB_6P10R5_y series (vertically shifted) which coupled with DSC further supports a microphase-separated morphology

Small angle X-ray scattering (SAXS) was used to gain insight into the nanometer scale morphology[31] of these polymers. Scattering maxima resulting from ordered domains allows for an estimation of characteristic dimensions using the equation $d = (2\pi)/q$ where d corresponds to the Bragg spacing and q is the scattering vector at the peak maximum. SAXS analysis was performed on compression molded films of the BB_6 homopolymer and BB_6P10R5_y series at 25 °C. The scattering profiles, depicted in **Figure 5** exhibit a peak for each composition and diffuse scattering for the segmented copolyesters at lower q values. **Table 1** contains the maximum q values for each peak and corresponding Bragg spacing. The calculated Bragg spacing values correlated well with previously reported BB_6 homopolymer lamellar spacing

values of 225 – 294 Å.[32,33] The consistent spacing between BB_6 and $BB6P10R5_y$ series suggested the scattering peak corresponds to the hard segment and further confirmed the microphase-separated morphology of these segmented copolyesters.

Table 4.1. Scattering vector maxima and calculated Bragg spacing from the SAXS profiles of the BB_6P10R5_y series

Weight % HS	q (nm^{-1})	d (nm)
35	0.18	34
50	0.18	35
75	0.19	34
100	0.19	33

DSC is a common technique employed to determine if a polymer possesses a liquid crystalline morphology; both the T_m and isotropic temperature (T_i) present an endotherm. Other characterization techniques such as polarized optical microscopy (POM), used to visually depict the LC texture, and wide-angle x-ray diffraction (WAXD) often couple with DSC to further confirm and characterize the anisotropic morphology.[23] **Figure 4** overlays the DSC thermograms for the BB_610R5_y series, where the hard segment homopolymer control is BB_6 (100 wt. % HS) and the independence of the thermal transitions for the hard and soft segments suggest a microphase-separated morphology. Preston et al.[34] and Watanabe et al.[33] extensively studied and characterized the LC morphology of BB_6 using DSC, SAXS and WAXD. The literature describes three classes of liquid crystalline textures which depend on the molecular ordering of the rigid rods; nematic, smectic, and cholesteric.[4] BB_6 displayed a smectic A texture, indicating a higher level of ordering than most LC polymers.[4,33] In the present study BB_6 exhibited three

transitions; a crystallization temperature, melting temperature, and isotropic temperature corresponding to a LC morphology as expected. All traces shown in **Figure 4** are from the second heating cycle in the DSC and the unresolved exothermic peaks for the T_m and T_i of BB_6 are most likely a result of the quench cooling procedure (100 °C/min) used.

A LC morphology was a key material property to preserve in the hard segment of the segmented copolyesters as the anisotropy induces shear thinning and allows for injection molding of intricate parts.[4,6] As mentioned above, BB_6 exhibited a small mesophase or processing window under the experimental conditions, and furthermore, an isotropic exotherm was not discernable in any of the second heat DSC traces of the segmented copolyesters. Polymer crystallization requires both time and a specific temperature(s) window, thus thermal transitions observed from DSC depend on both the heating and cooling rates.[35] Since the quench cooling procedure could constrain crystallization, we examined the first heating and cooling cycle of BB_6. BB_6 exhibited resolved T_m and T_i transitions in the first heat and cooling DSC thermograms (**Figure 11)**, corresponding closely with previous literature values (187 °C and 218 °C for the T_m and T_i, respectively) of a slow cooled (10 °C/min) BB_6 homopolymer.[33]

Each segmented copolyester in the BB_6P10R5_y series lacked evidence of an isotropic transition in the second heat DSC curves visible in **Figure 4**. To determine if the quench cooling procedure hindered crystallization as observed for BB_6, we examined the cooling curves and detected both a T_m and T_i for all compositions in the BB_6P10R5_y series. **Figure 6** overlays the quench cooling curves for the BB_6P10R5_y series, and **Table 2** reports the specific transition values. The two exothermic peaks indicated the copolyesters retain the desired LC morphology within the hard segment. The isotropic temperature exhibits a molecular weight dependence, yet more importantly, depends on rigidity and molecular ordering.[4,36] Additionally, structural

defects in the polymer chain can either decrease the mesophase or eradicate the LC morphology altogether.[4] For the BB_6P10R5_y series, T_i decreased with increasing soft segment content from 217 °C for BB_6 down to 171 °C for $BB6P10R5_{65}$. Although the thermal transitions provided evidence of a microphase-separated morphology, the specific length and distribution of the hard and soft polyester segments remain unknown. Therefore, the decrease in T_i with increasing soft segment could result from smaller hard segments (molecular weight effect) and/or the flexible soft segments acting as large defects. As expected from the second heat curves in **Figure 4**, the melting transitions remained similar for BB_6P10R5_{25} and BB_6P10R5_{50} and decreased slightly with an increase in SS.

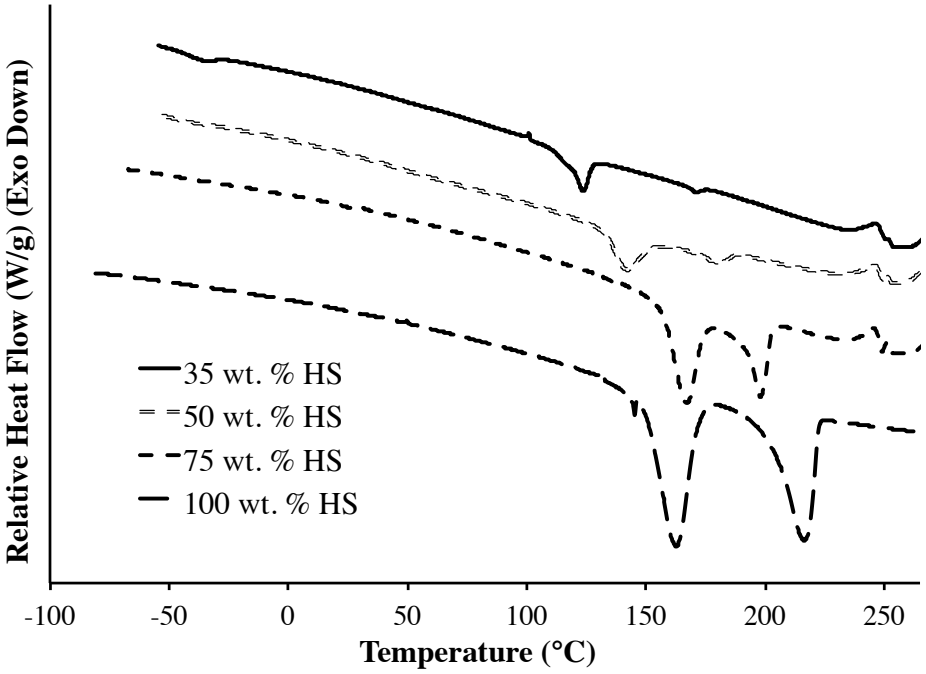

Figure 4.6. Quench cooling curves revealing a T_m and T_i for the complete BB_6P10R5_y series

Table 4.2. Thermal transitions from the quench cooling traces for the liquid crystalline BB_6P10R5_y series

Weight % HS	T_m (°C)	T_i (°C)
35	124	171
50	142	181
75	167	198
100	163	217

Second heat DSC thermograms of the BB_xPTMO_y series with even methylene spacers (4, 6, and 8 units) displayed independent T_m's for the SS and HS, close to the expected values of the specific homopolymers, and indicated a microphase-separated morphology as discussed above and shown in **Figure 3**. Similar to the BB_xP10R5_y series, T_m peaks broadened with lower wt. % HS content for the BB_6PTMO_y and BB_8PTMO_y series. The BB_5PTMO_{25}, however, displayed a HS exotherm with a large peak and shoulder providing a T_m and T_i of 180 °C and 194 °C, respectively; this data corresponded well with previously reported results and was indicative of a microphase-separated liquid crystalline morphology.[21] **Figure 12** displays the quench cooling and second heat DSC traces for BB_5PTMO_{25}. Previous literature noted the BB_6PTMO_y series displayed a LC morphology above 55 wt. % HS, however, did not provide specific transition temperatures.[21] Takahashi and Nagata[37] reported similar results for BB_6PTMO_y copolyesters, showing above 66 wt. % HS retained liquid crystallinity and values obtained from DSC cooling curves. Similar to the BB_6P10R5_y series described earlier, second heat thermograms for the BB_6PTMO_y series lacked evidence of isotropic transitions, however, the cooling curves exhibited both a T_m and T_i characteristic of a LC material.

Table 4.3. Melting and isotropic transitions determined from DSC quench cooling curves for various liquid crystalline BB_xPTMO_y segmented copolyesters (*shoulder)

Methylene Spacer Length (# C)	Weight % HS	T_m (°C)	T_i (°C)
4	35	248	279
4	50	249	285
4	75	237	285
5	75	77	168
6	35	113	165
6	50	143	180
6	75	149	196
6	100	163	217
8	35	104	117*
8	50	116	136
8	75	138	157

Table 3 summarizes the LC transition temperatures obtained from the quench cooling thermograms of BB_4PTMO_y series, BB_5PTMO_{25}, and both the BB_6PTMO_y and BB_8PTMO_y series. The BB_xPTMO_y series exhibited similar trends as described above for the BB_6P10R5_y series; both T_i and T_m decreased with increasing soft segment content. These values indicated the copolymers maintain a LC morphology within the hard segment despite approximately 65 wt. % of the segmented copolyester is comprised of the non-nematogenic soft segment. Limited literature on liquid crystalline polymers containing methylene spacer lengths of 4 or less exists, as the extremely high transition temperatures are often too close to or above the degradation

temperature.[4] DSC analysis of the BB_4PTMO_y series displayed high T_m's near 300 °C on the second heat and over the experimental temperature range (T_{max} = 325 °C) BB_4PTMO_{25} exhibited a T_i = 312 °C. The higher SS compositions only displayed a T_i upon cooling as tabulated above.

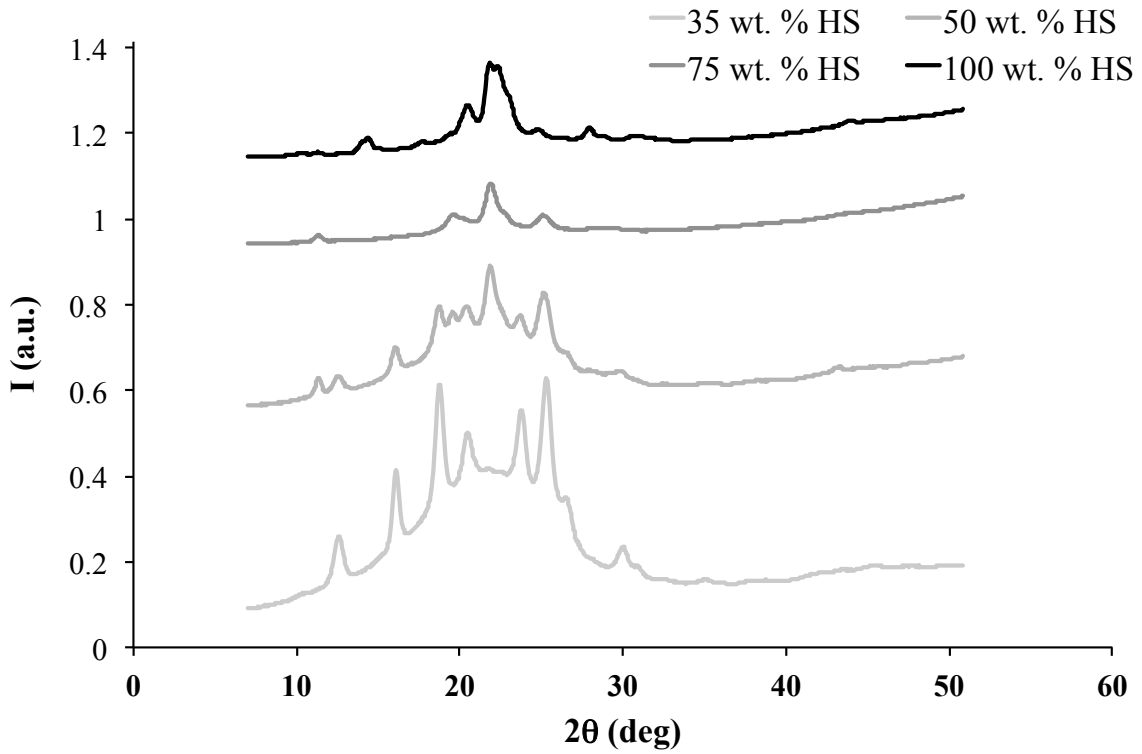

Figure 4.7. WAXD profiles of the BB_6P10R5_y series highlighting the highly crystalline hard segment and appearance of polymorphs upon soft segment incorporation

Wide angle X-ray diffraction (WAXD) probes the crystalline structure of materials on a smaller scale than SAXS and is capable of providing exact crystal lattices and polymer chain lengths.[38] WAXD utilizes the Bragg equation, $d = (2\pi)/q$, to determine crystal size and length scales. WAXD was performed on compression molded films of the BB_6P10R5_y series and the overlaid curves, shifted vertically for ease of comparison, are displayed in **Figure 7**. The lack of an amorphous halo for the BB_6 homopolymer (100 wt. % HS) indicated a highly crystalline material, congruent with previous literature.[37,39] An amorphous halo appeared upon

incorporation of the soft segment and increased with increasing flexible content. The segmented copolyesters maintained many peaks similar or identical to BB_6, as visible in **Figure 7**. Supplemental information **Table 5-8** contains all peak positions and calculated Bragg spacing for each polymer in the BB_6P10R5_y series. Interestingly, increasing the soft segment also introduced structure not observed in the homopolymer. These new peaks are attributed to soft segment induced polymorphs and shows a distinct difference from WAXD profiles Takahashi and Nagata[37] reported for BB_6PTMO segmented copolyesters with varying wt. % soft segment.

4.4.3 Thermomechanical Characterization and Tensile Testing

Many applications require materials with mechanical durability throughout the working temperature range. To compare the effect of methylene spacer length and HS content, **Figure 8a** depicts the DMA curves of BB_6PTMO_{50}, BB_8PTMO_{50}, BB_6PTMO_{25}, and BB_8PTMO_{25}. The general shape of the DMA trace reveals the PTMO SS glass transition temperature (T_g), melting temperature, followed by a rubbery plateau and ultimately flow. The overlay of these curves highlights the profound effect of flexibility on thermomechanical performance. All samples began with a similar storage modulus that dropped after SS melting to a plateau modulus dependent on SS content. This small synthetic alteration provides easily tunable thermomechanical properties based on a desired or specified working temperature. Solely focusing on the four compositions in **Figure 8a**, from 40 °C to 100 °C the achievable storage moduli range from ca. 10 MPa to 500 MPa.

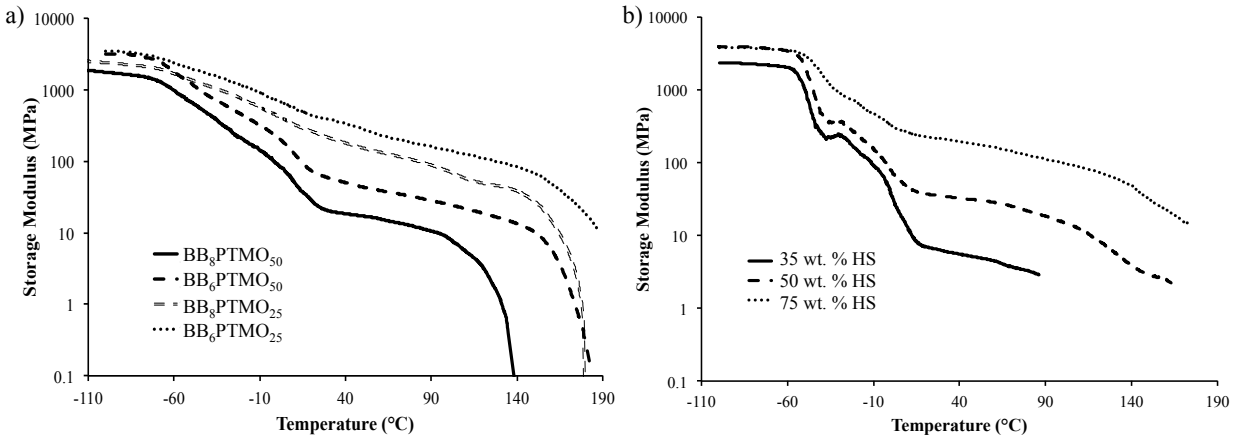

Figure 4.8. Overlaid DMA curves for BB_6PTMO_{50}, BB_8PTMO_{50}, BB_6PTMO_{25}, and BB_8PTMO_{25} (a) and thermomechanical analysis of the BB_6P10R5_y series (b)

The mechanical advantages of these segmented copolyesters are two-fold, as both the SS and HS affect different thermal and thermomechanical regions. As described above, the combination of SS content and HS structure impacted the plateau modulus providing tunable thermomechanical properties. However, the HS also controlled the upper working temperature, or flow region, of the material. For example, BB_6PTMO_{50} and BB_8PTMO_{25} exhibited similar flow temperatures with BB_6PTMO_{50} containing half as much HS as BB_8PTMO_{25}. A difference in plateau moduli of almost half an order-of-magnitude for these two copolyesters further demonstrated the advantages and capabilities of tunable transitions for applications with specific material property guidelines.

Figure 8b shows the thermomechanical analysis of the BB_6P10R5_y series. Unlike the BB_xPTMO_y series, the BB_6P10R5_y series first goes through a T_g, followed by a crystallization indicated with a slight increase in storage modulus, melting temperature, plateau modulus, and terminal flow. The transition temperatures corresponding to the SS correlated well with the DSC transitions observed for the 2K P10R5 oligoether (**Table 4**). As expected, a similar trend occurred with the BB_6P10R5_y series as with the BB_xPTMO_y segmented copolyesters; both the

plateau modulus and flow temperature increased with increasing HS content. The ability of a material to recover from a stress or deformation, known as hysteresis, is a key attribute of elastomeric materials.[40,41] To probe the ability of these segmented copolyesters to recover from thermomechanical deformation, a DMA experiment was performed on BB_6P10R5_{25} where heating stopped at 100 °C (prior to the flow temperature), the sample cooled back to -100 °C, and re-heated under the same conditions until flow. **Figure 9a** depicts the first heat and cooling curves. After heating to 100 °C, BB_6P10R5_{25} returned to the initial storage modulus. Furthermore, the second heat DMA trace overlaid the first heating curve almost perfectly and is shown in **Figure 9b**. These results demonstrated the thermomechanical hysteresis and mechanical integrity of these materials, which will allow for use in a broad range of potential applications.

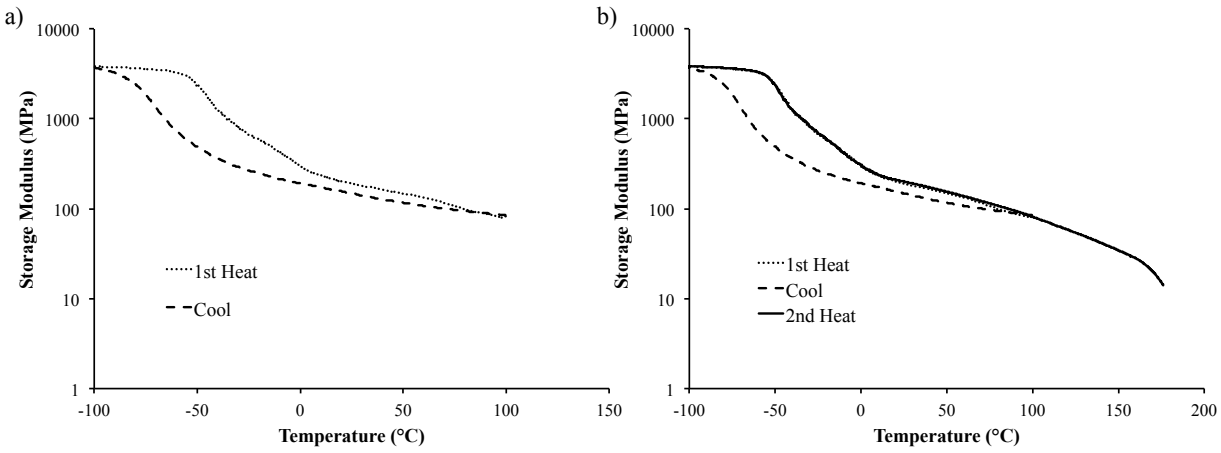

Figure 4.9. First heat and cooling DMA curves (a) and overlaid first heat, cool, and second heat traces (b) showing thermomechanical hysteresis of BB_6P10R5_{25}

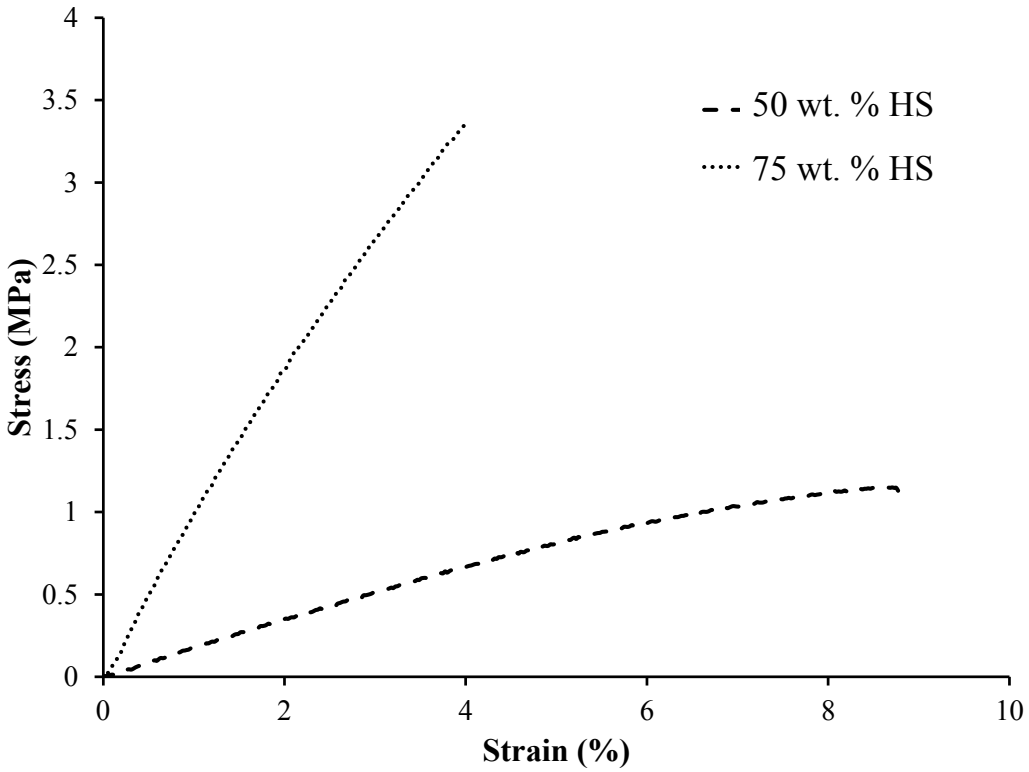

Figure 4.10. Representative tensile curves for BB_6P10R5_{50} and BB_6P10R5_{25}

Tensile testing of both BB_6P10R5_{50} and BB_6P10R5_{25} further probed the effect of HS composition on mechanical properties and ductility. **Figure 10** displays representative tensile curves for each composition. The average Young's modulus, calculated from the initial slope of the stress vs strain curve, is 19 ± 1 MPa for BB_6P10R5_{50} and 107 ± 12 MPa for BB_6P10R5_{25}. This demonstrated the large impact of HS content on the overall strength of the copolyesters. BB_6P10R5_{25} exhibited a higher stress at break than $BB_6P10R5_{50,}$ however, incorporating only 25 wt. % more SS, the strain at break doubled from 3.9 ± 0.4 % for BB_6P10R5_{25} to 8.2 ± 1.5 % for BB_6P10R5_{50}.

4.5 *Conclusions*

Melt transesterification afforded liquid crystalline segmented copolyesters containing various HS methylene spacer lengths and either PTMO or P10R5 SS oligoethers. ^{1}H NMR, TGA, DSC, SAXS, WAXD, DMA, and tensile testing provided structural determination, thermal, morphological, and thermomechanical analysis. Varying both copolymer structure and composition allowed for an investigation of the effect of HS methylene spacer length on thermal and thermomechanical properties, as well as exploring the ability of these randomly segmented polyesters to obtain a LC morphology. The effect of methylene spacer length on thermal properties followed the established even/odd trend; a higher T_m resulted from the shorter methylene spacer. For example, BB_4PTMO_{25} HS exhibited a T_m of 298 °C while the BB_8PTMO_{25} HS T_m was 186 °C. Thermomechanical analysis demonstrated the same trend, showing increasing plateau moduli with increasing HS content and a similar depressed temperature range for polyesters containing longer methylene spacers. Further characterization of the tensile properties of the novel BB_6P10R5_y series revealed the effect of HS composition, with an average Young's modulus for BB_6P10R5_{25} of 107 ± 12 MPa compared to the 19 ± 1 MPa for BB_6P10R5_{50} and a near doubling of the strain at break. Some key attributes of these segmented copolyesters include the microphase-separated morphology determined from both DSC and SAXS and liquid crystalline morphology retained in the hard segment. The straightforward one-pot synthesis and ease of varying comonomers resulted in a broad range of high-performance segmented (co)polyesters with tunable morphology, thermal, and thermomechanical properties capable of impacting a variety of electronic devices and aerospace materials.

4.6 *Acknowledgements*

This material is based upon work supported in part by the Virginia Space Grant Consortium, the National Science Foundation under Grant No. DMR-0923107, and the U.S. Army Research Laboratory and the U.S. Army Research Office under the Army Materials Center of Excellence Program, contract W911NF-06-2-0014. The authors would also like to thank Solvay for unrestricted financial support.

4.7 *References*

(1) Donald, A.; Windle, A.; Hanna, S. *Liquid Crystalline Polymers*; 2nd ed.; Cambridge University Press, 2006.
(2) Auman, B. C.; Percec, V. *Polymer* **1988**, *29*, 938.
(3) Lin, J.; Sherrington, D. C.; Nield, E.; Richards, R. W. *Macromolecules* **1992**, *25*, 7107.
(4) Ciferri, A. *Liquid Crystallinity in Polymers: Principles and Fundamental Properties*, 1991.
(5) Xie, H.-L.; Wang, S.-J.; Zhong, G.-Q.; Liu, Y.-X.; Zhang, H.-L.; Chen, E.-Q. *Macromolecules* **2011**, *44*, 7600.
(6) Economy, J.; Goranov, K.; Hergenrother, P., Ed.; Springer Berlin / Heidelberg: 1994; Vol. 117, p 221.
(7) D. Demus, J. G., G. W. Gray, H.-W. Spiess, V. Vill *Handbook of Liquid Crystals Vol. 3: High Molecular Weight Liquid Crystals*, 1998; Vol. 3.
(8) Chung, T.-S.; Cheng, M.; Goh, S. H.; Jaffe, M.; Calundann, G. W. *Journal of Applied Polymer Science* **1999**, *72*, 1139.
(9) Hu, Y. S.; Liu, R. Y. F.; Schiraldi, D. A.; Hiltner, A.; Baer, E. *Macromolecules* **2004**, *37*, 2136.
(10) Lin, Q.; Pasatta, J.; Long, T. E. *J. Polym. Sci., Part A: Polym. Chem.* **2003**, *41*, 2512.
(11) Trenor, S. R.; Shultz, A. R.; Love, B. J.; Long, T. E. *Chemical Reviews* **2004**, *104*, 3059.
(12) Calundann, G. W. 1980; Vol. US4184996 A.
(13) Roviello, A.; Sirigu, A. *Die Makromolekulare Chemie* **1982**, *183*, 895.
(14) Roviello, A.; Sirigu, A. *Die Makromolekulare Chemie* **1980**, *181*, 1799.
(15) Rogers, M. E.; Long, T. E. *Synthetic Methods in Step-Growth Polymers*, 2003.
(16) Fischer, H.; Poser, S. *Acta Polymerica* **1996**, *47*, 413.
(17) Walther, M.; Finkelmann, H. *Progress in Polymer Science* **1996**, *21*, 951.
(18) Aguilera, C.; Bartulin, J.; Hisgen, B.; Ringsdorf, H. *Die Makromolekulare Chemie* **1983**, *184*, 253.
(19) Finkelmann, H.; Kock, H.-J.; Rehage, G. *Die Makromolekulare Chemie, Rapid Communications* **1981**, *2*, 317.
(20) Tang, W.; Farris, R. J.; MacKnight, W. J.; Eisenbach, C. D. *Macromolecules* **1994**, *27*, 2814.
(21) Thuillier, P.; Tessier, M.; Maréchal, E. *Molecular Crystals and Liquid Crystals Science and Technology. Section A. Molecular Crystals and Liquid Crystals* **1994**, *254*, 1.
(22) Kang, H.; Lin, Q.; Armentrout, R. S.; Long, T. E. *Macromolecules* **2002**, *35*, 8738.
(23) Lin, Q.; Pasatta, J.; Wang, Z.-H.; Ratta, V.; Wilkes, G. L.; Long, T. E. *Polym. Int.* **2002**, *51*, 540.
(24) Arnold, F. E.; Van Deusen, R. L. *Macromolecules* **1969**, *2*, 497.
(25) Nunes, R. W.; Martin, J. R.; Johnson, J. F. *Polymer Engineering & Science* **1982**, *22*, 205.
(26) Yeh, J.-M.; Liou, S.-J.; Lai, C.-Y.; Wu, P.-C.; Tsai, T.-Y. *Chemistry of Materials* **2001**, *13*, 1131.
(27) Odian, G. G. *Principles of polymerization*; Wiley-Interscience: Hoboken, N.J., 2004.
(28) Szycher, M. *Szycher's handbook of polyurethanes*; CRC Press: Boca Raton, 1999.
(29) Nelson, A. M.; Long, T. E. *Macromolecular Chemistry and Physics* **2014**, *215*, 2161.

(30) Prisacariu, C.; SpringerLink *Polyurethane elastomers: from morphology to mechanical aspects*; New York: Wien, 2011.
(31) Stribeck, N. *X-Ray Scattering of Soft Matter*; Springer Verlag, 2007.
(32) Tokita, M.; Watanabe, J. *Polym. J. (Tokyo, Jpn.)* **2006**, *38*, 611.
(33) Tokita, M.; Takahashi, T.; Hayashi, M.; Inomata, K.; Watanabe, J. *Macromolecules* **1996**, *29*, 1345.
(34) Krigbaum, W. R.; Asrar, J.; Toriumi, H.; Ciferri, A.; Preston, J. *Journal of Polymer Science: Polymer Letters Edition* **1982**, *20*, 109.
(35) Nishi, T.; Wang, T. T. *Macromolecules* **1975**, *8*, 909.
(36) Blumstein, R. B.; Stickles, E. M.; Gauthier, M. M.; Blumstein, A.; Volino, F. *Macromolecules* **1984**, *17*, 177.
(37) Takahashi, T.; Nagata, F. *Journal of Macromolecular Science, Part B* **1991**, *30*, 25.
(38) In *Polymer Microscopy*; Springer New York: 2008, p 478.
(39) Krigbaum, W. R.; Watanabe, J. *Polymer* **1983**, *24*, 1299.
(40) Visakh, P. M.; Thomas, S.; Chandra, A. K.; Mathew, A. P. *Advance in Elastomers I: Blends and Interpenetrating Networks*; Springer Berlin Heidelberg, 2013.
(41) Gorce, J.-N.; Hellgeth, J. W.; Ward, T. C. *Polymer Engineering & Science* **1993**, *33*, 1170.

4.8 *Supporting Information*

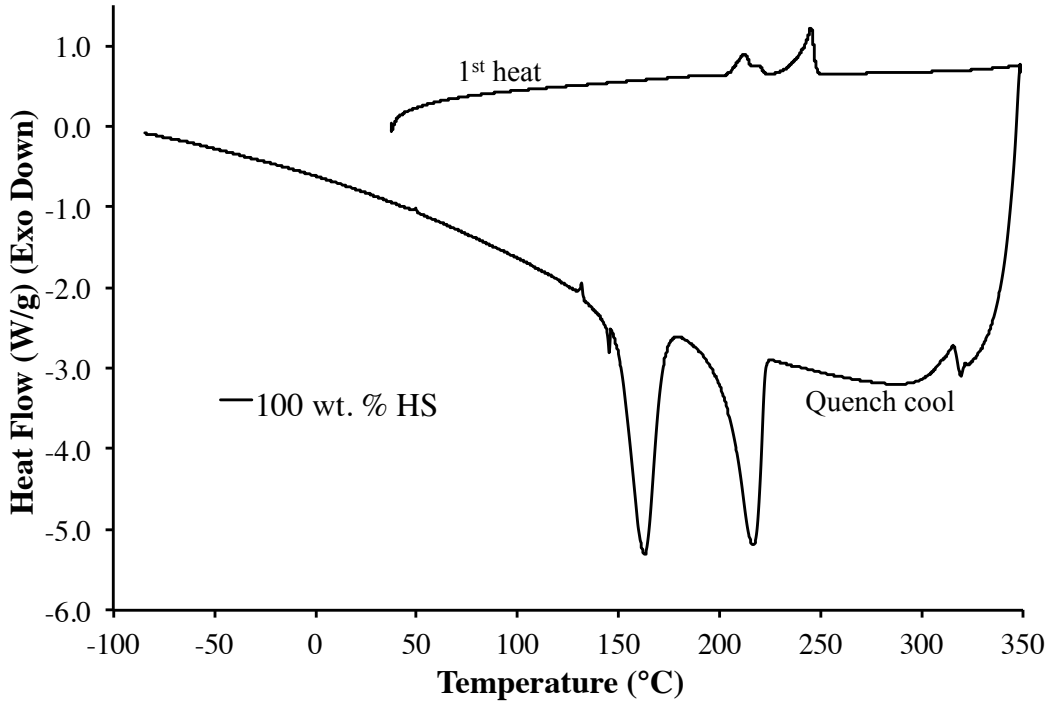

Figure 4.11. First heat and quench cooling cycle DSC thermogram of BB_6 homopolymer

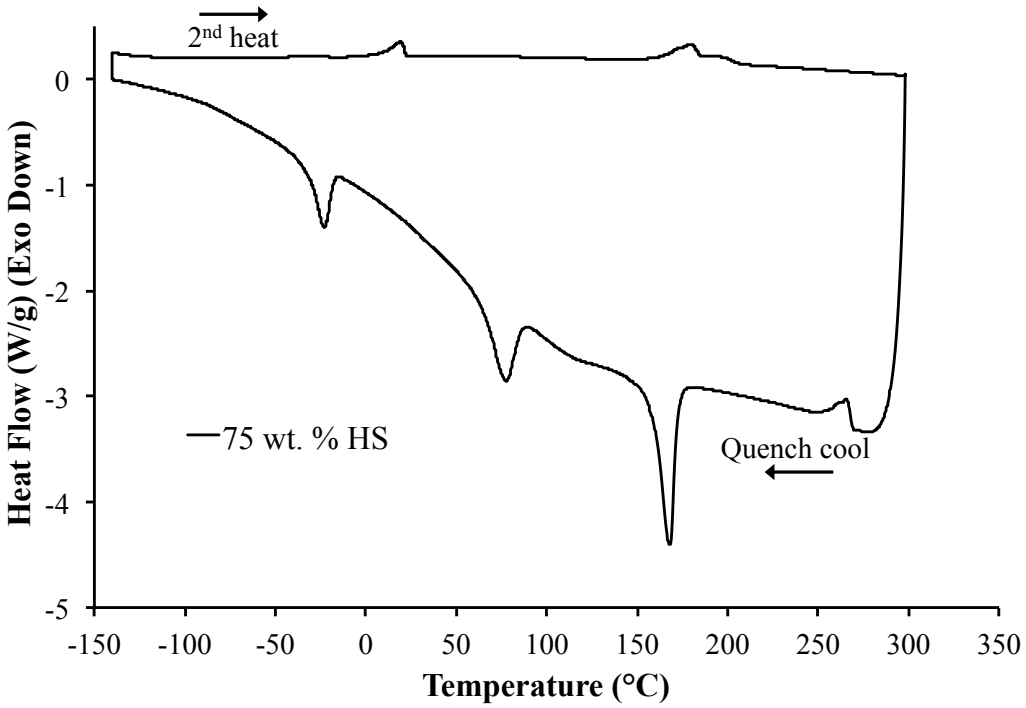

Figure 4.12. The quench cooling and second heat DSC curve for the liquid crystalline BB_5PTMO_{25} exhibiting a T_m and T_i for the hard segment and T_m for the soft segment

Table 4.4. Thermal transitions from DSC for the neat 2K P10R5 SS oligomer

SS	T_g (°C)	T_c (°C)	T_m (°C)
Pluronic®	-64	-25	17

Table 4.5. BB_6P10R5_{65} WAXD peaks and corresponding Bragg spacing

35 wt. % HS		
q (Å)	**2θ (deg)**	**d (Å)**
0.9	12.5	7.1
1.1	16.0	5.5
1.3	18.8	4.7
1.4	20.5	4.3
1.7	23.8	3.7
1.8	25.3	3.5
1.9	26.5	3.4
2.1	30.0	3.0
2.3	32.6	2.7
2.5	35.1	2.6
2.6	37.7	2.4
2.9	42.1	2.1
3.0	43.4	2.1
3.2	45.5	2.0

Table 4.6. BB_6P10R5_{50} WAXD peaks and corresponding Bragg spacing

50 wt. % HS		
q (Å)	**2θ (deg)**	**d (Å)**
0.8	11.3	7.8
0.9	12.6	7.0
1.1	16.1	5.5
1.3	18.7	4.7
1.4	19.6	4.5
1.4	20.4	4.4
1.5	21.8	4.1
1.7	23.7	3.8
1.8	25.2	3.5
1.9	26.4	3.4
2.0	28.1	3.2
2.1	29.8	3.0
2.3	32.7	2.7
2.5	35.3	2.5
3.0	43.2	2.1
3.3	47.7	1.9

Table 4.7. BB_6P10R5_{25} WAXD peaks and corresponding Bragg spacing

75 wt. % HS		
q (Å)	**2θ (deg)**	**d (Å)**
0.8	11.4	7.8
1.4	19.6	4.5
1.5	21.9	4.1
1.6	22.7	3.9
1.8	25.1	3.5
2.0	28.2	3.2
2.1	29.5	3.0
3.0	43.5	2.1

Table 4.8. BB_6 WAXD peaks and corresponding Bragg spacing

100 wt. % HS		
q (Å)	**2θ (deg)**	**d (Å)**
0.7	9.6	9.2
0.7	10.3	8.6
0.8	11.3	7.8
1.0	14.4	6.2
1.1	15.1	5.8
1.2	16.5	5.4
1.3	17.7	5.0
1.4	19.4	4.6
1.4	20.5	4.3
1.6	21.9	4.1
1.6	22.3	4.0
1.6	22.9	3.9
1.8	24.8	3.6
1.9	26.3	3.4
2.0	27.9	3.2
2.0	28.9	3.1
2.2	30.8	2.9
3.1	43.9	2.1

Chapter 5: Free Radical Polymerization of Caffeine-Containing Methacrylate Monomers

(Manuscript Just Accepted for Publication in the Journal of Polymer Science Part A: Polymer Chemistry)

Ashley M. Nelson, Sean T. Hemp, Jessica Chau, and Timothy E. Long

Department of Chemistry, Macromolecules and Interfaces Institute
Virginia Tech, Blacksubrg, VA 24061-0212

5.1 *Abstract*

The incorporation of acrylic functionality into caffeine enables the preparation of a vast array of novel thermoplastics and thermosets. A two-step derivatization provided a novel caffeine-containing methacrylate monomer capable of free radical polymerization. Copolymers of 2-ethylhexyl methacrylate and caffeine methacrylate (CMA) allowed for a systematic study of the effect of covalently bound caffeine on polymer properties. ^{1}H NMR and UV-vis spectroscopy confirmed caffeine incorporation at 5 and 13 mol %, and SEC revealed the formation of high molecular weight (co)polymers (> 40,000 g/mol). CMA incorporation resulted in a multi-step degradation profile with initial mass loss closely correlating to caffeine content. Differential scanning calorimetry, rheological, and thermomechanical analysis demonstrated that relatively low levels of CMA increased the glass transition temperature, resulting in higher moduli and elucidating the benefits of incorporating caffeine into polymers.

5.2 *Introduction*

Nature plays an inspirational role in polymer science, providing designs and templates for complex functions and properties as well as offering an abundance of renewable resources.[1,2] Research dealing with the incorporation of renewable or bio-based compounds into polymeric materials surged as environmental concerns and efforts towards sustainability increased.[3-5] Consideration of the effect of synthetic materials on the environment is pervasive in both academic and industrial laboratories.[6,7] One means to achieve the goals of green chemistry includes the synthesis of functional materials solely comprised of bioderived compounds, e.g., poly(lactic acid).[8] Alternatively, introducing small amounts of renewable compounds into a polymeric material offers a route to achieve increased sustainability while either attempting to maintain the original material properties or further tuning properties.[9] Monomers derived from corn feedstock, particularly sugar-based alcohols and acids such as 1,4:3,6-dianhydrohexitols and succinic acid found great success as they readily possess functional groups for derivatization and polymerization.[10-13]

Caffeine, a well-known stimulant present in coffee and chocolate, belongs to a class of molecules referred to as xanthines.[14,15] Other xanthine derivatives with a similar chemical structure include theophylline and theobromine, depicted in **Figure 1** below. Encapsulation, delivery, molecularly imprinted polymers (MIPs), and the effect on oxygen permeability of polyesters represent recent research topics for caffeine.[16-21] For example, Bowyer et al.[20] synthesized caffeine and theophylline MIPs using both microwave and thermally induced polymerization. The polymerization technique affected the rebinding affinity; microwave MIPs exhibited higher dissociation constants than the thermally induced MIPs. Caffeine nearly doubled the oxygen barrier as an additive in 500-mL poly(ethylene terephthalate) bottles.[16]

Oxygen transmission rates decreased from 0.046 cc/pkg/day for a bottle without caffeine to 0.0306 cc/pkg/day and 0.0261 cc/pkg/day with only 3 and 5 weight percent caffeine incorporation respectively. The patent invokes an antiplasticization effect of caffeine, however, the origin of this dramatic increase in gas barrier has remained unexplored.

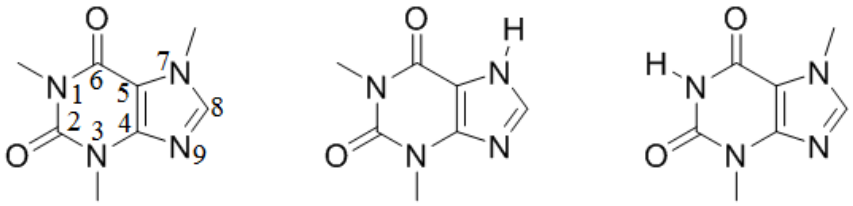

Figure 5.1. Chemical structures of caffeine (with atoms numbered for reference), theophylline, and theobromine

Natural polymers, chemicals, and chemical processes exhibit a high level of structural complexity, bestowing intricate functions and properties.[22] Many strive toward mimicking natural design when synthesizing polymers, such as the ability of a gecko to walk on walls, the color-changing capabilities of a chameleon, and our own biological code – deoxyribonucleic acid (DNA).[23-25] Polymerizable functional groups or reactive sites are essential for chemical derivatization and polymerization. Unlike adenine, caffeine does not contain a readily reactive functional group such as an amine. This aromatic heterocycle, which contains hydrogen bond accepting carbonyls, non-covalently interacts with receptors and remains unaltered chemically.[26] In the early 1970's, Salomon and coworkers[27,28] reported the ability to incorporate hydroxyl functionality at the 8-position of caffeine, adenine, adenosine, guanosine, and 2'-deoxyguanosine. **Figure 2** depicts the chemical similarity between adenosine, caffeine, and the nucleobase adenine. More recently, Alami et al.[29] alkenylated at the 8-position of caffeine with a Pd/Cu

catalyzed coupling reaction. Upon careful analysis of the literature, caffeine is present in many publications; however, derivatizing and covalently incorporating caffeine into a copolymer remains unexplored.

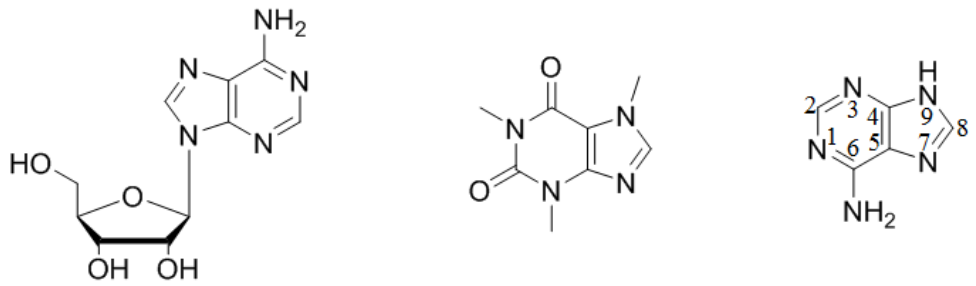

Adenosine Caffeine Adenine

Figure 5.2. Chemical structures of adenosine, caffeine, and adenine (with atoms numbered for reference)

In this manuscript, we describe for the first time the synthesis, polymerization, and physical characterization of caffeine-containing copolymers. A novel caffeine methacrylate (CMA) monomer, which is available from a photoreaction to introduce an alcohol and subsequent reaction with methacryloyl chloride, readily underwent free radical copolymerization with 2-ethylhexyl methacrylate (EHMA). Poly(EHMA) served as a control, and incorporation of various amounts of CMA allowed for an investigation of the effect of caffeine on acrylic copolymer properties. ^{1}H NMR spectroscopy confirmed CMA incorporation, and CMA altered the thermal, thermomechanical, rheological, and UV-vis absorbance properties. These copolymers demonstrate the capability and feasibility of incorporating the renewable resource caffeine into acrylic polymers and elucidate the influence of the heterocyclic structure on polymer properties.

5.3 *Experimental*

5.3.1 Materials

Caffeine (99 %), methacryloyl chloride (MAC; 97 %), Luperox® DI (di-*tert*-butyl peroxide, DBP; 98 %), and dioxane (spectrophotometric grade, 99+ %) were obtained from Sigma Aldrich and used as received. Triethylamine (TEA; Sigma Aldrich; ≥ 99 %) was distilled from calcium hydride prior to use. 2-ethylhexyl methacrylate (EHMA; Sigma Aldrich; 98 %) was eluted through an aluminum oxide column to remove inhibitor prior to use. 4,4'-Azobis(4-cyanopentanoic acid) (V-501; Sigma Aldrich; ≥ 98 %) was recrystallized from ethanol prior to use. Chloroform ($CHCl_3$), methanol (MeOH), isopropanol (IPA), and tetrahydrofuran (THF; stabilized with 0.025 % BHT) were purchased from Spectrum Chemicals and used as received. Ethanol (EtOH) was obtained from Decon Laboratories, Inc and used as received. Dry dichloromethane (DCM) was obtained upon treatment with a Innovative Technology Puresolve solvent system.

5.3.2 Analytical Methods

^{1}H NMR spectroscopy was performed on a Varian Inova or Agilent U4-DD2 400 MHz spectrometer with samples prepared in deuterated chloroform ($CDCl_3$) or deuterated dimethyl sulfoxide ($DMSO_{d6}$). Dynamic light scattering (DLS) using a Malvern Zetasizer Nano ZS at 25 °C provided the hydrodynamic diameter of the copolymers in THF. The (co)polymer solutions were filtered through a 0.45 μm PTFE syringe filter prior to analysis and the results are an average of 3 runs. Size exclusion chromatography (SEC) was performed in THF on a Waters 515 HPLC pump equipped with a Waters 717plus autosampler. Samples were analyzed at a

concentration of 1 mg/mL in THF through a series of three Polymer Laboratories PLgel 5 μm MIXED-C columns at a flow rate of 1 mL/min and results obtained using a Waters 2414 refractive index (RI) detector and Wyatt Technology Corporation Mini-dawn MALLS detector. Absolute molecular weight data was obtained using the d*n*/d*c* value for poly(EHMA) in THF determined offline with a Wyatt Technology Optilab® T-rEX refractive index detector. Thermal transitions of the (co)polymers were obtained using a TA Instruments Q50 TGA and TA Instruments Q1000 DSC affording degradation temperatures (T_d) and glass transition temperatures (T_g) respectively. A heating rate of 10 °C/min was used for the TGA and a heat/cool/heat method of 10 °C/min from room temperature to 100 °C, 10 °C/min from 100 °C to -80 °C, and 10 °C/min from -80 °C to 100 °C was used for the DSC and thermograms reported from the second heating, ensuring all samples had identical thermal history.

5.3.2.1 Photoreactions

Photoreactions were conducted in an Ace Glass photochemical safety cabinet using a 24.4475 cm 450 W ultraviolet (UV) immersion lamp connected to a 120 V, 60 Hz, 450 W UV power supply. The UV immersion lamp was placed inside a water-cooled condenser which fit inside a Pyrex® apparatus equipped with a N_2 inlet and outlet.

5.3.2.2 Thermomechanical Analysis

Dynamic mechanical analysis (DMA) was performed on a TA Instruments Q800 DMA in tension mode conducted at a frequency of 1 Hz. Samples were equilibrated at -50 °C, held for 5 min, and then heated at a rate of 3 °C/min until flow. Polymer films were solution-cast from

$CHCl_3$ onto a Mylar sheet, maintained at 20 °C overnight, placed in a vacuum oven at ca. 50 °C for at least 7.5 h, and finally vacuum was closed and the film remained at 50 °C for at least 22 h.

5.3.2.3 Ultraviolet-Visible Spectroscopy

A Ocean Optics Inc. USB 2000 spectrometer coupled to a CUV sample holder providing a 1 cm pathlength enabled ultraviolet-visible (UV-Vis) spectroscopy. An Analytical Inst. Systems Model DT 1000CE UV light source provided a wavelength range of 190 – 850 nm. All solutions were prepared in dioxane and measurements occurred in a quartz cuvette. 10^{-4} M caffeine control solutions and $2.6(10^{-5})$ M caffeine-containing copolymer solutions (normalized to caffeine content) were suitable for quantitative absorbance measurements.

5.3.2.4 Melt Rheology

A TA Instruments Discovery HR-2 hybrid rheometer equipped with an environmental test chamber (ETC) provided time-temperature superposition (TTSP) melt rheology data. The measurements were performed using an 8 mm parallel plate steel geometry. An amplitude sweep was conducted first to ensure frequency measurements were performed at a strain within the viscoelastic regime of the material, and master curves were shifted to a reference temperature (T_{ref}) of 30 °C. Complex viscosity data was also reported for all samples at 30 °C.

5.3.2.5 Synthesis of hydroxyl functionalized caffeine

The procedure involved an adaptation of a previously reported procedure[27] and the MeOH, EtOH, and IPA caffeine derivatives were all prepared in a similar manner. The photoreactions were conducted in the setup described above. For example, the synthesis of the MeOH derivative, 8-(hydroxymethyl)-1,3,7-trimethyl-3,7-dihydro-1*H*-purine-2,6-dione, follows.

10.0 g of caffeine, 87 mL of reverse osmosis (RO) water, and 350 mL of MeOH were added to the photoreactor glassware with a magnetic stir bar. 25 mL of DBP was then added to the reaction and a 15 min N_2 purge with stirring was allowed prior to UV irradiation. Upon irradiation, aliquots were extracted to monitor the progress of the reaction. Excess reagents were removed using a rotary evaporator and the crude mixture was dried in a vacuum oven (~50 mmHg) at ca. 90 °C overnight. The crude reaction mixture was used in the subsequent acid chloride reaction; however, isolation of the compound was possible using silica gel chromatography. The crude reaction mixture was dissolved in 1:1 $CHCl_3$:MeOH, loaded onto the column and eluted with a 9:1 $CHCl_3$:MeOH solvent mixture. Prior to running the column, thin layer chromatography (TLC) was performed to ensure good separation. Using the aforementioned solvent system, caffeine exhibited an R_f value of 0.46 and the product exhibited an R_f value of 0.23. After collecting the product from the column, a rotary evaporator removed the solvent and the product was dried in a vacuum oven at ca. 40 °C. The isolated product (93 % pure via NMR) was a white solid. HRMS: calcd for $C_9H_{12}N_4O_3$, 224.09; found, 224.09. ^{1}H NMR (400 MHz, DMSO-d_6, δ): 3.90 (s, 3H, -N-CH_3), 3.39 (s, 3H, -N-CH_3), 3.20 (s, 3H, -N-CH_3), 4.57 (d, 2H, -CH_2-), 5.64 (t, 1H, -O*H*).

8-(1-hydroxyethyl)-1,3,7-trimethyl-3,7-dihydro-1*H*-purine-2,6-dione (EtOH derivative). HRMS: calcd for $C_{10}H_{14}N_4O_3$, 238.11; found, 238.05. ^{1}H NMR (400 MHz, $CDCl_3$, δ): 3.95 (s, 3H, -N-CH_3), 3.49 (s, 3H, -N-CH_3), 3.33 (s, 3H, -N-CH_3), 4.94 (q, 1H, -C*H*-), 1.58 (d, 3H, -CH_3-), 2.85 (br, -O*H*).

8-(2-hydroxypropan-2-yl)-1,3,7-trimethyl-3,7-dihydro-1*H*-purine-2,6-dione (IPA derivative, crude). ^{1}H NMR (400 MHz, $CDCl_3$, δ): 4.10 (s, 3H, -N-CH_3), 3.43 (s, 3H, -N-CH_3), 3.27 (s, 3H, -N-CH_3), 1.62 (s, 6H, -(CH_3)$_2$), 2.72 (br, -O*H*).

5.3.2.6 Synthesis of caffeine methacrylate

Methacrylates were synthesized from both the MeOH and EtOH caffeine derivatives. Starting from the MeOH caffeine derivative, the following procedure describes the synthesis of (1,3,7-trimethyl-2,6-dioxo-2,3,6,7-tetrahydro-1*H*-purin-8-yl)methyl methacrylate (CMA). Dry DCM was added to the crude hydroxyl functionalized caffeine reaction mixture. The dissolved mixture in DCM was cannulated into a dry round-bottomed flask equipped with a magnetic stir bar. Using dry syringe techniques, TEA (0.1 mol equivalent excess compared to MAC) was added to the reaction and the contents were stirred in an ice bath. MAC was added to the reaction and the reaction was allowed to proceed, slowly warming up to room temperature with stirring overnight. A rotary evaporator removed excess reagents. Conventional free-radical polymerization was performed on the crude reaction mixture; however, dissolving the crude mixture in 20:1 $CHCl_3$:MeOH and eluting with 2:1 $CHCl_3$:acetone on a silica gel column allowed for CMA isolation. After collecting the appropriate fractions from the column, rotary evaporation removed the solvent and the product was dried in a vacuum oven at 50 °C overnight. HRMS: calcd for $C_{13}H_{16}N_4O_4$, 292.12; found, 292.12. ^{1}H NMR (400 MHz, $CDCl_3$, δ): 4.03 (s, 3H, -N-C*H*$_3$), 3.57 (s, 3H, -N-C*H*$_3$), 3.40 (s, 3H, -N-C*H*$_3$), 5.27 (s, 2H, -C*H*$_2$-), 6.16 (s, 1H, -*H*), 5.65 (t, 1H, -*H*), 1.95 (s, 3H, -C-C*H*$_3$).

1-(1,3,7-trimethyl-2,6-dioxo-2,3,6,7-tetrahydro-1*H*-purin-8-yl)ethyl methacrylate (from EtOH caffeine derivative). HRMS: calcd for $C_{14}H_{18}N_4O_4$, 306.13; found, 306.13. ^{1}H NMR (400 MHz, $CDCl_3$, δ): 4.01 (s, 3H, -N-C*H*$_3$), 3.56 (s, 3H, -N-C*H*$_3$), 3.38 (s, 3H, -N-C*H*$_3$), 6.02 (q, 1H, -C*H*-), 1.73 (d, 3H, -C-C*H*$_3$), 6.15 (t, 1H, -*H*), 5.63 (t, 1H, -*H*), 1.94 (t, 3H, -C-C*H*$_3$).

5.3.2.7 Free radical copolymerization of (1,3,7-trimethyl-2,6-dioxo-2,3,6,7-tetrahydro-1*H*-purin-8-yl)methyl methacrylate (CMA)

Conventional free radical polymerization afforded poly(ethylhexyl methacrylate) (poly(EHMA)) and caffeine-containing copolymers. All polymerizations were conducted in dioxane at 10 % solids using 4,4′-azobis(4-cyanopentanoic acid) (V-501) as the free radical initiator (0.67 mol % for EHMA and 1.0 mol % for the copolymerizations). The reagents were added to a single-neck, round-bottomed, flask equipped with a magnetic stir bar, sparged with an inert gas, and then allowed to react for approximately 24 h at 70 °C. Polymers were isolated upon precipitation into MeOH for poly(EHMA) and poly($EHMA_{95}$-*co*-CMA_5), 80:20 MeOH:H_2O for poly($EHMA_{87}$-*co*-CMA_{13}); all products were filtered and dried in vacuo at 50 °C overnight.

5.4 *Results and Discussions*

5.4.1 Synthesis and Copolymerization of Caffeine-containing Methacrylate

Caffeine lacks functional groups capable of undergoing polymerization, thus chemical modification was necessary to achieve a caffeine-based monomer. Previous literature reported the methodology to introduce hydroxyl functionality at the 8-position of a variety of purine derivatives using a peroxide-initiated photoreaction between the purine and alcohol.[27] This reaction served as a first step, placing the reactive hydroxyl group on caffeine allowing for further derivatization to a methacrylate. **Scheme 1** depicts the photoreaction and conditions used to synthesize the methanol caffeine derivative. The bond created in the photoreaction forms at the carbon directly adjacent to the hydroxyl group, therefore, different alcohols (methanol,

ethanol, and isopropanol) afforded caffeine with a primary, secondary, and tertiary hydroxyl, respectively.

Scheme 5.1. Synthesis of hydroxyl-functionalized caffeine using a peroxide-initiated photoreaction

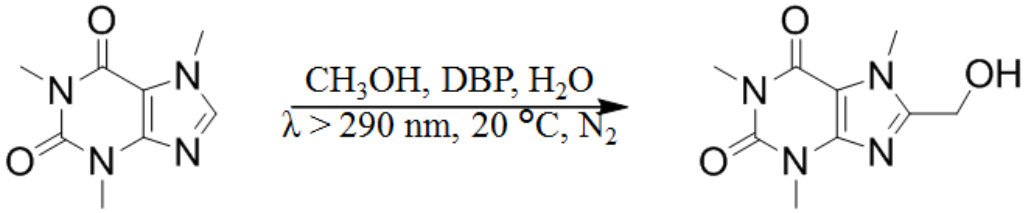

Figure 3 depicts the chemical structures and caffeine conversion as a function of exposure time for the three hydroxyl-functionalized caffeine derivatives. Caffeine conversion plateaued at 30 % for each reaction despite the stability difference between the three carbon radical intermediates (1° < 2° < 3°). Murgida et al.[30] studied the photoreaction of caffeine, theophylline, and theobromine (**Figure 1**) initiated with benzophenone. The proposed mechanism included a caffeine radical intermediate formed upon reaction of caffeine with the alcohol-based radical. The final product, hydroxyl-functionalized caffeine, ultimately formed from coupling of the radical intermediate of caffeine with either the alcohol-based radical or the benzophenone radical. Two routes prohibit the necessary caffeine radical intermediate: (1) combination of two alcohol-based radicals, and (2) combination of the photoinitiator radical with an alcohol-based radical. The molar excess of alcohol to both caffeine and peroxide in our reaction (173:1:6 respectively for the MeOH derivative) favors alcohol-based radical combination/termination, presumably eliminating the effect of radical stability on caffeine intermediate formation, resulting in similar conversion for each reaction.

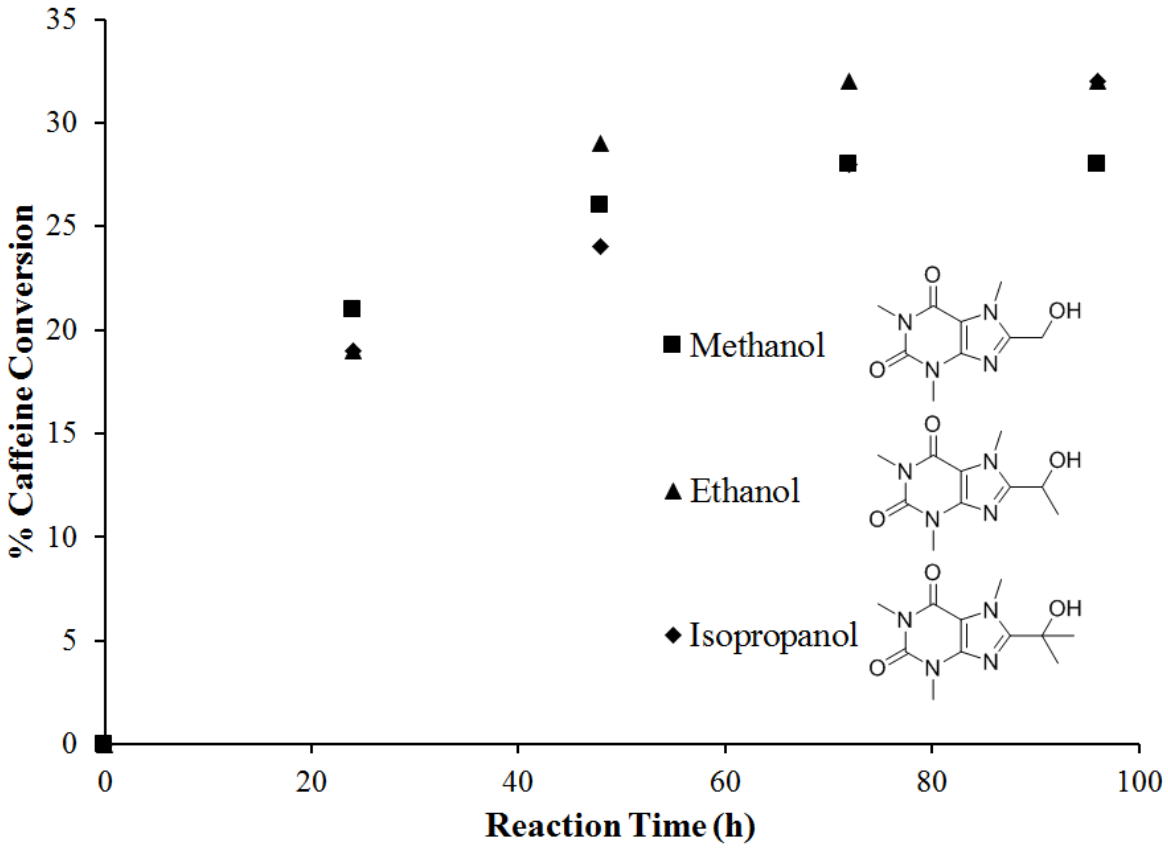

Figure 5.3. Photoreaction kinetics of caffeine with various alcohols as a function of time, determined using ^{1}H NMR spectroscopy, with primary (methanol), secondary (ethanol), and tertiary (isopropanol) radicals showing the independence of radical intermediate stability

Placing the hydroxyl group on caffeine provided a reactive chemical site for further derivitization to a polymerizable methacrylate. A commonly employed reaction with methacryloyl chloride (MAC), as depicted in **Scheme 2**, provided a caffeine methacrylate (CMA) monomer.[31,32] This second and final reaction in the monomer synthesis succeeded on the crude photoreaction mixtures, eliminating challenging isolation and purification steps. **Figure 13** displays the ^{1}H NMR spectrum for CMA. 2-ethylhexyl methacrylate (EHMA), which is a well-studied monomer providing a low glass transition temperature (T_g), served as a comonomer to observe the influence of caffeine on thermomechanical properties.[33-35] Conventional free

radical copolymerization in dioxane of commercially available EHMA, CMA, and V-501 as a radical initiator, as represented in **Scheme 3**, generated copolymers containing covalently bound caffeine. Varying feed ratios of CMA to EHMA afforded a series of caffeine-containing copolymers.

Scheme 5.2. Synthesis of caffeine methacrylate (CMA) monomer

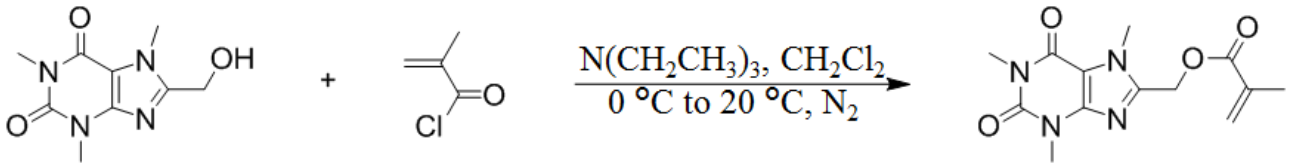

Scheme 5.3. Synthesis of caffeine-containing copolymers using conventional free radical polymerization

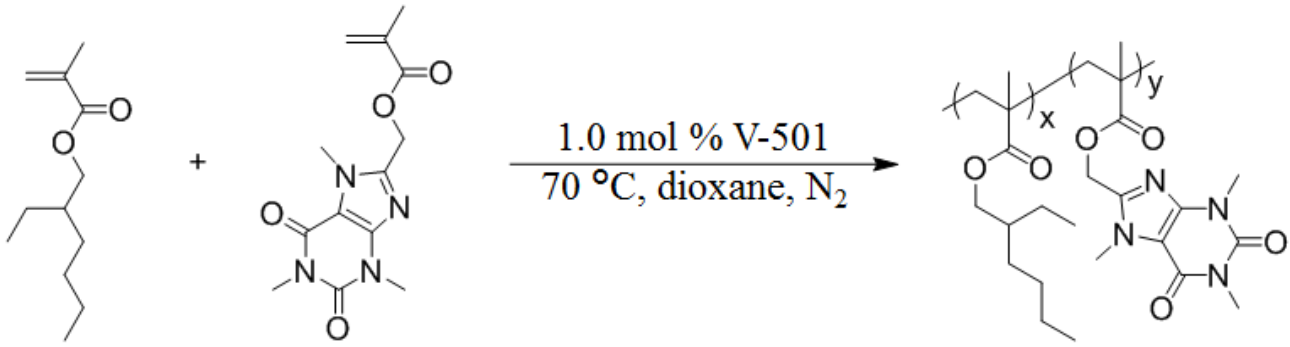

5.4.2 Structural Confirmation and Molecular Weight Analysis of Poly(EHMA$_x$-*co*-CMA$_y$)

Copolymerization proceeded on crude CMA to expedite synthesis and eliminate unnecessary solvent and waste from workup procedures. This strategy prevented a determination of an accurate CMA feed ratio, therefore NMR after polymer purification provided actual mol % CMA incorporation. **Figure 4** depicts the ^{1}H NMR spectra of poly(EHMA$_{95}$-*co*-CMA$_5$). The region below 2 ppm corresponds to the backbone peaks and pendant alkyls on EHMA; however, integration of the distinct resonances for the three methyl groups on caffeine and the methylene

adjacent to the ester for each monomer quantified mol % CMA. Purified control poly(EHMA) and CMA copolymers containing 5 and 13 mol % CMA (using integrations from resonance *a* and *d* in **Figure 4**) allowed for an investigation of the impact of CMA on polymeric properties. Precipitation revealed an initial solubility difference; poly($EHMA_{87}$-*co*-CMA_{13}) required an 80:20 MeOH:H_2O mixture as opposed to 100 % MeOH for poly(EHMA) and poly($EHMA_{95}$-*co*-CMA_5).

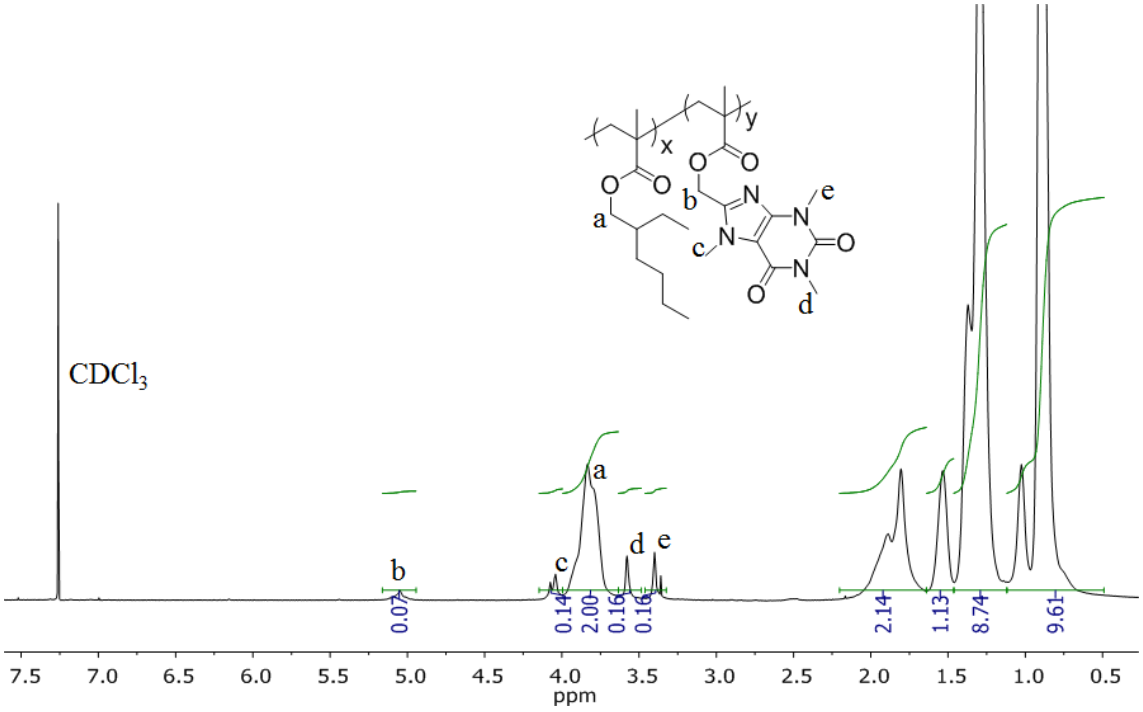

Figure 5.4. Structural confirmation of poly($EHMA_{95}$-co-CMA_5) using ^{1}H NMR spectroscopy

UV-Vis spectroscopy is a common analytical tool for evaluating conjugated molecules and polymers.[36,37] Researchers utilized UV-Vis measurements to quantify and detect caffeine for various applications including determining the concentration in coffee and investigating mutagenic activity.[38-40] **Figure 5** displays the UV-Vis absorption spectra for caffeine, poly($EHMA_{95}$-*co*-CMA_5), and poly($EHMA_{87}$-*co*-CMA_{13}), confirming successful caffeine incorporation. Neat caffeine exhibited a maximum wavelength (λ_{max}) of 276 nm while

poly(EHMA$_{95}$-*co*-CMA$_5$) and poly(EHMA$_{87}$-*co*-CMA$_{13}$) revealed similar elevated λ_{max} values of 282 nm and 283 nm, respectively. Increased conjugation enhances the stability of the π* state, which simultaneously decreases the energy required for the transition ultimately increasing the wavelength of absorption.[36,37] Therefore, the additional π bond and resonance present in the CMA-containing copolymers from the ester could account for the observed bathochromic shift.

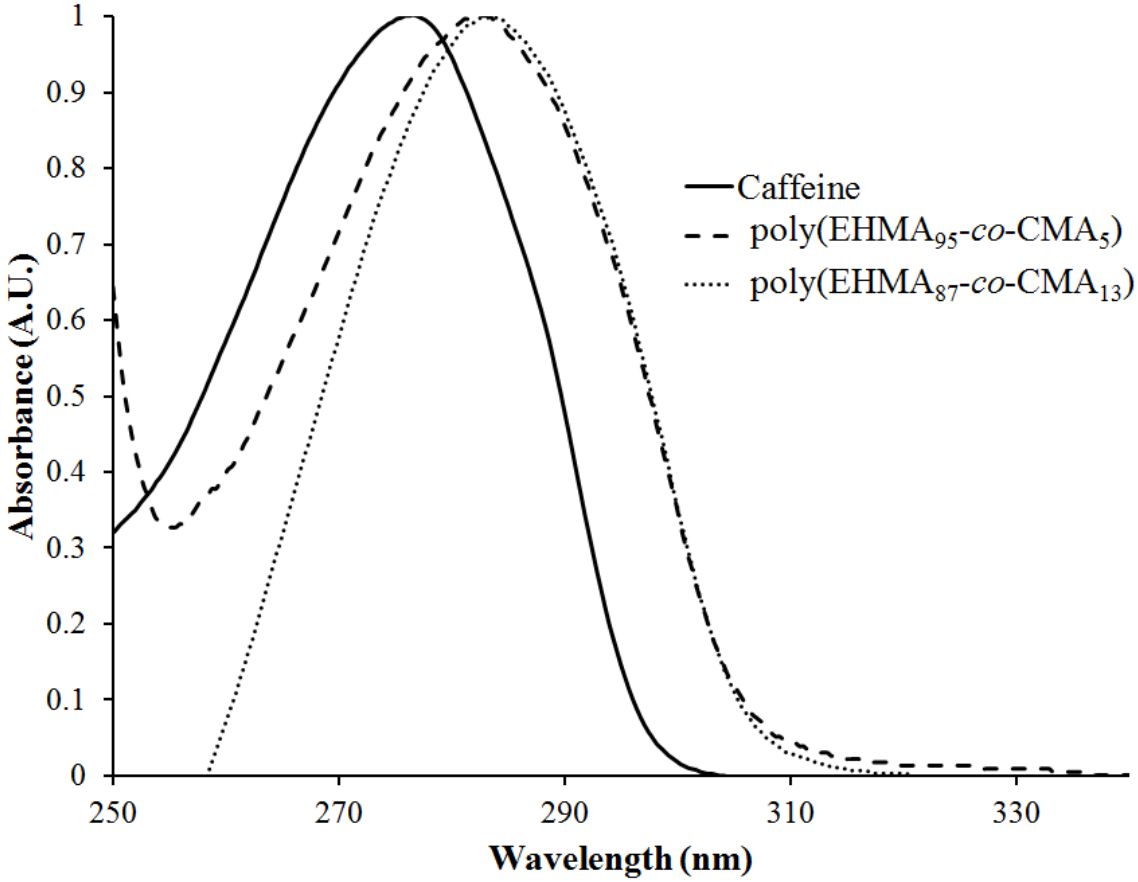

Figure 5.5. Normalized absorbance spectra for CMA-containing copolymers, including a caffeine control in dioxane showing a distinct red shift when caffeine is bound to the polymer backbone

Size exclusion chromatography (SEC) in THF provided absolute molecular weight analysis of poly(EHMA), poly(EHMA$_{95}$-*co*-CMA$_5$), and poly(EHMA$_{87}$-*co*-CMA$_{13}$). **Figure 6** depicts the light scattering (LS) traces and **Table 1** displays the corresponding weight-average

molecular weight (M_w) and polydispersity index (PDI) for each copolymer. Offline determination of the refractive index increment, d*n*/d*c*, for poly(EHMA) afforded absolute molecular weight. Using the d*n*/d*c* value addressed the chemical dissimilarity between the CMA-containing series and the polystyrene chromatography columns; however, it is important to emphasize that the poly(EHMA) d*n*/d*c* generated the molecular weight data for all three (co)polymers in the series. A separate determination of the d*n*/d*c* value for each copolymer composition would minimize the effect of compositional differences on the results.

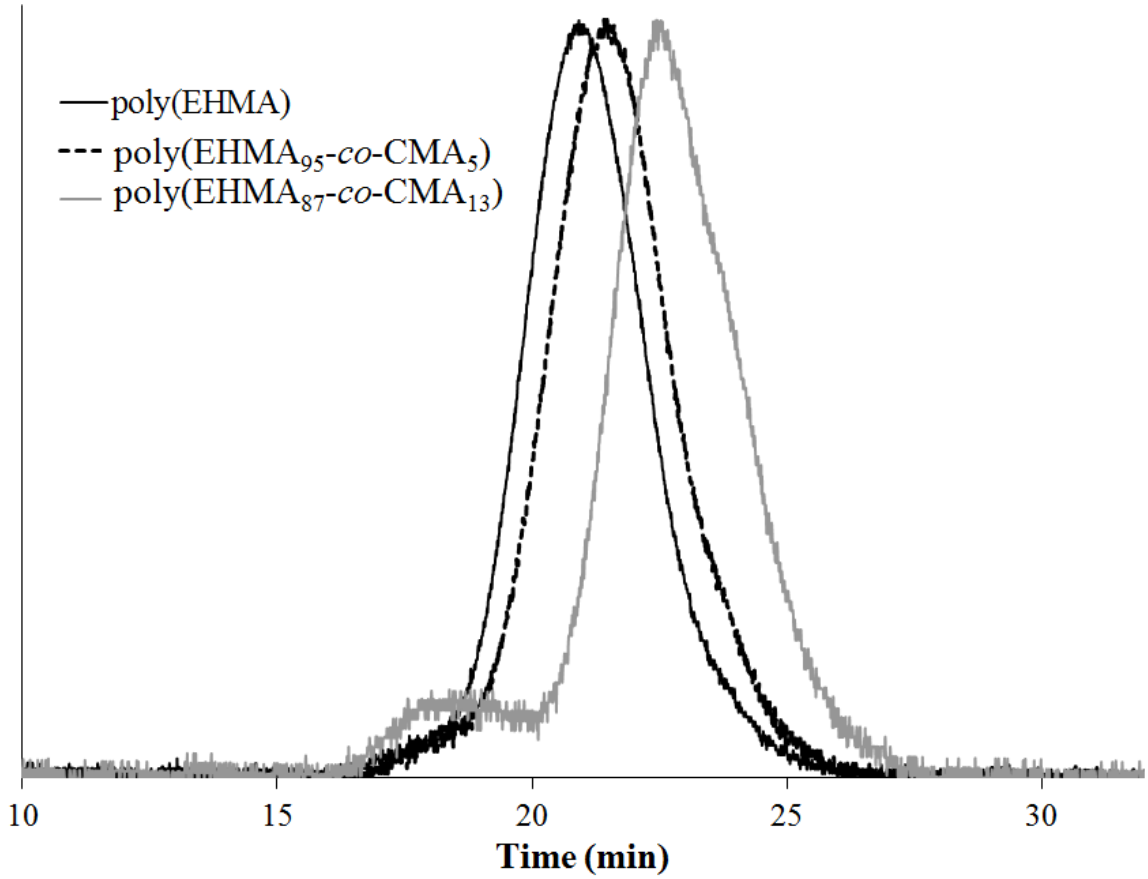

Figure 5.6. Light scattering SEC chromatograms of poly(EHMA) control and caffeine-containing copolymers

The three LS traces in **Figure 6** show poly(EHMA) eluting first corresponding to the highest M_w of 99.2 kg/mol (**Table 1**). Although lower, both poly($EHMA_{95}$-*co*-CMA_5) and

poly(EHMA$_{87}$-*co*-CMA$_{13}$) exhibited suitable M_ws for conventional free radical polymerization of 78.5 kg/mol and 40.1 kg/mol, respectively. A higher concentration of V-501 initiated the 5 and 13 mol % CMA copolymers compared to the poly(EHMA) control. Since polymerization rate scales according to the square root of initiator concentration, the increased V-501 concentration lowers the final attainable polymer molecular weight and presumably contributed to the observed decreased M_w.[41] Poly(EHMA) and poly(EHMA$_{95}$-*co*-CMA$_5$) displayed monomodal LS traces, whereas poly(EHMA$_{87}$-*co*-CMA$_{13}$) contained a high molecular weight shoulder and slight low molecular weight shoulder. This could originate from the isolation procedure and/or poor THF dissolution during chromatography for this particular copolymer composition. Dynamic light scattering (DLS) in THF of the (co)polymers showed monomodal hydrodynamic diameter distributions (99.9 % of mean volume) of 12 ± 5 nm, 9 ± 3 nm, and 8 ± 2 nm for poly(EHMA), poly(EHMA$_{95}$-*co*-CMA$_5$), and poly(EHMA$_{87}$-*co*-CMA$_{13}$), respectively. These results provided evidence for good solubility in THF to ensure reliable SEC data. In lieu of the high molecular weight shoulder present in poly(EHMA$_{87}$-*co*-CMA$_{13}$), DLS also specified hydrodynamic diameter as a function of intensity. An aggregation peak near 100 nm increased with increasing CMA content from 7 % for poly(EHMA) to 30 % and 49 % for poly(EHMA$_{95}$-*co*-CMA$_5$) and poly(EHMA$_{87}$-*co*-CMA$_{13}$), respectively. This aggregation could account for the observed shoulder in the poly(EHMA$_{87}$-*co*-CMA$_{13}$) SEC trace. **Figure 14** displays the hydrodynamic diameters for the (co)polymers as a function of mean volume % (**a**) and mean intensity % (**b**).

Table 5.1. Molecular weight and thermal degradation of caffeine-containing copolymers

Mol % CMA[a]	Wt. % CMA	M_w (kg/mol)[b]	PDI[b]	$T_{d1,onset}$ (°C)[c]	Wt. $Loss_{d1}$ (%) [c]	$T_{dfinal,onset}$ (°C) [c]
0	0	99.2	2.13	269	N.D.	N.D.
5	7	78.5	1.89	195	10	313
13	18	40.1	2.12	194	13	315

a: Calculated from ^{1}H NMR
b: Absolute molecular weight data obtained from THF SEC at 40 °C using d*n*/d*c* = 0.088
c: TA Instruments Q50 thermogravimetric analyzer (TGA) heating at 10 °C/min
N.D. = not detected

5.4.3 Thermal, Thermomechanical, and Rheological Characterization of Caffeine-containing Copolymers

Thermogravimetric analysis (TGA) provided weight loss as a function of temperature in a N_2 atmosphere for the (co)polymer series. Poly(EHMA) displayed a one-step degradation occurring at 228 °C while both poly($EHMA_{95}$-*co*-CMA_5) and poly($EHMA_{87}$-*co*-CMA_{13}) displayed multi-step degradation profiles. **Figure 7** depicts the decomposition curves and **Table 1** specifies the degradation temperatures (T_d) and corresponding % weight loss. CMA-containing copolymers displayed an initial degradation lower than poly(EHMA), however, the largest degradation step of the copolymers increased ~50 °C compared to poly(EHMA). The final degradation temperature increased from 269 °C for poly(EHMA) to 313 °C and 315 °C for poly($EHMA_{95}$-*co*-CMA_5) and poly($EHMA_{87}$-*co*-CMA_{13}), respectively. Additionally, the absence of early weight loss suggested the absence of volatile by-products.

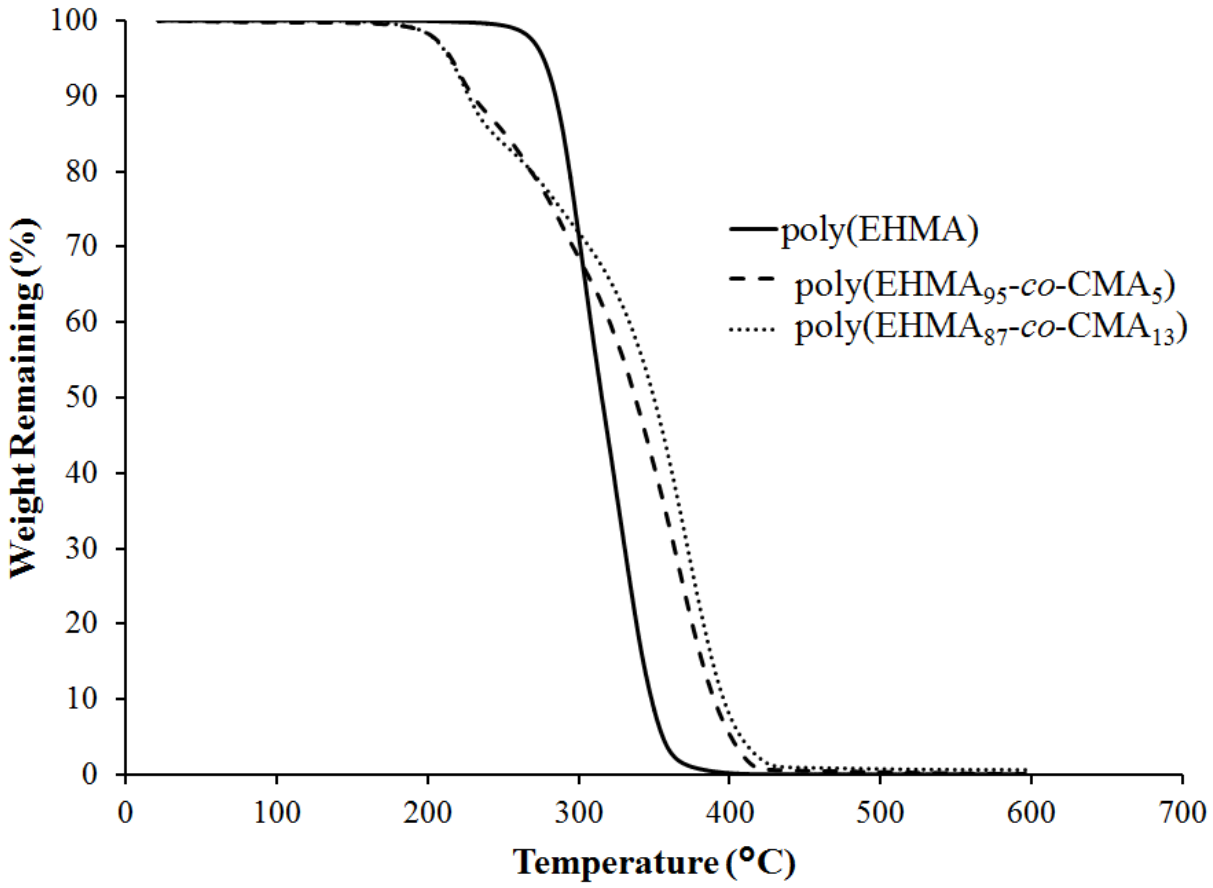

Figure 5.7. Two-step thermal degradation profile of caffeine-containing copolymers

Interestingly, the initial wt. loss in poly(EHMA$_{95}$-*co*-CMA$_5$) and poly(EHMA$_{87}$-*co*-CMA$_{13}$) closely correlated to the loss of pendant caffeine. Beta hydrogen elimination is a commonly reported degradation route for methacrylates with pendant side chains or groups.[42-44] CMA, however, does not contain any beta hydrogens eliminating the common route as a possible mechanism for caffeine loss. Fodor et al.[45] extensively researched the thermal decomposition of poly(*N*-vinylimidazole) using pyrolysis-gas chromatography/mass spectrometry (Py-GC/MS). This highly sensitive analytical technique identified 10 different small molecule byproducts, one of them being imidazole. **Figure 8** depicts the proposed mechanism (left) constructed to support imidazole as a decomposition product. As discussed above, the photoreaction in the first step of CMA synthesis occurs through a radical intermediate at the same position on caffeine in which

the proposed degradation mechanism occurs. With the propensity of caffeine to lose a hydrogen at the same attachment point, the right side of **Figure 8** proposes a mechanism of sidegroup elimination and subsequent hydrogen abstraction to explain the observed caffeine loss.

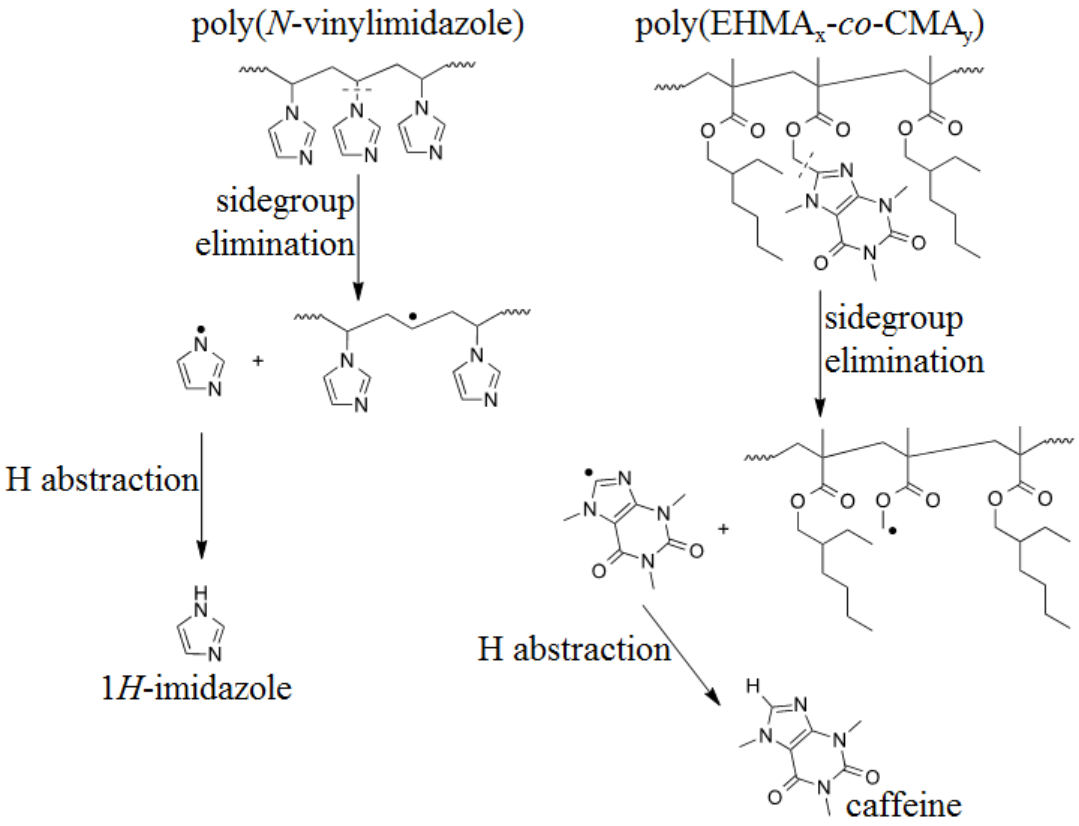

Figure 5.8. Proposed thermal degradation route of caffeine-containing copolymers resulting in the loss of free caffeine. Adapted with permission.[45]

Differential scanning calorimetry (DSC) revealed a broad glass transition temperature for poly(EHMA), poly(EHMA$_{95}$-*co*-CMA$_5$) and poly(EHMA$_{87}$-*co*-CMA$_{13}$). Although difficult to assign an exact value due to the breadth of the transition, the observed T_g of poly(EHMA) corresponded well with the literature value of ~-10 °C.[33] Incorporating caffeine increased the T_g of the polymers, visible from the plateau of the step-wise T_g shifting to the right for poly(EHMA$_{95}$-*co*-CMA$_5$) and higher for poly(EHMA$_{87}$-*co*-CMA$_{13}$). The lack of any

endothermic transitions indicated amorphous (co)polymers, and a single T_g suggested random copolymerization of the two methacrylates without microphase-separation. Placing hydrogen bonding sites pendant to the polymer backbone, Zhang et al.[46] observed highly-ordered lamellar morphologies. Cheng and coworkers[47] also observed H-bonding driven self-assembly upon synthesizing poly(acrylates) containing 7 mol % of an adenine-containing acrylate. Surprisingly, polymerizing a thymine-containing acrylate in concentrations up to 30 mol % incorporation did not exhibit any self-assembly. Caffeine does not hydrogen bond with itself, however, the aromatic structure is prone to π-π stacking.[48-50] It is proposed that placing the caffeine pendant group further from the backbone will increase mobility, enabling the aromatic groups to π-π stack and potentially resulting in a distinct caffeine-rich phase. Additionally, increasing CMA content will promote π-π stacking through a proximity effect.

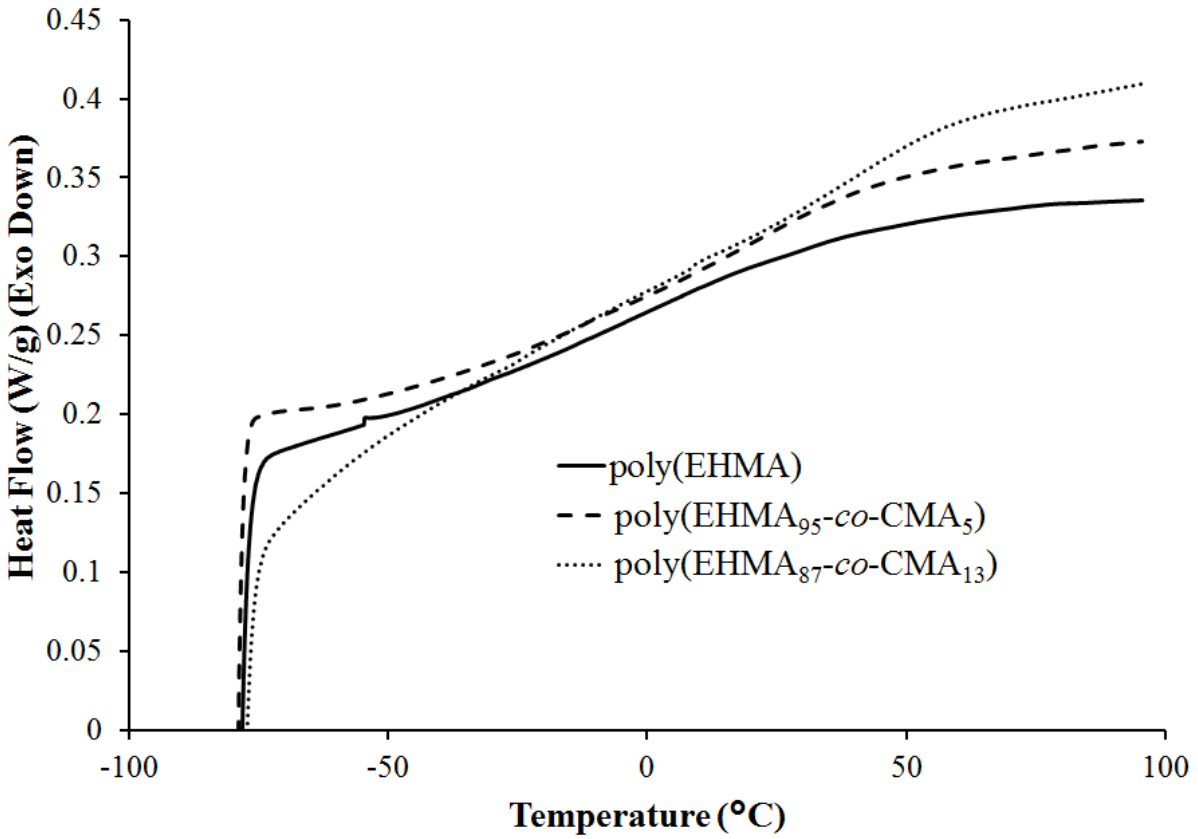

Figure 5.9. DSC shows broad T_g's for the copolymers, trending upward with increasing CMA content

Time-temperature superposition (TTSP) melt rheology and dynamic mechanical analysis (DMA) further investigated the effect of caffeine on thermal properties. **Figure 10** displays the master curves, obtained using a 30 °C reference temperature (T_{ref}), for the (co)polymer series. All polymers adhered to TTSP, which provided a broad range of rheological behavior over angular frequencies of 10^{-6} to ~10^{4} rad/s. The crossover of the storage (G') and loss (G") moduli (G' = G") occurred in each material and shifted to lower frequencies with increasing CMA.[51] Modulus also increased with increasing caffeine content. Contrary to the SEC results discussed previously where poly(EHMA) exhibited the highest M_n, a shift of the crossover point to lower frequencies often indicates higher molecular weight.[52] The shifted crossover point combined

with the enhanced modulus suggested caffeine pendant groups increased chain stiffness. Similarly complex viscosity, depicted in **Figure 11**, followed an increasing trend with CMA incorporation. Complex viscosity often scales with molecular weight, thus these results further supported that pendant caffeine functional groups largely influenced chain stiffness.

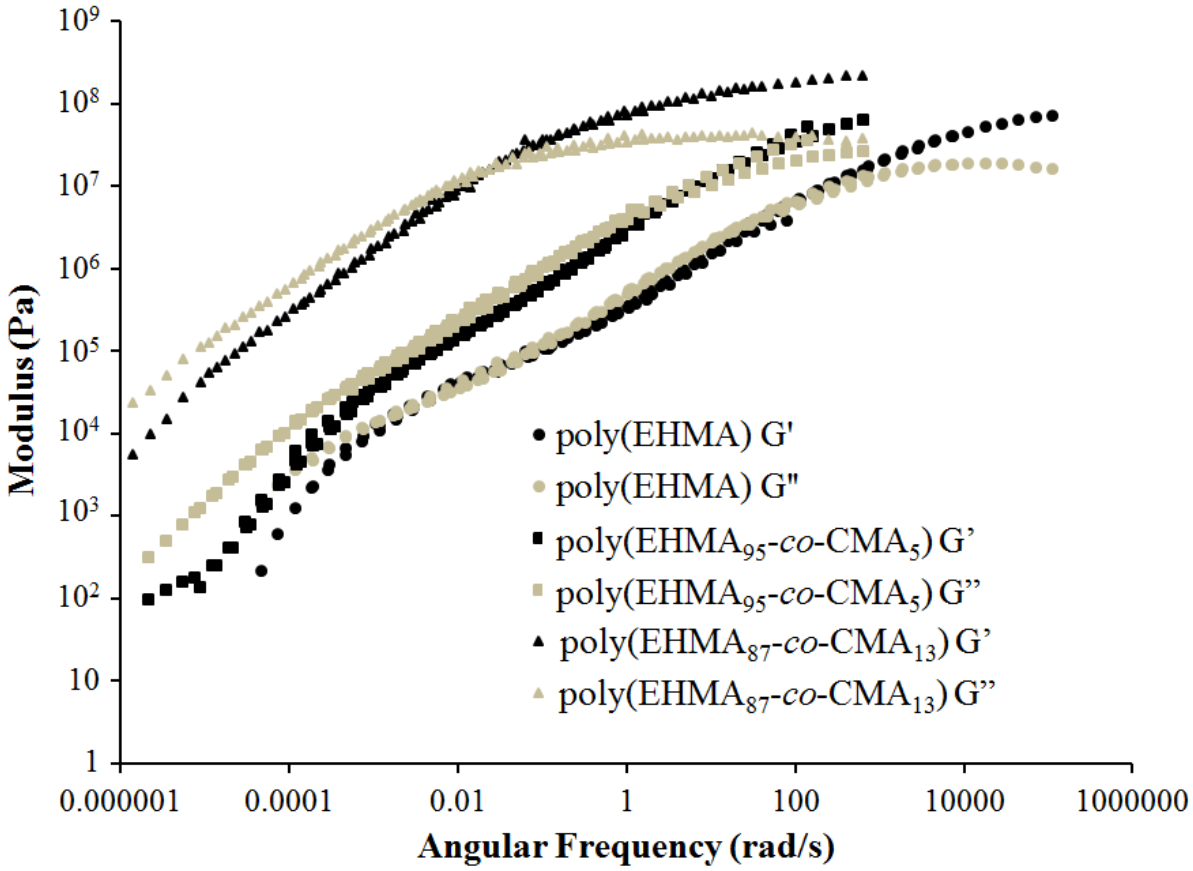

Figure 5.10. Melt rheology exhibits higher moduli with increasing CMA content

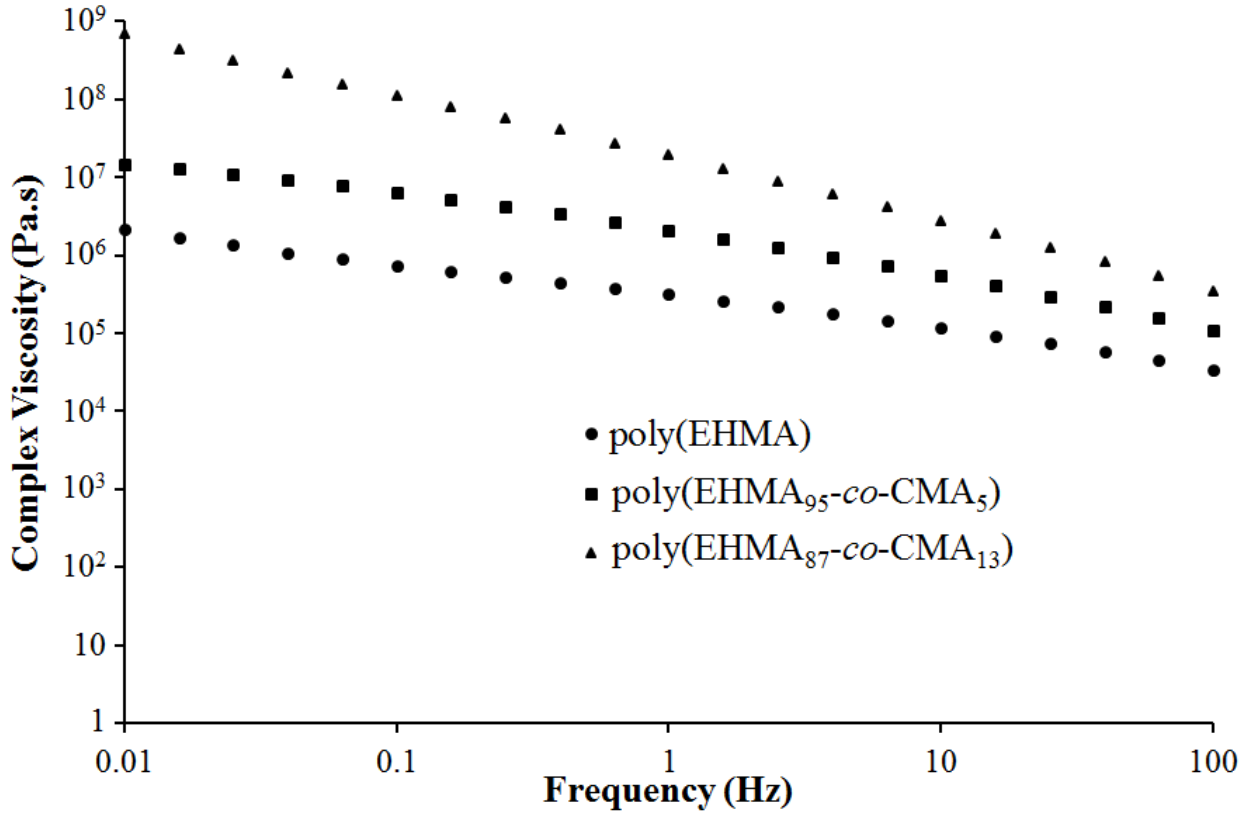

Figure 5.11. Complex viscosity of poly(EHMA) and caffeine-containing copolymers at 30 °C

All three (co)polymers formed films with solution casting from chloroform. **Figure 12** shows the DMA curves of poly(EHMA) and poly(EHMA$_{95}$-*co*-CMA$_5$) obtained from their respective films. Poly(EHMA$_{87}$-*co*-CMA$_{13}$) formed a film, however, films were glassy at room temperature, unlike the other two samples, and shattered while attempting to obtain a rectangular piece for thermomechanical testing. The stiffer, glassy, nature of poly(EHMA$_{87}$-*co*-CMA$_{13}$) correlated well to TTSP and viscosity data, demonstrating the influence of the caffeine pendant group on properties. Poly(EHMA) and poly(EHMA$_{95}$-*co*-CMA$_5$) exhibited DMA traces expected of amorphous materials; beginning with a glassy modulus at low temperatures and proceeding through a single transition (T_g) leading to flow. As observed in DSC, poly(EHMA$_{95}$-*co*-CMA$_5$) exhibited a slightly higher T_g than poly(EHMA), with a tan delta maximum occurring

at 55 °C and 49 °C, respectively. Additionally, a higher storage modulus with CMA was consistent.

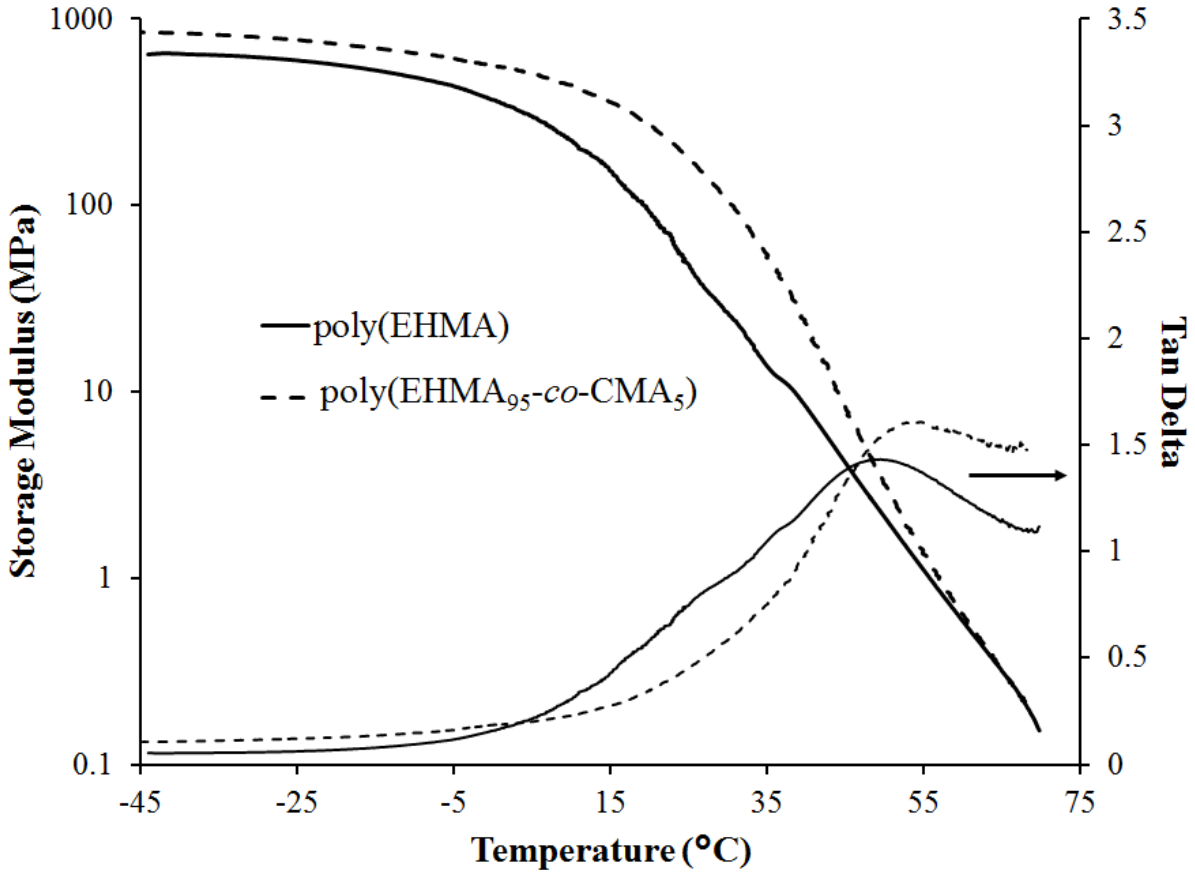

Figure 5.12. Thermomechanical analysis of 5 mol % CMA copolymer, showing an increased and extended glassy modulus compared to poly(EHMA) control

5.5 *Conclusions*

The successful synthesis and polymerization of a novel caffeine-containing methacrylate afforded copolymers containing covalently bound caffeine pendant groups. A free radical induced photoreaction and acid chloride reaction generated CMA requiring minimal isolation prior to polymerization. Using 2-ethylhexyl methacrylate as a comonomer, film-forming polymers containing 0, 5, and 13 mol % CMA provided insight into the effect of caffeine on

physical properties. Caffeine influenced both thermal stability and T_g, showing a unique multi-step thermal degradation profile similar to sidegroup elimination as observed for poly(*N*-vinylimidazole).[45] ^{1}H NMR confirmed caffeine content, and UV-vis spectroscopy exhibited a characteristic absorbance for caffeine, shifted to higher wavelengths attributed to the extra π bond and resonance in CMA-containing copolymers. Finally, caffeine improved polymer moduli suggesting the aromatic structure stiffened polymer chains. These novel materials demonstrated the effect of the naturally-occurring caffeine structure on polymer properties, including both thermal and thermomechanical influences. The higher T_g and storage moduli of low CMA contents (< 15 mol %) suggested that CMA could perform as a comonomer in acrylic polymers to impart specific physical properties and increase sustainability. Furthermore, future placement of caffeine further from the polymer backbone may encourage noncovalent π-π stacking and expand the library of caffeine-containing polymers, promoting microphase-separation for the synthesis of elastomers and broadening the understanding and potential of caffeine in material applications.

5.6 *Acknowledgements*

The authors would like to thank the U.S. Army Research Laboratory and the U.S. Army Research Office under the Army Materials Center of Excellence Program, contract W911NF-06-2-0014 for financial support. The authors would like to thank Michael H. Allen, Jr. and Richard N. Carmean for insightful discussions and assistance. The authors would also like to thank Dr. David Inglefield and Mingtao Chen for the offline determination of poly(EHMA) d*n*/d*c* in THF.

5.7 *References*

(1) Barron, A. E.; Zuckerman, R. N. *Current Opinion in Chemical Biology* **1999**, *3*, 681.
(2) Belgacem, M. N.; Gandini, A. *Monomers, Polymers and Composites from Renewable Resources*; Elsevier, 2008.
(3) Meier, M. A. R.; Metzger, J. O.; Schubert, U. S. *Chemical Society Reviews* **2007**, *36*, 1788.
(4) Mohanty, A. K.; Misra, M.; Drzal, L. T. *J Polym Environ* **2002**, *10*, 19.
(5) Ragauskas, A. J.; Williams, C. K.; Davison, B. H.; Britovsek, G.; Cairney, J.; Eckert, C. A.; Frederick, W. J.; Hallett, J. P.; Leak, D. J.; Liotta, C. L.; Mielenz, J. R.; Murphy, R.; Templer, R.; Tschaplinski, T. *Science* **2006**, *311*, 484.
(6) Gandini, A.; Lacerda, T. M. *Progress in Polymer Science*.
(7) Koch, C. A.; Patent, U. S., Ed.; AVery Dennison Corporation: US, 2014; Vol. US 8,796,351 B2.
(8) Madhavan Nampoothiri, K.; Nair, N. R.; John, R. P. *Bioresource Technology* **2010**, *101*, 8493.
(9) Yu, L.; Dean, K.; Li, L. *Progress in Polymer Science* **2006**, *31*, 576.
(10) Fenouillot, F.; Rousseau, A.; Colomines, G.; Saint-Loup, R.; Pascault, J. P. *Progress in Polymer Science* **2010**, *35*, 578.
(11) Song, H.; Lee, S. Y. *Enzyme and Microbial Technology* **2006**, *39*, 352.
(12) Chatti, S.; Schwarz, G.; Kricheldorf, H. R. *Macromolecules* **2006**, *39*, 9064.
(13) Lin, Q.; Pasatta, J.; Long, T. E. *J. Polym. Sci., Part A: Polym. Chem.* **2003**, *41*, 2512.
(14) Looser, E.; Baumann, T. W.; Wanner, H. *Phytochemistry* **1974**, *13*, 2515.
(15) Matissek, R. *Z Lebensm Unters Forsch* **1997**, *205*, 175.
(16) Shi, Y.; Schloss, F. M.; Weemes, D. A. Patent WO 2007/040960 **2007**.
(17) Paseta, L.; Potier, G.; Abbott, S.; Coronas, J. *Organic & Biomolecular Chemistry* **2015**, *13*, 1724.
(18) Belščak-Cvitanović, A.; Komes, D.; Karlović, S.; Djaković, S.; Špoljarić, I.; Mršić, G.; Ježek, D. *Food Chemistry* **2015**, *167*, 378.
(19) Kuznetsova, E. G.; Kuryleva, O. M.; Salomatina, L. A.; Sevast'yanov, V. I. *Biomed Eng* **2008**, *42*, 141.
(20) Turner, N. W.; Holdsworth, C. I.; Donne, S. W.; McCluskey, A.; Bowyer, M. C. *New Journal of Chemistry* **2010**, *34*, 686.
(21) Zayas, H.; Holdsworth, C. I.; Bowyer, M. C.; McCluskey, A. *Organic & Biomolecular Chemistry* **2014**, *12*, 6994.
(22) Trask, R. S.; Williams, H. R.; Bond, I. P. *Bioinspiration & Biomimetics* **2007**, *2*, P1.
(23) Huebsch, N.; Mooney, D. J. *Nature* **2009**, *462*, 426.
(24) Hardaker, S. S.; Gregory, R. V. *MRS Bulletin* **2003**, *28*, 564.
(25) Hemp, S. T.; Long, T. E. *Macromolecular Bioscience* **2012,** *12*, 29.
(26) Goswami, S.; Mahapatra, A. K.; Mukherjee, R. *Journal of the Chemical Society, Perkin Transactions 1* **2001**, 2717.
(27) Salomon, J.; Elad, D. *The Journal of Organic Chemistry* **1973**, *38*, 3420.
(28) Elad, D.; Steinmaus, H.; Rosenthal, I. *The Journal of Organic Chemistry* **1971**, *36*, 3594.
(29) Sahnoun, S.; Messaoudi, S.; Brion, J.-D.; Alami, M. *European Journal of Organic Chemistry* **2010**, *2010*, 6097.

(30) Murgida, D. H.; Aramendía, P. F.; Erra-Balsells, R. *Photochemistry and Photobiology* **1998**, *67*, 487.
(31) Saito, T.; Mather, B. D.; Costanzo, P. J.; Beyer, F. L.; Long, T. E. *Macromolecules* **2008**, *41*, 3503.
(32) Rikkou-Kalourkoti, M.; Panteli, P. A.; Patrickios, C. S. *Polymer Chemistry* **2014**, *5*, 4339.
(33) Elkins, C. L.; Park, T.; McKee, M. G.; Long, T. E. *Journal of Polymer Science Part A: Polymer Chemistry* **2005**, *43*, 4618.
(34) Sierant, M.; Kazmierski, S.; Rozanski, A.; Paluch, P.; Bienias, U.; Miksa, B. J. *New Journal of Chemistry* **2015**, *39*, 1506.
(35) Fleischhaker, F.; Haehnel, A. P.; Misske, A. M.; Blanchot, M.; Haremza, S.; Barner-Kowollik, C. *Macromolecular Chemistry and Physics* **2014**, *215*, 1192.
(36) Bruice, P. Y. *Organic Chemistry*; 7th ed.; Pearson Education, Inc: Upper Saddle River, NJ, 2014.
(37) Skoog, D. A.; Holler, F. J.; Crouch, S. R. *Instrumental Analysis*; Brooks/Cole, 2007.
(38) Belay, A.; Ture, K.; Redi, M.; Asfaw, A. *Food Chemistry* **2008**, *108*, 310.
(39) López-Martínez, L.; López-de-Alba, P. L.; García-Campos, R.; De León-Rodríguez, L. M. *Analytica Chimica Acta* **2003**, *493*, 83.
(40) Woziwodzka, A.; Gołuński, G.; Wyrzykowski, D.; Kaźmierkiewicz, R.; Piosik, J. *Chemical Research in Toxicology* **2013**, *26*, 1660.
(41) Odian, G. *Principles of Polymerization, Fourth Edition*; John Wiley & Sons, Inc.: Hoboken, NJ, 2004.
(42) Smith, S. D.; Long, T. E.; McGrath, J. E. *Journal of Polymer Science Part A: Polymer Chemistry* **1994**, *32*, 1747.
(43) Cervantes-Uc, J. M.; Cauich-Rodríguez, J. V.; Herrera-Kao, W. A.; Vázquez-Torres, H.; Marcos-Fernández, A. *Polymer Degradation and Stability* **2008**, *93*, 1891.
(44) Zulfiqar, S.; Zafar-uz-Zaman, M.; Munir, A.; McNeill, I. C. *Polymer Degradation and Stability* **1997**, *55*, 89.
(45) Fodor, C.; Bozi, J.; Blazsó, M.; Iván, B. *Macromolecules* **2012**, *45*, 8953.
(46) Zhang, K.; Fahs, G. B.; Aiba, M.; Moore, R. B.; Long, T. E. *Chemical Communications* **2014**, *50*, 9145.
(47) Cheng, S.; Zhang, M.; Dixit, N.; Moore, R. B.; Long, T. E. *Macromolecules* **2012**, *45*, 805.
(48) Hill, G. M.; Moriarity, D. M.; Setzer, W. N. *Scientia Pharmaceutica* **2011**, *79*, 729.
(49) Kostjukov, V. V.; Khomytova, N. M.; Hernandez Santiago, A. A.; Tavera, A.-M. C.; Alvarado, J. S.; Evstigneev, M. P. *The Journal of Chemical Thermodynamics* **2011**, *43*, 1424.
(50) Zhang, H.-M.; Chen, T.-T.; Zhou, Q.-H.; Wang, Y.-Q. *Journal of Molecular Structure* **2009**, *938*, 221.
(51) Malkin, A. Y.; Isayev, A. I. *Rheology - Concepts, Methods, and Applications (2nd Edition)*; ChemTec Publishing, 2012.
(52) Mezger, T. G. *The Rheology Handbook: For Users of Rotational and Oscillatory Rheometers*; Vincentz Network, 2006.

5.8 *Supporting Information*

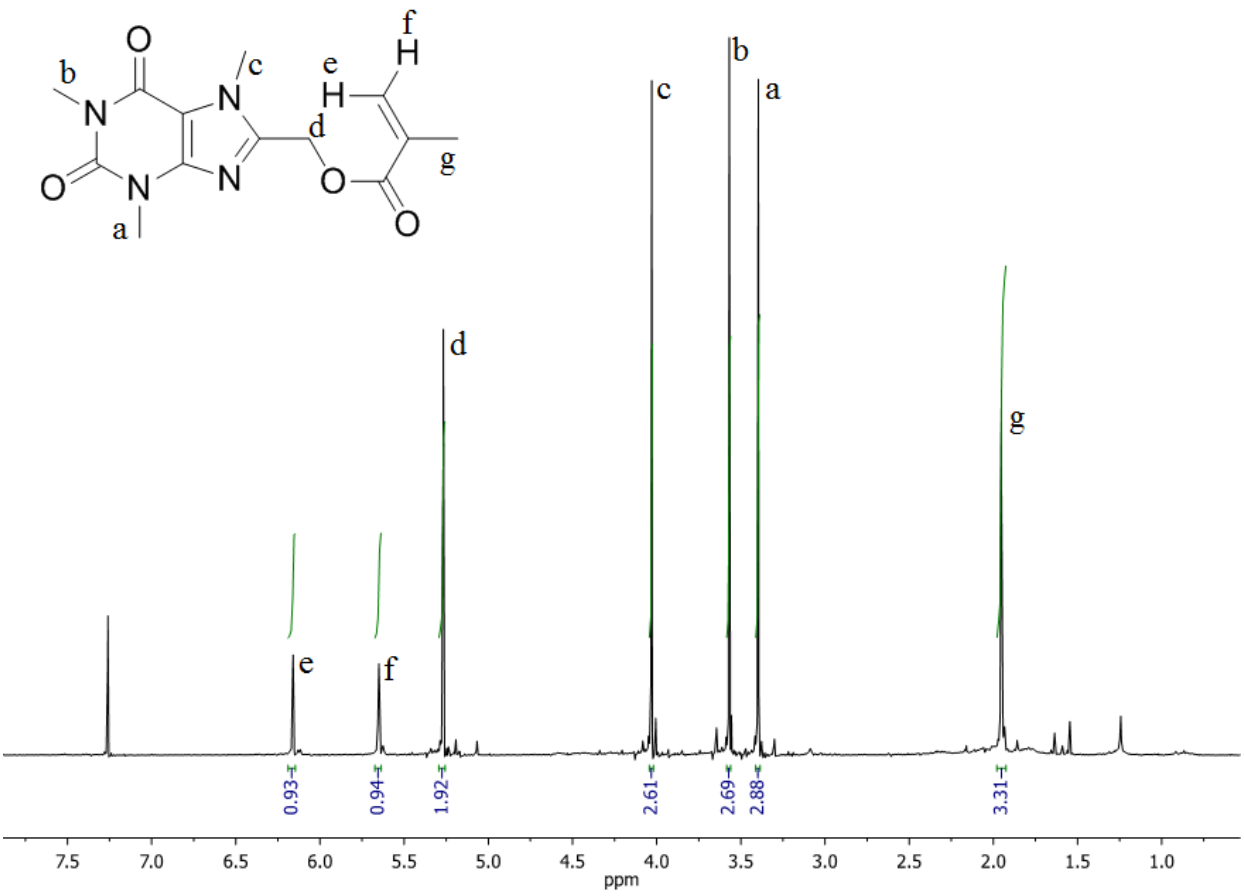

Figure 5.13. ^{1}H NMR spectroscopy confirms structure of novel caffeine methacrylate

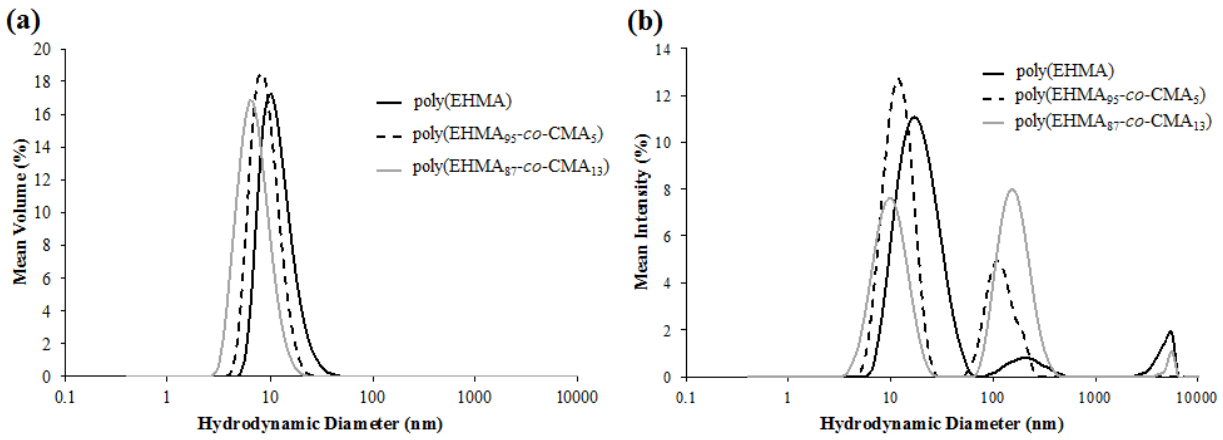

Figure 5.14. Particle size with respect to mean volume % (a) and mean intensity % (b) for the (co)polymers in THF

Chapter 6: Synthesis of Novel Amorphous Copolyesters and Crosslinking Additives from Plant-Based Monomers

Ashley M. Nelson, Keren Zhang, and Timothy E. Long

Department of Chemistry, Macromolecules and Interfaces Institute
Virginia Tech, Blacksubrg, VA 24061-0212

6.1 *Abstract*

Plant-based fatty acids are attractive aliphatic compounds for the synthesis of biodegradable polymeric materials due to versatile chemical functionality. Starting from methyl 9-decenoate (9-DAME), two synthetic paths resulted in novel amorphous aliphatic polyesters and a multifunctional branching/crosslinking agent. Hydration of 9-DAME afforded an isomeric mixture of AB hydroxyester or AB hydroxyacid monomers which ^{1}H NMR spectroscopy revealed 28 % 7- and 8-hydroxy isomers. Soluble polyesters were synthesized via melt transesterification and the low molar mass resolution of advanced polymer chromatography (APC) followed molecular weight growth as a function of polymerization time. Thermal analysis revealed amorphous copolyesters with T_g ~-60 °C, identical to poly(ε-caprolactone) (PCL). These novel copolyesters have applications ranging from biomedical devices to high-performance elastomers. Additionally, epoxidation of 9-DAME and then hydrolysis afforded an ABB'-dihydroxyester monomer. Unequal alcohol reactivity prevented the direct formation of hyperbranched polyesters, however, plant-based crosslinked polyesters resulted demonstrating the feasibility of the ABB'-dihydroxyester as a biodegradable branching and/or crosslinking additive.

6.2 *Introduction*

The importance and necessity of exploring the capabilities of bio-based resources in materials science is increasingly prevalent and acknowledged in both scientific and political realms.[1-3] Research efforts span from the synthesis of renewable monomers and polymers to the engineering of scale-up and industrial production.[4] Bio-based resources offer a plethora of functional monomers; including but not limited to fatty acids, ethylene, sugar-based diols, and lactic acid.[4-8] Fermentation, dehydration, and extraction are some of the techniques which aid in clean isolation of compounds from renewable resources.[4,7] The ability of bio-based compounds to function as (co)monomers and additives accesses a variety of materials with tunable properties and renewable content for a wide-range of applications.[9-13]

Sustainable polymers derived from bio-based feedstock's remain a controversial topic surrounding environmental implications.[4] Monomer synthesis, derivitization, polymerization processes, and the ultimate fate of the materials often mimic current petroleum-based practices resulting in environmentally unfriendly chemical usage and the inability to recycle or degrade. Green chemistry standards provide a unique set of idealized criterion that, albeit difficult to succeed in all areas, encourages environmental preservation and foresight when inventing new materials and/or processes.[14] Ester bonds are hydrolytically unstable, reverting back to an alcohol and acid particularly in acidic and/or basic conditions.[15] Utilizing this instability as an advantage, polyesters are biodegradable under structure-dependent conditions (time, temperature, acidic, basic, enzymatic, etc.).[16,17] Polyesters remain an attractive class of polymers synthesized from renewable resources as they inherently possess at least two green principles, bio-based monomers and degradability, and many bio-based compounds contain functionality enabling polyester synthesis.[18-21]

Poly(lactic acid) (PLA), a commercially produced aliphatic polyester synthesized from bio-derived lactic acid, or lactide, generates materials with tunable crystallinity.[7] Lactic acid is chiral and the lactide dimer exists as D, L, or meso. Copolymerization of the different isomers affords polyesters with glass transition temperatures (T_g's) around 60 °C and, unless amorphous, melting temperatures (T_m's) ranging from 130 °C to 180 °C. **Figure 1** depicts PLA **(a)** alongside another commercially produced and prevalent polymer, polypropylene (PP) **(b)**. With the chemical similarity evident in the repeating units shown below, comparable material properties result. PP processing dictates thermal properties which range from commercially available amorphous displaying a T_g = -10 °C to semi-crystalline isotactic PP with $T_m \cong 160$ °C (values obtained from Sigma Aldrich). Furthermore, Liu et al.[18] synthesized long-chain aliphatic polyesters from the renewable resource methyl ω-hydroxytetradecanoic acid. Polycondensation of the AB hydroxyacid monomer achieved high molecular weight semi-crystalline polyesters with T_m's around 100 °C and proposed performance and applications similar to polyethylene (PE). These examples demonstrate the desirable properties of aliphatic polyesters, highlighting opportunities for commercialization while maintaining the built-in degradation mechanism.

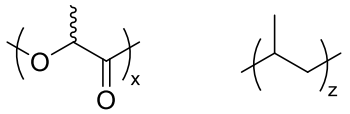

(a) (b)

Figure 6.1. Repeating units of PLA (a) and PP (b)

Monomers bearing functionality greater than 2 (f > 2) lead to hyperbranched and/or crosslinked materials.[22] These architectures often exhibit unique properties compared to the corresponding linear analogs and are explored for various applications including additives and coatings.[23] Plant-based oils, or fatty acids in particular, foster the synthesis of three-dimensional

architectures since many contain multiple alkenes which easily convert to epoxides.[8,24] Enzymatic epoxidation and polymerization afforded Uyama et al.[25] crosslinked polyester films from fatty acids. The crosslinked films displayed promising biodegradability, showing ~50 % degradation after a 50 d biochemical oxidation demand (BOD) test. Kim and Sharma[26] epoxidized 5 different bio-based oils containing varying ratios of saturated and unsaturated fatty acids. The resulting thermosets revealed elastic moduli ranging from 68 – 170 MPa.

Elevance Renewable Sciences Inc., a company dedicated to the use and engineering of bio-based compounds, pioneered the isolation of methyl 9-decenoate (9-DAME) in high purity and graciously teamed up with Virginia Tech in the exploration of novel polymers. Alkenes are versatile functional groups lending to a variety of chemical transformations.[27] Warwel et al.[28] demonstrated this versatility specifically on plant-based monomers, including 9-DAME, and focused on metathesis reactions and enzymatic epoxidation to generate polyesters, polyethers, and small-molecule surfactants. In the present study, a formic acid hydration and epoxidation of 9-DAME provided two different routes to step-growth monomers. Hydration achieved an isomeric mixture of AB monomers readily polymerized using high-temperature polycondensation techniques. Hydrolysis of the terminal epoxide efficiently generated two active sites, resulting in ABB' hydroxyester monomer. The following manuscript describes the synthesis of bio-derived monomers/additives, and the synthesis and characterization of the resulting polyesters and crosslinked networks. These initial monomers and polyesters elucidate 9-DAME as a platform bio-based chemical for obtaining renewable polymers with desirable properties.

6.3 *Experimental*

6.3.1 Materials

Methyl 9-decenoate (9-DAME) was provided from Elevance Renewable Sciences, Inc. (^{1}H NMR in supporting information, **Figure 10**). Formic acid (FA; 97 %), potassium hydroxide (KOH; 85 %), and potassium carbonate (K_2CO_3; 99 %; anhydrous) were obtained from Alfa Aesar. Dibutyltin oxide ($SnOBu_2$; 98 %), antimony(III) oxide (Sb_2O_3; 99 %; 5 micron powder), *meta*-chloroperoxybenzoic acid (*m*- CPBA, ≤77%), sodium hydroxide solution (NaOH, 1.0 M in water), sodium sulfite ($NaSO_3$, ≥98%), sodium bicarbonate ($NaHCO_3$, ≥99.7), sodium chloride (NaCl, ≥99%), and aluminum oxide (Al_2O_3, activated basic Brockmann I) were obtained from Sigma Aldrich. A titanium tetraisopropoxide catalyst solution ($Ti(OiPr)_4$; 0.01 g Ti/mL) was prepared in anhydrous 1-butanol (99.8 %; Sigma Aldrich) according to previous literature.[29] Hydrochloric acid (HCl) and isopropanol (IPA) were purchased from Spectrum Chemicals. Dichloromethane (DCM) and was obtained from Fisher Scientific. All water used was purified using a reverse osmosis process. All reagents were used as received.

6.3.2 Analytical Methods

Nuclear magnetic resonance (NMR) spectroscopy was performed on a Bruker Avance II 500 MHz NMR or Agilent U4-DD2 400 MHz NMR at ambient temperature in deuterated chloroform ($CDCl_3$). A TA Instruments thermogravimetric analyzer (TGA) Q50 afforded degradation profiles in a N_2 atmosphere at a heating rate of 10°C/min from room temperature to 600 °C. A TA Instruments differential scanning calorimeter (DSC) Q1000 provided thermal transitions. All values reported are from the second heat in a heat/cool/heat procedure with a

ramp of 10 °C/min to an upper temperature (ranging from 100 °C to 200 °C), quench cooled at 100 °C/min to a lower temperature (-80 °C to -100 °C), and heated again at a rate of 10 °C/min to the same upper temperature. Relative molecular weights (relative to polystyrene (PS) standards) were obtained from a Waters Acquity advanced polymer chromatography (APC) refractive index detector using column set 450 Å x 150 mm, 200 Å x 150 mm, 45 Å x 150 mm in tetrahydrofuran stabilized with 0.025 wt. % BHT at a flow rate of 1 mL/min. An Agilent 6220A time-of-flight (TOF) liquid chromatography/mass spectrometry (LC/MS) run in 60/40 MeOH/H_2O (v/v) with 0.1 % formic acid at a flow rate of 0.4 mL/min and a 10 L/min nebulizer provided accurate mass. A TSQ Quantum triple quadrupole LC-MS equipped with a Luna 5 μm C18 150 x 2.0 mm column and a mobile phase of acetonitrile (ACN)/H_2O of 5/95 (v/v) with 0.1 % formic acid at a flow rate of 0.2 mL/min provides LC-MS results. The sample spectra is obtained using the following procedure: in 10 min the mobile phase changes to 95/5 ACN/H_2O, holds for 5 min, and then in 1 min pumps back to 5/95 ACN/H_2O and equilibrates for another 5 min.

6.3.3 Monomer and Polymer Synthesis

6.3.3.1 Synthesis of AB Polyester Monomer

9-DAME (20 g) and formic acid (50 mL) were added to a 250 mL round bottomed flask equipped with a magnetic stir bar and water condenser. The reaction setup was lowered into an oil bath and allowed to reflux (~90 °C) with constant stirring for at least 24 h. The condenser was then removed and the round-bottomed flask was equipped with a distillation apparatus to facilitate the removal of excess formic acid via vacuum distillation. The temperature of the oil bath was then lowered to approximately 60 °C and KOH in a mixture of water and IPA was

added to the reaction and allowed to stir for a minimum of 3 h. The reaction mixture was pushed through a basic alumina column and excess solvent removed using rotary evaporation. A transparent yellow oil was obtained and dried in the vacuum oven overnight. ^{1}H NMR was used to determine monomer structure and the isomeric mixture. Formylate-ester product often remained after the aforementioned workup and was determined based on the distinct ^{1}H NMR resonance of the aldehyde proton around 8 ppm. To deformylate, the oil was dissolved in IPA and KOH in IPA/water was added to the reaction and allowed to stir at 60 °C. It was determined that vigorous stirring aided in deformylation. The reaction mixture was neutralized using an aqueous HCl solution. To reduce impurities, one batch of product was extracted into DCM multiple times and the solvent removed using a rotary evaporator. To remove salt remaining in the oil, the extracted batch of product was filtered through a 5 μm membrane filter. Depending on the monomer batch/purity, a silica or basic alumina flash column was performed. Finally, the product was dried in the vacuum oven at c.a. 50 °C. The neutralization and isolation procedures were repeated as needed to remove formate ester and obtain an isomeric mixture, generated from 1,2-hydride shifts, of the AB monomer. Workup conditions influenced the structure of the obtained product(s) and are discussed in detail in the results and discussion section. One monomer batch resulted in an isomeric mixture of AB hydroxyesters (LC/MS). AB hydroxyesters: methyl 9-hydroxydecanoate, methyl 8-hydroxydecanoate, methyl 7-hydroxydecanoate. LC/MS [M+H] = 203.04. Masses corresponding to formate ester, dimers, and starting material were also observed. It is necessary to note TOF-MS observed 200.14 which would suggest a product with unsaturation, however, LC-MS and ^{1}H NMR do not corroborate these findings and we are assuming this is a result of an ionization or mobile-phase interaction. The discussion section will further address these results.

A different monomer batch provided an isomeric mixture of AB hydroxyacids and AB hydroxyacid dimers of 7-hydroxydecanoic acid, 8-hydroxydecanoic acid, and 9-hydroxydecanoic acid. LC/MS [M+H] = 189.11 and 359.27; TOF-MS = 358.27.

6.3.3.2 Synthesis of ABB' Monomer

In the first step, *m*-CPBA (33 g, 0.14 mol) and DCM (200 mL) were added to a 500 mL round-bottomed flask equipped with a magnetic stir bar. The reaction setup was placed into an ice bath with constant stirring until *m*-CPBA dissolved. 9-DAME (20 g, 0.11 mol) was then added into the solution and allowed to stir overnight. Vacuum filtration removed white precipitate from the solution and rotary evaporation removed DCM. Additional white precipitate was removed again through a vacuum filtration. The filtrate was washed with saturated $NaSO_3$ solution twice, NaOH 1.0 M solution 3 times, $NaHCO_3$ twice, and brine twice. Light yellow oil was obtained and placed in a -20 °C freezer overnight. The oil was filtered through a 5 μm membrane filter and dried in vacuo. The structure and purity of the 9,10-epoxydecanoate intermediate were confirmed using NMR spectroscopy (**Figure 11**) and MS. [M+Na] = 201.15.

In the second step, 9,10-epoxydecanoate (2.0 g, 10 mmol) was refluxed overnight with 40 mL water. The organic phase was then collected and dried in vacuo to obtain methyl 9,10-dihydroxydecanoate (MDHD) as a white solid (2.0 g, >90% yield). [M+Na] = 241.14. ^{1}H NMR is in supporting information, **Figure 12**.

6.3.3.3 Polyester Synthesis

All polyesters were synthesized using either melt transesterification or melt polycondensation. Catalyst type and amount(s), specific reaction times, and temperatures varied slightly and are specified in the body of the manuscript. As a representative example, the

following describes the melt transesterification of the isomeric mixture of AB hydoxyester monomer. 1 g of the isomeric mixture of AB hydroxyester was added to a dry 50 mL round-bottomed flask. Approximately 600 ppm dibutyltin oxide (0.0013 g) was added to the reaction and the round-bottomed flask was equipped with a mechanical stirrer and distillation apparatus through a t-neck adapter, which also provided a N_2 inlet. The reaction setup was purged with N_2 and evacuated at least 3 times to ensure complete oxygen removal. The reaction was then lowered into a silicon oil bath heated to ca. 80 °C and allowed to react for approximately 2 h with continuous stirring and N_2 purge. The temperature was increased to 120 °C for another 2 h, then 170 °C and 200 °C each for 1 h. High vacuum (<0.15 mmHg) was then applied and the reaction continued for another 2 h at 200 °C. Using the stir rod and/or a spatula, the resulting transparent liquid polymer was removed from the round-bottomed flask and characterized without any further workup or purification.

6.4 *Results and Discussion*

6.4.1 Synthesis and Polymerization of AB Plant-based Monomer

Methyl 9-decenoate (9-DAME), an oily liquid at room temperature, contains a methyl ester and terminal alkene. Hydration is a common and facile route to add water across a double bond, removing the unsaturation and introducing hydroxyl functionality.[27] **Scheme 1** displays the formic acid hydration of 9-DAME to produce AB polyester monomers. In the acid catalyzed hydration mechanism a carbocation forms on the more substituted (secondary) carbon. While present, 1,2-hydride shifts moved the carbocation down the carbon chain giving rise to the isomeric mixture of AB monomers depicted below.[30] The second step in the reaction scheme, the addition of potassium hydroxide (KOH), removed formate ester and occasionally hydrolyzed

the ester to an acid. This reaction affords secondary alcohols as opposed to hydroboration oxidation and ozonide hydrogenation and borohydride reduction which provide primary alcohols.[27,31] Additionally, it is proposed the isomeric mixture of AB monomer combined with the odd, non-symmetric, methylene spacer could prevent crystallization of the resulting polyesters.[32] As mentioned previously, ω-hydroxyacids with 12 methylene units afforded crystalline polyesters with $T_m \cong 100$ °C and crystallization temperatures also reported for poly(ω-hydroxyacids) containing methylene spacers of 1 – 5, 9-12, 14, and 15.[18,22]

Scheme 6.1. Synthesis of isomeric mixture of AB hydroxyester or hydroxyacid monomers for step-growth polymerization

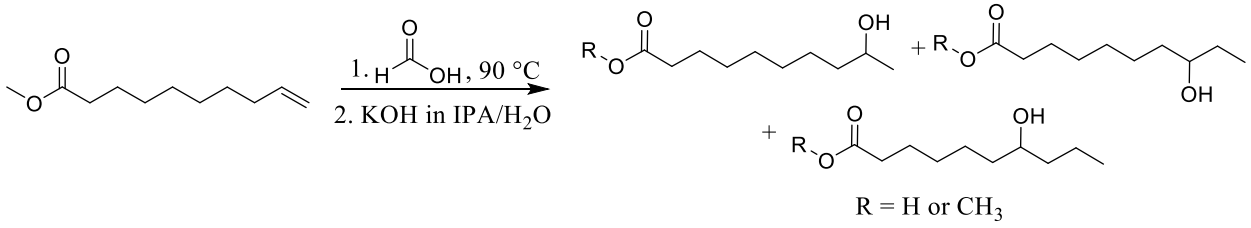

As mentioned previously, 9-DAME is liquid at room temperature and the isomeric mixture of AB monomers remained an oil, hindering purification. Throughout the reaction and workup ^{1}H NMR monitored alkene and formate ester and solubility in organic solvents indicated successful neutralization. **Figure 2** depicts the ^{1}H NMR spectra of a batch of AB hydroxyester plant-based step-growth monomer. The primary methyl groups from the 7- and 8-hydroxy (8-OH) isomers (**c**) appeared upfield relative to the 9-OH isomer, and the methine carbons also shifted upfield (peak **e** compared to peak **d**). The different shifts enabled calculation of the ratio of 7-OH and 8-OH (combined) to 9-OH monomer. The methylene adjacent to the ester carbonyl shifted downfield compared to the other methylenes and to the same position for each isomer, thus setting the integration to 2 revealed the isomeric ratio. In **Figure 1**, peak **c** integrates to 0.82

H. If 7-OH and 8-OH formed the entire batch, **c** would integrate to 3 H. Therefore the ratio, 0.82 H/3 H, elucidates 27 % 7- and 8-OH AB monomer. Comparing the methine resonances, peak **e** corroborated the percentage of 7- and 8-OH isomers with an integration of approximately 0.28 H, or ~28 %. This integration included two broad peaks, a much smaller peak at $\delta = 0.07$ which is proposed as either a separate peak from a distinct 7- or 8-OH isomer or potentially a small amount of the 9-isomer hydroxyl proton, and an unidentified sharp peak on the side of one of the broad peaks, both which could skew the isomer ratio if they correspond to a different structure. Furthermore, the integration of resonance **d** corresponded to 68 % of the 9-OH isomer. To summarize, approximately 68 % of AB hydroxyester monomer batch shown below contained the hydroxyl group at the 9-position and the remaining ca. 28 % a combination of the 7-OH and 8-OH isomers.

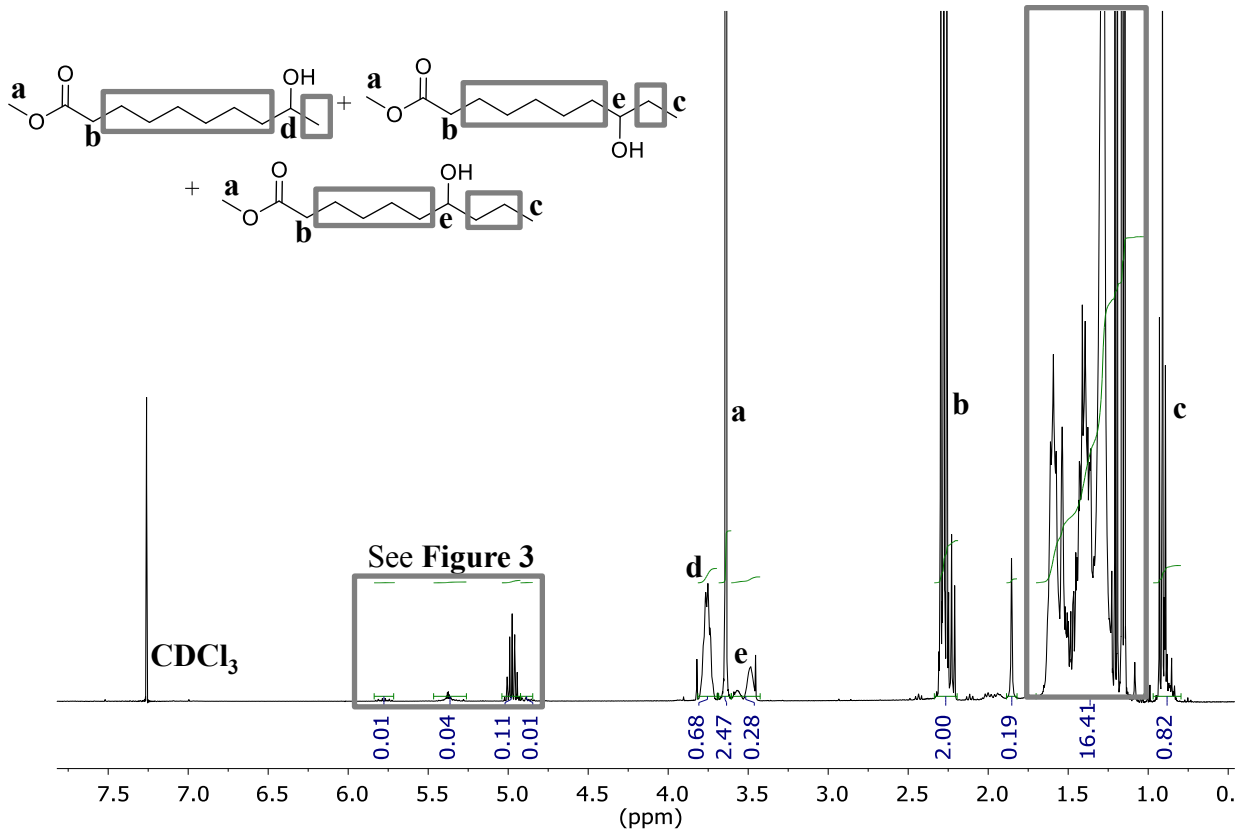

Figure 6.2. ^{1}H NMR spectroscopy of isomeric mixture of AB hydroxyester monomer confirms isomeric mixture and shows evidence of dimer

Looking closer at **Figure 1**, peaks downfield from the methyl ester instigated further structural and purity analyses of the AB hydroxyester. A possible contaminant included unreacted 9-DAME. 9-DAME starting material (^{1}H NMR in **Figure 11**) exhibited alkene resonances at 5.80 and 4.95 ppm in $CDCl_3$. **Figure 3** exhibits an enlarged area of the 4.6 – 6 ppm region of the above ^{1}H NMR spectra. The two resonances labeled **g** and **h** suggested a small amount (~1 %) of unreacted 9-DAME and both TOF-MS and LC-MS confirmed the presence of the starting material. LC-MS also revealed mass equal to dimers of the AB hydroxyester. In a dimer, the proton of the methine adjacent to the ester should shift downfield compared to the hydroxy methine groups. **Figure 3** illustrates the AB hydroxyester dimer of the 9-OH isomer and the methine proton, labeled **f**, assigned to the ^{1}H NMR resonance at ca. 5 ppm.

The integration of 0.11 equates to approximately 11 % AB hydroxester dimer present. This percentage combined with the previously discussed **d** and **e** integrations equal 107 %, not accounting for overlapping potential impurity peaks or the hydroxyl proton mentioned above.

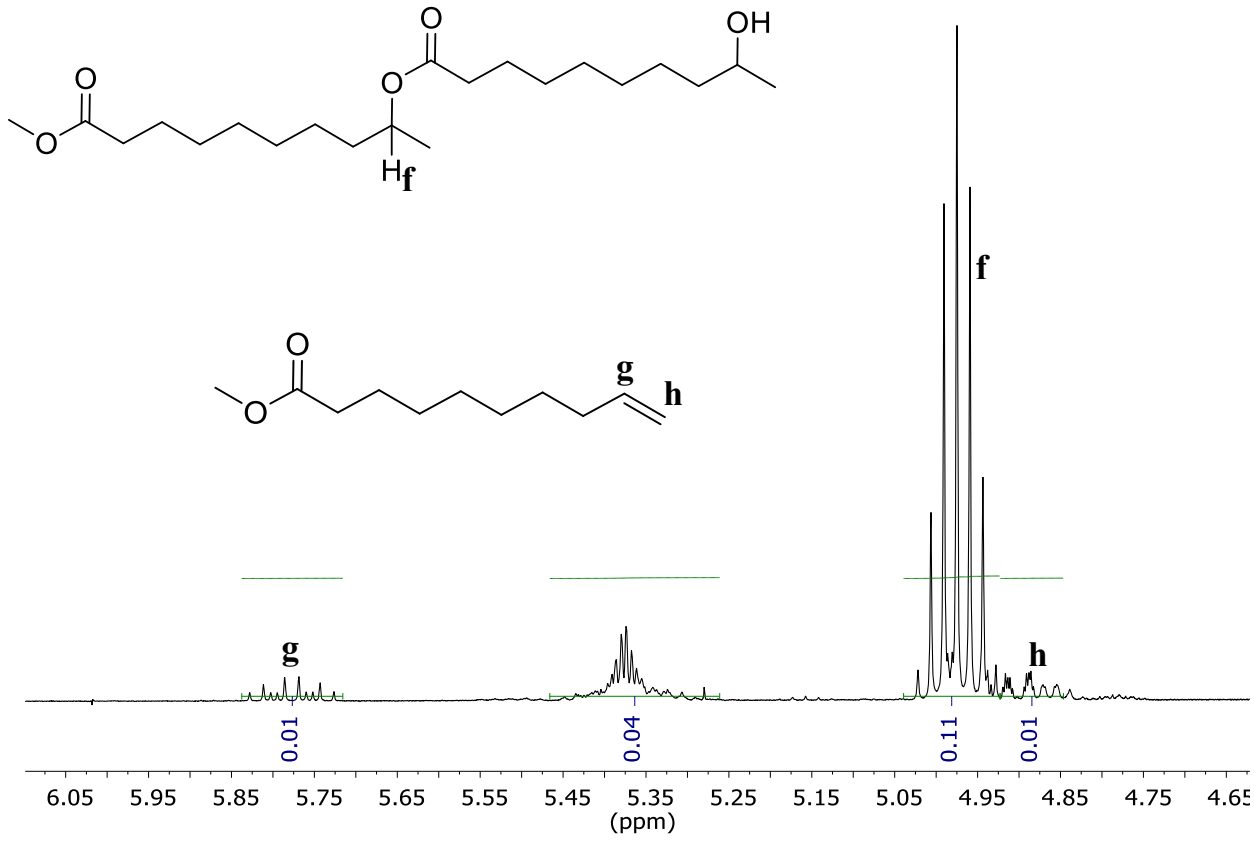

Figure 6.3. Zoomed in ^{1}H NMR spectra reveals evidence of AB hydroxyester dimer (top) and unreacted 9-DAME (bottom)

Not discernable in ^{1}H NMR, LC-MS also revealed the hydroxyester batch of monomer contained some formate ester product as well as other compounds, which remain unidentified. TOF-MS results suggested a site of unsaturation in the AB hydroxyester monomer, inconsistent with LC-MS. A site of unsaturation would not hinder the desired polymerization procedure, however, the polyester products, discussed in further detail later, did not exhibit evidence of unsaturation. Furthermore, workup of a different batch of monomer showed the ester hydrolyzed

to an acid and MS also revealed dimerization of the AB-hydroxyacid. Melt polymerization is a facile and common route to achieve high molecular weight polyesters pending the monomers can withstand elevated temperatures for extended periods of time.[18,33] Melt transesterification and direct esterification, reactions between an alcohol and either ester or acid respectively, tolerate initial offset stoichiometry and afford high molecular weight polyesters due to a vacuum step at the end of the polymerization which essentially forces 1:1 stoichiometry.[22] These high temperature reactions feature additional benefits such as a lack of solvent and byproducts. The application of vacuum drives esterification reactions to completion, efficiently removing the methanol or water byproduct and distilling off excess monomer and/or impurities. For this reason, the differing ester and acid functionalities and possible impurities in the plant-based AB monomers were of little concern.

Scheme 6.2. Melt polymerization of bio-based AB monomers readily achieves polyesters, eliminating solvents and excess purification

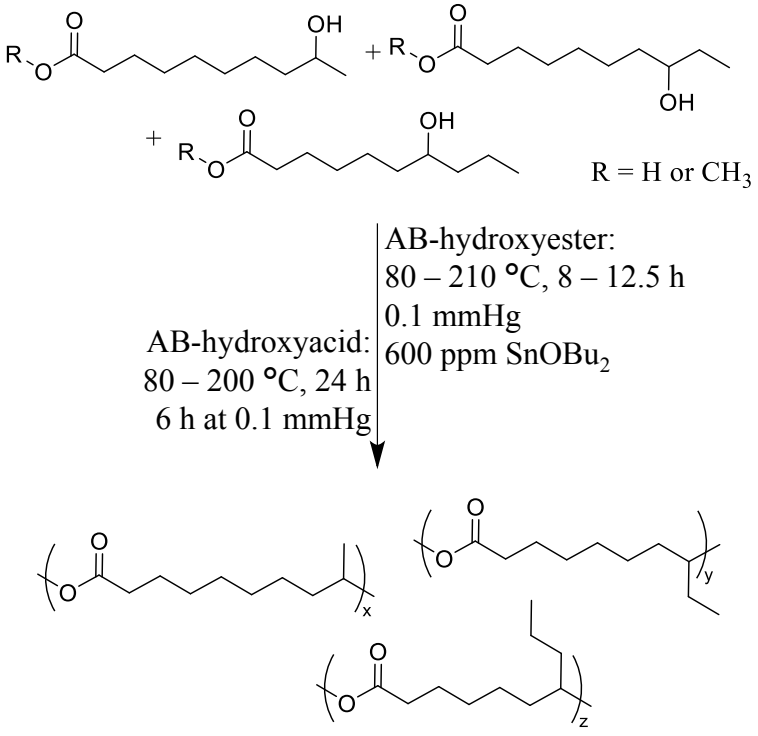

Scheme 2 depicts the melt polymerization of the isomeric mixture of AB plant-based monomers and expected repeating units. The resulting viscous polyesters readily dissolved in chloroform ($CHCl_3$) and tetrahydrofuran (THF). The conditions recorded above for the AB hydroxyester incorporate various polymerizations conducted to aid in the understanding of the rate and extent of reaction of the novel isomeric monomer mixture. Dibutyltin oxide ($SnOBu_2$), a catalyst for secondary alcohols, remained constant throughout the study while time and temperature varied.[11,34] **Figure 4** displays the ^{1}H NMR and ^{13}C (inset) NMR for the 8 h polymerization. Setting integration of the methylene adjacent to the ester to 2 facilitated comparisons with the monomer (**Figure 1**). The diminished methyl ester peak, from an integration of 2.47 H to 0.07 H, suggested polymerization proceeded yet not to 100 % conversion. Peak **c** remained unchanged, as expected, and the integration of **a** increased to near 1 H, confirming the growing methine resonance as observed from the monomer dimerization. Additionally, note the (near) disappearance of the unidentified peaks in the monomer ^{1}H NMR, suggesting the vacuum step efficiently removed impurities, unless present as endgroups in too low of a concentration to detect. Alkenes characteristically exhibit ^{13}C NMR resonances in the 80 - 140 ppm range, therefore, the lack of peaks in that region (**Figure 4** inset) provided further evidence that an unsaturated product (and resulting polyester) were not obtained.[27]

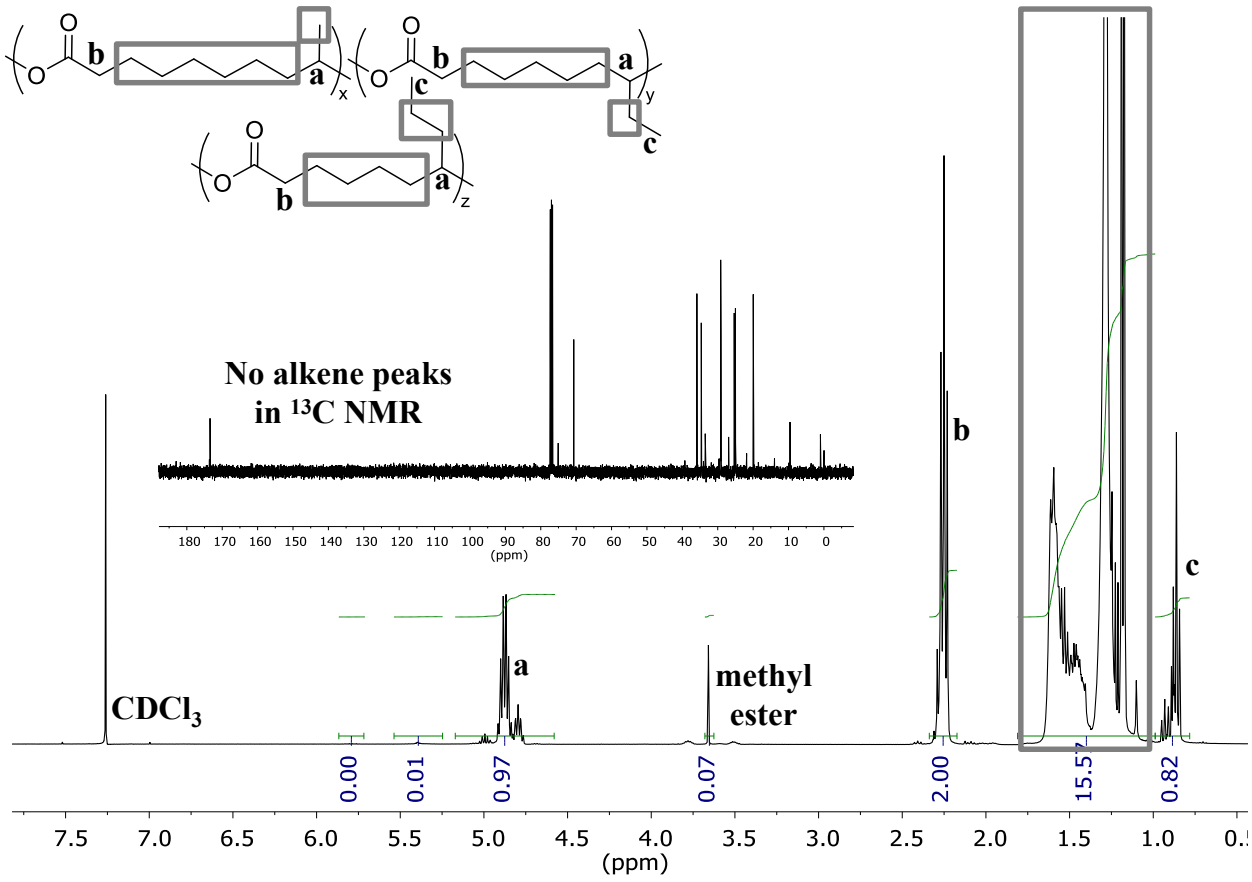

Figure 6.4. [1]H NMR spectroscopy confirms bio-based polyester structure and shows expected disappearance of methyl ester from monomer

Advanced polymer chromatography (APC) is a contemporary separation system from Waters which provides molecular weight data in minutes, readily accommodates a variety of solvents, and is capable of discerning low molecular weight species.[35] This unprecedented low molecular weight resolution enabled APC to monitor the transesterification reaction of the novel plant-based AB hydroxyester. **Figure 5** displays the APC chromatograms for the various reaction aliquots described in **Table 1** and the number-average molecular weight (M_n), weight-average molecular weight (M_w), and polydispersity index (PDI) values, all relative to polystyrene (PS) standards. The first 2 aliquots, taken after 2 h at 80 °C and an additional 2 h at 120 °C (4 h total), eluted too close to the solvent front for good resolution, however, the remaining time

points showed a steady increase in molecular weight with respect to time (and temperature). Multiple sharp peaks in the 5 h chromatogram indicated varying low molecular weight species, expected in the initial stages of melt transesterification.[22] As the reaction proceeded, smoother APC traces resulted and the molecular weight increased while the PDI approached the expected value of 2 for step-growth polymerizations.[36] After 8 h, 2 of those under reduced pressure, the plant-based polyester reached an M_w of 10000 g/mol and PDI of 1.83. The ^{1}H NMR results from **Figure 4** indicated methyl ester remained after 8 h. Suggested future work includes extending this conversion study to longer times at the lower temperatures and correlating with ^{1}H NMR to monitor the disappearance of the methyl ester. Additionally, unreacted 9-DAME or other monofunctional compounds in the monomer batch could act as endcapping agents, limiting achievable molecular weight.[36]

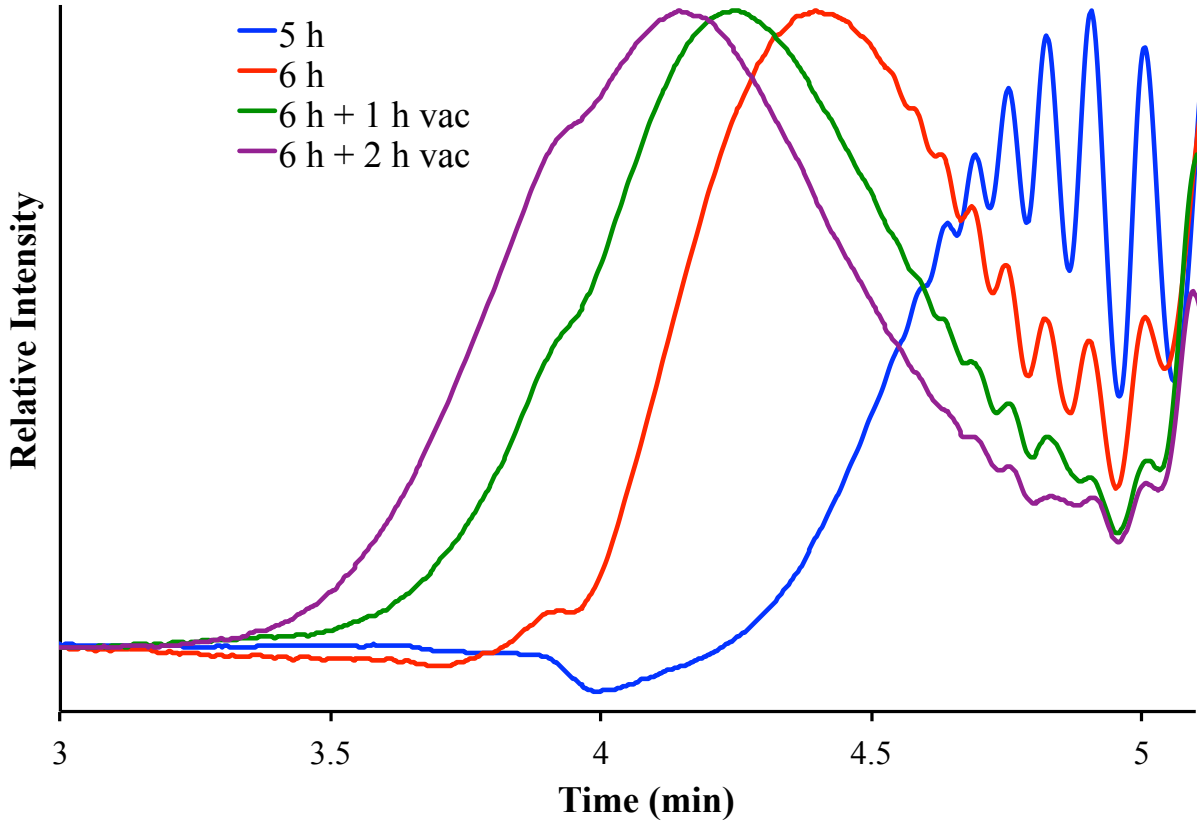

Figure 6.5. Advanced polymer chromatography (APC) provides excellent separation of low molecular weight species, allowing for monitoring molecular weight as the reaction proceeds

Table 6.1. Relative molecular weights of hydroxyester polymerization as a function of reaction time

Temperature (°C)	Polymerization Time (total h)	M_n (g/mol)[a]	M_w (g/mol)[a]	PDI[a]
80	2	N.D.	N.D.	N.D.
120	4	N.D.	N.D.	N.D.
170	5	1000	1700	1.59
200	6	3000	4500	1.52
200	6 + 1 @ 0.15 mmHg	4800	7600	1.58
200	6 + 2 @ 0.15 mmHg	5500	10000	1.83

a: Molecular weights determined from THF APC; relative to PS standards
N.D. = not determined

Polymerization of the AB hydroxyacid, depicted in **Scheme 2**, proceeded in the absence of catalyst and for substantially longer reaction times than the AB hydroxyester monomer. Direct esterifications eliminate water as the reaction progresses. The higher boiling point of water compared to the transesterification byproduct, MeOH, demands increased reaction time, particularly in the absence of catalyst.[22] **Figure 6** overlays the ^{1}H NMR spectra of the AB hydroxyacid monomer (bottom) and resulting polyester (top). Similar to the AB hydroxyester isomeric mixture, the primary methyl groups on the 7- and 8-OH isomers, labeled **b** in **Figure 6**, shifted upfield compared to the secondary methyl group of the 9-OH isomer. Almost identical to the AB hydroxyester monomer, peak **b** integrates to 0.83 when peak **a** is set to 2, resulting in about 28 % 7- and 8-OH. The methine protons of the 7- and 8-hydroxyesters, peak **d**, also shifted upfield relative to the 9-hydroxyester methine (**e**) and a similar, broad peak, appeared next to **d** as noted in the AB hydroxyester ^{1}H NMR discussion. The overlaid ^{1}H NMR spectra of

the monomer and polyester clearly indicate monomer dimers, as observed in both LC-MS and TOF-MS, via small peaks in the monomer around 4.8 ppm corresponding to the methine adjacent to the acid which increases upon polymerization. Interestingly, the ratio of 7- and 8-OH isomer present in the final polymerization based on the methyl resonance **b** decreased to 21 % ($\delta = 0.64$) suggesting different reactivity between the isomers whereas the AB hydroxyester polymer did not elucidate any difference in isomer reactivity.

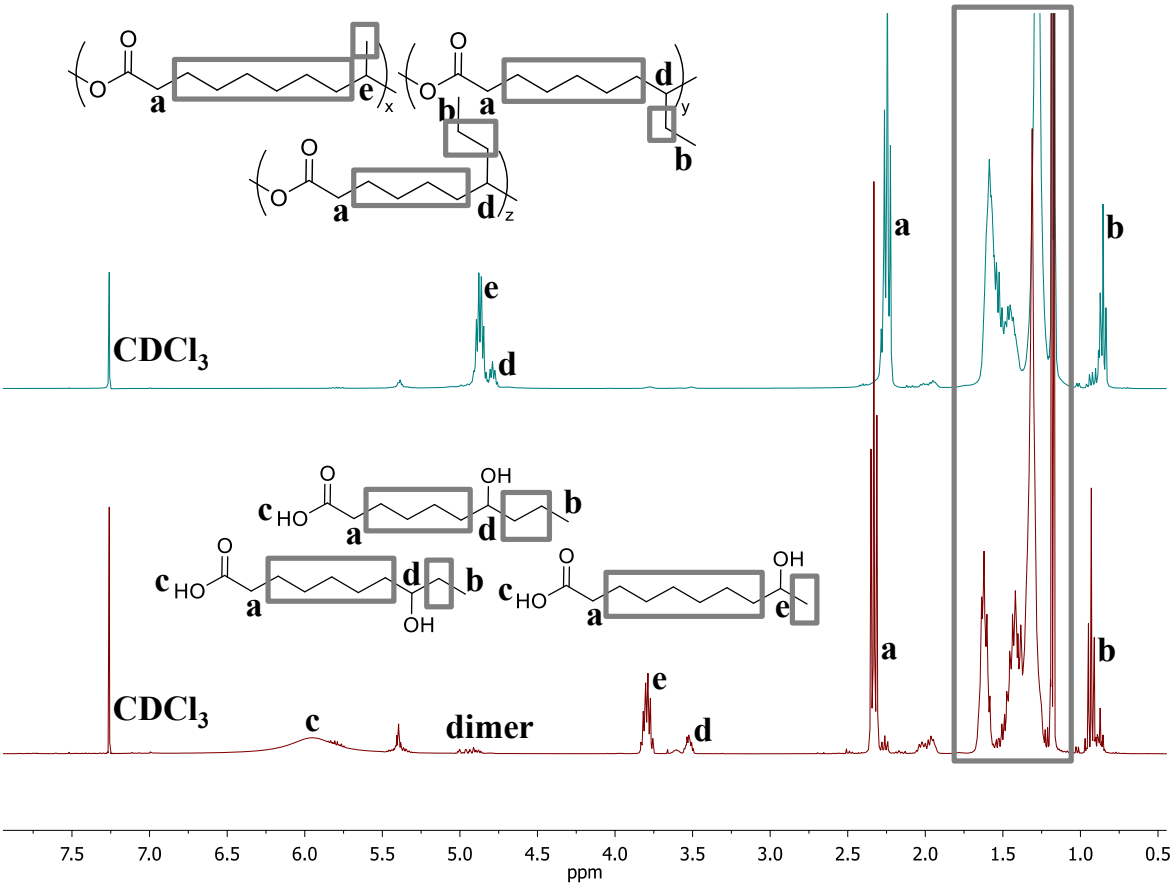

Figure 6.6. ^{1}H NMR spectra of AB hydroxyacid monomer (bottom) exhibiting presence of dimer and polymer (top) revealing the disappearance of the carboxylic acid upon polymerization

6.4.2 Thermal Analysis of Plant-based Polyesters

Thermogravimetric analysis (TGA) provided weight loss as a function of temperature for the plant-based AB monomers and resulting polyesters. **Figure 7** shows the degradation profiles. Both AB monomers started to lose mass at low temperatures, 139 °C for the AB hydroxyester and 159 °C for the AB hydroxyacid. These temperatures aided in determining an appropriate polymerization procedure and dictated the initial low temperature (80 °C) reaction steps to avoid possible monomer degradation and/or sublimation. The resulting polyesters exhibited similar degradation profiles with onset degradation temperatures ($T_{d,onset}$) for the largest mass loss around 320 °C. Slight mass loss occurred at lower temperatures for the polyesters generated from the 9 and 12.5 h polymerizations, $T_{d,5\%}$ = 295 °C and 225 °C, respectively. The mass seemed to originate near the monomer T_d, implying degradation products since the vacuum step should have removed any low molar mass compounds or unreacted monomer.

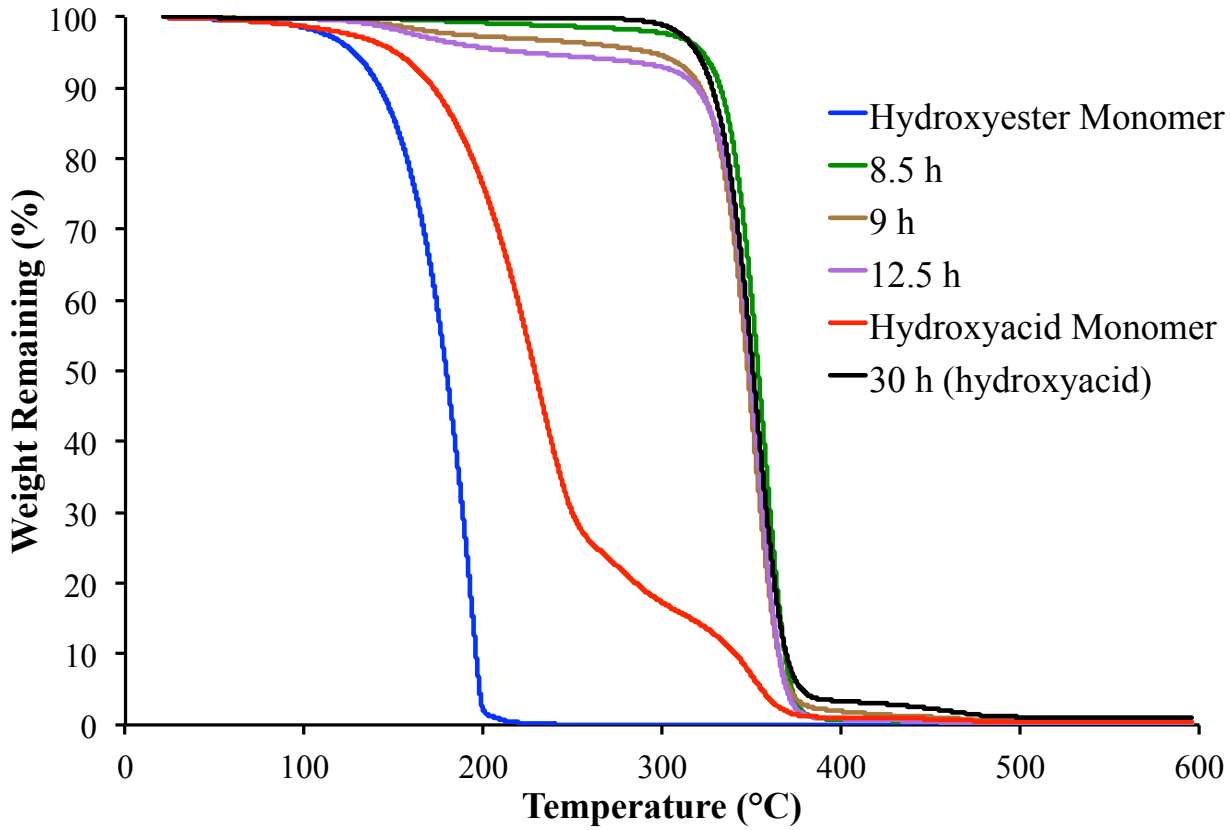

Figure 6.7. Thermal degradation profiles of bio-based AB monomers and resulting polyesters after different reaction procedures

Differential scanning calorimetry (DSC) of the AB hydroxyester monomer revealed a crystallization temperature of -23 °C and a melting temperature of 18 °C, consistent with it being a liquid at room temperature. **Figure 8** displays the DSC thermograms for the bio-based polyesters. A single glass transition temperature (T_g) occurred for each composition near -60 °C. The isomeric mixture of monomers introduced irregularity and crystallization did not occur on the time-scale and temperature range of the experiment. Poly(ε-caprolactone) (PCL), a commercially produced and degradable aliphatic polyester exhibits a T_g = -60 °C and a T_m = 60 °C.[22] PCL, synthesized through ring opening polymerization of ε-caprolactone performs in a variety of applications, mostly biological, including tissue engineering and drug delivery

devices.[37] The amorphous plant-based polyester offers ease of processability, potentially enhanced degradation due to the absence of crystalline domains, and could perform as a renewable substitute to PCL in biological applications desiring decomposition. Further applications include incorporating the bio-based oligoesters into segmented polyurethanes to serve as a low-T_g soft segment for thermoplastic elastomers.[38]

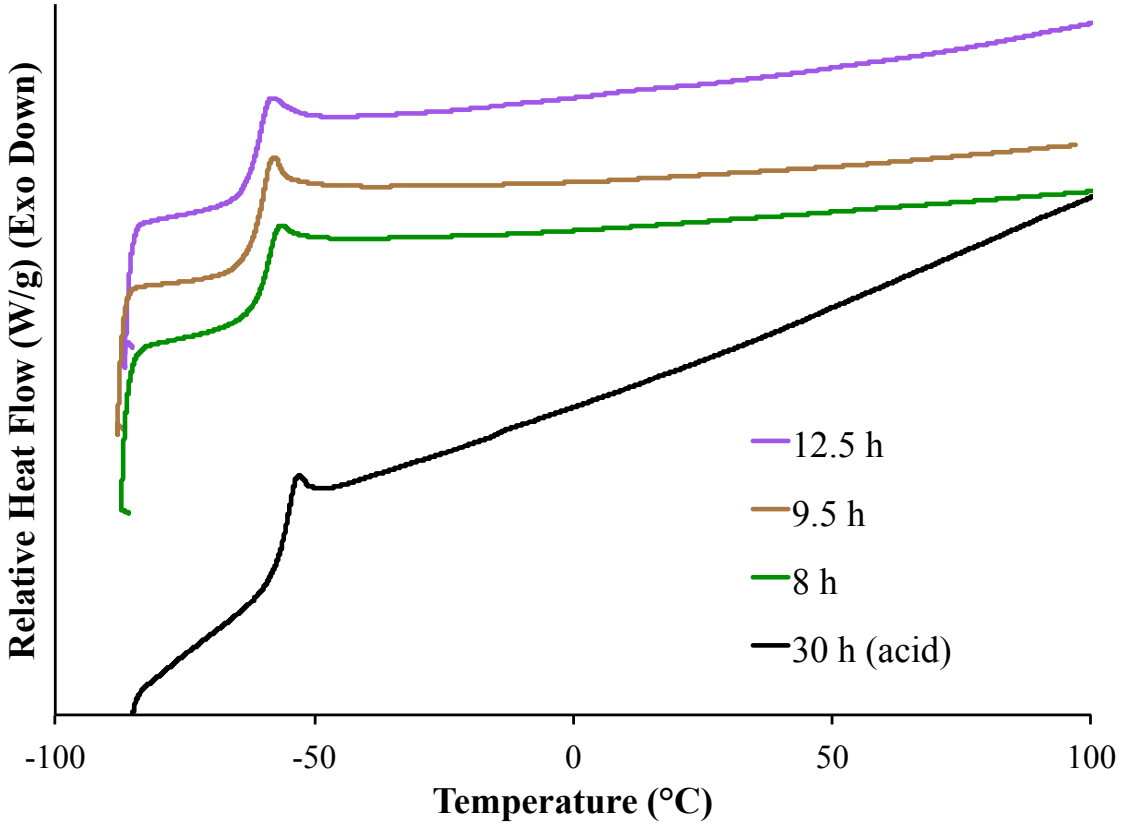

Figure 6.8. Isomeric mixture of bio-based monomers affords low T_g amorphous copolyesters

6.4.3 Synthesis and Crosslinking of ABB' Plant-based Monomer

Warwel et al.[28] elegantly displayed the opportunities an alkene functional group offers in the design and synthesis of polymers. Acyclic diene metathesis (ADMET) polymerization of dialkenes, ring opening polymerization of epoxides generated from enzymes, and polymerizable

unsaturated diesters obtained from methathesis reactions are some of the avenues explored. Utilizing the alkene, **Scheme 3** depicts the epoxidation of 9-DAME **(a)** and subsequent hydrolysis **(b)** to afford an ABB' dihydroxyester step-growth monomer (MDHD). *Meta*-chloroperoxybenzoic acid (*m*-CPBA) efficiently converted the alkene to an epoxide (> 98 % yield). In the event of scale-up or industrial production and to improve environmental implications, a hydrogen peroxide/formic acid reaction, with or without an enzyme catalyst, could reduce chlorinated solvents and byproducts.[8,28] Refluxing in water generated the final product with minimal workup. **Figure 12** and **Figure 13** in the supporting information present the ^{1}H NMR spectra of the epoxide and MDHD, respectively.

Scheme 6.3. Two step synthesis of ABB' hydroxyester step-growth monomer and/or crosslinking additive. (a) Epoxidation of 9-DAME (b) Hydrolysis of epoxidized 9-DAME yields MDHD

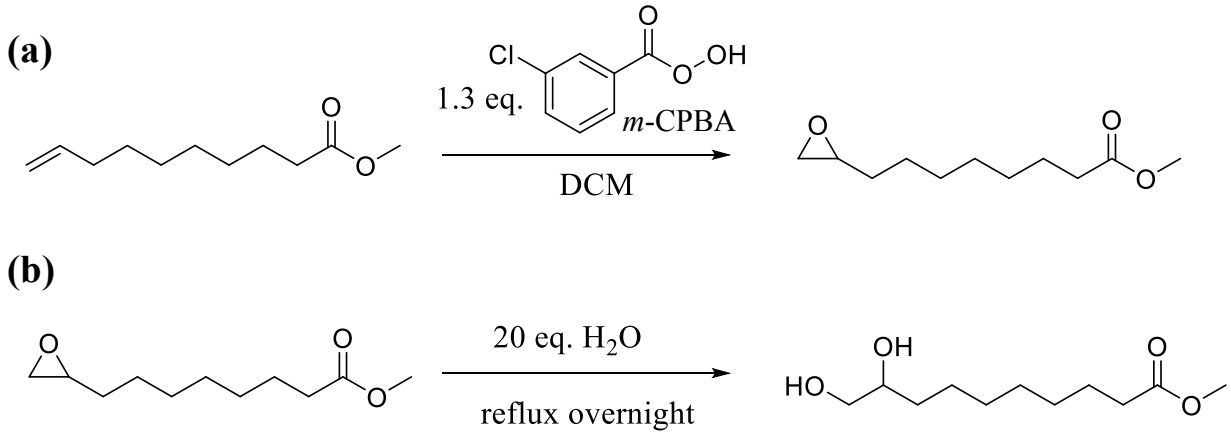

Step-growth monomers containing functionality greater than 2 (f > 2) generate dendritic, hyperbranched, branched, or crosslinked polymers.[22,39,40] Specifically, the self-condensation of AB_2 monomers containing a mixture of ester-forming functional groups often produces hyperbranched polyesters, demonstrated with a variety of both aromatic and aliphatic trifunctional monomers.[41,42] The successful synthesis of hyperbranched structures using AB_2

monomers depends on equally reactive B groups.[22,40,43] Unequal reactivity between functional groups can induce crosslinking since the polymerization acts like a pseudo $A_2 + B_3$ system, where the concentration of B_3 is crucial to avoid gelation.[40,43] In an $A_2 + B_3$ polymerization gelation is avoided through the introduction of a monofunctional monomer.[40] Researchers proved a ratio of monofunctional to trifunctional monomers greater than or equal to 3 produces high molecular weight, gel-free, polymers.

MDHD is classified as an ABB' monomer because it contains one primary and one secondary hydroxyl group. Primary and secondary hydroxyls often transesterify at different rates; the less encumbered primary group reacting faster.[44] As discussed above, unequal reactivity could hinder the ability to achieve hyperbranched polyesters from MDHD alone. Bao and coworkers[21] reported hyperbranched polyesters from a similar ABB' monomer derived from a thiolene click reaction between 10-DAME and 1-thioglycerol. 9 different polymerization procedures with varying catalyst type, reaction time, and reaction temperatures produced high molecular weight hyperbranched polyesters. Based on this literature precedence, MDHD was evaluated as a monomer for the synthesis of hyperbranched polyesters.

Scheme 6.4. Melt transesterification of MDHD ABB' monomer affords crosslinked networks

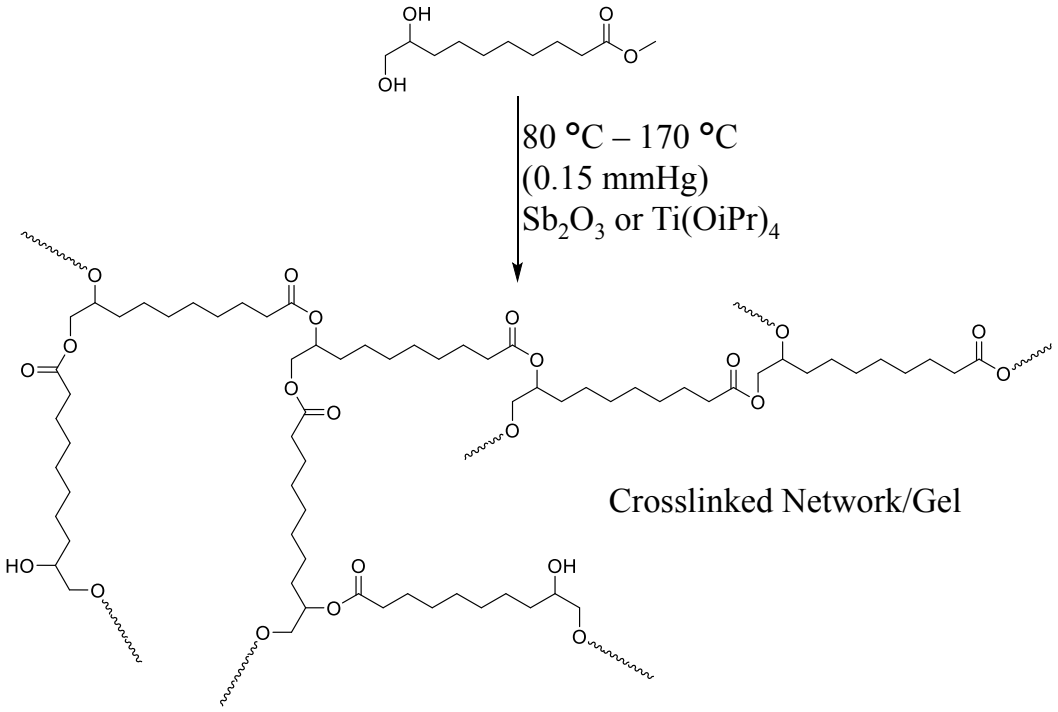

Scheme 4 displays the melt transesterification of MDHD and proposed hyperbranched polyester structure. Following similar transesterification procedures from the ABB' monomer discussed above (methyl 11-((2,3-dihydroxypropyl)thio)undecanoate), **Table 1** shows 4 different polymerization procedures employed using MDHD.[21] In all instances, the MDHD-containing polyesters gelled in the melt. Despite changing the catalyst, polymerization time, and vacuum application, MDHD did not afford hyperbranched polyesters under the conditions evaluated. The literature procedures used 0.5 g catalyst/0.1 mol monomer in each polymerization. For MDHD, lower amounts of the highly active titanium tetraisopropoxide ($Ti(OiPr)_4$) catalyst were added, unsuccessfully, in an attempt to diminish the pseudo $A_2 + B_3$ reaction.[22] Common $Ti(OiPr)_4$ catalyst amounts for transesterification are in the ppm range, much less than employed for this synthesis, nonetheless, gelation as a result of the unequal reactivity of the two hydroxyl functional groups was not unexpected.[33,45,46] The reactivity and successful transesterification of

MDHD to form crosslinked networks succeeded in demonstrating the ability of this monomer as a bio-based degradable polyester branching and crosslinking additive.[40,47,48]

Table 6.2. Synthetic procedures and thermal analysis of ABB' polyester crosslinked networks

Catalyst	Polymerization Time (total h)[a]	$T_{d,5\%}$ (°C)[b]	$T_{d,onset}$ (°C)[b]	T_g (°C)[c]
$Ti(OiPr)_4$[d]	6 + 0.33 @ 0.15 mmHg	252	--	-34
Sb_2O_3[e]	6 + 0.28 @ 0.15 mmHg	320	375	-20
$Ti(OiPr)_4$[f]	9	319	364	-18
Sb_2O_3[e]	9	350	371	-9

a: All polymerizations proceeded for 2 h @ 80 °C, 2 h @ 120 °C, and the remaining time at 170 °C
b: Data obtained from a TA Instruments TGA Q50, N_2 atmosphere, 10 °C/min heating
c: Data obtained from a TA Instruments DSC Q1000; values reported are from the second heat
d: ~1.4 % catalyst
e: 0.5 g catalyst/0.1 mol monomer
f: ~0.45 % catalyst

6.4.4 Thermal Characterization of Crosslinked Networks

Thermal analysis of the crosslinked polyesters revealed a multi-step degradation profile with $T_{d,5\%}$ ranging from 252 °C – 350 °C. **Figure 9** shows the TGA curves for MDHD and 4 polyester networks. The reaction conditions subjected upon MDHD were not optimized to synthesize crosslinked polyesters with high gel fractions and exact gel fractions were not determined. Oligomers not participating in the crosslinked network could cause the observed initial mass loss and multiple degradation steps. DSC provided thermal transitions for the polyester networks, visible in **Figure 10**. Low T_g's resulted and some networks exhibited a T_m, however, exact thermal properties remain undetermined as potential oligomer contaminant could plasticize and/or crystallize the unextracted polyester networks. These initial studies served as a

proof-of-concept that MDHD, an ABB' plant-based monomer, could successfully function as a novel branching or crosslinking additive.

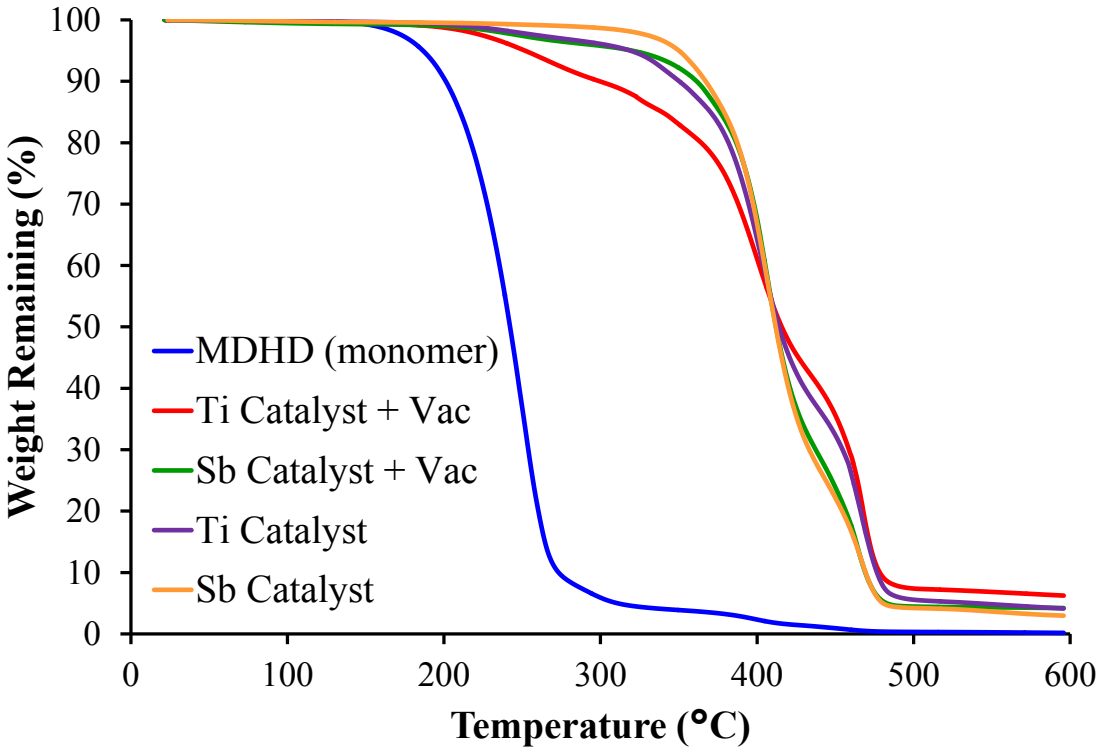

Figure 6.9. Thermal degradation profiles of novel MDHD-based polyester networks

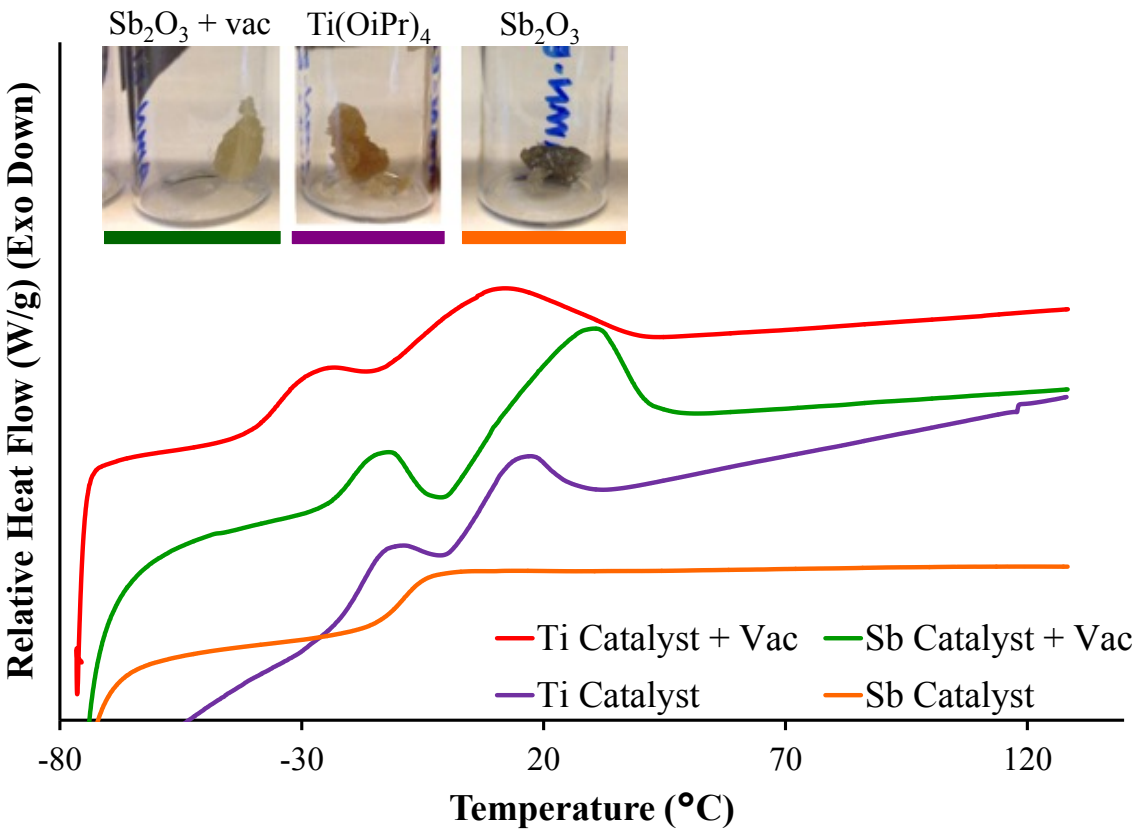

Figure 6.10. Thermal analysis of bio-based polyester networks

6.5 *Conclusions*

The development of sustainable materials is a highly active and discussed research area.[2,49,50] 9-DAME, a plant-based fatty acid containing a terminal alkene, proved as a successful platform for novel bio-based polyesters and a multi-functional branching/crosslinking additive. A formic acid hydration introduced secondary diol functionality while maintaining the original ester, or acid upon hydrolysis, functionality. 1,2-hydride shifts produced an isomeric mixture of the AB monomer and ^{1}H NMR elucidated about 28 % 7- and 8-OH isomers. Melt transesterification generated novel amorphous polyesters and APC monitored molecular weight as a function of reaction time showing M_w growth from 1700 to 10,000 g/mol. The isomeric

mixture resulting in an irregular polymer structure was used to explain the lack of crystallinity and the novel aliphatic polyesters exhibited $T_g \cong$ -60 °C, identical to commercially prevalent PCL.[22] These novel polyesters could serve as plant-based degradable substitutes for PCL, provide a renewable, low-T_g, soft segment in thermoplastic polyurethane elastomers, and even impact emerging applications such as microstereolithography 3D printing after acrylic endgroup functionalization.[37,38,51] Furthermore, a two-step synthesis transformed 9-DAME into an ABB' monomer. Epoxidation of the alkene and subsequent hydrolysis generated a primary and secondary alcohol functionality. The synthesis of hyperbranched polyesters was unsuccessful and attributed to the unequal reactivity between primary and secondary hydroxyl groups. The plant-based ABB' monomer, MDHD, formed crosslinked polyester networks in the melt under catalyzed transesterification conditions confirming reactivity and enabling use as a bio-based degradable branching or crosslinking additive.

6.6 *Acknowledgements*

This research was funded by Elevance Renewable Sciences, Inc. The author's would like to thank Elevance and their technical team for financial support, insightful discussions, and supplying 9-DAME. The author's would like to thank Waters for donating the APC and Ryan Mondschein, fellow graduate student and Long group member, for discussions and insight in regard to ^{1}H NMR and MS interpretation and running APC. A special thank you to Dr. Mehdi Ashraf-Khorassani and William Bebout for running and discussing the LC/MS and TOF-MS, respectively.

6.7 *References*

(1) Singh, S. P.; Ekanem, E.; Wakefield Jr, T.; Comer, S. *International Food and Agribusiness Management Review* **2003**, *5*, 14.
(2) Mooney, Brian P. *Biochemical journal*, *418*, 219.
(3) Gandini, A. *Macromolecules* **2008**, *41*, 9491.
(4) Gandini, A.; Lacerda, T. M. *Progress in Polymer Science*.
(5) Feng, X.; East, A. J.; Hammond, W. B.; Zhang, Y.; Jaffe, M. *Polymers for Advanced Technologies* **2011**, *22*, 139.
(6) Fenouillot, F.; Rousseau, A.; Colomines, G.; Saint-Loup, R.; Pascault, J. P. *Progress in Polymer Science* **2010**, *35*, 578.
(7) Lunt, J. *Polymer Degradation and Stability* **1998**, *59*, 145.
(8) Meier, M. A. R.; Metzger, J. O.; Schubert, U. S. *Chemical Society Reviews* **2007**, *36*, 1788.
(9) Bahr, M.; Bitto, A.; Mulhaupt, R. *Green Chemistry* **2012**, *14*, 1447.
(10) Bakhshi, H.; Yeganeh, H.; Mehdipour-Ataei, S. *J. Biomed. Mater. Res. Part A* **2013**, *101A*, 1599.
(11) Wu, J.; Eduard, P.; Thiyagarajan, S.; Jasinska-Walc, L.; Rozanski, A.; Guerra, C. F.; Noordover, B. A. J.; van Haveren, J.; van Es, D. S.; Koning, C. E. *Macromolecules* **2012**.
(12) Helou, M.; Carpentier, J.-F.; Guillaume, S. M. *Green Chemistry* **2011**, *13*, 266.
(13) Koch, C. A.; Patent, U. S., Ed.; AVery Dennison Corporation: US, 2014; Vol. US 8,796,351 B2.
(14) Anastas, P.; Eghbali, N. *Chemical Society Reviews* **2010**, *39*, 301.
(15) Li, S. *Journal of Biomedical Materials Research* **1999**, *48*, 342.
(16) Grizzi, I.; Garreau, H.; Li, S.; Vert, M. *Biomaterials* **1995**, *16*, 305.
(17) Hakkarainen, M. In *Degradable Aliphatic Polyesters*; Springer Berlin Heidelberg: 2002; Vol. 157, p 113.
(18) Liu, C.; Liu, F.; Cai, J.; Xie, W.; Long, T. E.; Turner, S. R.; Lyons, A.; Gross, R. A. *Biomacromolecules* **2011**, *12*, 3291.
(19) Liu, G.; Kong, X.; Wan, H.; Narine, S. *Biomacromolecules* **2008**, *9*, 949.
(20) Wu, J.; Eduard, P.; Jasinska-Walc, L.; Rozanski, A.; Noordover, B. A. J.; van Es, D. S.; Koning, C. E. *Macromolecules* **2012**, *46*, 384.
(21) Bao, Y.; He, J.; Li, Y. *Polymer International* **2013**, *62*, 1457.
(22) Rogers, M. E.; Long, T. E. *Synthetic methods in step-growth polymers*; Wiley-Interscience: Hoboken, N.J., 2003.
(23) Gao, C.; Yan, D. *Progress in Polymer Science* **2004**, *29*, 183.
(24) Bonnaillie, L. M.; Wool, R. P. *Journal of Applied Polymer Science* **2007**, *105*, 1042.
(25) Uyama, H.; Kuwabara, M.; Tsujimoto, T.; Kobayashi, S. *Biomacromolecules* **2003**, *4*, 211.
(26) Kim, J. R.; Sharma, S. *Industrial Crops and Products* **2012**, *36*, 485.
(27) Bruice, P. Y. *Organic Chemistry*; 7th ed.; Pearson Education, Inc: Upper Saddle River, NJ, 2014.
(28) Warwel, S.; Brüse, F.; Demes, C.; Kunz, M.; Klaas, M. R. g. *Chemosphere* **2001**, *43*, 39.
(29) Kang, H.; Lin, Q.; Armentrout, R. S.; Long, T. E. *Macromolecules* **2002**, *35*, 8738.

(30) Peterson, P. E.; Allen, G. *The Journal of Organic Chemistry* **1962**, *27*, 1505.
(31) Diaper, D. G. M.; Mitchell, D. L. *Canadian Journal of Chemistry* **1960**, *38*, 1976.
(32) Ham, G. E. *Journal of Polymer Science* **1962**, *61*, 293.
(33) Lin, Q.; Pasatta, J.; Long, T. E. *J. Polym. Sci., Part A: Polym. Chem.* **2003**, *41*, 2512.
(34) Kelsey, D. R.; Scardino, B. M.; Grebowicz, J. S.; Chuah, H. H. *Macromolecules* **2000**, *33*, 5810.
(35) Waters 2015; Vol. 2015.
(36) Odian, G. *Principles of Polymerization, Fourth Edition*; John Wiley & Sons, Inc.: Hoboken, NJ, 2004.
(37) Woodruff, M. A.; Hutmacher, D. W. *Progress in Polymer Science* **2010**, *35*, 1217.
(38) Yilgör, I.; Yilgör, E.; Wilkes, G. L. *Polymer* **2015**, *58*, A1.
(39) Odian, G. G. *Principles of polymerization*; Wiley-Interscience: Hoboken, N.J., 2004.
(40) McKee, M. G.; Unal, S.; Wilkes, G. L.; Long, T. E. *Progress in Polymer Science* **2005**, *30*, 507.
(41) Malmstroem, E.; Johansson, M.; Hult, A. *Macromolecules* **1995**, *28*, 1698.
(42) Lin, Q.; Long, T. E. *Journal of Polymer Science Part A: Polymer Chemistry* **2000**, *38*, 3736.
(43) Voit, B. I.; Lederer, A. *Chemical Reviews* **2009**, *109*, 5924.
(44) Otera, J. *Chemical Reviews* **1993**, *93*, 1449.
(45) Unal, S.; Lin, Q.; Mourey, T. H.; Long, T. E. *Macromolecules* **2005**, *38*, 3246.
(46) Unal, S.; Long, T. E. *Macromolecules* **2006**, *39*, 2788.
(47) McKee, M. G.; Wilkes, G. L.; Colby, R. H.; Long, T. E. *Macromolecules* **2004**, *37*, 1760.
(48) Chandorkar, Y.; Bhagat, R. K.; Madras, G.; Basu, B. *Biomacromolecules* **2014**, *15*, 863.
(49) Shearouse, W. C.; Lillie, L. M.; Reineke, T. M.; Tolman, W. B. *ACS Macro Letters* **2015**, *4*, 284.
(50) Hillmyer, M. A.; Tolman, W. B. *Accounts of Chemical Research* **2014**, *47*, 2390.
(51) Schultz, A. R.; Lambert, P. M.; Chartrain, N. A.; Ruohoniemi, D. M.; Zhang, Z.; Jangu, C.; Zhang, M.; Williams, C. B.; Long, T. E. *ACS Macro Letters* **2014**, *3*, 1205.

6.8 *Supporting Information*

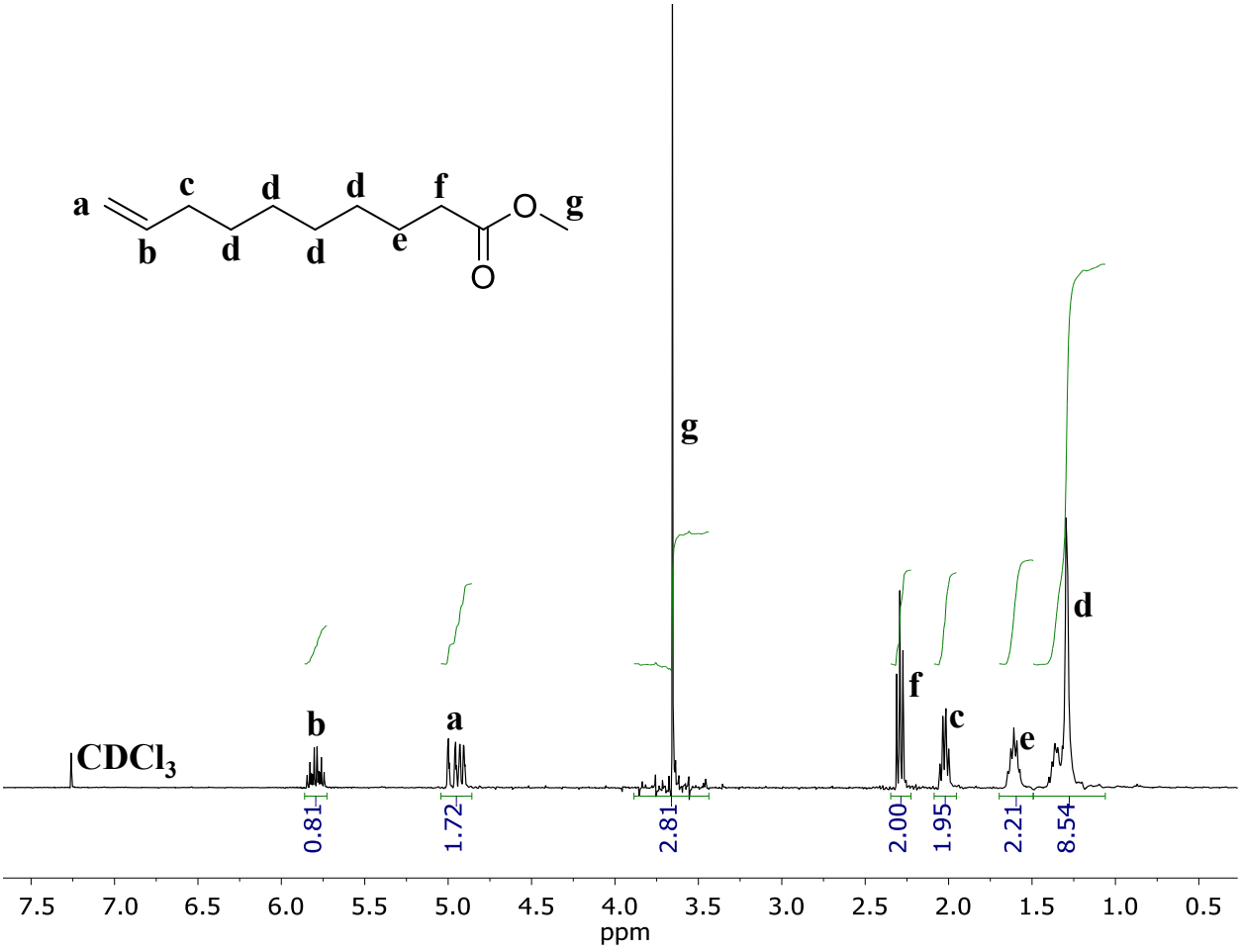

Figure 6.11. ^{1}H NMR spectroscopy of as-received 9-DAME

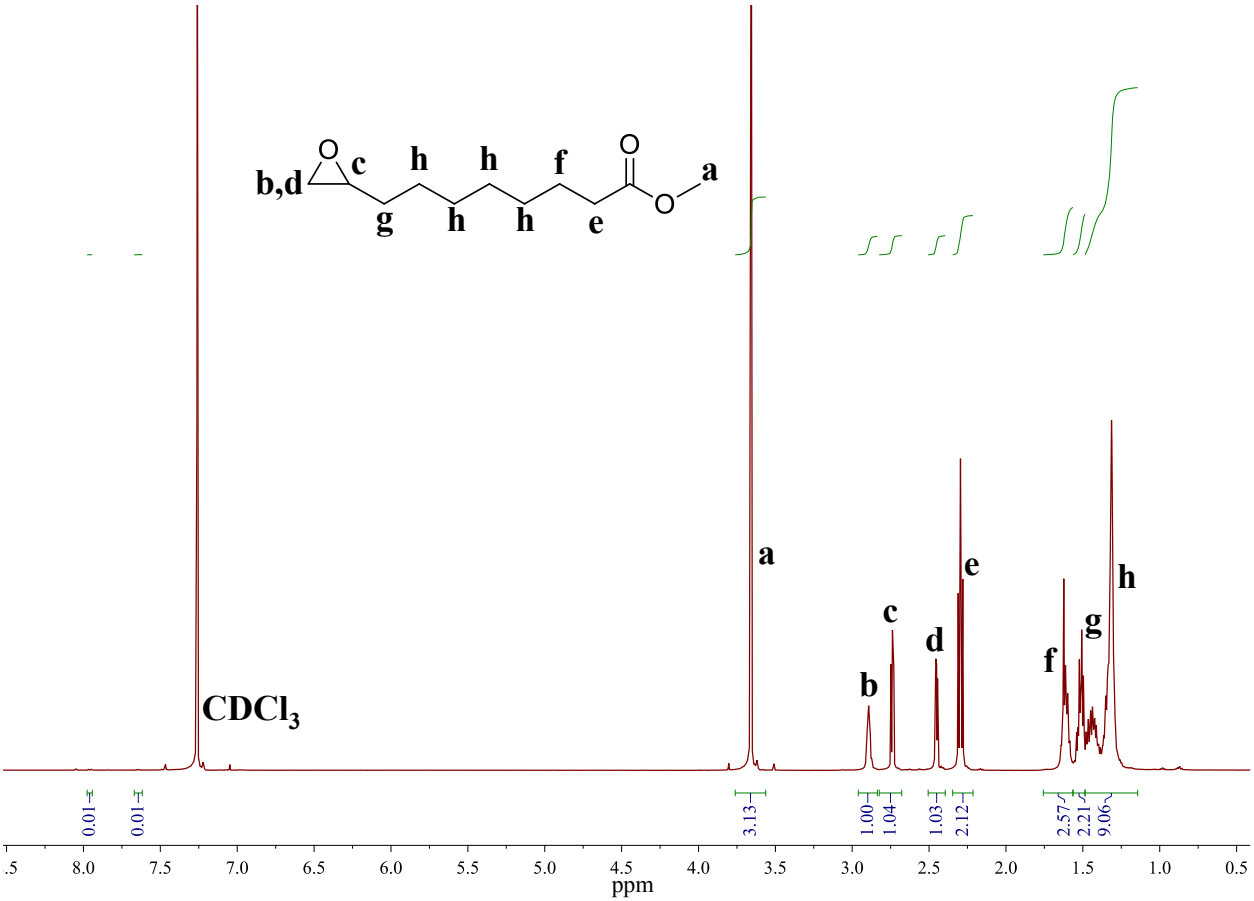

Figure 6.12. ^{1}H NMR spectroscopy of 9,10-epoxydecanoate

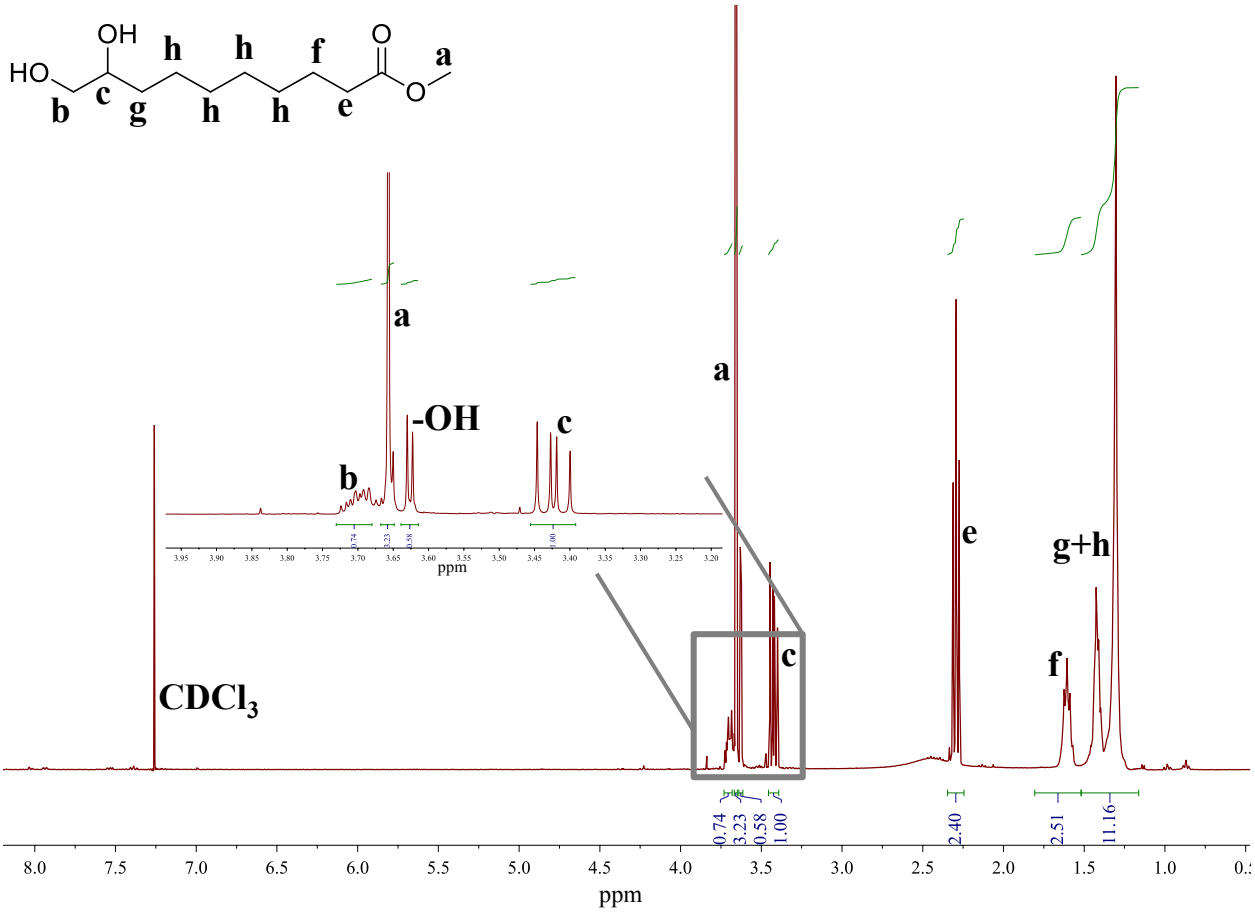

Figure 6.13. ^{1}H NMR spectroscopy confirms structure of MDHD ABB' monomer

Chapter 7: Synthesis, Properties and Applications of Ion-Containing Polyurethane Segmented Copolymers

(Published in *Macromolecular Chemistry and Physics* **2014**, *215*, 2161.)

Ashley M. Nelson and Timothy E. Long

Department of Chemistry, Macromolecules and Interfaces Institute
Virginia Tech, Blacksubrg, VA 24061-0212

7.1 *Abstract*

Despite the well-established foundation of polyurethane chemistry in both industry and academia, research continues at a vigorous pace to refine synthetic processes and discover new functional materials. Incorporating ionic groups into polymers is a synthetic parameter capable of tailoring polymer properties and enabling emerging technologies. This review focuses on recent efforts in the field of ion-containing segmented polyurethane copolymers. Multiple synthetic strategies to incorporate both cationic and anionic sites, including a particular focus on waterborne polyurethane dispersions and green synthetic methods are examined. Fundamental structure-property relationships based on ionic structure, content, and placement are explored and many applications, including biomedical products and polymer electrolytes for energy devices are discussed.

7.2 *Introduction*

Polyurethanes represent a very well-established class of step-growth polymers, and their synthesis was described nearly 80 years ago.[1,2] The commercial impact of polyurethanes is broad with uses ranging from foams and insulation to adhesives and encapsulants.[3,4] Due to extensive research, a myriad of suitable monomers and synthetic strategies were developed to enable polyurethanes to impact such diverse markets. One particularly advantageous feature is the ability for polyurethanes to function as thermoplastic elastomers (TPEs).[3] A microphase separated physical network forms upon introduction of a low glass transition temperature (T_g) oligomer, often a polyether or polyester such as poly(ethylene glycol) (PEG) or poly(tetramethylene oxide) (PTMO), to the polyurethane reaction. The hydrogen bonding, depicted in **Figure 1**, between the urethane carbonyl oxygen and urethane hydrogen coupled with crystallization construct the hard segment (HS) domains while the functionalized flexible spacers comprise the soft segments (SS) in an alternating fashion. The microphase separated morphology of segmented polyurethanes is the foundation for their versatility, with the ability to further tune materials for a specific application with other synthetic parameters such as chemical composition and molecular weight. Yilgör, Yurtsever, and Wilkes et al.[5-7] extensively studied various model segmented polyurethane systems to further understand the morphology and factors influencing morphology on a fundamental structure-property level.

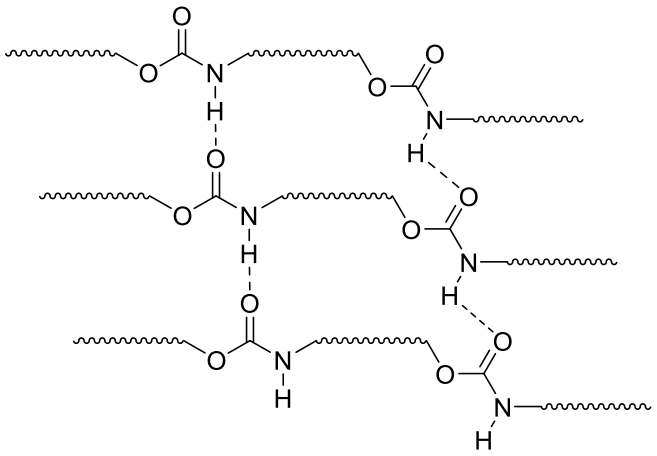

Figure 7.1. Hydrogen bonding, shown with dashed lines, between the hydrogen and carbonyl oxygen in urethane bonds.

Many comprehensive reviews and peer-reviewed journal articles focus on fundamental structure-property relationships of segmented polyurethanes.[8-11] The influence of different synthetic methods and HS/SS composition (chemical composition and number-average molecular weight (M_n) of both the individual segments and final polyurethane) and the resultant impact on the thermal, mechanical, elastomeric, and morphological properties have provided a fundamental understanding of segmented polyurethane copolymers. Performance tunable polymeric materials are desirable, as a keen understanding of the change in properties with various compositional parameters facilitates the design of specific properties for the intended application.[12-14] The search continues for novel compositions with unique properties, and technology-driven innovation affording new monomers, functionalized oligomers, and morphological design rendering segmented polyurethanes the focus of many industrial and academic research.[15-18]

The introduction of ionic groups to polymers is a recurring theme and one of continued interest; charge further tunes properties and expands potential applications.[19,20] Water solubility for coatings applications, deoxyribonucleic acid (DNA) binding for gene delivery, and ionic

conductivity represent areas where ion incorporation has significantly impacted.[21-23] Segmented polyurethanes offer exceptional versatility in their design as the ion type, location of the ionic site (HS, SS, or both), and the charge content are variable. In fact, Jaudouin et al.[24] published a review in 2012 discussing a single family of charged polyurethanes, polyurethane ionomers. Ionomers are a unique class of polymers containing a maximum of 15 mol % charge with applications ranging from waterborne coatings to biomedical applications. The following review focuses on very recent literature, highlighting new directions, elucidating structure-property relationships, and exploring emerging applications of segmented ion-containing polyurethanes. The various synthetic strategies to introduce charge are discussed in detail as well as the influence of charge placement on polyurethane properties.

7.3 *Synthesis of Ion-Containing Segmented Polyurethanes*

A urethane bond forms when an alcohol reacts with an isocyanate.[1,3,4] This energetically favored reaction between diols and diisocyanates drives the production of high molecular weight polyurethanes. Segmented polyurethanes require a slightly altered synthetic strategy to afford the desired blocky architecture. A telechelic functionalized oligomer serves as the SS. The end-group functionality of the oligomer and accompanying comonomers determine the type of segmented polyurethane, hence segmented polyurethanes occasionally contain an extra descriptor such as poly(urethane-esters) or poly(urethane-ureas) when a diacid or diamine is introduced, respectively.

Traditional segmented polyurethane synthesis proceeds through two popular routes, i.e., the one-shot and prepolymer methods.[1,4] Despite the synthetic route, the starting materials are identical; a polyol, a diisocyanate, and a diol. The diol is often referred to as the chain extender,

and the reaction of the diisocyanate with the diol forms the HS. As the name implies, the one-shot method involves the addition of all the reagents at the same time and the resulting polymer is immediately injection molded. The prepolymer, or two-shot, method requires first end-capping the oligomer with isocyanate functionality and then adding the chain extender in a subsequent step. **Figure 2** illustrates the two-step prepolymer route to segmented polyurethanes, distinguishing the SS and HS blocks comprised of the functionalized polyol, and diisocyanate and diol chain extender, respectively. The prepolymer method provides superior control of the polymer architecture because complete functionalization of the isocyanate-functionalized oligomer is predetermined as opposed to the presence of competing reactions of the polyol and diisocyanate, and diol and diisocyanate occurring simultaneously. For example, 1:1 stoichiometry of isocyanate-end-capped oligomer to chain extender would result in a small, well-defined HS consisting of only one chain extender and two diisocyanate units.

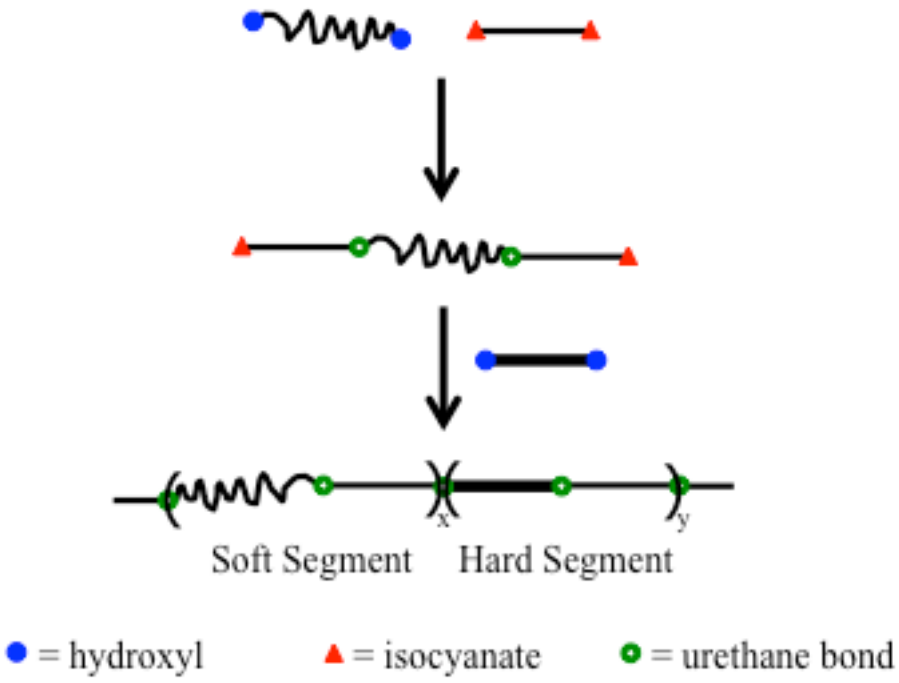

Figure 7.2. Prepolymer route to segmented polyurethanes.

Expanding upon the aforementioned synthetic strategies, there are two popular approaches to incorporate ionic sites into polyurethanes, i.e. using preformed charged monomers or a post-polymerization modification reaction such as alkylation.[25,26] In either route, the ionic content will reside in either the HS or SS at varying levels simply depending on the monomer(s) chosen and desired amounts.[27] The effect of charge placement and content on polymer properties is discussed in detail in later sections of this review. The inherent versatility in segmented polyurethane synthesis gives rise to a seemingly limitless array of possible architectures with the required functionalities (diol, diisocyanate, polyol), including anionic, cationic, and even zwitterionic monomers.[28-32] For example, **Scheme 1** shows the synthetic route for a zwitterionic sulfobetaine diol.[31]

Scheme 7.1. Synthesis of a zwitterionic diol.[30,31]

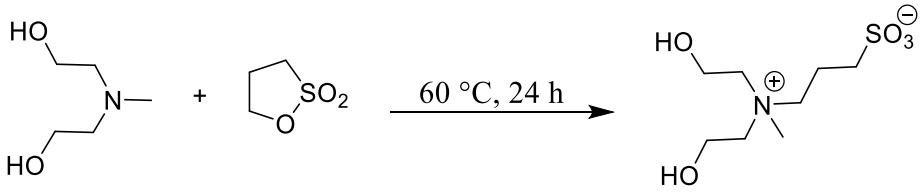

Incorporation of ionic groups exclusively in the HS involves the diisocyanate or chain extender with charged sites or a functional group which becomes charged upon further reaction. **Figure 3** depicts a selection of monomers employed in the synthesis of ion-containing segmented polyurethanes, where the charge solely resides in the HS.[26-28,33,34] Details pertaining to the resultant polyurethanes are discussed in subsequent sections; however, this group of monomers emphasizes the chemical and structural diversity of ion-containing polyurethanes. This diversity facilitates the complex design of polyurethanes for targeted applications. Compounds **A**, **B**, and **E** are cationic although differ in the specific ion type; phosphonium, calcium, and imidazolium, respectively. The anionic monomers, **C** and **D**, also contain different

ionic groups, sulfonate and carboxylate. Additionally, each monomer depicted contains a different counterion. The counterion is often a result of the reagents used in the monomer synthesis, but is tunable with a simple anion (or cation) exchange reaction.[26-28,35] Wang and coworkers[28] utilized compound **D** in the synthesis of ion-containing segmented polyurethanes and upon cation exchange reactions, the investigators evaluated the effect of 9 different ionic liquid (IL) countercations (including sodium, ammonium, imidazolium, and phosphonium ions) on various polyurethane properties.

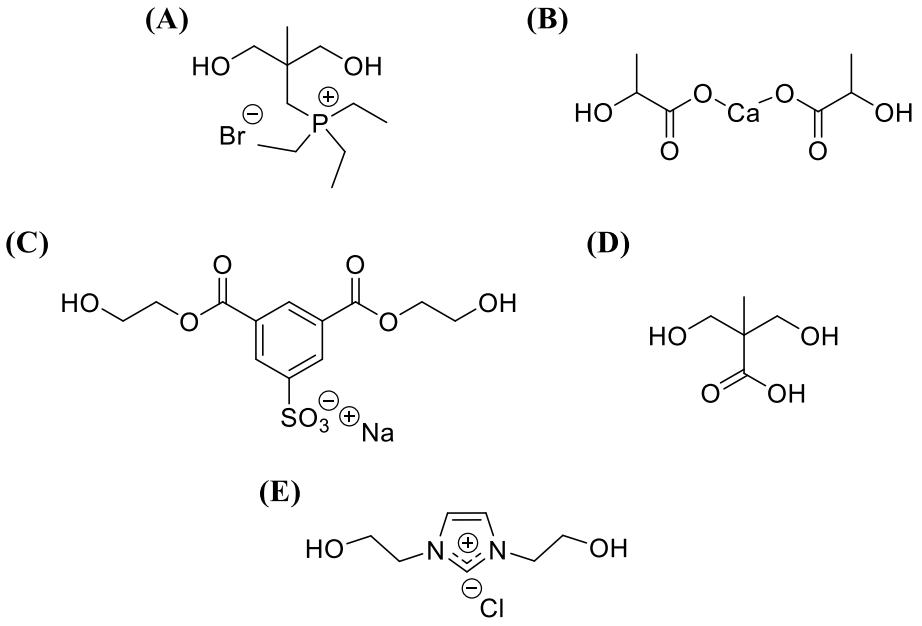

Figure 7.3. Some polyurethane monomers which place ionic groups in HS.[26-28,33,34]

Commercially available oligomeric polyols are often used in the synthesis of segmented polyurethanes as an easily accessible starting material with known M_n and confirmed difunctionality, which eliminate the needs for (multi-step) reactions and arduous purification.[26,34,36] Common oligomers include PEG, PTMO, poly(propylene glycol) (PPG), and poly(caprolactone) (PCL).[26,34,36,37] These oligomers are offered in multiple M_n's, which is convenient for probing the effect of SS M_n on polymer properties; however, most commercially

available oligomers are neutral and lack necessary functionality for incorporating charged species. As a result, the synthesis of segmented polyurethanes with charge specifically in the SS requires novel oligomers. Despite the synthetic challenges, several ion-containing SSs exist as a result of the efforts of many research groups.[27,31,38-45] Ammonium, sulfonate, and carboxylate-containing SSs were prepared, providing similar ionic variety as charged HS monomers. The location and amount of ionic groups within the SS, and ultimately in the resulting segmented polyurethane, depends on the synthesis of the SS. Kurt et al.[42,43] synthesized alkyl bromide-containing poly(oxetanes) which was amenable to a quantitative substitution reaction to afford pendant ammonium groups. A transesterification reaction of PEG with dimethyl 5-sulfoisophthalate sodium salt resulted in a sulfonated SS with only one ionic group per SS unit.[27] **Figure 4** depicts the chemical structures of some commercially available (**F**, **G**, and **I**) and ion-containing SSs (**H** and **J**), showing the variation in ion placement.[27,42,43] Throughout this review many other ion-containing SSs, including the effect of ionic content and placement on polymer properties will be discussed.

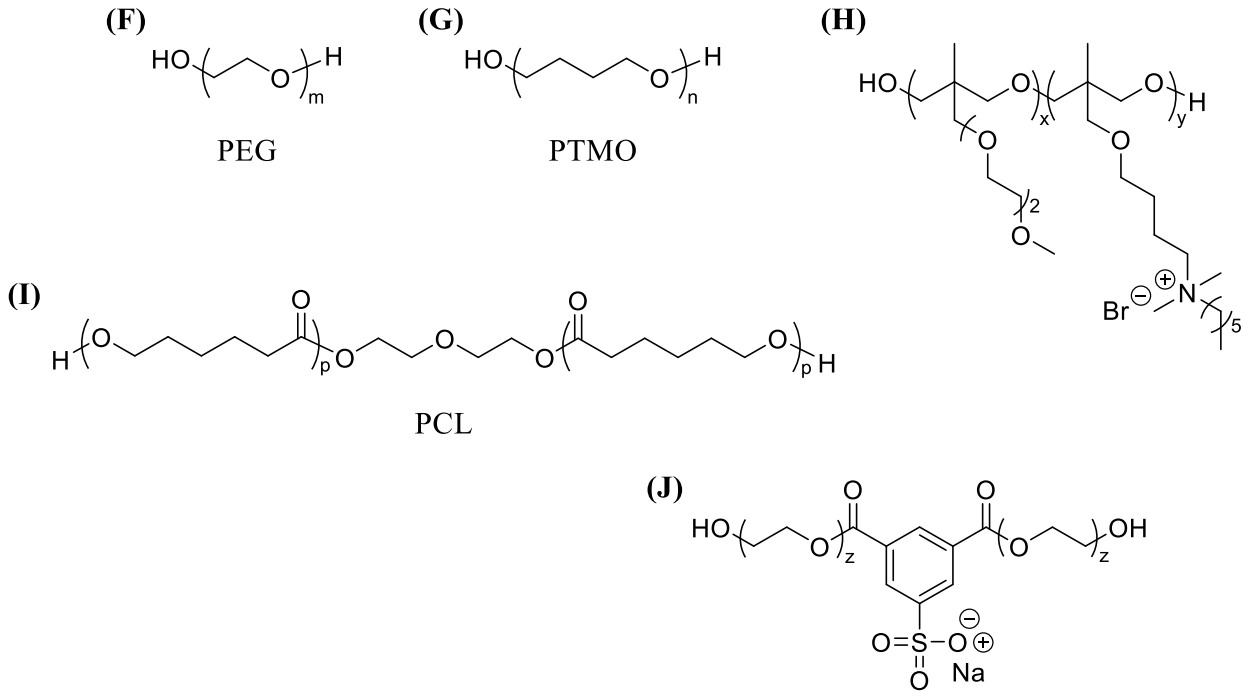

Figure 7.4. Polyols used in the synthesis of segmented polyurethanes.[27,42,43]

7.4 *Ion-Containing Biobased Polyols and Waterborne Polyurethane Dispersions*

There are numerous efforts to increase sustainability and limit the negative environmental impact of chemical processes for materials synthesis.[46-48] This field, often referred to as green chemistry, is prevalent in all aspects of polymer chemistry, including polyurethanes.[49] According to Clark[50], the ideal synthesis is atom efficient, simple, safe, only requires one-step, does not waste any reagents, uses available materials, has a 100 % yield, and is environmentally friendly. While fulfilling all of these items at once is challenging, small changes focused on one or two points further advance the understanding, capabilities, and implementation of green chemical processes. In relation to ion-containing segmented polyurethanes, the use of naturally occurring SSs, waterborne polyurethanes, and the elimination of isocyanate-based synthetic strategies is reviewed in more detail.

The use of naturally occurring compounds as starting materials adheres to the principles of green chemistry.[51] Oleic acid, castor oil, soybean oil, and natural rubber were all converted to functionalized polyols and subsequently used in the synthesis of ion-containing polyurethanes for various applications.[39,40,52-56] The chemical structures of castor oil and soybean oil contain a glycerol core with functional groups along primarily hydrocarbon chains.[39,53] **Figure 5** illustrates the structural resemblance between glycerol and castor oil. Velayutham et al.[45,52] applied a similar design to obtain an oleic acid-containing polyol, reacting glycerol, phthalic anhydride, and oleic acid in a two-step procedure. Linear step-growth polymerization requires perfectly difunctional monomers and near 100 % conversion to obtain high molecular weight polymers.[4] The introduction of multi-functional monomers (f >2), such as A_2B or B_3 monomers where A and B represent different functional groups, leads to branched, hyperbranched, or crosslinked polymers.[4,57-59] The polyols derived from oleic acid, soybean oil, and castor oil all possess f>>2, thus the one-shot method afforded crosslinked polyurethanes upon curing.[39,40,45,52,53,60]

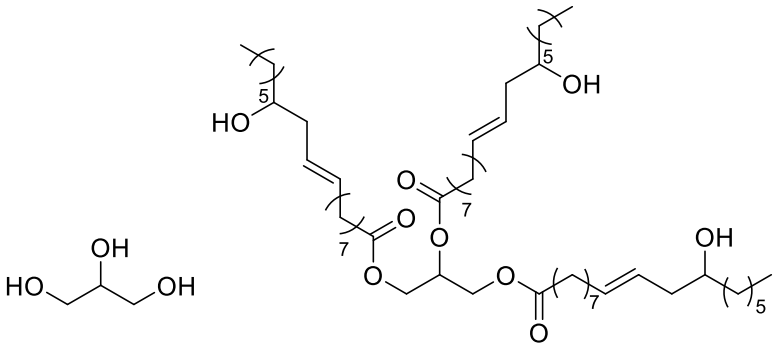

Figure 7.5. The chemical structures of glycerol and castor oil.

The oleic acid-containing oligomer represents the only polyol in the earlier literature with inherent ionic content due to the presence of unreacted pendant carboxylic acid groups, where

conductivity measurements confirmed ionization.[52] Epoxidized soybean oil (ESBO) and castor oil both contain reactive functional groups, epoxides and hydroxyl groups respectively, which facilitate chemical modifications.[39,40,53] For example, ring-opening the epoxide groups with an azide and performing a "click" reaction with a tertiary amine-containing alkyne followed by alkylation resulted in ammonium-containing multi-functional ESBO-based polyols.[40] Alternatively, Yari et al.[53] reacted the secondary diols in castor oil with a diisocyanate and subsequently glycidol to form urethane bonds while introducing the epoxide group. After curing the modified castor oil in the presence of an ammonium salt and amine chain extender, ion-containing crosslinked polyurethanes with varying ionic content were obtained.

Another green approach to materials synthesis is the removal or replacement of hazardous solvents and volatile organic compounds (VOCs).[1,50] Waterborne polyurethanes, or waterborne polyurethane dispersions (PUDs), are a widely investigated and represent an industrially prevalent class of segmented ion-containing polyurethanes.[1,15,61-63] PUDs function as excellent adhesives and coatings, imparting the properties of a segmented polyurethane in an easily applicable environmentally safe aqueous solution.[1] In the synthesis of PUDs, the basic polyurethane chemistry remains unchanged; the reactions between the polyol, diisocyanate, and chain extender formulate the high molecular weight segmented structure. The significant difference lies with the process when the polyurethane is water soluble or dispersible, and the means to achieve water solubility/dispersibility.

PUD synthesis combines principles from both traditional segmented polyurethanes and emulsion polymerization.[1,64] The nature of the monomers (hydrophobic, hydrophilic, ionic) dictate the synthetic procedure required to obtain the desired segmented aqueous-based

polyurethane. Szycher[1] describes in detail four common synthetic processes for PUDs. Commonalities include a prepolymer formation step, which is similar to the traditional diisocyanates prepolymer method described earlier.[1,4] Herein, we will focus on the specifics of the solution, also termed the acetone process, since the majority of PUDs discussed in this review were synthesized accordingly. **Scheme 2** illustrates the solution process for the synthesis of a fluorescent dye-containing PUD.[65] In the first step, tolylene-2,4-diisocyanate (TDI), PPG, and 2,2-bis(hydroxymethyl)propionic acid (DMPA) react to form an isocyanate end-capped prepolymer containing a pendant carboxylic acid. The SS and HS (labeled) repeating units are comprised of PPG and TDI, and TDI and DMPA, respectively. Subsequent addition of triethylamine (TEA) deprotonates the carboxylic acid, introducing pendant ammonium carboxylate groups, which aid in the formation of a stable aqueous dispersion. Stoichiometric control throughout the polymerization process enables tunable charge content, and PUDs are often reported in weight percent solids.[54,66] This process is also termed the "acetone process", as the addition of solvent reduces the viscosity of the PUD and is easily removed after polymerization.[1] In **Scheme 2** the fluorescent dye ACN (1 mol TDI:0.14 mol ACN) was added after the addition of acetone.[65]

Scheme 7.2. PUD synthesis via the solution process.[65]

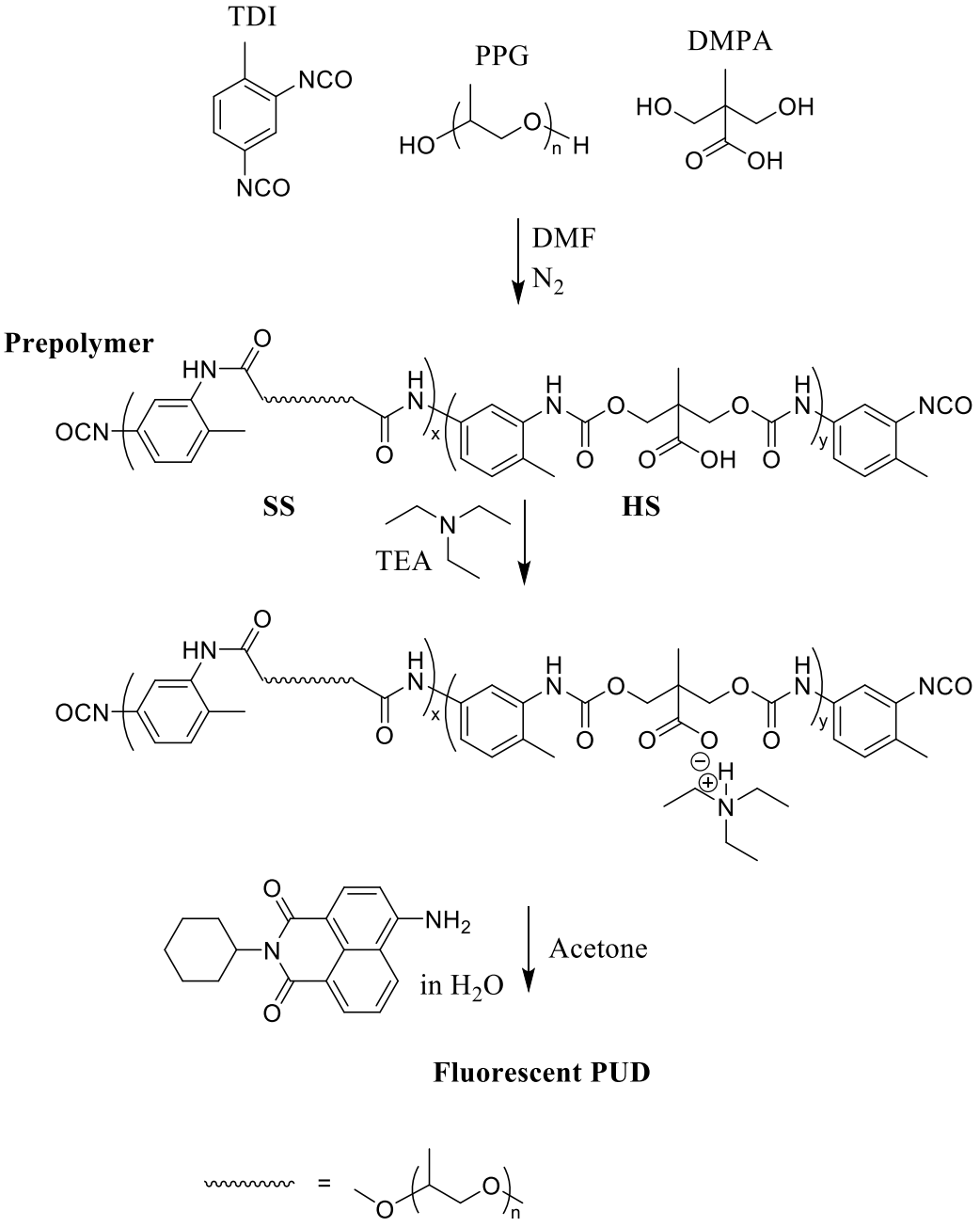

Ionic groups facilitate water-compatibility and are easily incorporated through deprotonation, alkylation, or a preformed charged monomer; most PUDs are ion-containing segmented systems.[1,25,36,55,65,67] The diversity of potential ionic groups is identical to the

traditional ion-containing segmented polyurethanes as summarized in the previous section. The fluorescent PUD described above is classified as an anionic PUD due to the carboxylic acid-containing starting monomer.[65] DMPA and 2,2-bis(hydroxymethyl)butyric acid (DMBA) are common diols that afford anionic PUDs.[38,41,44,54,56,62-75] Garrison et al.[55] synthesized cationic PUDs containing methoxylated soybean oil through the alkylation of N-methyldiethanolamine (MDEA) with acetic acid, providing ammonium cations in the backbone with carboxylate counterions. Although not the focus of this review, uncharged hydrophilic monomers afford neutral PUDs.[1]

Isocyanates are classified as hazardous compounds and require precautionary measures to maintain not only safe surroundings, but also to avoid any adverse exposure.[1,76] Isocyanates readily react with moisture in the air to produce carbon dioxide.[1] This gas-forming reaction in a closed container can potentially lead to over-pressurization, which is dangerous whether it occurs on a laboratory or industrial scale. From a biological standpoint, isocyanate vapors are known to cause respiratory issues and in general, isocyanates are toxic.[1,49,76] Finally, the synthesis of small molecule isocyanates often involves the toxic reagent, phosgene.[1,77] From a green chemistry perspective, an environmentally and biologically friendly replacement for isocyanates in polyurethane remains as an active research area.[78-80]

Isocyanate-free strategies for the preparation of polyurethanes remains an active field of study.[49,81] Cyclic carbonate ring-opening is an attractive alternative to isocyanates for the synthesis of polyurethanes.[80,81] The reaction of an amine with a cyclic or linear carbonate yields the desired urethane linkage.[81] Unlike the phosgene-based isocyanate synthesis, the reaction of an epoxide with carbon dioxide in the presence of a catalyst forms a 5-membered cyclic

carbonate with tunable pendant functionalities based on the initial epoxide.[82] The process typically employs a functionalized epoxide, and **Scheme 3** displays the formation of a cyclic carbonate and the products of the ring-opening reaction with a primary amine.[82] Note the reaction produces a pair of constitutional isomers each containing a pendant hydroxyl functionality. Similarly, the polymerization of a difunctional cyclic carbonate and diamine affords linear polyurethanes bearing pendant primary and secondary hydroxyl groups.[49] Rokicki et al.[83] elegantly coupled the ring-opening of ethylene carbonate with a diamine and further transesterification with a diol to produce polyurethanes with pendant hydroxyl groups. Adapting this synthetic strategy to include an oligomeric polyol rather than a low molar mass diol enables segmented poly(hydroxy-urethanes), however, the HS only consists of two urethane linkages.[84] Many challenges remain for the synthesis of segmented polyurethanes without using isocyanates, and the absence of significant literature describing ion-containing segmented polyurethanes from carbonates challenges polymer chemists to continue the search for environmentally friendly chemical processes.

Scheme 7.3. Isocyanate-free route to the 5-membered cyclic carbonate and the subsequent ring opening reaction with a primary amine, revealing the hydroxy-urethane chemistry.[82]

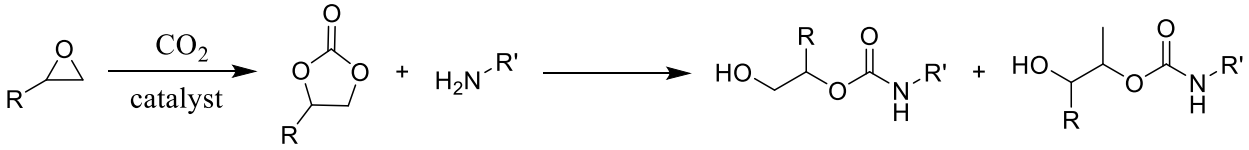

7.5 *Effect of Ion-Incorporation on Segmented Polyurethane Properties*

The ability to tune the charge content in ion-containing segmented polyurethane copolymers arises from the synthetic design. The stoichiometric ratio of charged to uncharged monomers or the extent of post-polymerization charge incorporation reactions (i.e. alkylation or

deprotonation) allows for the systematic variation of ionic content and elucidates structure-property relationships. As previously mentioned, ionic groups in PUDs often provide the hydrophilicity necessary to obtain a stable aqueous dispersion. Varying the amount of DMPA in 0.5 weight percent increments, Lei et al.[68] synthesized PUDs with ionic content ranging from 3 – 5 weight % and investigated the influence on dispersion and adhesive properties. Dynamic light scattering (DLS) provided a measurement of the hydrodynamic dimension and zeta potential of the segmented polyurethane particles in solution. Both the observed hydrodynamic diameter and zeta potentials decreased with increasing charge, with sizes ranging from 80.8 – 146.7 nm for the 5 and 3 weight % DMPA content. The larger particles also exhibited a shorter shelf-life, indicating a less stable dispersion. Polyurethane dispersions containing an identical diisocyanate and DMPA but different polyol (PCL_{2K} *versus* poly(butylene adipate)$_{3K}$, where the subscripted value corresponds to the approximate M_n) showed a similar dependence on hydrodynamic diameter with varying ionic content.[69] Hydrodynamic diameters of 76 nm and 159 nm were obtained for 4 and 6 weight % DMPA content, respectively. These results suggest that the ionic content plays a more significant role in nanoparticle formation than the chemical structure of the SS. Surface characterization of PCL-based segmented polyurethane films exhibited increased surface tension, interfacial tension, and contact angle values with increasing ionic content.[68] Peel testing revealed an increase in peel strength from 3 – 4 weight % DMPA, and then a gradual decrease upon 4 – 5 % incorporation. The synergy between surface tension, surface wetting, and the resulting effect on adhesion was used to explain the differences in peel strength.

Saetung et al.[56] synthesized PUDs from natural rubber polyols, varying both the ionic content and M_n of the polyol precursor. DLS revealed a similar trend of decreasing nanoparticle

size with increasing ionic content and dispersion stability. Differential scanning calorimetry (DSC) probed the thermal properties of the PUD films and revealed T_g's remained constant through a range of charge content (1.6 – 7.5 weight % DMPA). However, keeping the ionic content constant (4.2 weight %) and decreasing the M_n of the polyol from 2000 g/mol to 1000 g/mol increased the T_g from -60 °C to -53 °C, respectively. Alternatively, an increase in polyol M_n from 2000 g/mol to 4000 g/mol only slightly depressed the T_g from -60 °C to -63 °C. These results suggest the ionic content in PUDs more significantly impact the dispersion properties than the physical properties of the dry films.[56,68] Cakić and coworkers[66] varied the ionic content in polycarbonate-based PUDs and examined the influence of charge on the thermal and thermomechanical properties, and morphology of the resulting dry polyurethane films. In contrast to the constant T_g's observed throughout a range of different charge contents with the natural rubber based PUDs, the polycarbonate-based PUDs exhibited an increase in T_g with increasing ionic content.[56,66] As the ionic content increased from 4.5 to 7.5 to 10 weight % (PUD1, PUD2, and PUD3 respectively) from DMPA incorporation, the T_g increased ~9 °C per increment. **Figure 6** depicts the storage modulus (G') *versus* temperature curves for the polycarbonate-based PUDs. The increased storage modulus with increasing ionic content is attributed to the physical crosslinks formed from ionic aggregation. Increasing the amount of DMPA also, inherently, increases the length of the HS in the overall segmented polyurethane, thus the increased storage modulus observed with increasing ionic content is a function of both higher HS content and ionic interactions. The disparate results between the natural rubber-based PUDs and polycarbonate-based PUDs emphasize the abundance of tunable synthetic parameters (monomers, M_n's, % solids) and film preparation techniques, affording a broad range of attainable material properties.[56,66]

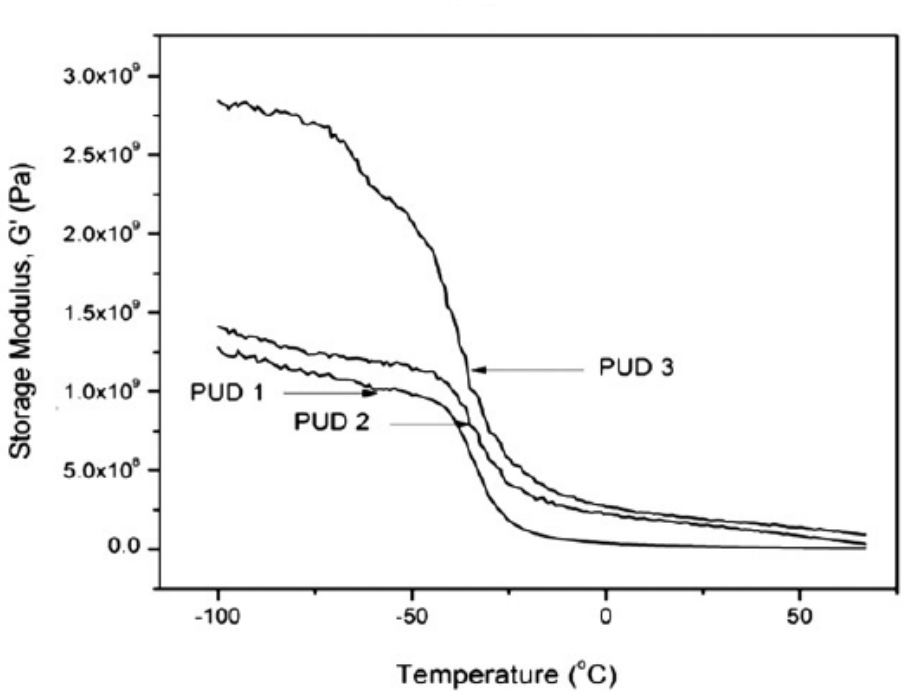

Figure 7.6. Modulus as a function of temperature for polycarbonate-based PUD films with varying ionic content. Reproduced with permission from ref.[66]

Gao et al.[27] synthesized a series of ion-containing polyurethanes strategically placing sulfonate groups in only the HS and only the SS to allow for a fundamental study of the effect of ion-placement on polyurethane properties. Ionic compounds **C** and **J** (from **Figure 3** and **4**) provided the charge in the HS and SS, respectively. The thermal, thermomechanical, and tensile properties, hydrogen-bonding, and morphology were investigated. DSC revealed the T_g's of the ion-containing polyurethanes increased as compared to the neutral control; and the ionic groups in the HS further increased the T_g compared to when the ionic groups resided solely in the SS. These results suggested stronger electrostatic interactions when the ions were located in the less mobile HS. **Table 1** summarizes the thermal transitions of the segmented polyurethane copolymers. Atomic force microscopy (AFM) and small angle X-ray scattering (SAXS) probed the surface and bulk morphology respectively of the segmented polyurethanes. Coupled with

wide-angle X-ray diffraction (WAXD) for characterizing crystallinity and variable temperature Fourier transform infrared (FTIR) spectroscopy to observe the hydrogen-bonding (H-bonding), a microphase-separated morphology was confirmed for the neutral polyurethane, as well as when the ionic groups resided in the SS. When the charge was in the HS, however, a phase-mixed morphology resulted.

Table 7.1. Thermal transitions of segmented polyurethanes with sulfonate groups in the hard and soft segments. Reproduced with permission from ref.[27]

Location of Ionic Groups	T_g (°C)	T_m (°C)
HS	-5	110
SS	-26	--
Neutral	-52	34, 107

Sophisticated synthetic design enabled Lee et al.[62] to synthesize PUDs containing ionic groups only in the SS, only in the HS, or only on the chain ends, while maintaining overall structural similarity. In PUDs with identical percent solids, weight percent HS, and SS/HS monomers, the smallest hydrodynamic diameter and zeta-potential was observed with terminal ions and the largest with ions in the HS.[62] As revealed in the PUDs discussed above, an increase in ionic content gives rise to smaller particles which form more stable dispersions.[56,68,69] In this case, the ionic content is the same for each PUD, and the results from this study show the impact of chain/ionic mobility on particle formation.[62] In regards to the viscosity and zeta potential of the PUDs, the opposite trend occurred. A viscosity of 24 cP was reported for the charge in the HS and 69 cP for the terminal position. Swelling the films in water revealed the PUD containing ions in the HS achieved the highest percent swelling with the ions in the SS and at the chain ends

displaying results similar to one another. In the same laboratory, Jung et al.[64] synthesized photo-curable PUDs with ions placed at the chain ends or in the HS and observed similar results as a function of ion placement.

Continuing our survey of some fundamental structure-property relationships of ion-containing segmented polyurethane copolymers, Zhang et al.[26] synthesized a novel phosphonium diol with varying alkyl chain lengths. Using the phosphonium diol as a chain extender in the traditional prepolymer method and systematically varying the HS to SS ratio, a series of phosphonium-containing segmented polyurethanes with ethyl (compound **A** in **Figure 3**) or butyl pendant alkyl chains resulted. A thorough investigation of polyurethane properties as a function of both HS content, correlating to ionic content, and alkyl chain length ensued. The alkyl spacer length dramatically affected the tensile properties of the segmented polyurethanes. **Figure 7** shows the stress versus strain curves for the 75 weight percent HS polyurethanes with the triethyl and tributyl phosphonium cations (TEP and TBP respectively). The ion-containing segmented polyurethanes displayed increased strain at break compared to the neutral control, and yielded Young's moduli of 10.0 ± 0.5 MPa, 21.0 ± 5.6 MPa, and 134 ± 16 MPa for the uncharged, TEP, and TBP polyurethanes respectively. Uniquely, these polyurethanes were water dispersible and bound DNA with the longer, butyl chain. Other research groups also explored the effect of alkyl chain length on polyurethane properties.[29,36] Through an alkylation reaction of MDEA with alkyl bromides varying in chain lengths from 4 – 18 carbons, Wynne et al.[29] synthesized a library of ammonium diols. Subsequent reaction of the ammonium diols with a commercially available tri-functional isocyanate endcapped oligomer afforded polyurethane networks. The thermal, thermomechanical, and antibacterial properties of the networks as a

function of alkyl chain length was examined. Both the octyl and octadecyl systems showed promise as antibacterial coatings.

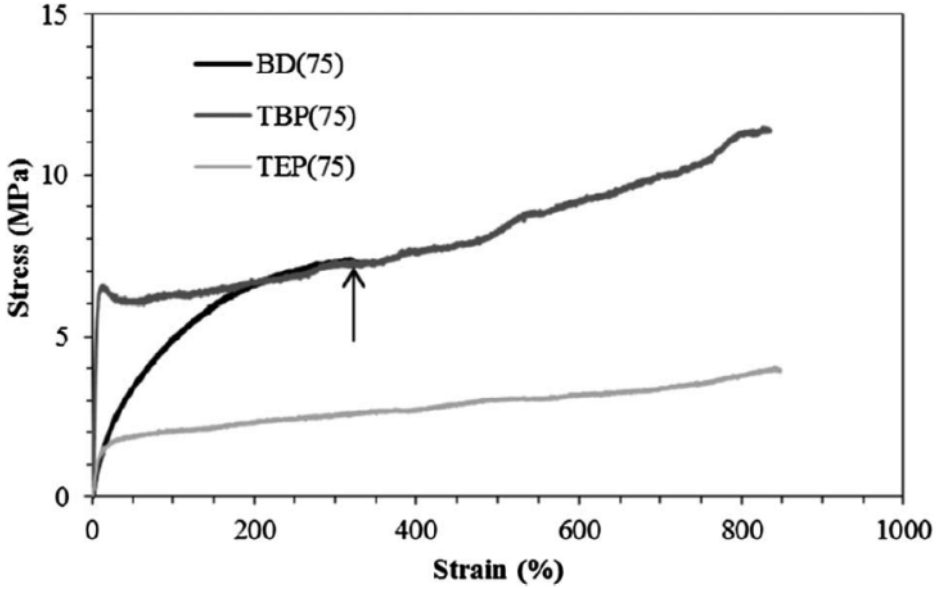

Figure 7.7. Tensile curves of the uncharged, TEP and TBP polyurethanes with 75 weight percent HS content. Reproduced with permission from ref.[26]

The research of Ramesh and Nair broadens the field of ion-containing polyurethanes to include the divalent calcium cation.[34,37,85] Utilizing commercially available calcium $_{L}$-lactate hydrate (compound **B** in **Figure 3**), PTMO, and hexamethylene diisocyanate (HDI) in the one-shot polymerization process, segmented calcium-containing polyurethanes were achieved.[34] Compared to a neutral control, dynamic mechanical analysis (DMA) displayed a higher storage modulus and T_g for the calcium-containing polyurethane. The ion-containing polyurethane outperformed the control in all areas of tensile testing (tensile strength, modulus, toughness, and elongation at break) and blood compatibility experiments with the calcium-containing segmented polyurethanes displayed encouraging results. In a similar study that substituted the calcium salt of *p*-hydroxybenzoic acid as the ion-containing chain extender, the amount of ionic content was

varied and the resulting effect on the thermal, thermomechanical, and tensile properties of the ion-containing polyurethanes was discussed.[85]

7.6 *Applications of Ion-Containing Segmented Polyurethanes*

The impact of ion-containing segmented polyurethanes spans various fields as a direct result of the chemical and structural diversity affording a multitude of performance tunable polymer systems.[33,44,70] Biomedical applications, polymer electrolytes, and the coatings industry are just some of the areas benefitting from the advancement of these materials. Highlighting some technology-driven research combines the various synthetic techniques and importance of understanding structure-property relationships in the design of functional segmented polyurethanes. In the following section, some recent research in relation to the three aforementioned subjects is described.

The biocompatible nature of ion-containing segmented polyurethanes stimulates abundant research aimed at various biomedical applications including biodegradable scaffolds, antimicrobicides, blood compatibilizers, and there potential use in drug delivery systems.[25,31,53,55,70,86-89] Biodegradability is an important feature when designing scaffolds as their function is to aid in regeneration, not remain as permanent replacements.[90] A common route to biodegradable segmented polyurethanes is the use of a biodegradable polyol, such as PCL, in the SS.[70,90,91] De Oliveira et al.[70] synthesized PUDs containing biodegradable PCL in the SS and DMPA as the ionic moiety to achieve dispersion. Mixing the PUDs with bioactive glass nanoparticles in a poly(vinyl alcohol) (PVA) solution and either drying or freeze drying afforded films and foams, respectively. **Figure 8** depicts the PUD and resulting film and foam composites. A scanning electron microscopy (SEM) image of the foam composite containing

10 % of the nanoparticle elucidates the porous structure achieved with the freeze-drying process. To confirm biocompatibility of the polyurethane/nanoparticle/PVA composites, cells were subjected to the decomposition products. After 24 h, an acceptable percentage of cells remained. Additionally, to assess the ability of the composites to function as tissue scaffolds, an *in vitro* study revealed hydroxyapatite remained on the surface after soaking in a biological medium. These results indicate potential for *in vivo* success.

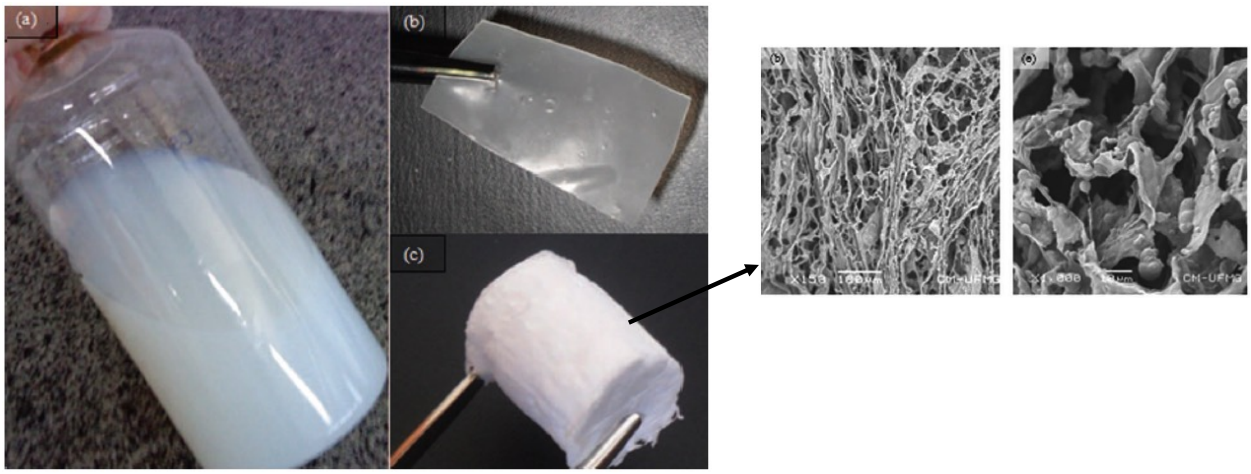

Figure 7.8. The PUD (a), representative film (b) and foam (c) of the PUD/PVA/glass nanoparticle composites, and SEM image of the foam containing 10 % bioactive glass nanoparticle. Adapted with permission from ref.[70]

Antimicrobial surfaces and materials function in one of two ways, as bacteria repellents or bacteria killers.[92] Often, cationic polymers are effective at killing bacteria upon contact. Most bacteria carry a negative charge; electrostatic interactions between the bacteria and positively charged polymer result in bacterial cell rupture and ultimately cell death. Garrison and coworkers[55] synthesized ammonium-containing segmented PUDs using methoxylated soybean oil, as described in an earlier section. PUDs with differing ionic content and identical hydroxyl number, equal hydroxyl number and charge ratio, and an anionic control (using DMPA) were

prepared to elucidate the effect of charge on antimicrobial performance. In general, PUDs with higher ammonium content displayed improved antibacterial properties, however, the PUD with the lowest hydroxyl number, corresponding to the lowest ammonium content and least crosslinked material, outperformed the other PUDs prepared with the same charge ratio. This result demonstrated the significance of polymer mobility on antibacterial properties. Ultraviolet-visible (UV-Vis) spectroscopy confirmed the hypothesis of bacterial cell death through rupturing of the cell wall. The antimicrobial properties of castor oil based crosslinked ammonium-containing polyurethane membranes were also investigated.[53] The membrane containing the largest amount of ionic content exhibited superior antibacterial properties. Cytotoxicity studies revealed an increase in ionic content correlated to increased cytotoxicity. Thoroughly washing the crosslinked materials and replicating the experiment showed all of the membranes, despite ionic content, were not cytotoxic. It was determined that the washing step removed unreacted, excess small molecule ammonium salt which is known to cause cell death.[93]

Unless the direct aim of a device is to inhibit blood flow, it is important for materials introduced into the body to function in the presence of blood and avoid causing unnecessary complications.[94] After publishing successful results showing increased blood compatibility of PCL polymerized using a zwitterionic sulfobetaine initiator, taking advantage of the diol functionality Cao and coworkers[30,31] synthesized zwitterionic segmented polyurethanes. **Scheme 1** depicts the synthetic route to the novel sulfobetaine diol which converted to a polyol after ring-opening PCL off each hydroxyl group. Chain extension of the polyol with HDI afforded biodegradable zwitterionic polyurethanes with a very small HS content. The zwitterionic polyurethanes exhibited lower protein adsorption for hydrated samples compared to a neutral

MDEA-containing control polyurethane. **Figure 9** models the observed effect of molecular weight and ionic content on the charge migration after soaking in water and the subsequent effect on protein adsorption for the zwitterion-containing polyurethanes. The results of clotting time and hemolysis studies were also in the range of acceptable values, indicating blood compatibility. Li et al.[86] functionalized the endgroups of traditional segmented polyurethanes with a zwitterionic phospholipid. All compositions showed a drastic decrease (greater than 90 %) in protein adsorption, corresponding to increased blood compatibility, in relation to the unfunctionalized neutral segmented polyurethane copolymer. The structure of the zwitterionic phospholipid (inset) and protein adsorption results are displayed in **Figure 10**, where the zwitterionic-endcapped segmented polyurethanes are denoted FPCPU-T, FPCPU-P, and FPCPU-H corresponding to PTMO, PPG, and polycarbonate SSs. PEU represents the nonionic control.

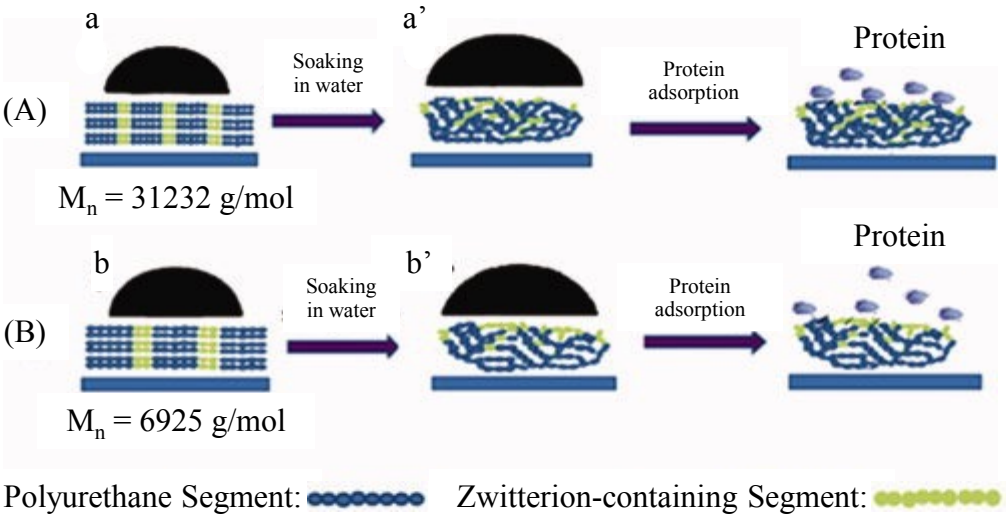

Figure 7.9. A model demonstrating the rearrangement of zwitterion-containing polyurethanes with different M_n's in water, based on contact angle analysis, and the resultant effect on protein adsorption. Adapted with permission from ref.[31]

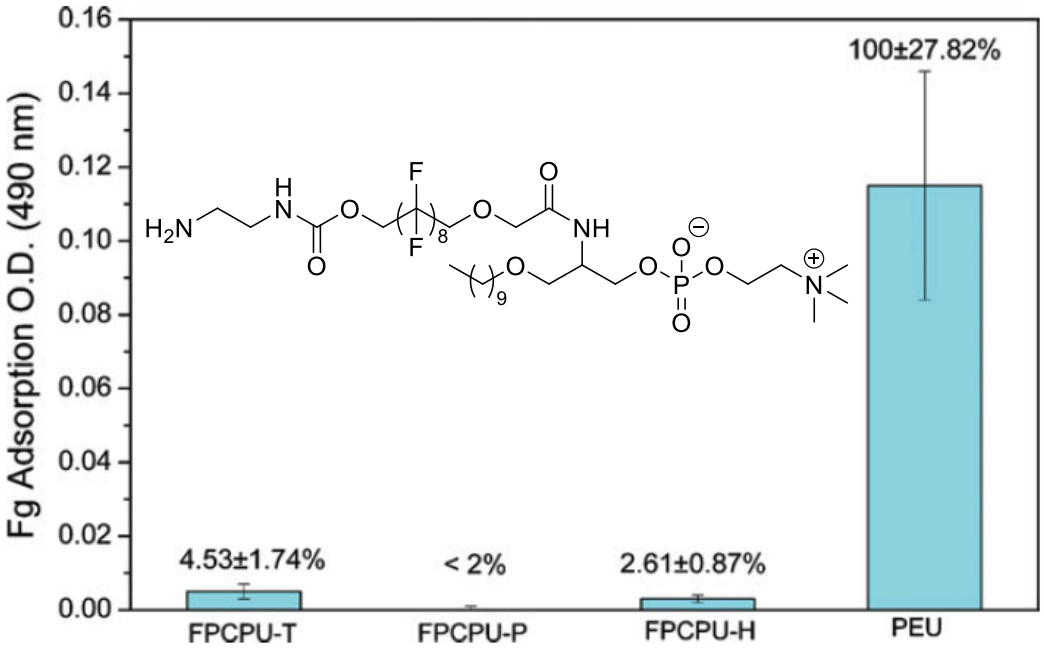

Figure 7.10. The chemical structure of the zwitterionic phospholipid endcapping agent and protein adsorption results for zwitterionic-containing segmented polyurethanes with various SS polyol components. Adapted with permission from ref.[86]

Utilizing electrostatic interactions of ion-containing segmented polyurethanes, Feng et al.[88,89] employed layer-by-layer (LBL) assembly to produce films and investigated their ability to adsorb and release model compounds as a direct correlation to potential drug delivery applications. Two different LBL materials were fabricated with alternating layers of cationic polyurethane and poly(acrylic acid) (PAA) or anionic polyurethane and poly(allylamine hydrochloride) (PAH). Dyes, methylene blue (MB) and methylene orange (MO), were the model drug for each system, respectively, and chosen for ease of quantification. A systematic investigation on the effect of the number of layers, charge of the exposed layer, solution pH, and salt content on the loading and release properties of the anionic polyurethane/PAH multilayer films ensued.[89] Cationic charge on the top layer increased loading efficiency, however, exposing the anionic polyurethane improved release. Loading increased with decreasing pH and

increasing salt concentration. Both the cationic polyurethane/PAA and anionic polyurethane/PAH films showed reversible adsorption and release of the respective dyes for more than 10 cycles. These results suggest potential success for multilayer films constructed with ion-containing polyurethanes in the area of drug delivery.[88,89]

The development and improvement of polymer electrolytes, specifically for use in lithium ion batteries, is an extremely active area of research.[95-99] As mentioned throughout this review, ion-containing segmented polyurethanes possess desirable material properties, including thermal and thermomechanical stability, and tensile strength. The ability to tune these properties with structural diversity and ionic content render them excellent candidates for the range of material needs in the field of polymer electrolytes.[100,101] Liu and coworkers[102] synthesized cationic segmented polyurethanes with varying alkyl chain lengths achieved via post-polymerization alkylation reactions of MDEA and bromoalkanes. Mixing lithium perchlorate ($LiClO_4$) and the ammonium-containing segmented polyurethanes in different ratios afforded a series of polymer electrolytes containing Li salt in different weight ratios for each alkyl chain length (2, 8, and 14 carbons). Independent of alkyl chain length, as salt content increased both the degradation temperature (T_d) and T_g decreased. 50 weight % Li salt in the cationic segmented polyurethane with an octyl chain displayed the highest room temperature conductivity of 1.07×10^{-4} S/cm. A trend of increasing ionic conductivity with increasing Li salt was observed for all cationic segmented polyurethanes.

Ionic conductivity depends on both the concentration and mobility of ions, thus solid salts in polymer matrices with T_g's above room temperature reach a conductivity plateau.[103] ILs, by definition, are salts with melting temperatures (T_m's) below 100 °C.[104] Incorporating ILs

possessing T_m's near or below room temperature in polymer electrolytes increases ionic mobility, pushing past the conductivity barrier and introducing a new class of polymer electrolytes.[103] Utilizing an imidazolium diol (compound **E** in **Figure 3**), Gao et al.[33] synthesized a cationic segmented polyurethane. Mixing 1-ethyl-3-methylimidazolium ethyl sulfate (EMIm ES), a liquid at room temperature, with the imidazolium-containing segmented polyurethane in varying weight ratios and casting into Teflon® molds afforded IL-containing polymer electrolyte films. **Figure 11a** depicts the DMA curves for the IL-containing polymer electrolyte films. As IL content increased both the storage modulus and HS T_g decreased suggesting the IL disrupted the hydrogen bonding in the HS yet did not interact with the SS in enough capacity to influence the T_g. A 106 MPa difference between the storage moduli of the 5 and 30 weight % IL samples at 40 °C shows the range of mechanical integrity, easily altered with simply increasing or decreasing IL content. Ionic conductivity as a function of temperature and IL content, displayed in **Figure 11b**, showed conductivity increased with increasing temperature and IL incorporation. A proposed model of ionic interactions and potential IL placement was constructed, **Figure 12**, to pictorially represent the influence of ion incorporation on polyurethane self-assembly and aid in the explanation of enhanced material properties.

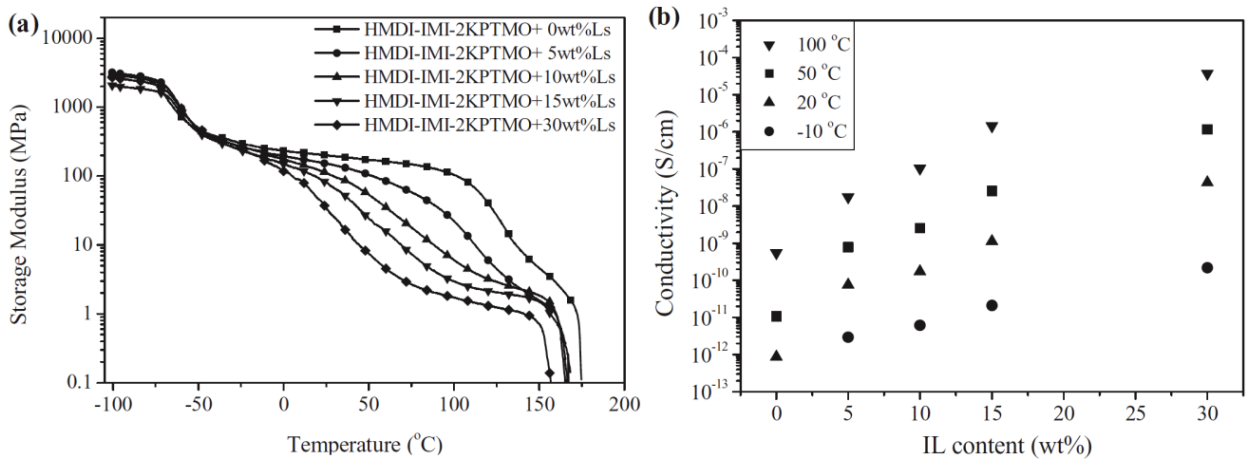

Figure 7.11. DMA curves (a) and conductivity (b) of imidazolium-containing polyurethanes with varying amounts of IL. Adapted with permission from ref.[33]

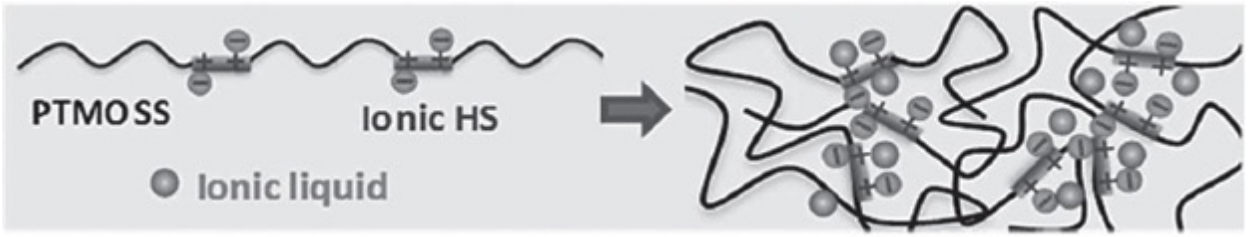

Figure 7.12. Cartoon showing proposed ionic aggregation and IL intercalation providing enhanced thermomechanical strength and ionic conductivity. Reproduced with permission from ref.[33]

Coatings are a dominant application for ion-containing waterborne PUDs, with structure-dependent built-in functionalities designed for various applications including hydrophobicity, oil repelling, adhesive strength, and corrosion resistance.[15,38,44,71,105] As described above in relation to blood compatibility, placing functional groups on the end of ion-containing polyurethanes can significantly impact polymer properties.[86] Similarly, placing photoactive groups on the end of waterborne PUDs efficiently provides UV-curable PUDs.[41,72-75] 2-Hydroxyethyl acrylate (HEA) and 2-hydroxyethyl methacrylate (HEMA) are two commonly employed photoactive molecules, which readily react with isocyanate end-groups to produce a urethane bond and upon addition of a photoinitiator and UV-light afford UV-crosslinked films from PUDs. **Scheme 4** shows the

reaction of HEMA with an isocyanate group and the resulting photocurable acrylate-functionalized product.

Scheme 7.4. Functionalization reaction of isocyanate-endcapped polyurethanes with UV-active HEMA.

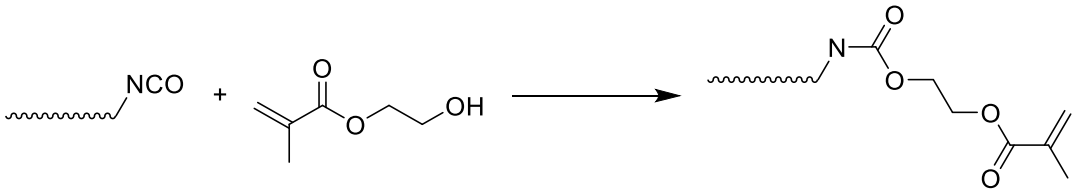

Employing the aforementioned HEMA-endcapping strategy, Dong et al[72] prepared UV crosslinked anionic polyurethanes. The reaction of DMBA with PPG afforded the ion-containing SS and the addition of pyromellitic dianhydride (PMDA) into the synthesis resulted in anionic imide-containing photocurable PUDs. Increasing PMDA content correlated to an increase in T_g, Shore A hardness, and tensile strength. Hwang and Kim[74] also synthesized a series of photocrosslinkable anionic waterborne PUDs using the HEMA-endcapping strategy which, after curing, exhibited tunable surface energies and tensile properties. The ionic content was incorporated into the HS using DMPA, and a polycarbonate polyol dominated the SS, however, small amounts of hydroxyl-terminated perfluoropolyether (PFPE) (0.1, 0.25, 0.5, and 1 mol %) were added to the polyurethane synthesis. Results of contact angle analysis, X-ray photoelectron spectroscopy, and tensile testing demonstrated a broad range of both surface and mechanical properties achievable from photocrosslinked ion-containing polyurethane films incorporating small amounts of a fluorinated polyol. Both of the discussed PUD systems illustrate the recurring theme of structural diversity and tunability inherently present in the design, synthesis, and resulting properties of ion-containing segmented polyurethane copolymers.

7.7 *Conclusions*

The synthesis, structure-property relationships, and broader impact of ion-containing segmented polyurethanes on various fields of study has been discussed. Focusing on recent literature, an overview of the synthetic methods affording ion-containing polyurethane copolymers, including waterborne PUDs, green efforts, and the multiple avenues to successful incorporation of ionic content (anionic, cationic, and zwitterionic) into polyurethanes was provided. Using both novel and commercially available charge-containing diols and polyols or post-polymerization reactions to afford ionic groups, an array of ion-containing segmented polyurethanes with performance tunable properties have been prepared globally in both academic and industrial laboratories. The material properties and ease of synthesis result in a class of polymers with applications spanning multiple platforms, a few of which were discussed in detail. The incorporation of biodegradability into already biocompatible systems allows ion-containing polyurethanes to play an important role in many biomedical applications, including regenerative medicine and antimicrobials. Excellent film and coating properties combined with engineering conductive membranes affords polymer electrolytes and endgroup functionalization has provided photocrosslinkable coatings form waterborne PUDs. The field of ion-containing polyurethanes is abundant, versatile, and will continue to flourish and develop with the creativity and innovation of today's scientists.

7.8 *Acknowledgements*

The authors would like to thank the U.S. Army Research Laboratory and the U.S. Army Research Office under the Army Materials Center of Excellence Program, contract W911NF-06-

2-0014 for supporting polyurethane research in our group. The authors would also like to thank Bayer MaterialScience for financial support and insightful discussions.

7.9 *References*

(1) Szycher, M. *Szycher's handbook of polyurethanes*; CRC Press: Boca Raton, 1999.
(2) Rinke, H.; Schild, H.; Siefken, W.; C08G18/32 ed.; Office, U. S. P., Ed. U.S., 1938; Vol. US2511544 (A).
(3) Odian, G. G. *Principles of polymerization*; Wiley-Interscience: Hoboken, N.J., 2004.
(4) Rogers, M. E.; Long, T. E. *Synthetic methods in step-growth polymers*; Wiley-Interscience: Hoboken, N.J., 2003.
(5) Sheth, J. P.; Wilkes, G. L.; Fornof, A. R.; Long, T. E.; Yilgor, I. *Macromolecules* **2005**, *38*, 5681.
(6) Yılgör, E.; Yılgör, İ.; Yurtsever, E. *Polymer* **2002**, *43*, 6551.
(7) Yilgor, I.; Yilgor, E.; Guler, I. G.; Ward, T. C.; Wilkes, G. L. *Polymer* **2006**, *47*, 4105.
(8) Abouzahr, S.; Wilkes, G. L.; Ophir, Z. *Polymer* **1982**, *23*, 1077.
(9) Chattopadhyay, D. K.; Webster, D. C. *Progress in Polymer Science* **2009**, *34*, 1068.
(10) Lee, D.-K.; Tsai, H.-B. *Journal of Applied Polymer Science* **2000**, *75*, 167.
(11) Petrović, Z. S.; Ferguson, J. *Progress in Polymer Science* **1991**, *16*, 695.
(12) İçli, M.; Pamuk, M.; Algi, F.; Önal, A. M.; Cihaner, A. *Chemistry of Materials* **2010**, *22*, 4034.
(13) Robertson, N. J.; Kostalik, H. A.; Clark, T. J.; Mutolo, P. F.; Abruña, H. D.; Coates, G. W. *Journal of the American Chemical Society* **2010**, *132*, 3400.
(14) Xie, T. *Nature* **2010**, *464*, 267.
(15) *3M™ Paint Defender Spray Film, 90001*; MSDS No. 30-4587-9 [Online]; 3M: St. Paul, MN, July 19, 2013. http://s7d9.scene7.com/is/content/GenuinePartsCompany/1772711pdf?PDF (accessed May 2, 2014).
(16) *HyFlex® 11-435*; Product Sheet [Online]; Ansell: Brussels, Belgium. http://industrialcatalogue.ansell.eu/pdf_datasheet/36/HyFlex11-435_en_productsheet.pdf (accessed May 2, 2014).
(17) Valero-Navarro, A.; Medina-Castillo, A. L.; Fernandez-Sanchez, J. F.; Fernández-Gutiérrez, A. *Biosensors and Bioelectronics* **2011**, *26*, 4520.
(18) Jiang, G.; Tuo, X.; Wang, D.; Li, Q. *J Mater Sci: Mater Med* **2012**, *23*, 1867.
(19) Eisenberg, A. K. M. *Ion-containing polymers : physical properties and structure*; Academic Press: New York, 1977.
(20) Bazuin, C. G.; Eisenberg, A. *Industrial & Engineering Chemistry Product Research and Development* **1981**, *20*, 271.
(21) Gieselman, M. B.; Reynolds, J. R. *Macromolecules* **1992**, *25*, 4832.
(22) Heath, W. H.; Senyurt, A. F.; Layman, J.; Long, T. E. *Macromolecular Chemistry and Physics* **2007**, *208*, 1243.
(23) Argun, A. A.; Ashcraft, J. N.; Hammond, P. T. *Advanced Materials* **2008**, *20*, 1539.
(24) Jaudouin, O.; Robin, J.-J.; Lopez-Cuesta, J.-M.; Perrin, D.; Imbert, C. *Polymer International* **2012**, *61*, 495.
(25) Chen, F.; Hehl, J.; Su, Y.; Mattheis, C.; Greiner, A.; Agarwal, S. *Polymer International* **2013**, *62*, 1750.
(26) Zhang, M.; Hemp, S. T.; Zhang, M.; Allen, M. H.; Carmean, R. N.; Moore, R. B.; Long, T. E. *Polymer Chemistry* **2014**.

(27) Gao, R.; Zhang, M.; Dixit, N.; Moore, R. B.; Long, T. E. *Polymer* **2012**, *53*, 1203.
(28) Wang, S.-W.; Liu, W.; Colby, R. H. *Chemistry of Materials* **2011**, *23*, 1862.
(29) Wynne, J. H.; Fulmer, P. A.; McCluskey, D. M.; Mackey, N. M.; Buchanan, J. P. *ACS Applied Materials & Interfaces* **2011**, *3*, 2005.
(30) Cao, J.; Chen, Y.-W.; Wang, X.; Luo, X.-L. *J. Biomed. Mater. Res. Part A* **2011**, *97A*, 472.
(31) Cao, J.; Yang, M.; Lu, A.; Zhai, S.; Chen, Y.; Luo, X. *J. Biomed. Mater. Res. Part A* **2013**, *101A*, 909.
(32) Williams, S. R.; Wang, W.; Winey, K. I.; Long, T. E. *Macromolecules* **2008**, *41*, 9072.
(33) Gao, R.; Zhang, M.; Wang, S.-W.; Moore, R. B.; Colby, R. H.; Long, T. E. *Macromolecular Chemistry and Physics* **2013**, *214*, 1027.
(34) Nair, P. A.; Ramesh, P. *Polym J* **2012**, *44*, 1009.
(35) Lee, H.-T.; Lin, L.-H. *Macromolecules* **2006**, *39*, 6133.
(36) Król, B.; Król, P. *Colloid Polym. Sci.* **2009**, *287*, 189.
(37) Nair, P. A.; Ramesh, P. *J. Biomed. Mater. Res. Part A* **2013**, *101A*, 1876.
(38) Athawale, V. D.; Kulkarni, M. A. *Journal of Applied Polymer Science* **2010**, *117*, 572.
(39) Bakhshi, H.; Yeganeh, H.; Mehdipour-Ataei, S. *J. Biomed. Mater. Res. Part A* **2013**, *101A*, 1599.
(40) Bakhshi, H.; Yeganeh, H.; Mehdipour-Ataei, S.; Solouk, A.; Irani, S. *Macromolecules* **2013**, *46*, 7777.
(41) Choi, H. Y.; Bae, C. Y.; Kim, B. K. *Progress in Organic Coatings* **2010**, *68*, 356.
(42) Kurt, P.; Wood, L.; Ohman, D. E.; Wynne, K. J. *Langmuir* **2007**, *23*, 4719.
(43) Kurt, P.; Wynne, K. J. *Macromolecules* **2007**, *40*, 9537.
(44) Mishra, A. K.; Mishra, R. S.; Narayan, R.; Raju, K. V. S. N. *Progress in Organic Coatings* **2010**, *67*, 405.
(45) Velayutham, T. S.; Abd Majid, W. H.; Ahmad, A. B.; Gan, Y. K.; Gan, S. N. *Journal of Applied Polymer Science* **2009**, *112*, 3554.
(46) Meier, M. A. R.; Metzger, J. O.; Schubert, U. S. *Chemical Society Reviews* **2007**, *36*, 1788.
(47) Anastas, P.; Eghbali, N. *Chemical Society Reviews* **2010**, *39*, 301.
(48) Kobayashi, S.; Makino, A. *Chemical Reviews* **2009**, *109*, 5288.
(49) Matsumura, S.; Soeda, Y.; Toshima, K. *Appl Microbiol Biotechnol* **2006**, *70*, 12.
(50) H. Clark, J. *Green Chemistry* **1999**, *1*, 1.
(51) Tang, S. Y.; Bourne, R. A.; Smith, R. L.; Poliakoff, M. *Green Chemistry* **2008**, *10*, 268.
(52) Velayutham, T. S.; Majid, W. H. A.; Gan, S. N. *Journal of Applied Polymer Science* **2011**, *121*, 1796.
(53) Yari, A.; Yeganeh, H.; Bakhshi, H.; Gharibi, R. *J. Biomed. Mater. Res. Part A* **2014**, *102*, 84.
(54) Madbouly, S. A.; Xia, Y.; Kessler, M. R. *Macromolecules* **2013**, *46*, 4606.
(55) Garrison, T. F.; Zhang, Z.; Kim, H.-J.; Mitra, D.; Xia, Y.; Pfister, D. P.; Brehm-Stecher, B. F.; Larock, R. C.; Kessler, M. R. *Macromolecular Materials and Engineering* **2014**, doi: 10.1002/mame.201300423.
(56) Saetung, A.; Kaenhin, L.; Klinpituksa, P.; Rungvichaniwat, A.; Tulyapitak, T.; Munleh, S.; Campistron, I.; Pilard, J.-F. *Journal of Applied Polymer Science* **2012**, *124*, 2742.
(57) Unal, S.; Lin, Q.; Mourey, T. H.; Long, T. E. *Macromolecules* **2005**, *38*, 3246.

(58) Unal, S.; Long, T. E. *Macromolecules* **2006**, *39*, 2788.
(59) Unal, S.; Ozturk, G.; Sisson, K.; Long, T. E. *Journal of Polymer Science Part A: Polymer Chemistry* **2008**, *46*, 6285.
(60) Yeganeh, H.; Hojati-Talemi, P. *Polymer Degradation and Stability* **2007**, *92*, 480.
(61) *Dispercoll U 54*; MSDS No. 81020583 [Online]; Bayer MaterialScience LLC: Pittsburgh, PA, 2010. http://www.productsafetyfirst.bayer.com/SDSSearchPage.aspx?qpn=Dispercoll%20U%2054&qmn=&qn=EN&qa=US& (accessed May 16, 2014).
(62) Lee, S. K.; Kim, B. K. *J. Colloid Interface Sci.* **2009**, *336*, 208.
(63) Lee, D.-K.; Tsai, H.-B.; Yang, Z.-D.; Tsai, R.-S. *Journal of Applied Polymer Science* **2012**, *126*, E275.
(64) Jung, D. H.; Kim, E. Y.; Kang, Y. S.; Kim, B. K. *Colloids and Surfaces a-Physicochemical and Engineering Aspects* **2010**, *370*, 58.
(65) Hu, X.; Zhang, X.; Liu, J.; Dai, J. *Polymer International* **2014**, *63*, 453.
(66) Cakic, S. M.; Spirkova, M.; Ristic, I. S.; B-Simendic, J. K.; M-Cincovic, M.; Poreba, R. *Mater. Chem. Phys.* **2013**, *138*, 277.
(67) Wu, F.; Li, Y. J.; Chen, R. J.; Chen, S. *Chin. Chem. Lett.* **2009**, *20*, 115.
(68) Lei, L.; Xia, Z.; Cao, G.; Zhong, L. *Colloid Polym. Sci.* **2014**, *292*, 527.
(69) Orgiles-Calpena, E.; Aran-Ais, F.; Torro-Palau, A. M.; Orgiles-Barcelo, C.; Miguel Martin-Martinez, J. *Journal of Adhesion Science and Technology* **2009**, *23*, 1953.
(70) de Oliveira, A. A. R.; de Carvalho, S. M.; de Fátima Leite, M.; Oréfice, R. L.; de Magalhães Pereira, M. *Journal of Biomedical Materials Research Part B: Applied Biomaterials* **2012**, *100B*, 1387.
(71) Shin, M.; Lee, Y.; Rahman, M.; Kim, H. *Polymer* **2013**, *54*, 4873.
(72) Fang, Z.; Zhou, M.; Zhong, J.; Qi, Y.; Li, L.; Dong, Q. *High Perform. Polym.* **2013**, *25*, 668.
(73) Zhang, S.; Yu, A.; Liu, S.; Zhao, J.; Jiang, J.; Liu, X. *Polym. Bull.* **2012**, *68*, 1469.
(74) Hwang, H.-D.; Kim, H.-J. *J. Colloid Interface Sci.* **2011**, *362*, 274.
(75) Qiu, F.; Xu, H.; Wang, Y.; Xu, J.; Yang, D. *Journal of Coatings Technology and Research* **2012**, *9*, 503.
(76) Bello, D.; Herrick, C. A.; Smith, T. J.; Woskie, S. R.; Streicher, R. P.; Cullen, M. R.; Liu, Y.; Redlich, C. A. *Environmental health perspectives* **2007**, *115*, 328.
(77) Hearne, S. A. *Environment: Science and Policy for Sustainable Development* **1996**, *38*, 4.
(78) Brocas, A.-L.; Cendejas, G.; Caillol, S.; Deffieux, A.; Carlotti, S. *Journal of Polymer Science Part A: Polymer Chemistry* **2011**, *49*, 2677.
(79) Pyo, S.-H.; Persson, P.; Mollaahmad, M. A.; Sörensen, K.; Lundmark, S.; Hatti-Kaul, R. In *Pure and Applied Chemistry* 2011; Vol. 84, p 637.
(80) Helou, M.; Carpentier, J.-F.; Guillaume, S. M. *Green Chemistry* **2011**, *13*, 266.
(81) Hahn, C.; Keul, H.; Möller, M. *Polymer International* **2012**, *61*, 1048.
(82) Caló, V.; Nacci, A.; Monopoli, A.; Fanizzi, A. *Organic Letters* **2002**, *4*, 2561.
(83) Rokicki, G.; Piotrowska, A. *Polymer* **2002**, *43*, 2927.
(84) Clements, J. H. *Industrial & Engineering Chemistry Research* **2003**, *42*, 663.
(85) Nair, P. A.; Ramesh, P. *Journal of Applied Polymer Science* **2011**, *122*, 1946.
(86) Li, J.; Zhang, Y.; Yang, J.; Tan, H.; Li, J.; Fu, Q. *J. Biomed. Mater. Res. Part A* **2013**, *101A*, 1362.

(87) Podsiadlo, P.; Qin, M.; Cuddihy, M.; Zhu, J.; Critchley, K.; Kheng, E.; Kaushik, A. K.; Qi, Y.; Kim, H.-S.; Noh, S.-T.; Arruda, E. M.; Waas, A. M.; Kotov, N. A. *Langmuir* **2009**, *25*, 14093.
(88) Ding, C.; Xu, S.; Wang, J.; Liu, Y.; Hu, X.; Chen, P.; Feng, S. *Polym. Adv. Technol.* **2012**, *23*, 1283.
(89) Jian, W.; Xu, S.; Wang, J.; Feng, S. *J. Appl. Polym. Sci.* **2013**, *129*, 2070.
(90) Guelcher, S. A. *Tissue Engineering Part B: Reviews* **2008**, *14*, 3.
(91) Ayres, E.; Oréfice, R. L.; Yoshida, M. I. *European Polymer Journal* **2007**, *43*, 3510.
(92) Gour, N.; Ngo, K. X.; Vebert-Nardin, C. *Macromolecular Materials and Engineering* **2013**, doi: 10.1002/mame.201300285.
(93) Nagamune, H.; Maeda, T.; Ohkura, K.; Yamamoto, K.; Nakajima, M.; Kourai, H. *Toxicology in Vitro* **2000**, *14*, 139.
(94) Ratner, B. D. *Journal of Biomedical Materials Research* **1993**, *27*, 283.
(95) Cui, W.-W.; Tang, D.-Y. *Journal of Applied Polymer Science* **2012**, *126*, 510.
(96) Lian, F.; Wen, Y.; Ren, Y.; Guan, H. *Journal of Membrane Science* **2014**, *456*, 42.
(97) Soo Lee, A. S.; Lee, J. H.; Lee, J.-C.; Hong, S. M.; Hwang, S. S.; Koo, C. M. *Journal of Materials Chemistry A* **2014**, *2*, 1277.
(98) Yin, K.; Zhang, Z.; Yang, L.; Hirano, S.-I. *J. Power Sources* **2014**, *258*, 150.
(99) Zhang, L.; Chaloux, B. L.; Saito, T.; Hickner, M. A.; Lutkenhaus, J. L. *Macromolecules* **2011**, *44*, 9723.
(100) Wang, Y.; Chen, K. S.; Mishler, J.; Cho, S. C.; Adroher, X. C. *Applied Energy* **2011**, *88*, 981.
(101) Agrawal, R. C.; Pandey, G. P. *Journal of Physics D: Applied Physics* **2008**, *41*, 223001.
(102) Liu, L. B.; Wu, X. W.; Li, T. D. *J. Power Sources* **2014**, *249*, 397.
(103) Shin, J.-H.; Henderson, W. A.; Passerini, S. *Electrochemistry Communications* **2003**, *5*, 1016.
(104) Armand, M.; Endres, F.; MacFarlane, D. R.; Ohno, H.; Scrosati, B. *Nat Mater* **2009**, *8*, 621.
(105) Król, P.; Król, B.; Stagraczyński, R.; Skrzypiec, K. *Journal of Applied Polymer Science* **2013**, *127*, 2508.

Chapter 8: Melt-Stable Imidazolium-Containing Copolyesters as Potential Non-viral Gene Delivery Vehicles

Ashley M. Nelson[1], Allison M. Pekkanen[2], Neil L. Forsythe[1], John H. Herlihy[1], Musan Zhang[1], M. Nichole Rylander[2], and Timothy E. Long[1,]

[1]*Macromolecules and Interfaces Institute, Department of Chemistry*
Virginia Tech, Blacksburg, VA 24061-0212

[2]*School of Biomedical Engineering and Sciences*
Virginia Tech, Blacksburg, VA 24061

8.1 *Abstract*

The inherent biocompatible and biodegradable nature of polyesters renders them excellent candidates for a variety of biological applications. Incorporating ionic groups further expands the potential impact, encompassing charge-dependent functions such as deoxyribonucleic acid (DNA) binding, antibacterial properties, and pH responsiveness. Catalyst-free polycondensation of a bromomethyl imidazolium-containing (BrMeIm) diol with neopentylglycol (NPG) and adipic acid (AA) afforded a series of novel charged copolyesters with pendant imidazolium sites. Varying ionic content impacted thermal properties and offered a wide-range, -41 °C to 40 °C, of composition-dependent glass transition temperatures (T_gs). In spite of the melt and thermal stability, ionic concentrations ≥15 mol % dispersed in water, initiating their evaluation as non-viral gene delivery vectors. A gel shift assay confirmed the novel cationic copolyesters successfully bound DNA at an N/P ratio of 4 for 50 and 75 mol % charged copolyesters (P(NA_{50}-*co*-ImA_{50}) and P(NA_{25}-*co*-ImA_{75})) and 5 for 100 mol % Im (PImA). Polyplexes exhibited insignificant cytotoxicity at high concentrations (200 μg/mL) and

a Luciferase transfection assay revealed the ionic (co)polyesters transfected DNA significantly better than controls. Furthermore, electrospinning PImA with poly(ethylene oxide) (PEO) at an 80:20 ratio of PImA:PEO produced fibers for additional antimicrobial coatings and/or adhesive applications. The successful transfection of these novel (co)polyesters inspired future imidazolium-containing polyester design based on structure-property-function relationships for improved transfection and understanding.

8.2 *Introduction*

Polyesters span many different markets ranging from high-performance materials to low glass transition temperature (T_g) adhesives.[1-3] Biodegradability, resulting from hydrolytically unstable ester bonds, and biocompatibility are two additional benefits of a polyester backbone, which make them excellent candidates for biological applications.[4-7] Step-growth and ring-opening polymerization methods generate polyesters, utilizing mainly diacids or diesters and diols or cyclic lactone monomers, respectively.[8] Focusing solely on step-growth transesterification (diester and diol) and condensation (diacid and diol) reactions, an array of well-studied difunctional monomers provide vast structural diversity, enabling chemists the ability to design polyesters with specific functions and properties.[3,8] The development of novel monomers poses a synthetic challenge, however, as successful linear step-growth polymerization demands monomers of high purity (>99 %) and perfect difunctionality (f=2).

Similar to polyesters, charged, or ion-containing polymers enable structural and material diversity in a variety of applications including conductive materials, water purification membranes, antibacterial coatings, and non-viral gene delivery.[9-12] The ability to impact such different fields stems from the manipulation and/or placement of the ionic groups into

polymers.[13,14] The polymer structure, type of ion, amount of ion, and desired end-use all influence the resulting polymer properties. Introduction of ionic groups occurs through polymerization of an ion-containing monomer or post-polymerization reactions. Each method imparts control of ion concentration, which many systematic studies revealed crucial as small changes in ionic content can greatly alter material properties.[15-17]

Ion-containing polyesters continue as a highly researched topic with seemingly limitless possibilities as a result of different ionic groups yielding anionic and cationic backbones or endgroups, all exhibiting structure and ion dependent counterion effects, electrostatic interactions, ionic conductivity, and more.[16,18-20] For example, utilizing commercially available sulfonated dimethyl isophthalate, Zhang et al.[16] synthesized polyester block copolymers containing pendant sulfonate anions in the hard or soft segments. When placed in the soft segment, a microphase-separated morphology resulted and tensile testing revealed elastomeric properties which the authors attributed to electrostatic interactions. Another field of study ion-containing polymers, specifically cationic polymers, play a critical role in is non-viral gene delivery.[21] This involves complexation of positively charged polymers, often phosphonium or ammonium cations, with the negatively charged backbone of deoxyribonucleic acid (DNA) or ribonucleic acids (RNAs). Ideally DNA or RNAs coded with a specific function binds to a non-toxic polymer forming a polyplex, which undergoes endocytosis and then releases the nucleic acid into the cell to perform the programmed function.

Poly(ethylene imine) (PEI) is recognized as the current gold standard in non-viral gene delivery; however, cytotoxicity prevents long-term stable transfection and creates a need for a non-toxic transfection-efficient polymer.[22-24] The Long[25] research group compared ammonium and phosphonium cations and the influence of alkyl chain length on successful transfection. A

longer alkyl spacer enhanced transfection, and the phosphonium-containing polymers outperformed the ammonium analogs. Well-defined diblock copolymers designed to both bind DNA and stabilize the polyplexes showed the effect of molecular weight on transfection and elucidated unexpected cell-line dependent results.[26] These systematic studies provided valuable insight into understanding the effect of polymer structure and properties on the endocytotic pathway and subsequent release. The biodegradable and biocompatible nature of polyesters coupled with performance tunable properties and noncovalent interactions make cationic polyesters promising non-viral gene delivery vehicles.[27] Abundant research on biodegradable nanoparticles comprised of mostly non-ionic poly($_{D,L}$-lactide-*co*-glycolide) (PLGA) polyesters, and some development of cationic PLGA-derivatives, for non-viral delivery further supports cationic polyesters as efficient and nontoxic polymeric vectors.[28-30] Although limited research exists, bio-inspired linear polymers poly($_{L}$-lysine), poly($_{D,L}$-lactide-*co*-4-hydroxy-$_{L}$-proline), and poly[α-(4-aminobutyl)-$_{L}$-glycolic acid] delivered promising results, confirming polyesters are capable of efficient transfection.[5,22,31] Finally, Xu et al.[32] utilized self-biodegradation to design a novel poly(beta-amino ester) to enhance DNA release after endocytosis and observed transfection efficacy greater than Jet PEI. Synthetic restrictions, alluded to previously, inhibit the continual development of novel polyester compositions impeding the success and potential of polyesters in this field of study.

The imidazole ring is a naturally occurring compound present in the amino acid histidine and forms an imidazolium cation upon alkylation.[33,34] Exploration and use of this particular ionic group traverses from biological (antibacterial, non-viral gene delivery) applications to electroactive devices.[17,34,35] Allen and coworkers[17] synthesized poly(1-vinylimidazole) and post-polymerization reactions with alkyl bromides containing different alkyl spacer lengths and

hydrogen-bonding groups allowed for a systematic study of the effect of ionic content and noncovalent interactions on transfection. Increased ionic and hydroxyl functionality improved transfection, yet >25 mol % charge negatively impacted toxicity. Currently, we are aware of only one report of linear polyesters containing pendant imidazolium groups; a post-polymerization click reaction allowed Mincheva et al.[36] to graft imidazolium sidechains only containing a maximum of 17 % ionic content and evaluated for increased carbon nanotube (CNT) dispersion. In other imidazolium containing linear polyesters, the imidazolium group resides in the polymer backbone, decreasing accessibility for efficient DNA binding.[20,37] Furthermore, examining polyesters with pendant imidazolium groups as potential non-viral gene delivery vehicles remains unexplored.[34]

Herewithin, we report the synthesis and characterization of novel copolyesters containing pendant imidazolium groups. Catalyst-free high-temperature melt polycondensation of an imidazolium diol, neopentylglycol, and adipic acid afforded a systematic series of charged copolyesters demonstrating tunable thermal transitions and hydrophilicity. The imidazolium group imparted water solubility above 30 weight % (wt. %) ionic content, allowing for the evaluation as non-viral gene delivery vectors. Gel shift assays, toxicity studies, and transfection experiments showed the influence of the polyesters on successful polyplex endocytosis and DNA release. Additionally, electrospinning with poly(ethylene oxide) (PEO) afforded mats with potential antibacterial activity. These novel imidazolium-containing copolyesters provide a platform for new chemistries and materials capable of advancing non-viral gene delivery technologies.

8.3 *Experimental*

8.3.1 Materials

1-butylimidazole (BuIm, 98%), 1-methylimidazole (MeIm, ≥99 %), neopentylglycol (NPG, 99 %), dimethyl adipate (DMA, ≥99 %), and poly(ethylene oxide) (PEO, M_v ~300,000 g/mol) were obtained from Sigma-Aldrich and used as received. Adipic acid (AA, ≥99.5 %) was purchased from Fluka Analytical and used as received. Ethyl acetate (EtOAc, Fisher Scientific) and methanol (MeOH, Spectrum Chemical), both HPLC grade, were used as received. 2-(bromomethyl)-2-methyl-1,3-propanediol was prepared according to previous literature (^{1}H NMR available in supplementary information, **Figure 12**).[38] A catalyst solution of 0.01 g titanium tetraisopropoxide per 1 mL 1-butanol was prepared in accordance with previous literature.[39]

8.3.2 Analytical Methods

^{1}H nuclear magnetic resonance (NMR) spectroscopy was performed on an Agilent U4-DD2 400 MHz spectrometer at room temperature in either deuterated chloroform ($CDCl_3$) or deuterated water (D_2O). A TA Instruments thermogravimetric analyzer (TGA) Q50 provided weight loss as a function of temperature in a N_2 atmosphere at a 10 °C/min heating rate from room temperature to 600 °C. Charged polyesters were dried in a vacuum oven prior to running. For isothermal TGA, the sample was heated at a rate of 20 °C/min until the desired 180 °C and weight loss monitored over 12 h at the elevated temperature. A TA Instruments differential scanning calorimeter (DSC) Q1000 or Q2000 equipped with a refrigerated cooling system afforded glass transition (T_g), melting (T_m), and crystallization (T_c) temperatures. A

heat/cool/heat cycle, ramping at a rate of 10 °C/min to an upper temperature ranging from 60 to 180 °C, cooling at either 50 or 100 °C/min to ≤-60 °C, and heated at a rate of 10 °C/min to the same upper temperature used in the first heat, was performed on each sample and the values reported from the second heat. All polyester DSC samples were dried in a vacuum oven at ca. 50 °C and ran immediately to avoid water uptake. A TA Instruments dynamic vapor sorption analyzer (TGA-SA) Q5000SA provided water uptake as a function of relative humidity. Samples were first dried in the instrument for either 2 h or until < 0.01 weight % change for 5 min and then equilibrated at ambient temperature (20 °C for noncharged control, 25 °C for 100 mol % Im) and 0 % relative humidity (RH). RH was increased in 5 % increments, samples were held at each increment for either 2 h or < 0.01 weight % change for 10 min, up to 95 % RH.

8.3.3 Synthesis of Imidazolium-containing Diols

1-(3-hydroxy-2-(hydroxymethyl)-2-methylpropyl)-3-methyl-1*H*-3λ^4-imidazol-1-ium bromide (bromomethyl imidazolium diol, BrMeIm diol) and 3-butyl-1-(3-hydroxy-2-(hydroxymethyl)-2-methylpropyl)-1*H*-3λ^4-imidazol-1-ium (bromobutyl imidazolium diol, BrBuIm diol) were prepared and isolated in a similar manner. 2-(bromomethyl)-2-methyl-1,3-propanediol (12.72, 1.0 mol eq) and MeIm (5.85 mL, 1.05 mol eq) were added to a round-bottomed flask equipped with a magnetic stir bar. After a 30 min N_2 purge, the round-bottomed flask was lowered into a heated oil bath (~ 100 °C) and allowed to stir for >2 d to ensure complete substitution. While still hot, MeOH was added to dilute the reaction and it was slowly precipitated into EtOAc. After stirring overnight, the white crystals were filtered, subsequently rinsed with cold EtOAc, and dried in a 50 °C vacuum oven. Whittington et al.[40] previously reported the synthesis of this *N*-methyl derivative as a yellow oil, however, we obtained a white

crystalline solid. ^{1}H NMR (**Figure 1**), mass spectrometry (*MS*), TGA, and DSC confirmed the structure and thermal properties. MS: calcd, 185.13; found, 185.13. $T_{d,onset}$ = 307 °C. T_g = -22 °C. T_c = 90 °C. T_m = 113 °C.

BrBuIm diol was isolated as a yellow oil. ^{1}H NMR available in supporting information, **Figure 13**. MS: calcd, 227.18; found, 227.18. $T_{d,onset}$ = 271 °C. T_g = -38 °C.

8.3.4 Neutral Control Polyester Synthesis

Melt transesterification afforded the noncharged polyester control, poly(neopentylene adipate) (PNA). Neopentylglycol (5.8366 g, 1.2 mol eq), dimethyl adipate (8.14 g, 1.0 mol eq), and titanium tetraisopropoxide solution (0.06 mL, 40 ppm) were added to an oven dried 100 mL round-bottomed flask. A mechanical stir rod, t-neck, and distillation apparatus were affixed to the round-bottomed flask after the reagents were added and then the reaction was purged with N_2 and vacuum three times to ensure an inert environment. During the purging process any condensed or sublimed monomer was melted back into the reaction using a butane torch. With a constant N_2 purge, the reaction was lowered into a molten metal bath heated to 170 °C and allowed to react with stirring for 2 h. The temperature was then raised to 220 °C for an additional 2 h and finally vacuum (0.15 mmHg) was pulled maintaining a temperature of 220 °C for another 2 h. The reaction was removed from the heat and allowed to cool under a N_2 atmosphere. The resulting polymer was removed from the round-bottomed flask and used without further purification.

8.3.5 Imidazolium-Containing (Co)polyesters Synthesis

Catalyst-free melt polycondensation generated all imidazolium-containing (co)polyesters in similar manner. A 1:1 molar ratio of diacid to total diol was used in each synthesis and

BrMeIm diol was dried in a vacuum oven overnight at 50 °C prior to use. The following procedure describes the synthesis of the imidazolium homopolyester (100 mol % Im). BrMeIm diol (2.1208 g) and adipic acid (1.1690 g) were added to a dry 50 mL round-bottomed flask and the reaction was setup and degassed as described earlier for the neutral control polyester. The reaction was then lowered into a 130 °C silicon oil bath and allowed to react with stirring and a N_2 purge for approximately 12 h. The temperature was increased to 200 °C for an additional 12 h and vacuum (0.15 mmHg) was then pulled for 6 h at 200 °C to complete the reaction. The polyester was removed from the round-bottomed flask and used without any further purification.

8.3.6 Gel Electrophoresis

To prepare the 8-well agarose gels, agarose (600 mg, Bio-Rad) was dissolved in warm reverse osmosis (RO) water (54 mL). TRIS acetate-EDTA (TAE) buffer solution (6 mL of 10X concentrate, Sigma-Aldrich) was then added and once the mixture was β cooled SYBR® Green I nucleic acid gel stain (6 μL, Sigma-Aldrich) was pipetted into the solution. The solution was then poured into the gel tray, 8-well combs carefully placed and used to remove any bubbles, covered, and allowed to harden. Polyplexes were formed in the following manner: in order, DNA (1 μL of a 1 μg/μL solution of gWiz™ High-Expression beta-galactosidase vector from Aldevron), water, and polymer (a volume of 1 mg/mL solution to reach the desired nitrogen/phosphate (N/P) ratios) were added to a micro-centrifuge tube to a total volume of 30 μL and mixed using a micropipette. After a 30 min incubation, loading buffer (30 wt. % glycerol (99 %, Sigma-Aldrich) in water, 6 μL) was added to each polyplex and then pipetted into the wells of the agarose gel. Gels were run horizontally in a 1X TAE buffer solution at 70 V for 40 min using a Bio-Rad PowerPac Basic power supply. Images were taken using UVP's

MultiDoc-It™ Imaging System. Full DNA binding was obtained at an N/P ratio of 4 for 50 and 75 mol % Im and 5 for 100 mol % Im.

8.3.7 Polyplex Stability Study

Polyplexes were formed in a similar manner as described above for the fully bound N/P ratios, however, volumes were adjusted to obtain 1 mL total. 100 μL aqueous polymer solution (necessary μL polymer for N/P ratio using 1μL DNA) was added to 100 μL aqueous DNA solution (1μL gWiz™ beta-gal), vortexed, and then incubated for 30 min. 800 μL of water was then added to the polyplex, the solution was vortexed, and then placed in a disposable cuvette for dynamic light scattering (DLS) measurements. A Malvern Zetasizer Nano ZS measured hydrodynamic diameter at 25 °C and the reported volume particle size distributions, including standard deviation, are an average of 3 runs.

8.3.8 Cell Culture

HeLa cervical cancer cells were obtained from the American Type Culture Collection (ATCC) and were cultured at 37 °C with 5% CO_2 in Dulbecco's Modified Eagle Medium (DMEM) supplemented with 10% Fetal Bovine Serum (FBS) and 1% penicillin/streptomycin.

8.3.9 Cytotoxicity Protocol

Prior to exposure to polyplex solutions, HeLa cells were lifted from the culture plate with 0.25 % Trypsin-EDTA and seeded into 96 well plates at a density of 5,000 cells/well. The cells were allowed to attach and proliferate for 24 hours at 37 °C with 5% CO_2. Cell media was aspirated and cells were rinsed with phosphate buffered saline (PBS) prior to application of polyplex solutions. Polyplex solutions were prepared by mixing DNA with polymer in water,

allowing 30 minutes for polyplexes to form. Stock polyplex solution was then diluted in serum-free DMEM to the desired concentration, applied to cells, and allowed to incubate for 2 h. After incubation, polyplex solutions were removed, cells rinsed with PBS, and fresh media was applied. HeLa cells were allowed to incubate with media for 24 hours, after which the CellTiter-Glo® assay was performed according to manufacturer's protocol. Briefly, existing media was removed, cells were rinsed with PBS, and fresh media was applied to each well. After equilibrating to room temperature, equal volume of CellTiter-Glo® reagent was added to each well, rocked gently for 2 minutes, and allowed to equilibrate for 10 minutes. Luminescence was read using a Promega GloMax 96 Microplate Luminometer. All measurements were normalized to positive and negative controls on the same plate (n=5), and data is presented as an average ± standard deviation. Statistical analysis (ANOVA with Tukey's HSD) was performed with JMP software (p=0.05).

8.3.10 Transfection Assay

Prior to transfection, HeLa cells were lifted from the culture plate using 0.25 % Trypsin-EDTA and seeded into 96 well plates at a density of 5,000 cells/well. Cells were allowed to attach and proliferate for 24 hours at 37 °C with 5% CO_2. Cell media was aspirated and cells were rinsed with PBS before exposure to polyplex solutions consisting of polyester and gWiz-Luc DNA at minimum N/P ratios for full binding. Superfect and Jet-PEI were prepared and applied to cells according to manufacturer's protocols. Polyplex solutions were formed in water, diluted in Opti-MEM, and subsequently applied to cells with a final concentration of 1 μg DNA/well. After 2 h incubation, polyplex solutions were removed, HeLa cells rinsed with PBS, and fresh serum-containing media was added to each well. Cells were incubated at 37 °C with 5%

CO_2 for 48 hours prior to performing a Promega luciferase assay according to manufacturer's protocol. Briefly, media was removed, cells washed with PBS, and cells were lysed with 1x Reporter Lysis Buffer. Following one freeze-thaw cycle to ensure complete cell lysis, 100 μL of Luciferase Assay Reagent was added to cell lysate and read using a Promega GloMax 96 Microplate Luminometer. Total protein was measured with the BCA protein assay and absorbance was read using a SpectraMax M2 plate reader. All measurements were normalized to total amount of protein in each sample, and data is presented as an average ± standard deviation.

8.3.11 Electrospinning

An electrically grounded Plexiglass® box served as an electrospinning chamber. A Gamma High Voltage Research power supply and Spellman CZE1000R power supply were used for the syringe tip and collection plate, respectively. A New-Era Pump Systems single syringe pump allowed for constant solution dispensing. Images of electrospun fibers/mats were obtained using a Jeol Neoscope JCM-5000 benchtop scanning electron microscope (SEM).

8.4 *Results and Discussion*

8.4.1 Synthesis of Imidazolium-containing (Co)polyesters

En route to novel cyclic carbonates, Mindemark and Bowden[38] synthesized alkyl halide-containing 1,3-propanediol intermediates. Zhang et al.[41] and Whittington et al.[40] recognized the potential for ion-containing primary diols and substitution reactions with trialkylphosphines and 1-methylimidazole, respectively, resulted in novel charged diols. Utilizing a slightly altered reaction and workup procedure, we prepared the previously reported methyl and a novel butyl

imidazolium diol derivatives. **Scheme 1** depicts the substitution reaction of 2-(bromomethyl)-2-methyl-1,3-propanediol, performed in bulk, with both 1-methylimidazole (MeIm) and 1-butylimidazole (BuIm) resulting in alkyl imidazolium diols with bromide counterions. Precipitation into ethyl acetate (EtOAc) removed the slight excess of MeIm and BuIm charged and any impurities, resulting in highly pure BrMeIm diol and BrBuIm diol confirmed with mass spectrometry (MS) and ^{1}H NMR.

Scheme 8.1. Substitution reaction affords alkyl imidazolium diols

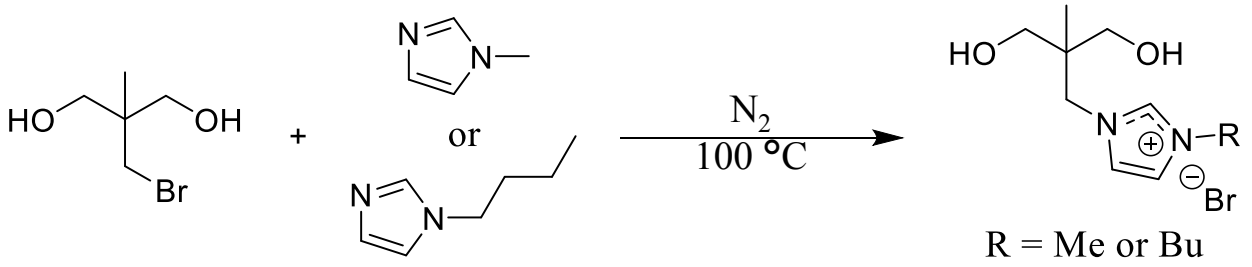

The ^{1}H NMR spectra for BrMeIm diol and BrBuIm diol are shown in **Figure 1** and **Figure 13**, respectively, exhibiting expected integrations and peaks labeled accordingly. The ionic diols readily dissolved in D_2O, explaining the absence of the hydroxyl proton resonances. The desired high-temperature melt polycondensation polymerization method required high purity and thermal stability, rendering these crucial properties for the successful synthesis of imidazolium-containing (co)polyesters. Previously reported as a yellow oil without any specified thermal transitions, our diol precipitated as a white crystalline solid with a glass transition temperature (T_g) of -22 °C, crystallization temperature (T_c) of 90 °C, melting temperature (T_m) of 113 °C, and an onset degradation temperature ($T_{d,onset}$) of 307 °C.[40] The 113 °C T_m of BrMeIm diol exceeded the 100 °C limit for classification as an ionic liquid (IL), however, the BrBuIm diol only displayed a T_g (-38 °C) throughout a temperature range of -60 °C

to 180 °C.[42] The single T_g suggested the longer butyl alkyl chain prohibited packing into a crystalline lattice, designating BrBuIm diol an IL.

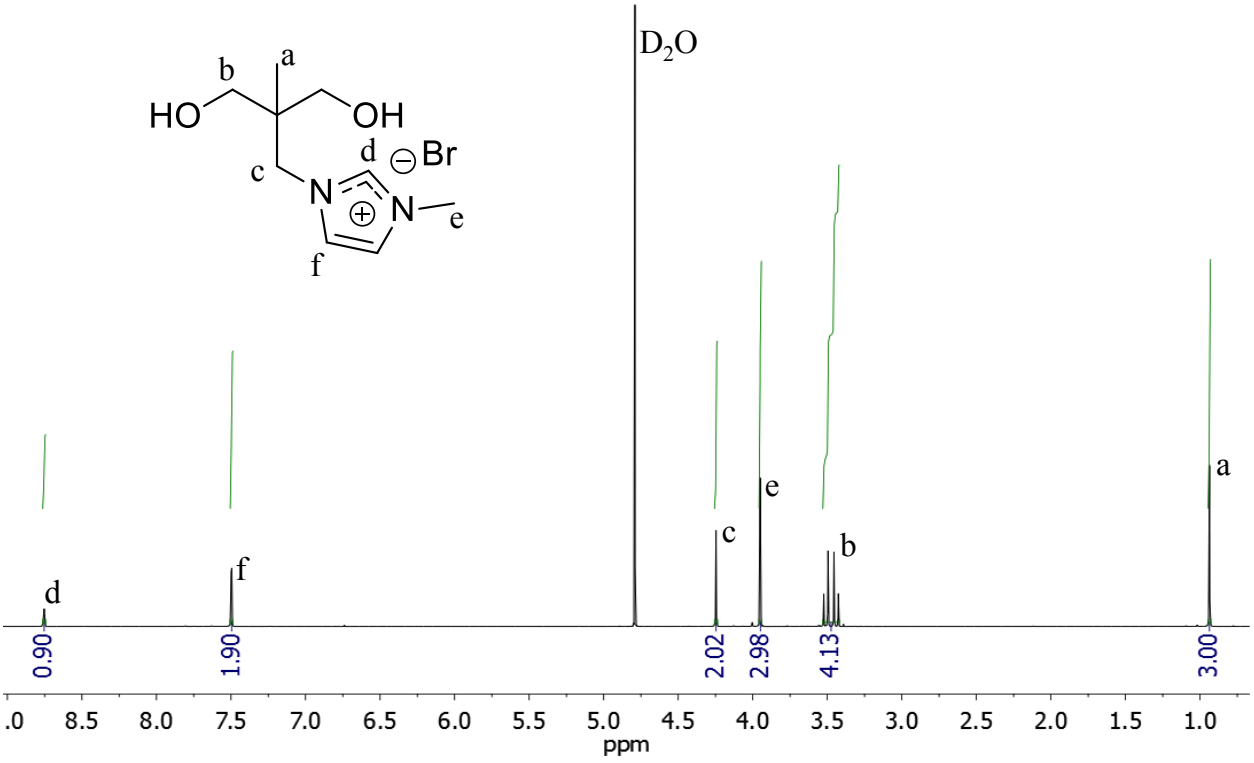

Figure 8.1. ^{1}H NMR spectroscopy confirms structure of bromomethyl imidazolium diol

We employed two different step-growth polymerization strategies for the synthesis of the noncharged control polyester poly(neopentylene adipate) and the imidazolium-containing (co)polyesters. Both polymerization techniques proceeded in bulk and the minimal or lack of catalyst allowed polymer isolation without any purification or workup. A titanium tetraisopropoxide ($Ti(OiPr)_4$) catalyzed melt transesterification, the reaction of a dimethylester and diol with methanol (MeOH) elimination driving the reaction to high conversion, afforded the neutral control polyester. **Scheme 2** displays the synthetic procedure and polyester repeating unit. The structural similarity of neopentylglycol (NPG) to the BrMeIm and BrBuIm diols and

literature precedence suggesting sterics prevent transesterification both contributed to NPG as the selected comonomer diol.[43] Beginning with a transesterification resistant diol allows for further development to well-defined block copolyesters, improving the understanding of various structure-property relationships and a possible need for the targeted biological applications.

Scheme 8.2. Synthesis of noncharged polyester, poly(neopentylene adipate) (PNA)

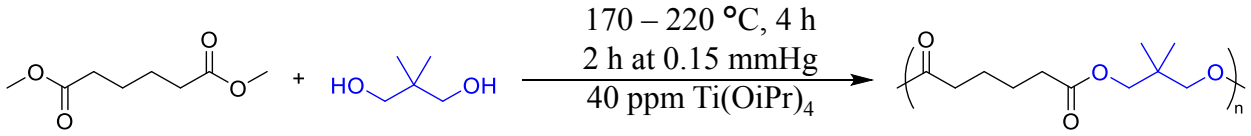

Polycondensation, the reaction of a diacid and diol with water elimination driving the reaction to the right, generated imidazolium-containing (co)polyesters. Multiple motives contributed to polycondensation as the preferred method for the ion-containing (co)polyester synthesis. A benefit of melt transesterification is the ability to charge a slight molar excess of low boiling point monomers, contrary to usual step-growth reactions requiring exact 1:1 stoichiometry.[8] The high temperatures and high vacuum at the end of the reaction removes any unreacted or small molecule byproducts, essentially forcing a 1:1 stoichiometry and reaching high conversion. Ionic monomers often possess exceedingly high boiling points, even under reduced pressure.[42] Therefore, any excess unreacted BrMeIm diol would remain in the polymer, lower the achievable molecular weight, and act as a plasticizer. To avoid the contaminate, 1:1 stoichiometry is required and the reaction conditions must ensure the comonomers (NPG and adipic acid (AA)) do not sublime or distill throughout the polymerization. Efficient water elimination occurs slowly so often initial steps in polycondensations progress at relatively low temperatures for extended periods of time and/or polymers are subsequently solid-stated..[3,8,44] Extended low temperature initial reaction conditions proved ideal for polymerization of BrMeIm diol as they provided ample opportunity for the monomers to form dimers, trimers, etc and

removed the possibility of monomer loss via distillation later in the reaction. Finally, polycondensation proceeded in absence of any heavy metal catalyst to eliminate potential cytotoxicity. **Scheme 3** depicts the imidazolium-containing (co)polyester synthesis.

Scheme 8.3. Catalyst-free melt polycondensation affords imidazolium-containing (co)polyesters

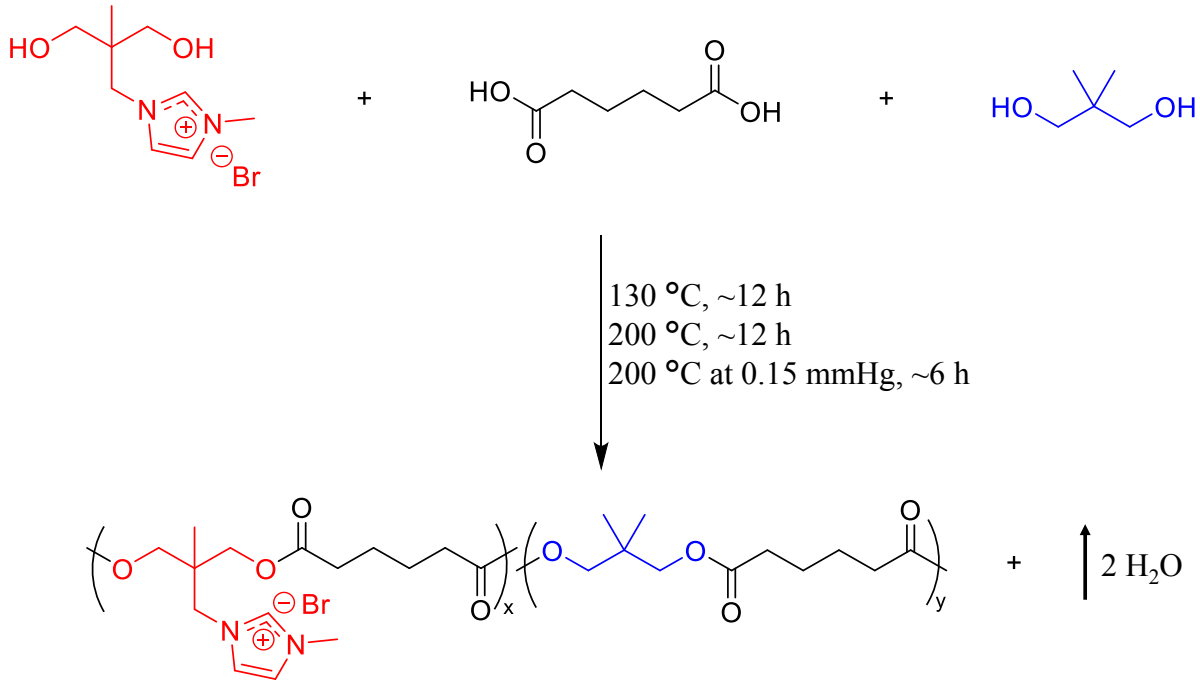

Charging different ratios of the BrMeIm diol and NPG, maintaining 1:1 stoichiometry of overall diol:diacid, afforded a series of imidazolium-containing (co)polyesters, poly(neopentylene adipate)$_x$-*co*-poly(BrMeIm adipate)$_y$ abbreviated P(NA$_x$-*co*-ImA$_y$) where x and y are the respective charged mol % of the neutral and imidazolium repeating units respectively. A total of 6 copolyesters with ionic content ranging from 10 – 75 mol % (12 – 88 wt. %), the imidazolium homopolyester (PImA), and the noncharged control (PNA) provided an array of charge content and structural diversity for investigating structure-property relationships with respect to ion concentration. Ionic content of 15 mol % and greater achieved hydrophilic water dispersible polyesters, enabling the exploration of biological applications. **Figure 2**

depicts the ^{1}H NMR spectra of PImA. Mnova NMR analysis software permitted a fixed integration of 4.00 for the adipic acid protons labeled **a** (**Figure 2)** and the remaining integrations correlated as expected. This confirmed all BrMeIm diol successfully polymerized, as free diol would increase integrations for the corresponding peaks. Interestingly, each hydrogen on the imidazolium monomer (resonances **c**, **d**, **e**, **f**, **g**, and **h** in **Figure 2**) exhibited distinct peak splitting, which equaled the expected value for full incorporation. We hypothesize the splitting resulted from tacticity, or the arrangement of the imidazolium groups along the backbone respective to neighboring protons.[45]

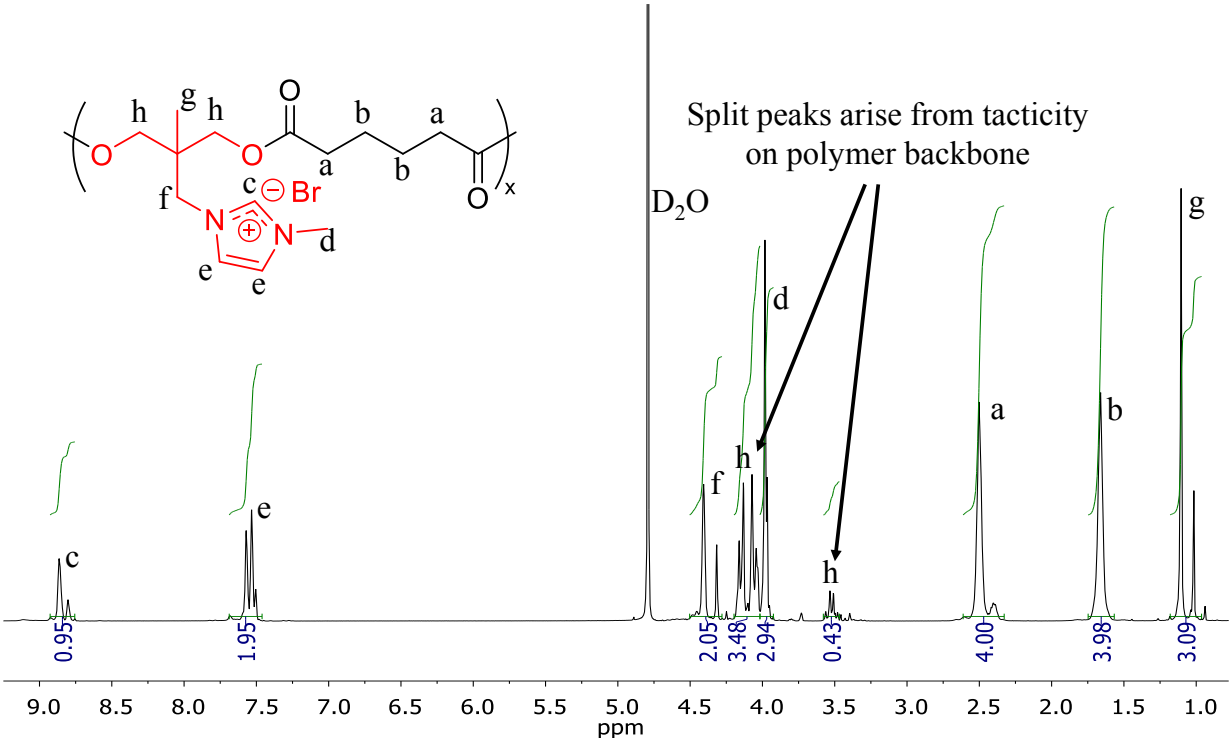

Figure 8.2. ^{1}H NMR spectroscopy confirms structure of melt stable imidazolium homopolyester, PImA

Unfortunately, high temperature melt polymerization of the novel BrBuIm diol proved unsuccessful. Hofmann elimination is a common thermally induced degradation pathway for ammonium cations containing beta-hydrogens.[46-48] The butyl alkyl spacer of BrBuIm diol,

unlike the single methyl group of BrMeIm diol, contains beta-hydrogens permitting the aforementioned elimination reaction. Initial thermogravimetric analysis (TGA) of BrBuIm diol revealed a promising one-step degradation profile with $T_{d,5\%}$ = 232 °C and $T_{d,onset}$ = 271 °C. A homogeneous melt prevailed throughout the first 12 h low temperature step in an attempted polymerization, however, upon increasing the temperature to 200 °C an undesirable brown color occurred and after 9 h the reaction no longer appeared homogeneous. An isothermal TGA of the BrBuIm diol monomer at 180 °C reflected the expected thermal instability, suffering a 15 % wt. loss after 2 h. **Figure 3** displays the isothermal TGA curve and proposed Hofmann elimination mechanism of BrBuIm diol. If all BrBuIm diol underwent Hofmann elimination, complete 1-butene loss equals 18 % wt., very close to the observed 16 % after 12 h. Additionally, hydrobromic acid (HBr) byproduct could induce the observed brown coloring and would inhibit the formation of ester bonds, further reinforcing Hofmann elimination's detrimental effect on BrBuIm diol polymerization.

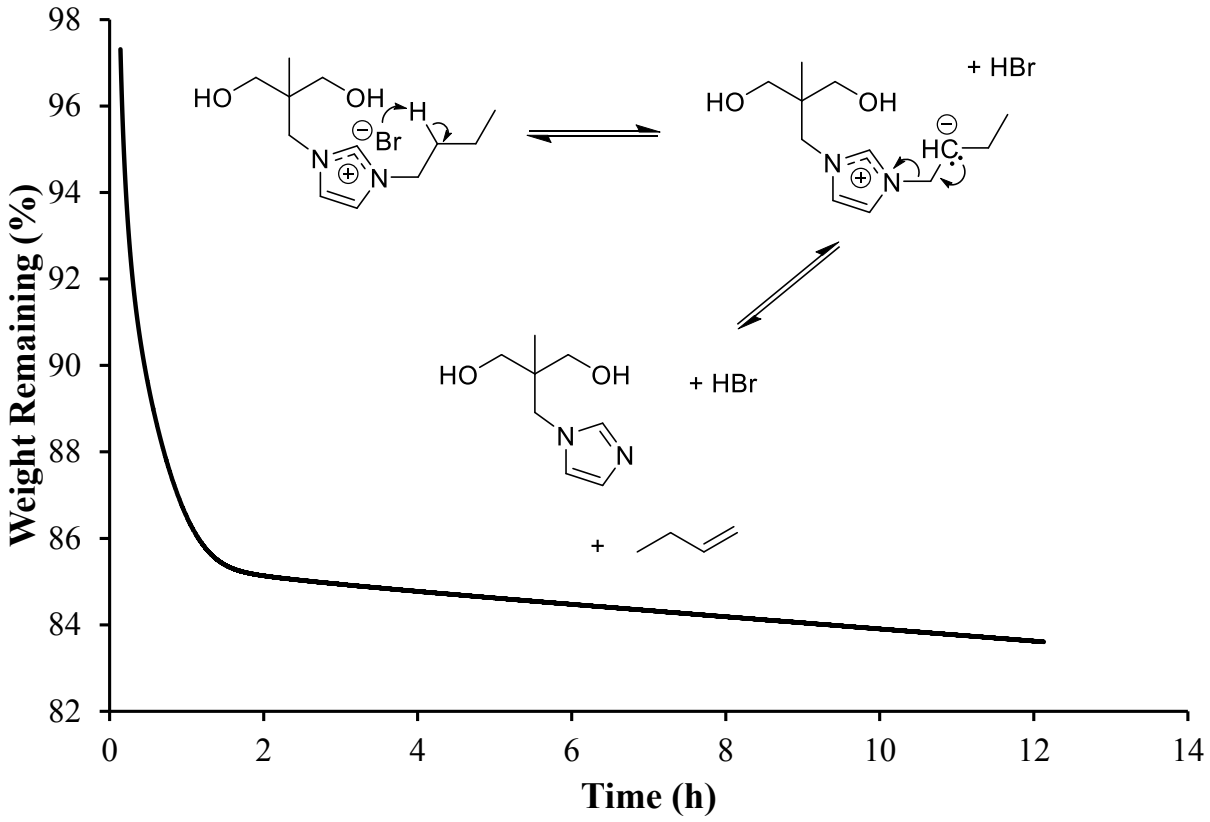

Figure 8.3. 12 h TGA isotherm of BrBuIm diol at 180 °C and proposed Hofmann elimination arrow-moving mechanism (inset)

8.4.2 Thermal and Sorption Analysis of Imidazolium Polyesters

General acid-base chemistry explains the hydrophilic nature of ionic groups.[49] Incorporating charged species into polymers provides multi-functional hydrophilic sites capable of imparting or tuning water solubility and directing self-assembly, for example.[50-52] As briefly noted earlier, water dispersible imidazolium-containing (co)polyesters resulted with ≥15 mol % charge. Thermogravimetric sorption analysis (TGA-SA) provided a direct comparison of the hydrophilicity of the organic soluble noncharged control and water soluble PImA. **Figure 4** depicts the water uptake, represented as percent weight gain, curves for the PNA and PImA homopolyesters as a function of increasing relative humidity (RH). After ramping RH to 95 %,

the noncharged control gained negligible weight (0.7 %) while PImA gained 41.2 wt. %. The increased water uptake of PImA both demonstrated and quantified the effect of ionic content on the amorphous polyester hydrophilicity.

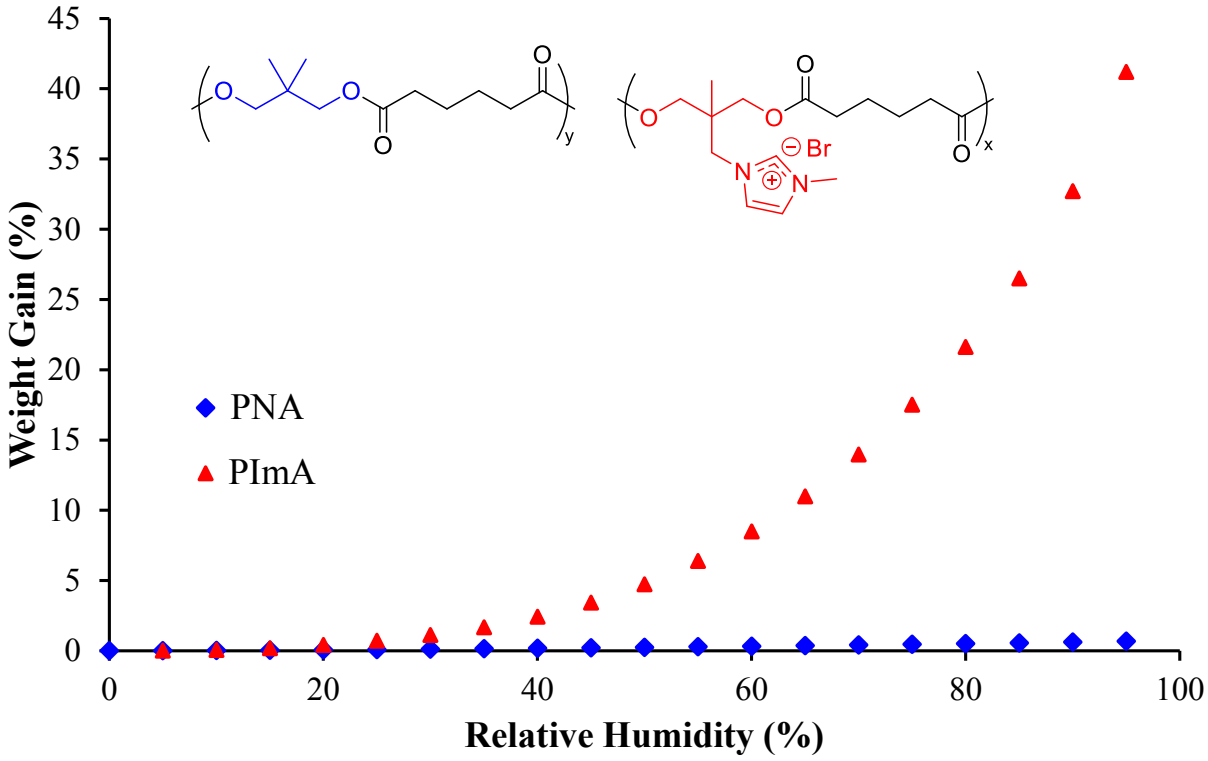

Figure 8.4. Water sorption analysis demonstrating increased hydrophilicity of PImA (red) compared to PNA (blue)

Figure 5 shows the one-step TGA degradation profiles of PNA, P(NA_{50}-*co*-ImA_{50}), P(NA_{25}-*co*-ImA_{75}), and PImA. As observed and discussed above, the ion-containing polyesters pick up water. Vacuum drying all charged polyesters at 50 °C prior to thermal analysis diminished water influencing and prohibiting determination of an accurate T_d. All (co)polyesters demonstrated good thermal stability, with $T_{d,onsets}$ > 300 °C well beyond the 200 °C and 220 °C melt polymerization temperatures. The neutral control exhibited a slightly higher $T_{d,onset}$ of 352 °C, whereas the imidazolium-containing (co)polyesters started to lose mass closer to 300 °C.

Residual char systematically increased with increasing imidazolium content, a reflection of the high degradation temperatures of ionic species, often shown in correlation with flame retardancy.[53,54]

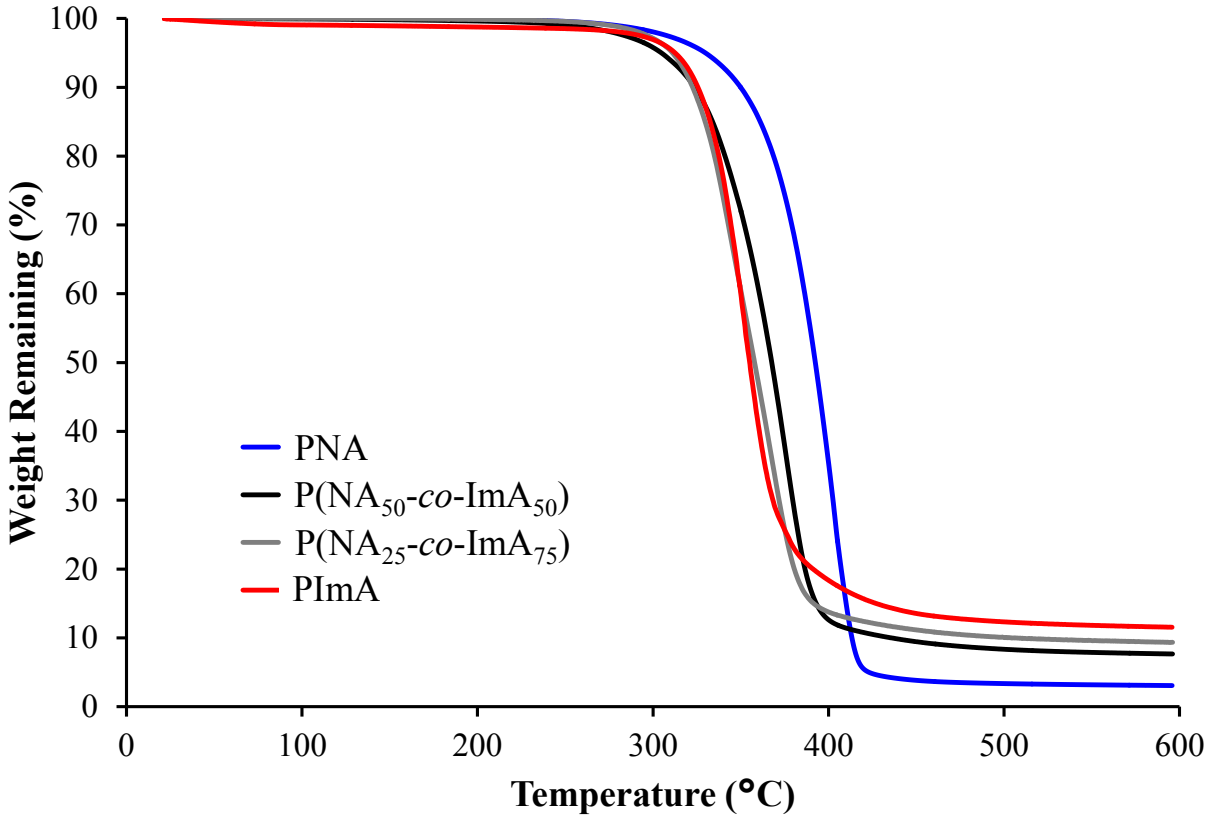

Figure 8.5. Degradation profiles of imidazolium-containing (co)polyesters and neutral control. Char residue scales with imidazolium content.

Differential scanning calorimetry (DSC) revealed a single T_g for each (co)polyester in the series, indicating amorphous materials within experimental temperature and time restrictions. T_g increased with increasing ionic content, spanning a large 80 °C temperature range of -41 °C to 40 °C. Tunable thermal transitions, accessing T_g's both above and below room temperature, elucidated an advantageous structure-property relationship of these novel ion-containing copolyesters. One T_g also implied an absence of microphase-separation; thus comparing

experimental values to those obtained using the Fox equation provided an indication of the randomness of the copolymerization.[55,56] With known homopolymer T_g's, the Fox equation (**Equation (1)**) predicts copolymer T_g's assuming a random copolymerization and phase mixing. The Fox equation requires temperature units in Kelvin, $T_{g,1}$ and $T_{g,2}$ are the T_g's of the homopolymers, w_1 and w_2 correspond to the weight fractions of each homopolymer, and T_g is the predicted transition temperature for the copolymer of interest. **Figure 6** displays the observed T_g for each copolyester as a function of wt. % Im and the predicted values from the Fox equation. Good agreement with predicted T_g's occurred at high ionic content suggesting a random copolymerization with efficient phase-mixing, however, the lower wt. % Im copolyesters deviated from the calculated values exhibiting slightly lower T_g's than theoretically determined.

$$\frac{1}{T_g} = \left(\frac{w_1}{T_{g,1}}\right) + \left(\frac{w_2}{T_{g,2}}\right) \qquad \textbf{Equation (1)}$$

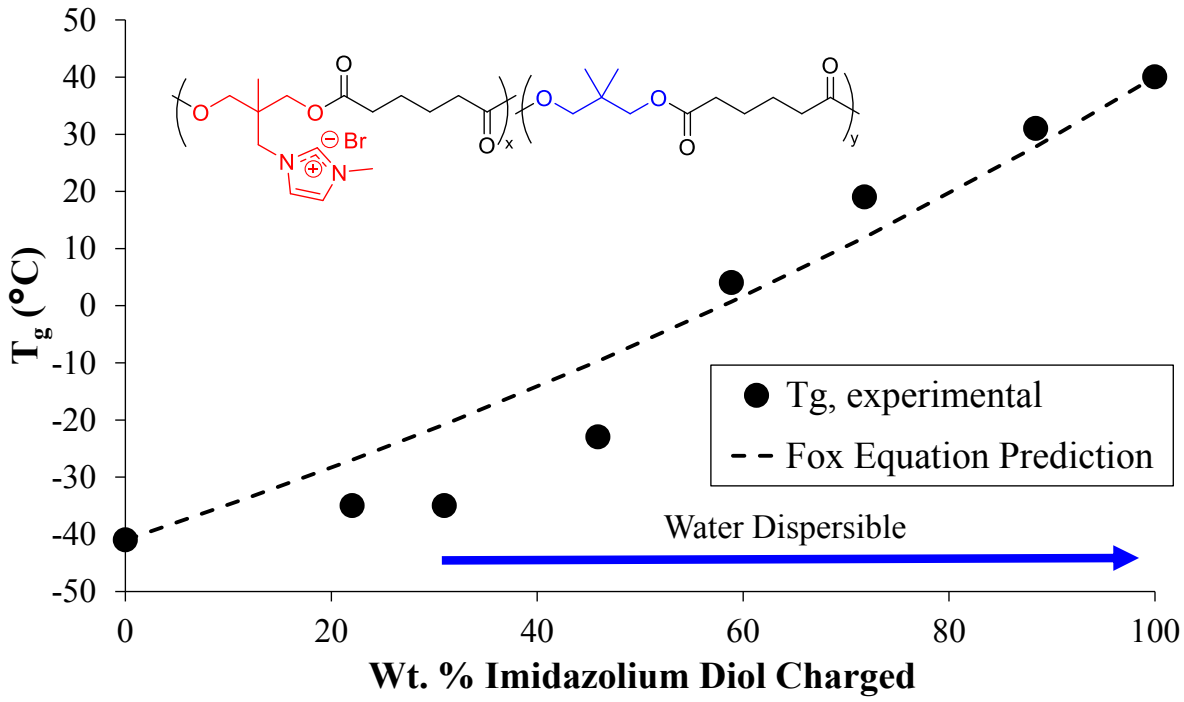

Figure 8.6. Fox equation plot demonstrating increasing glass transition temperature (T_g) with increasing ionic content

8.4.3 Imidazolium (Co)polyesters as Non-viral Gene Delivery Vectors

With literature precedence supporting the inherent biocompatibility of polyesters and efficient deoxyribonucleic acid (DNA) binding with imidazolium cations, we evaluated the ability of these novel water soluble imidazolium-containing copolyesters as potential non-viral gene delivery vectors.[5,6,17,57] P(NA_{50}-*co*-ImA_{50}), P(NA_{25}-*co*-ImA_{75}), and PImA polyesters served for initial studies since all three readily dissolved in water and previous literature shows improved transfection efficiency with increased charge content.[17] Electrophoretic gel shift assays are efficient and expedient at revealing DNA binding capabilities since any free or unbound DNA travels out of the loading well toward the positive electrode. The agarose gels contained 8-wells, the first loaded only with DNA as a control and the others contained

polyplexes prepared in water at different nitrogen/phosphorous (N/P) ratios. All copolyesters partially bound DNA at an N/P ratio of 2 and fully bound at an N/P of 4 for P(NA_{50}-*co*-ImA_{50}) and P(NA_{25}-*co*-ImA_{75}) and an N/P of 5 for PImA. **Figure 7** depicts the gel shift assay results for each (co)polyester. Comparing to relevant literature, Zhang et al.[57] synthesized poly(3-butyl-1-vinylimidazolium $_L$-proline salt) (PV4-Pro) and reported full DNA binding at an N/P ratio of 3.2, correlating well with the N/P of 4 and 5 observed for the imidazolium-containing (co)polyesters. Previously reported poly(1-ethyl-3-vinylimidazolium bromide-co-1-vinylimidazole) copolymers containing 25 mol % quaternization ($PEVIM_{25}$) did not bind until an N/P ratio of 10, however; 100 mol % ion content and the addition of a single hydrogen-bonding hydroxyl group (PHEVIM) reduced the binding N/P ratio to 2.[17] Different protocols, DNA, cell lines, charge density, and other factors alluded to above limited any exact comparisons between current literature and the binding of the novel imidazolium (co)polyesters, yet this initial experiment proved the imidazolium-containing copolyesters successfully bound DNA at analogous N/P ratios. Furthermore, the culmination of results highlights the sensitivity of efficient DNA binding to overall polymer composition.

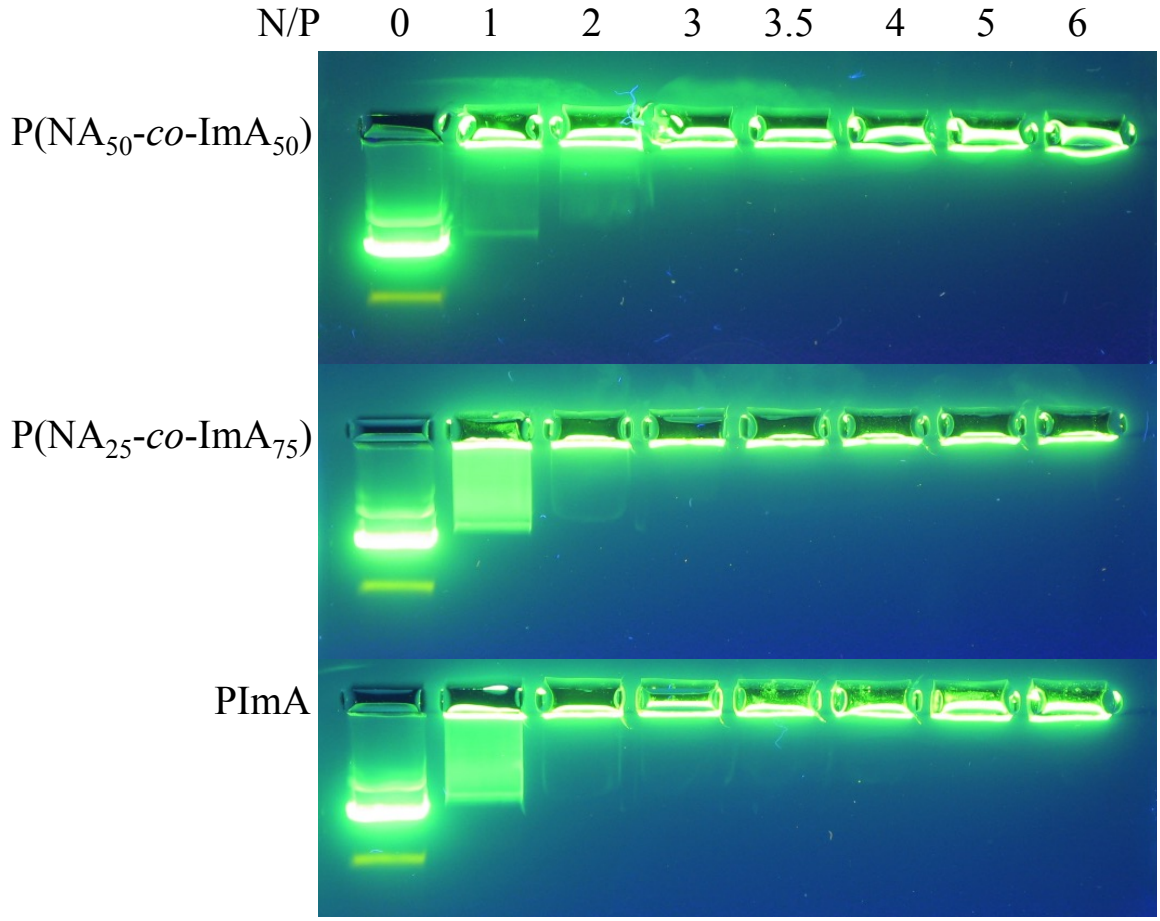

Figure 8.7. DNA gel binding assay shows imidazolium-containing (co)polyesters completely bind DNA at N/P ratios of 4 (P(NA_{50}-*co*-ImA_{50}) and P(NA_{25}-*co*-ImA_{75})) and 5 (PImA)

Dynamic light scattering (DLS) measured polyplex (formed using the specified minimum N/P ratios from gel binding studies) size and stability in solution over 24 h. Research stresses the importance of small stable particles, suggesting smaller polyplexes facilitate endocytosis.[21,58] Additionally, polyplexes must remain intact throughout cellular treatment and uptake. **Figure 8** shows the results for each (co)polyester at 7 different time-points over a 24 h study, where the zero time-point corresponds to the first measurement after a 30 min incubation allotted for

polyplex formation. Polyplexes formed from all three (co)polyesters remained stable in salt-free and serum-free water over 24 h with small hydrodynamic diameters (generally <100 nm). The cytotoxicity and transfection protocols allowed a 2 h polyplex incubation period, prompting the initial hourly recordings. These gentle conditions illustrated the strong electrostatic binding between the imidazolium-containing (co)polyesters and DNA and absence of polyplex aggregation or dissociation.

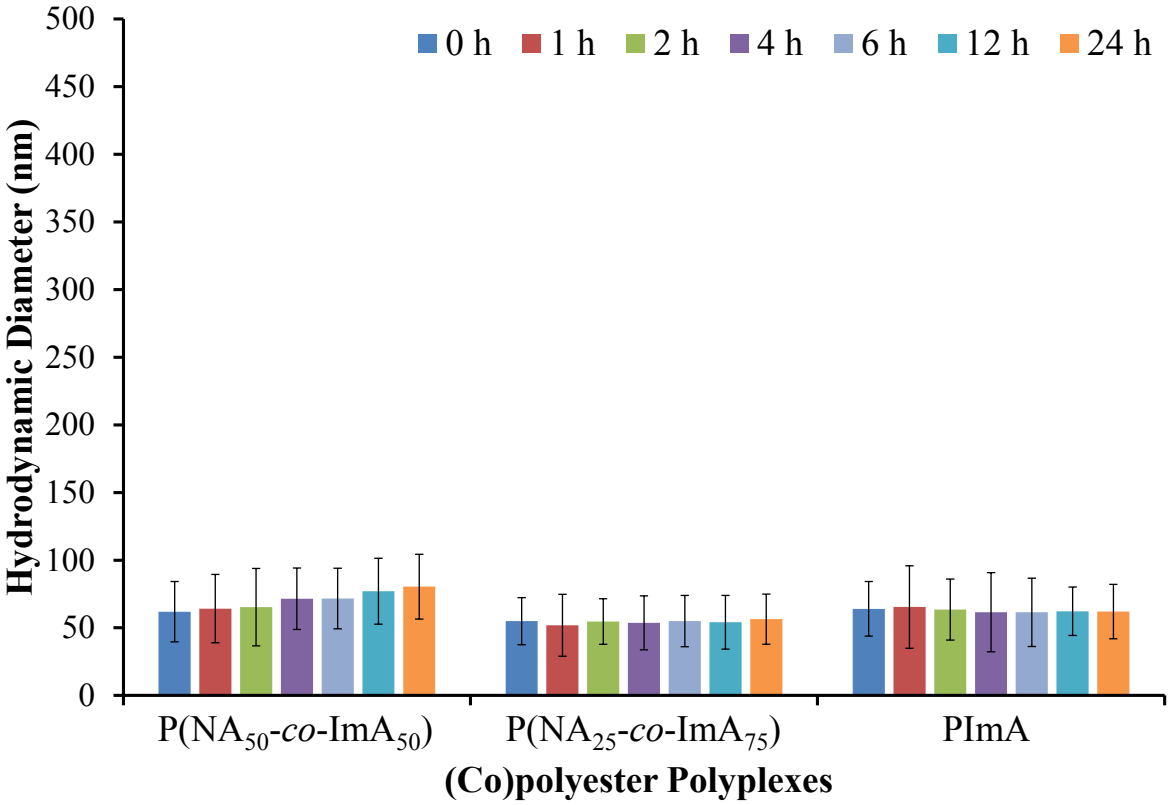

Figure 8.8. Hydrodynamic diameter of polyplexes from dynamic light scattering showing stability over 24 h in water

Cytotoxicity is arguably one of the most important parameters, as successful DNA delivery and release is quickly negated if ultimately cell death occurs. Many reports demonstrated the biocompatible nature of polyesters, however, biocompatibility does not

guarantee negligible cytotoxicity and studies reported (excess) cationic charge decreased cell viability.[6,17,25,59] HeLa cells, a human cervical cancer cell line, treated with polyplexes formed at the indicated N/P ratios for the P(NA_{50}-*co*-ImA_{50}), P(NA_{25}-*co*-ImA_{75}), and PImA polyester vectors displayed insignificant toxicity with respect to control cells over a range of concentrations reaching 200 μg/mL. **Figure 9** displays the results from the CellTiter-Glo® assay. Many samples exceeded 100 % cell viability, indicating cell growth in lieu of polyplex exposure. Although not a direct comparison, the previously described PHEVIM polyplexes containing >25 % ionic content triggered a cytotoxic response in African green monkey COS-7 cells at large N/P ratios (≥20).[17] Acknowledging different protocols and cell lines can drastically affect results; from a structure-property observation the imidazolium-containing copolyesters reinforced the value of a polyester backbone, as even 100 mol % Im charge did not induce cytotoxicity.[26] Zhang and coworkers[57] only reported cytotoxicity measurements of free PV4-Pro, which reduced cell viability to ca. 80 % at concentrations ≥15 μg/mL, consistent with fully charged free-PHEVIM.[17]

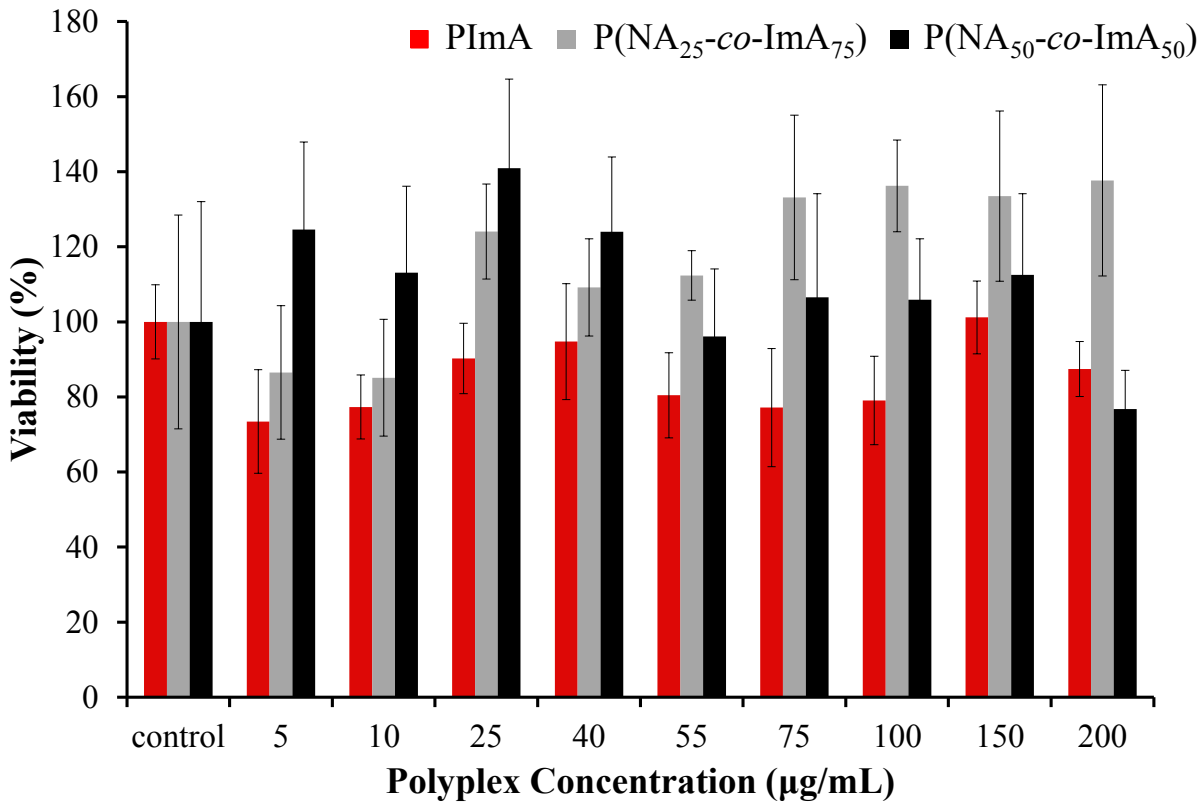

Figure 8.9. Cytotoxicity assay demonstrating insignificant toxicity in HeLa cells and confirming biocompatibility of imidazolium-containing (co)polyesters (error bars are the standard deviation from the average of n=5 samples)

A Luciferase assay determined quantitative transfection efficiency for P(NA_{50}-*co*-ImA_{50}), P(NA_{25}-*co*-ImA_{75}), and PImA compared to untreated control cells and two commercial benchmarks, Jet PEI® and Superfect®. The minimum amount of polyester (lowest N/P ratio) required for full DNA binding, as specified above, formed the respective polyplexes and the experiment proceeded in Opti-MEM. **Figure 10** depicts the transfection results in relative light units (RLU)/mg protein for each polymer vector and control cells. All three imidazolium-containing (co)polyesters successfully transfected with significant improvement, about two orders of magnitude, over untreated control cells. At these specific N/P ratios used the copolymers underperformed compared to industry standards. Continuing the comparison to

vinylimidazole polymers; in serum-containing media only ~0.5 % PV4-Pro transfected at N/P=4 which increased to around 7 % at an N/P=16.[57] These results suggest increasing the N/P ratio providing excess cation would significantly improve transfection efficiency for P(NA_{50}-*co*-ImA_{50}), P(NA_{25}-*co*-ImA_{75}), and PImA. $PEVIM_{25}$ required an N/P=10 before efficient DNA binding and displayed transfection ca. 1.5 orders of magnitude greater than PImA in serum-free media.[17] Increasing the N/P ratio to 25 slightly enhanced transfection to ~10^7 RLU/mg protein yet remained orders of magnitude below Superfect®. The pendant hydroxyl functionality of PHEVIM achieved transfection close to Superfect® (within an order of magnitude) at low N/P ratios in serum-free media, further demonstrating the incredible structural effects and sensitivity of endocytosis and endosomal release.

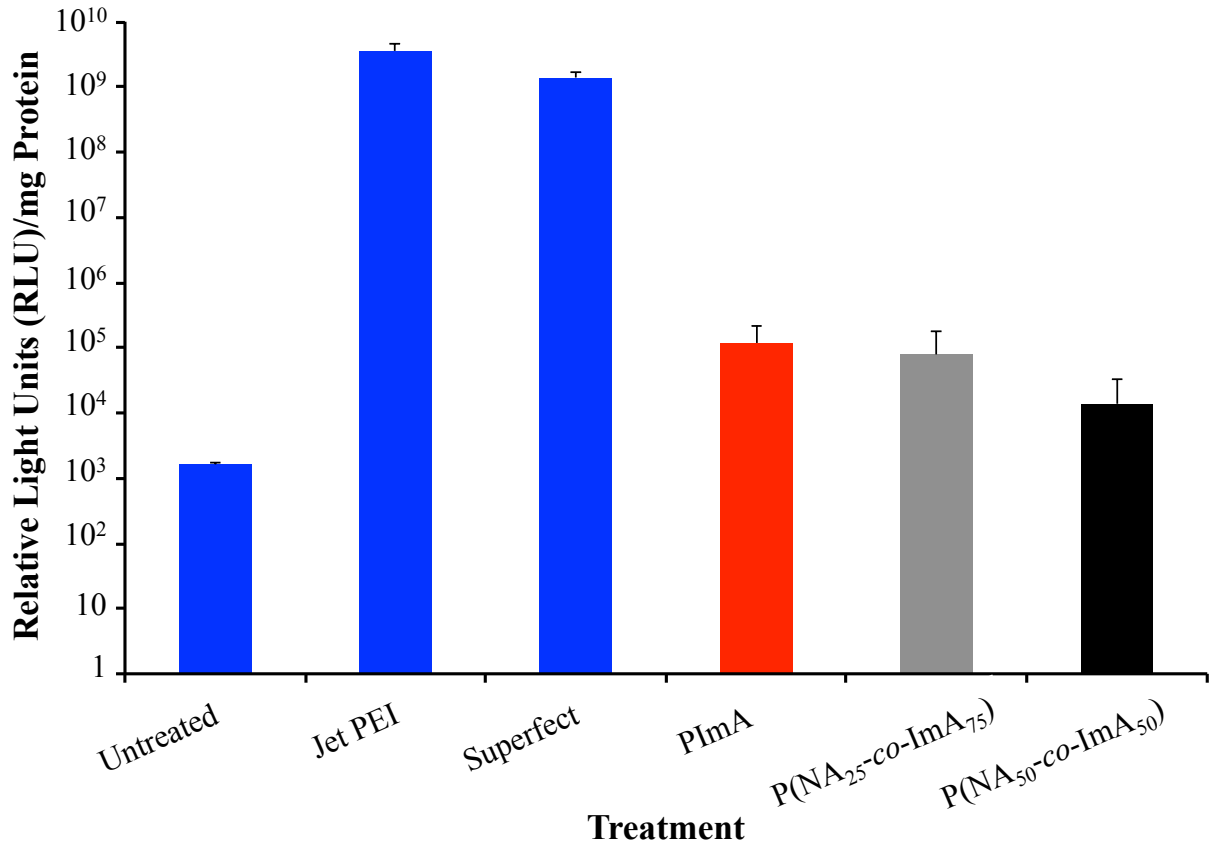

Figure 8.10. Charged polyesters transfected significantly better than controls at low N/P ratios in serum-free media

The transfection results combined with the cytotoxicity assay confirmed the novel melt-stable imidazolium-containing (co)polyesters exhibited potential as non-toxic non-viral gene delivery vectors. With excellent research studies and literature reporting various structure-property relationships in regard to materials and transfection, we propose the following explanations for the observed transfection and potential solutions demonstrating the platform technology these charged copolyesters provide. The core-shell model of polyplex formation suggests excess polycation decorates the polymer/DNA or RNA complex (core), decreasing aggregation, increasing stability, and ultimately improving transfection.[21] Therefore, an N/P ratio in excess of the minimum required for efficient DNA binding would promote the formation

of a stabilized polyplex. The biocompatible nature of the imidazolium-containing (co)polyesters would hopefully allow increased N/P ratios without sacrificing cell viability. Furthermore, block copolymers designed with one block for stabilization and another to bind DNA/RNAs, demonstrated excellent cell viability and transfection on par with Jet PEI.[26] The versatile and facile melt polycondensation synthetic strategy accommodates oligomeric diols affording randomly segmented (co)polyesters.[60,61] Copolymerization of BrMeIm diol with an oligomeric poly(ethylene oxide) (PEO) diol and adipic acid offers a route to obtain imidazolium-containing segmented copolyesters to investigate the influence of a randomly distributed stabilizing "block" along the backbone on polyplex stability and transfection.

It is improbable all endosomal escape occurs through the same mechanism, however, two of the most common theories cited include the proton sponge effect and electrostatic destabilization of the membrane.[25,62-64] Astafieva and coworkers[65] reported delivering Pluronic® P85 alongside poly(4-vinylpyridine-*stat*-*N*-ethyl-4-vinylpyridinium bromide) (PEVP) increased transfection efficiency and reasoned the amphiphilic nature of the Pluronic® block copolymer mimicked the proton sponge effects attributed to PEI's success.[21] As mentioned above, melt polycondensation successfully affords segmented copolyesters using functionalized oligomers, thus a Pluronic® diol offers another route to explore structure-property-transfection relationships. Degradation of the imidazolium copolyesters in the endosome could have introduced buffering capacity and thus invoke the proton sponge hypothesis as a potential explanation for the observed transfection. In the future, copolymerization with a less hydrolytically stable comonomer could further enhance degradation and increase transfection efficiency. Finally, literature showed alkyl spacer length affects transfection efficiency; a butyl alkyl spacer disrupted the endosomal membrane promoting escape and transfection whereas

transfection did not occur with a shorter ethyl alkyl spacer.[25] These results further highlight the significance of the imidazolium-containing (co)polyester transfection with only a methyl group and suggest either a different copolymerization strategy such as the low temperature solution polymerization with an acid chloride to eliminate Hofmann degradation of BrBuIm diol or further monomer derivitization to remove beta-hydrogens.[66]

8.4.4 Electrospinning and Other Potential Applications

The imidazolium ionic group exhibits antimicrobial effects, both as a small molecule salt and when covalently incorporated into materials.[34,67,68] Due to the pendant imidazolium groups, the novel (co)polyesters could function in applications desiring antimicrobial properties such as wound healing bandages.[69,70] To further demonstrate the versatility and potential of the melt-stable imidazolium-containing polyesters for various applications, electrospinning evaluated the fiber forming capabilities of PImA. PImA formed fibers upon blending with high molecular weight PEO, visible in **Figure 11**. Electrospinning is a sensitive technique with many variables requiring optimization some of which include polymer concentration, voltages, and solvent.[71-73] The two scanning electron microscopy (SEM) images, depicted in **Figure 11**, demonstrate the severe influence of parameters and optimization on effective fiber formation. The left image revealed relatively uniform fibers achieved from a 30 wt. % solution of 70:30 PImA:PEO in water. Alternatively, the image on the right shows although fiber size remained relatively uniform, upon increasing to 80 % polyester and raising the overall solution concentration to 32 wt. %, an inconsistent fiber morphology resulted. Finally, the tunable thermal transitions of the imidazolium-containing (co)polyester series and limitless comonomers for future material development provides opportunities for an array of structure-property-morphology relationships

as well as emerging applications including but not limited to pressure-sensitive adhesives, biocompatible and biodegradable membranes, and ion-conducting polymers.

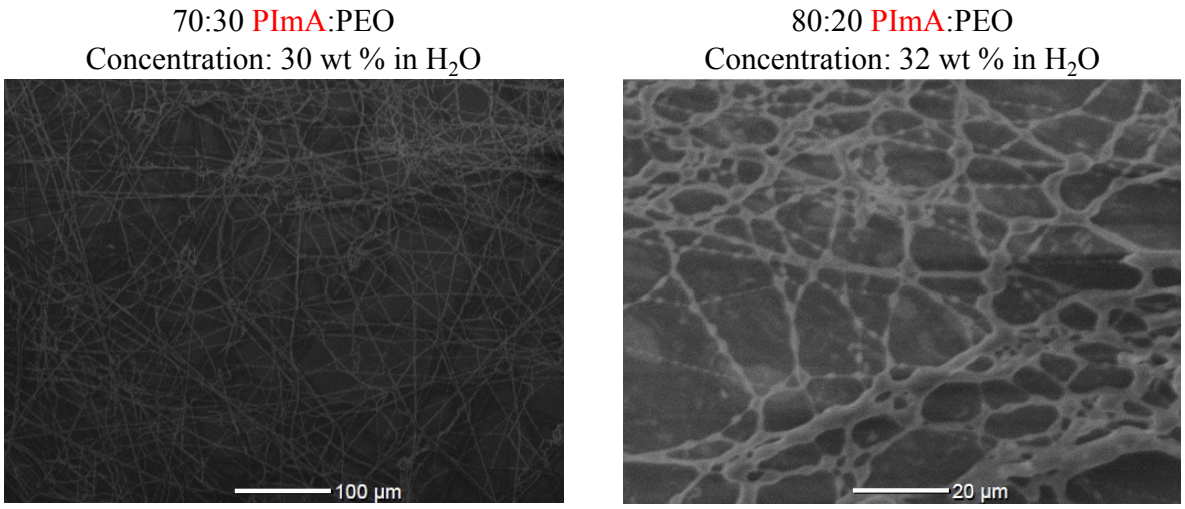

Figure 8.11. SEM images of electrospun fibers from blends of PImA and 300,000 g/mol poly(ethylene oxide) for potential antimicrobial and adhesive applications. 18 mm collector distance, left: +/-15 kV, right: +10 kV –15 kV

8.5 *Conclusions*

In this manuscript we described the synthesis, characterization, and non-viral gene delivery potential of a novel series of imidazolium-containing (co)polyesters. Melt polycondensation of BrMeIm diol with NPG and AA comonomers provided thermally stable amorphous (co)polyesters with T_g's ranging from -41 °C to 40 °C. A newly synthesized BrBuIm diol unfortunately succumbed to Hofmann elimination, rendering melt polymerization insufficient. ^{1}H NMR confirmed polyester structure and exhibited unique splitting attributed to tacticity. Water dispersibility prevailed above 15 mol % ionic content (31 wt. %) and initiated the evaluation of readily soluble P(NA_{50}-*co*-ImA_{50}), P(NA_{25}-*co*-ImA_{75}), and PImA as potential non-viral gene delivery vectors. Gel electrophoresis identified minimum N/P ratios of 4 for

P(NA_{50}-*co*-ImA_{50}) and P(NA_{25}-*co*-ImA_{75}) and 5 for PImA completely bound DNA. A cytotoxicity assay elucidated the expected biocompatible nature of the linear (co)polyesters revealing insignificant polyplex cytotoxicity at all concentrations assessed. A Luciferase transfection assay produced encouraging results as P(NA_{50}-*co*-ImA_{50}), P(NA_{25}-*co*-ImA_{75}), and PImA transfected significantly better than untreated control cells. A discussion offered a plethora of ideas with respect to improving the material design of these novel systems to increase transfection efficiency in hopes of competing with the current industry standards, including segmented copolyesters and ideal N/P ratio evaluations. Additionally, electrospinning with PEO yielded imidazolium-containing polyester-based fibers for antimicrobial and adhesive applications. This report successfully describes the first evaluation of imidazolium-containing polyesters as potential non-viral gene delivery vectors with promise for future material advancement.

8.6 *Acknowledgements*

This work was supported in part by the U.S. Army Research Laboratory and the U.S. Army Research Office under the Army Materials Center of Excellence Program, contract W911NF-06-2-0014. The authors would also like to thank Virginia Tech's Institute for Critical Technology and Applied Sciences (ICTAS) for laboratory space promoting interdisciplinary research and Chainika Jangu for setting up a TGA-SA experiment.

8.7 *References*

(1) Turner, S. R.; King, B.; Ponasik, J.; Adams, V.; Connell, G. *High Perform. Polym.* **2005**, *17*, 361.
(2) Ozturk, G. I.; Pasquale, A. J.; Long, T. E. *J. Adhes.* **2010**, *86*, 395.
(3) Scheirs, J.; Long, T. E. *Modern Polyesters: Chemistry and Technology of Polyesters and Copolyesters*; Wiley, 2005.
(4) Zhang, X.-Q.; Tang, H.; Hoshi, R.; De Laporte, L.; Qiu, H.; Xu, X.; Shea, L. D.; Ameer, G. A. *Biomaterials* **2009**, *30*, 2632.
(5) Lim, Y.-B.; Han, S.-O.; Kong, H.-U.; Lee, Y.; Park, J.-S.; Jeong, B.; Kim, S. *Pharm Res* **2000**, *17*, 811.
(6) Cameron, D. J. A.; Shaver, M. P. *Chemical Society Reviews* **2011**, *40*, 1761.
(7) Fakirov, S. *Biodegradable Polyesters*; Wiley, 2015.
(8) Rogers, M. E.; Long, T. E. *Synthetic methods in step-growth polymers*; Wiley-Interscience: Hoboken, N.J., 2003.
(9) Susan, M. A. B. H.; Kaneko, T.; Noda, A.; Watanabe, M. *Journal of the American Chemical Society* **2005**, *127*, 4976.
(10) Wang, F.; Hickner, M.; Kim, Y. S.; Zawodzinski, T. A.; McGrath, J. E. *Journal of Membrane Science* **2002**, *197*, 231.
(11) Gour, N.; Ngo, K. X.; Vebert-Nardin, C. *Macromolecular Materials and Engineering* **2013**, doi: 10.1002/mame.201300285.
(12) Heath, W. H.; Senyurt, A. F.; Layman, J.; Long, T. E. *Macromolecular Chemistry and Physics* **2007**, *208*, 1243.
(13) Nelson, A. M.; Long, T. E. *Macromolecular Chemistry and Physics* **2014**, *215*, 2161.
(14) Eisenberg, A. K. M. *Ion-containing polymers : physical properties and structure*; Academic Press: New York, 1977.
(15) Gao, R.; Zhang, M.; Dixit, N.; Moore, R. B.; Long, T. E. *Polymer* **2012**, *53*, 1203.
(16) Zhang, M.; Zhang, M.; Moore, R. B.; Long, T. E. *Polymer* **2013**, *54*, 3521.
(17) Allen, M. H.; Green, M. D.; Getaneh, H. K.; Miller, K. M.; Long, T. E. *Biomacromolecules* **2011**, *12*, 2243.
(18) Tudryn, G. J.; Liu, W.; Wang, S.-W.; Colby, R. H. *Macromolecules* **2011**, *44*, 3572.
(19) Bednarek, M.; Basko, M.; Biedroń, T.; Kubisa, P.; Pluta, M. *Polym. Bull.* **2014**, *71*, 1891.
(20) Choi, U. H.; Mittal, A.; Price Jr, T. L.; Lee, M.; Gibson, H. W.; Runt, J.; Colby, R. H. *Electrochimica Acta* **2015**.
(21) Kabanov, A. V.; Felgner, P. L.; Seymour, L. W. *Self-Assembling Complexes for Gene Delivery: From Laboratory to Clinical Trial*; Wiley, 1998.
(22) Li, Z.; Huang, L. *Journal of Controlled Release* **2004**, *98*, 437.
(23) Mintzer, M. A.; Simanek, E. E. *Chemical Reviews* **2009**, *109*, 259.
(24) Green, J. J.; Langer, R.; Anderson, D. G. *Accounts of Chemical Research* **2008**, *41*, 749.
(25) Hemp, S. T.; Allen, M. H.; Green, M. D.; Long, T. E. *Biomacromolecules* **2012**, *13*, 231.
(26) Hemp, S. T.; Smith, A. E.; Bryson, J. M.; Allen, M. H.; Long, T. E. *Biomacromolecules* **2012**, *13*, 2439.
(27) Reul, R.; Nguyen, J.; Biela, A.; Marxer, E.; Bakowsky, U.; Klebe, G.; Kissel, T. *International Journal of Pharmaceutics* **2012**, *436*, 97.
(28) Panyam, J.; Labhasetwar, V. *Advanced Drug Delivery Reviews* **2003**, *55*, 329.
(29) Ravi Kumar, M. N. V.; Bakowsky, U.; Lehr, C. M. *Biomaterials* **2004**, *25*, 1771.
(30) Vila, A.; Sánchez, A.; Tobío, M.; Calvo, P.; Alonso, M. J. *Journal of Controlled Release* **2002**, *78*, 15.
(31) Park, J. S.; Choi, Y. H.; Kim, S. W.; Google Patents: 2001.
(32) Xu, P.; Li, S.-Y.; Li, Q.; Ren, J.; Van Kirk, E. A.; Murdoch, W. J.; Radosz, M.; Shen, Y. *Biotechnology and Bioengineering* **2006**, *95*, 893.
(33) Hofmann, K. *The Chemistry of Heterocyclic Compounds, Imidazole and Its Derivatives*; Wiley, 2009.
(34) Anderson, E. B.; Long, T. E. *Polymer* **2010**, *51*, 2447.
(35) Ranke, J.; Stolte, S.; Störmann, R.; Arning, J.; Jastorff, B. *Chemical Reviews* **2007**, *107*, 2183.
(36) Mincheva, R.; Meyer, F.; Verge, P.; Raquez, J.-M.; Billiet, L.; Du Prez, F.; Dubois, P. *Macromolecular Rapid Communications* **2011**, *32*, 1960.
(37) Lee, M.; Choi, U. H.; Salas-de la Cruz, D.; Mittal, A.; Winey, K. I.; Colby, R. H.; Gibson, H. W. *Advanced Functional Materials* **2011**, *21*, 708.

(38) Mindemark, J.; Bowden, T. *Polymer* **2011**, *52*, 5716.
(39) Kang, H.; Lin, Q.; Armentrout, R. S.; Long, T. E. *Macromolecules* **2002**, *35*, 8738.
(40) Whittington, C. P.; Daily, L. A.; Miller, K. M. *Polymer* **2014**, *55*, 3320.
(41) Zhang, M.; Hemp, S. T.; Zhang, M.; Allen, M. H.; Carmean, R. N.; Moore, R. B.; Long, T. E. *Polymer Chemistry* **2014**, *5*, 3795.
(42) Armand, M.; Endres, F.; MacFarlane, D. R.; Ohno, H.; Scrosati, B. *Nat Mater* **2009**, *8*, 621.
(43) Moad, G.; Groth, A.; O'Shea, M. S.; Rosalie, J.; Tozer, R. D.; Peeters, G. *Macromolecular Symposia* **2003**, *202*, 37.
(44) Moon, S.-I.; Taniguchi, I.; Miyamoto, M.; Kimura, Y.; Lee, C.-W. *High Performance Polymers* **2001**, *13*, S189.
(45) Odian, G. *Principles of Polymerization, Fourth Edition*; John Wiley & Sons, Inc.: Hoboken, NJ, 2004.
(46) Dullius, J. E. L.; Suarez, P. A. Z.; Einloft, S.; de Souza, R. F.; Dupont, J.; Fischer, J.; De Cian, A. *Organometallics* **1998**, *17*, 815.
(47) Hemp, S. T.; Zhang, M.; Allen, M. H.; Cheng, S.; Moore, R. B.; Long, T. E. *Macromolecular Chemistry and Physics* **2013**, *214*, 2099.
(48) Scammells, P. J.; Scott, J. L.; Singer, R. D. *Australian Journal of Chemistry* **2005**, *58*, 155.
(49) Bruice, P. Y. *Organic Chemistry*; 7th ed.; Pearson Education, Inc: Upper Saddle River, NJ, 2014.
(50) Dragan, E. S. *New Trends in Ionic (Co)polymers and Hybrids*; Nova Science Publishers, 2007.
(51) Lee, S. K.; Kim, B. K. *J. Colloid Interface Sci.* **2009**, *336*, 208.
(52) Rahman, M. M.; Kim, H.-D. *Journal of Applied Polymer Science* **2006**, *102*, 5684.
(53) Zhang, Y.; Chen, L.; Zhao, J.-J.; Chen, H.-B.; He, M.-X.; Ni, Y.-P.; Zhai, J.-Q.; Wang, X.-L.; Wang, Y.-Z. *Polymer Chemistry* **2014**, *5*, 1982.
(54) Ge, X.-G.; Wang, C.; Hu, Z.; Xiang, X.; Wang, J.-S.; Wang, D.-Y.; Liu, C.-P.; Wang, Y.-Z. *Journal of Polymer Science Part A: Polymer Chemistry* **2008**, *46*, 2994.
(55) Wunderlich, B. *Thermal Analysis of Polymeric Materials*; Springer, 2005.
(56) Hiemenz, P. C.; Lodge, T. P. *Polymer Chemistry, Second Edition*; CRC Press, 2007.
(57) Zhang, Y.; Chen, X.; Lan, J.; You, J.; Chen, L. *Chemical Biology & Drug Design* **2009**, *74*, 282.
(58) Gebhart, C. L.; Kabanov, A. V. *Journal of Controlled Release* **2001**, *73*, 401.
(59) Ikada, Y.; Tsuji, H. *Macromolecular Rapid Communications* **2000**, *21*, 117.
(60) Pepic, D.; Zagar, E.; Zigon, M.; Krzan, A.; Kunaver, M.; Djonlagic, J. *European Polymer Journal* **2008**, *44*, 904.
(61) Takahashi, T.; Nagata, F. *Journal of Macromolecular Science, Part B* **1991**, *30*, 25.
(62) Akinc, A.; Thomas, M.; Klibanov, A. M.; Langer, R. *The Journal of Gene Medicine* **2005**, *7*, 657.
(63) Behr, J.-P. *CHIMIA International Journal for Chemistry* **1997**, *51*, 34.
(64) Xu, Y.; Szoka, F. C. *Biochemistry* **1996**, *35*, 5616.
(65) Astafieva, I.; Maksimova, I.; Lukanidin, E.; Alakhov, V.; Kabanov, A. *FEBS Letters* **1996**, *389*, 278.
(66) Cheremisinoff, N. P. *Handbook of Polymer Science and Technology*; Taylor & Francis, 1989.
(67) Colonna, M.; Berti, C.; Binassi, E.; Fiorini, M.; Sullalti, S.; Acquasanta, F.; Vannini, M.; Di Gioia, D.; Aloisio, I.; Karanam, S.; Brunelle, D. J. *Reactive and Functional Polymers* **2012**, *72*, 133.
(68) Nigmatullin, R.; Gao, F. *Macromolecular Materials and Engineering* **2012**, *297*, 1038.
(69) Dai, T.; Tanaka, M.; Huang, Y.-Y.; Hamblin, M. R. *Expert Review of Anti-infective Therapy* **2011**, *9*, 857.
(70) Zahedi, P.; Rezaeian, I.; Ranaei-Siadat, S.-O.; Jafari, S.-H.; Supaphol, P. *Polymers for Advanced Technologies* **2010**, *21*, 77.
(71) Gupta, P.; Elkins, C.; Long, T. E.; Wilkes, G. L. *Polymer* **2005**, *46*, 4799.
(72) McKee, M. G.; Hunley, M. T.; Layman, J. M.; Long, T. E. *Macromolecules* **2006**, *39*, 575.
(73) McKee, M. G.; Layman, J. M.; Cashion, M. P.; Long, T. E. *Science* **2006**, *311*, 353.

8.8 *Supporting Information*

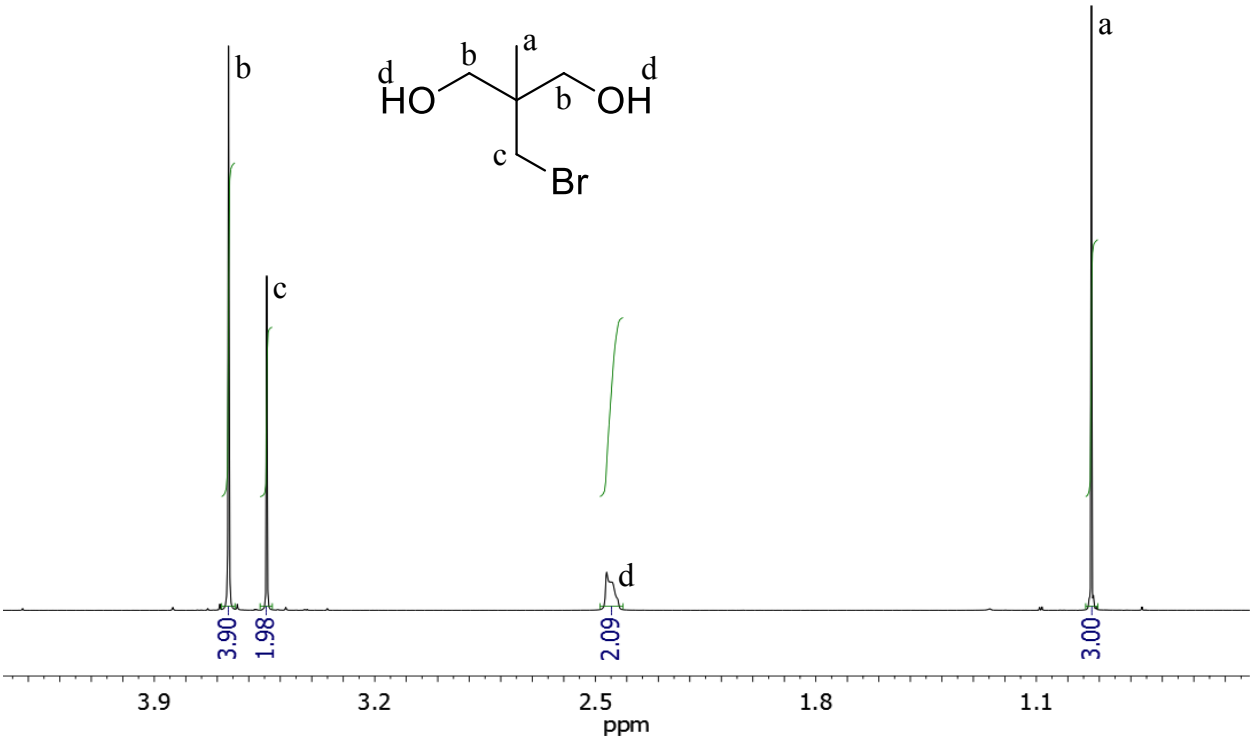

Figure 8.12. ^{1}H NMR spectroscopy confirms structure of bromo-containing intermediate diol

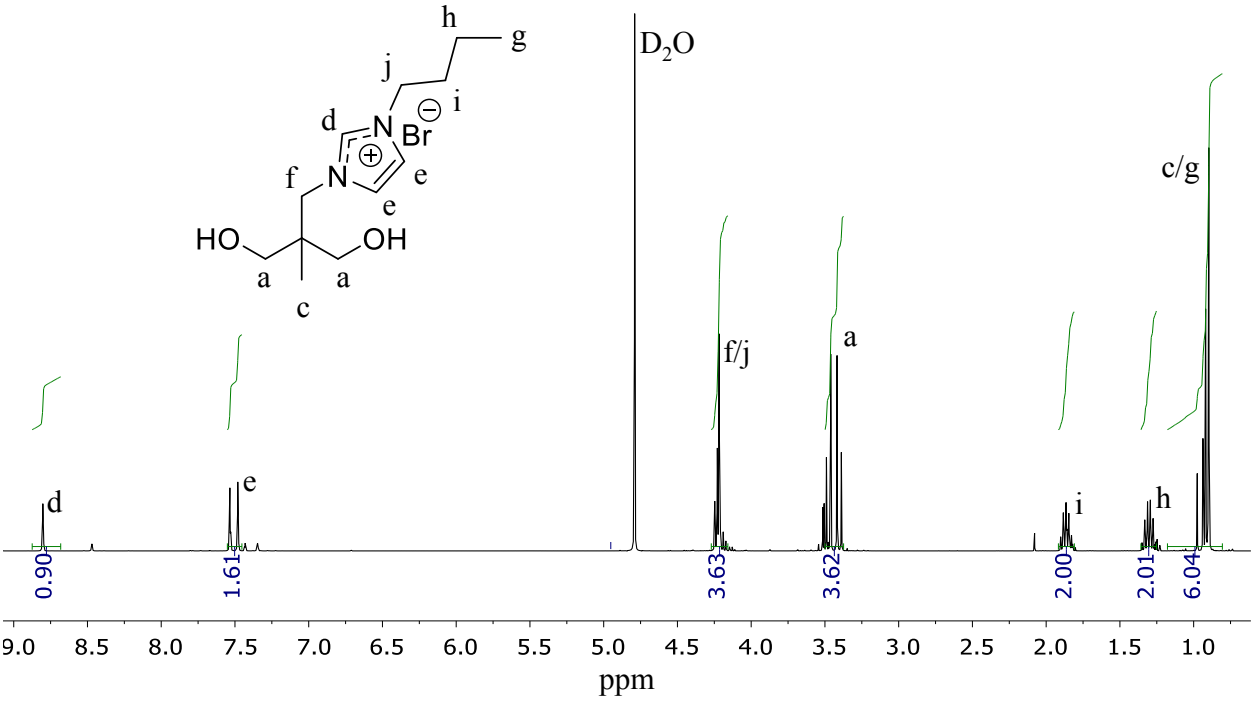

Figure 8.13. ^{1}H NMR spectroscopy confirms structure of novel bromobutyl imidazolium diol

Chapter 9: Overall Conclusions

Step-growth polymerization and the design of novel functional monomers enabled the synthesis of polyesters for electronic, aerospace, and biological applications. Fundamental structure-property-morphology relationships remained at the forefront and afforded tunable properties resulting from a thorough understanding of systematic evaluations. Familiarity with current literature guided projects for impactful, relevant, research including topics such as the incorporation of renewable resources, novel ion-containing monomers, and the synthesis of high-performance bisphenol-A (BPA) free polymeric materials.

A series of liquid crystalline copolyesters containing SDE exhibited promising thermomechanical, rheological, and tensile properties for use as electronic encasings that would ideally photocrosslink upon UV exposure and enhance mechanical properties over the lifetime of a product. These copolymers could potentially overcome limitations of current commercial electronic encasings plagued with degradative, property sacrificing, side-reactions in harsh UV environments. Additionally, the incorporation of a flexible soft segment into high-performance liquid crystalline copolyesters resulted to impart potential elasticity and investigate fundamental structure-property-morphology relationships. 4,4'-biphenyl dicarboxylate (BDE) functioned as the mesogen and polyether polyols, notably a blocky Pluronic® oligoether which resulted in novel segmented copolyester compositions, constructed the flexible segment. Differential scanning calorimetry and X-ray scattering confirmed microphase-separated morphologies and a liquid crystalline morphology remained even with 65 weight % soft segment. The aliphatic-containing hard segment dictated the thermal properties and a doubling of the tensile strain at break, up to about 8 % with 50 weight % soft segment, occurred. The range of thermal,

thermomechanical, and tensile properties combined with proposed UV stability made both the segmented and non-segmented high-performance liquid crystalline (co)polyesters of interest to the aerospace industry.

The design of novel step-growth monomers and polyesters for biological applications centered around the transformation of a plant-based fatty acid into an AB monomer and a diol containing pendant imidazolium functionality. Hydration of methyl 9-decenoate (9-DAME), a plant-derived fatty acid gifted from Elevance Renewable Sciences Inc., achieved an isomeric mixture of AB monomers. Melt polycondensation afforded amorphous aliphatic polyesters with a glass transition temperature (T_g) equal to -60 °C, the same as commercially prevalent poly(ε-caprolactone). These low-T_g polyesters offer sustainability and degradability for applications ranging from sutures to elastomers. Demonstrating the versatility of 9-DAME, epoxidation and hydrolysis of the alkene produced an ABB' monomer that gelled upon self-condensation and could function as a degradable bio-based branching and/or crosslinking agent for polyesters and polyurethanes.

Synthesis and polycondensation of a bromomethyl imidazolium diol with adipic acid generated water dispersible melt-stable (co)polyesters. Precedence for successful nucleic acid delivery with imidazolium-containing chain-growth polymers instigated gel binding and cytotoxicity studies of the novel (co)polyesters. Polyesters containing 50, 75, and 100 mol % ionic content bound deoxyribonucleic acid (DNA) at low charge ratios and the resulting polyplexes did not induce cytotoxic affects. A quantitative transfection assay displayed successful delivery and release of the nucleic acid to human cervical cancer cells (HeLa), with room for improvement to reach the current industry standard, poly(ethyleneimine). These

copolyesters also electrospun into fibers when blended with poly(ethylene oxide) and provided tunable T_gs, -41 ° to 40 °C, increasing with increasing ionic content.

Finally, continuing the use of renewable resources, a two-step monomer synthesis afforded a novel caffeine-containing methacrylate (CMA). Free radical copolymerization with 2-ethylhexyl methacrylate (EHMA) generated the first polymeric materials to contain covalently bound caffeine. High molecular weight, film-forming, amorphous copolymers permitted thermomechanical and rheological analysis. Caffeine increased the modulus of the copolyesters, even at low mol % incorporation, to the extent that at 13 mol % CMA the prepared film was too glassy to withstand thermomechanical testing; markedly different from low T_g poly(EHMA).

In summary, a fundamental, systematic approach to the design of polymers encouraged exploring and evaluating results for a wide-range of applications; constantly catalyzing new ideas and research directions for further development and impact.

Chapter 10: Suggested Future Work

10.1 *Segmented Liquid Crystalline Copolyesters*

Combining a couple of the topics explored throughout this dissertation, **Scheme 1** depicts a synthetic route to obtain ion-containing segmented liquid crystalline copolyesters. Melt transesterification of commercially available dimethyl 5-sulfoisophthalate sodium salt with varying ratios of oligomeric polyol (poly(tetramethylene oxide) is depicted and other oligomers such as Pluronics® could substitute) and methylene diol would readily achieve either ionomers (> 15 mol % ionic content) or charged segmented copolyesters. This polymerization would produce 4 different repeating units and instigate studies to understand which segment, hard or soft, the ionic group preferentially resides. Additionally, a systematic study on the effect of ionic content on the liquid crystalline morphology and other material properties, as well as the influence of methylene spacer length and structure would provide an understanding of structure-property-morphology relationships. The ionic content could result in segmented liquid crystalline copolyesters which swell in water or self-assemble more readily due to electrostatic interactions. Qin Lin's previous work on non-segmented ion-containing liquid crystalline copolyesters would provide good comparisons of polyester properties and the impact of incorporating the soft segment.[1] The synthetic scheme suggests the addition of sodium acetate (NaOAc) as described in Kang et al.[2]

Scheme 10.1. Synthesis of ion-containing segmented liquid crystalline copolyesters

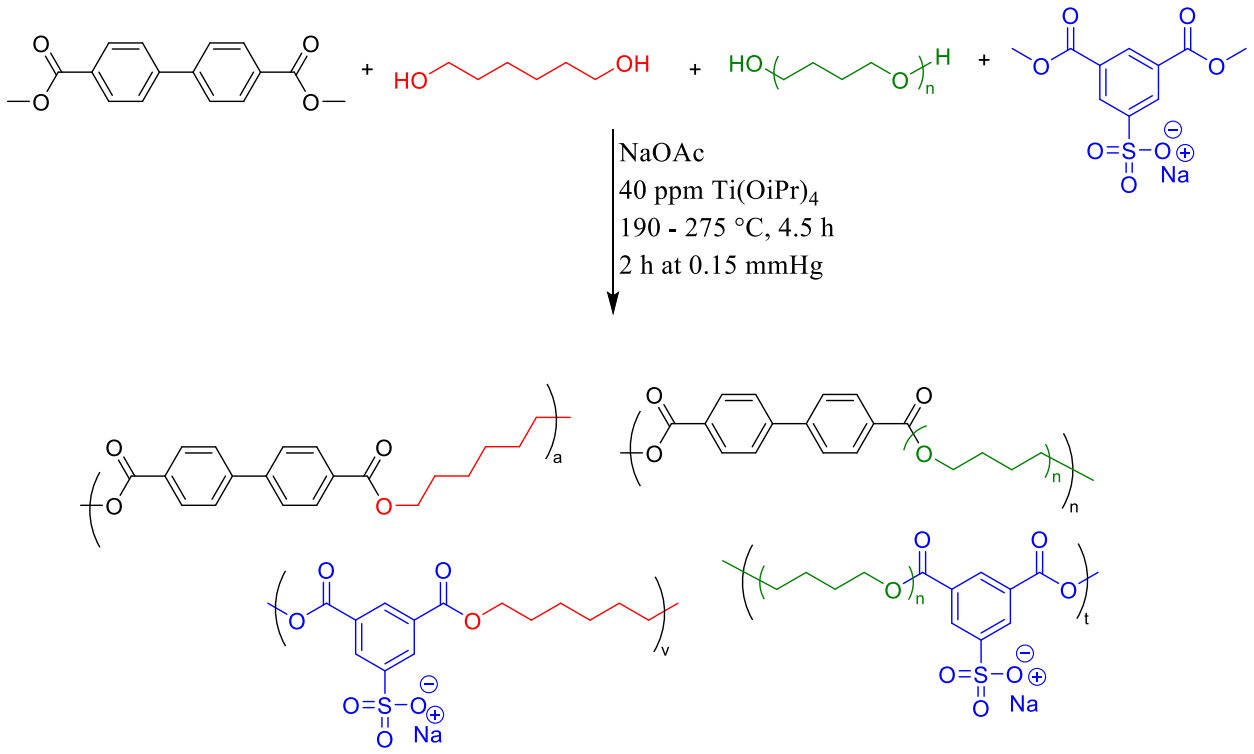

Continuing the exploration and modification of segmented liquid crystalline copolyesters, **Scheme 2** shows a route to obtain branched segmented liquid crystalline copolyesters. The trifunctional oligomer, glycerol propoxylate (M_n ~1500 g/mol), commercially available from Sigma Aldrich, serves as the branching agent. Structure-property relationships of interest include the effect of branching agent on maintaining a liquid crystalline morphology and the influence on the thermal transitions. Additionally, synthesizing branched copolyesters could help improve the solubility of these often insoluble materials while preserving the desirable properties of liquid crystalline copolyesters such as high melting transitions and shear thinning to ease processability. **Figure 1** shows another commercially available trifunctional diblock polyol, glycerol propoxylate-*block*-ethoxylate (M_n ~4000 g/mol), to further probe the influence of the

soft segment structure on resulting material properties as discussed on similar linear segmented liquid crystalline copolyesters in **Chapter 4**.

Scheme 10.2. Copolymerizing with a trifunctional polyol to obtain branched segmented liquid crystalline copolyesters

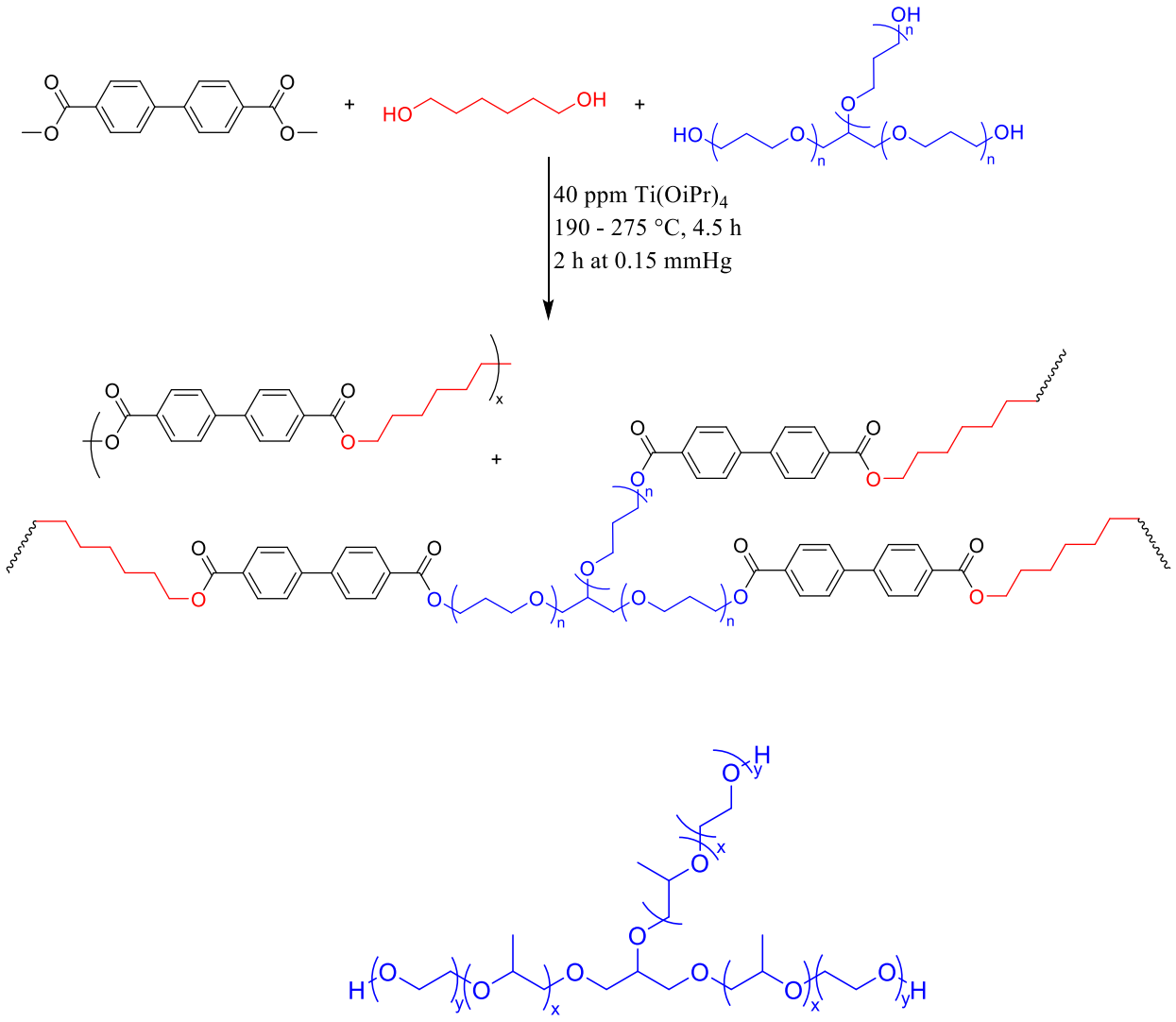

Figure 10.1. Commercially available trifunctional diblock polyether

10.2 *Incorporating Caffeine into Polyesters*

The caffeine-containing methacrylate copolymers synthesized and characterized in **Chapter 5** did not display any evidence of pi-pi stacking or a microphase-separated morphology.

We hypothesized the proximity of caffeine to the polymer backbone prevented any self-assembly via non-covalent interactions. **Scheme 3** reveals a synthetic route to synthesize caffeine endcapped polyesters. Offsetting stoichiometry would allow the monofunctional commercially available caffeine derivative, theophylline-7-acetic acid, to endcap polyesters. To facilitate molecular motion and promote caffeine group association flexible comonomers, such as diethylene glycol and adipic acid, would afford a material with a low glass transition temperature (T_g). Initial experiments include investigating the ability of the caffeine endgroups to self-assemble and characterizing the resulting morphologies using X-ray scattering and microscopy. Varying polyester molecular weight and structure and determining the effect on caffeine association would elucidate structure-property-morphology relationships for designing functional materials. Exploring if the pi-pi stacking of caffeine endgroups could result in a supramolecular polymer, similar to protein assembly, would broaden the scope of the project. Potential bio-relevance as a result of inherent receptor binding could also be of interest. **Scheme 4** displays the synthesis of a caffeine containing diol using the caffeine photoreaction described in **Chapter 5** and the bromomethyl diol from **Chapter 8** to further expand the library of caffeine-containing monomers. Melt polymerization of the caffeine diol could overcome the solubility challenges from **Chapter 5**, potentially achieving (co)polyesters with high caffeine content and further examining the capability of the pendant caffeine to associate.

Scheme 10.3. Proposed synthesis of caffeine endcapped oligoesters

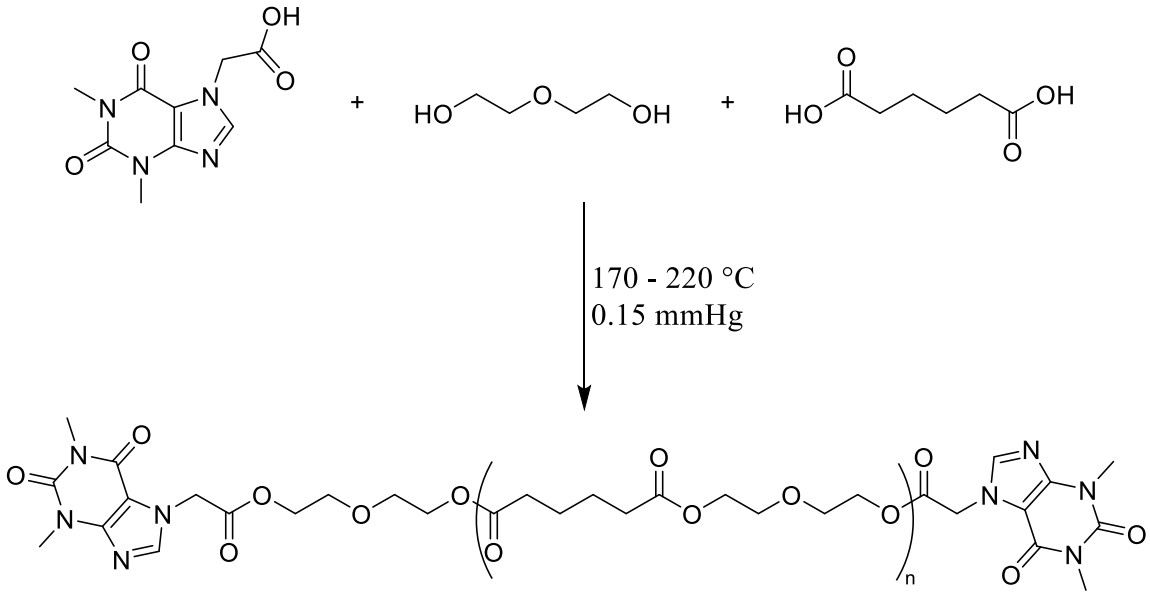

Scheme 10.4. Substitution reaction to generate a caffeine diol

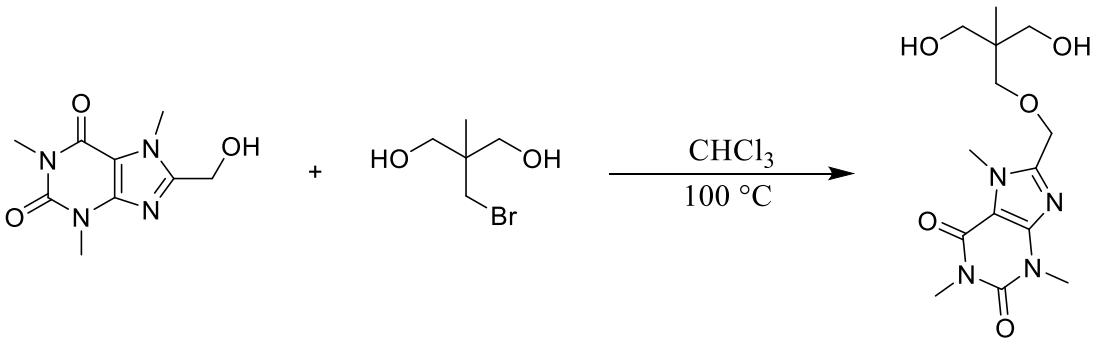

10.3 *Novel Step Growth Monomers*

Hedrick and coworkers devised a versatile synthetic strategy for the synthesis of ester and amide functionalized carbonates for ring-opening polymerization (ROP).[3, 4] The cyclic carbonate, depicted in **Scheme 5**, contains an X and R group where X = nitrogen or oxygen and R can accommodate many pendant groups, with a previous step requiring RXH. Utilizing the readily reactive 6-membered cyclic carbonate, **Scheme 5** proposes a room temperature (RT) reaction with a diamine to afford hydroxyurethane diester or hydroxyurethane diamide step-

growth monomers with functionality of 4 (f=4) for use as additives, branching agents, and/or crosslinking agents. Previous research groups published the synthesis of sulfonated dimethyl fumarate (step 1 in **Scheme 6**).[5, 6] Furthermore, current unpublished work from Chainika Jangu, a fellow colleague in the Long research group, demonstrated the success of steps 2 and 3 in **Scheme 6** on sodium 4-vinylbenzenesulfonate. Adopting these same strategies with the melt-stable diester, dimethyl fumarate, enables the synthesis of a diester with a pendant trifluorosulfonimide group. Alkylation of the nitrogen generates an ion-containing monomer for use in the synthesis of conductive polyesters.

Scheme 10.5. Ring-opening functionalized cyclic carbonates to obtain multifunctional monomers

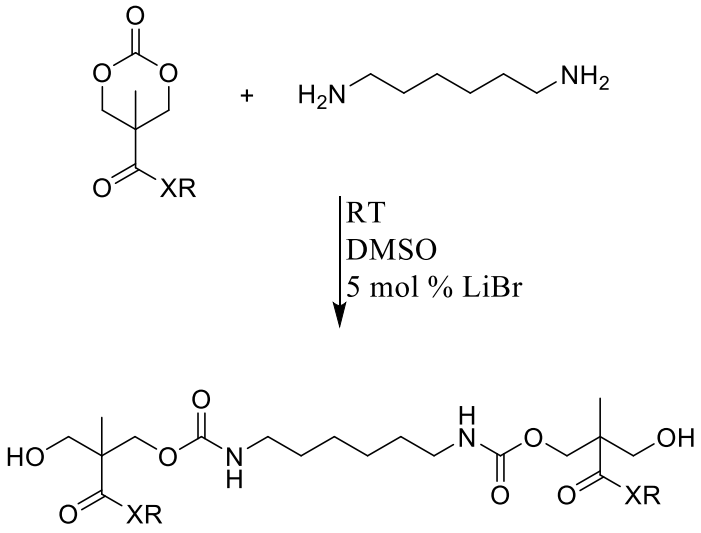

Scheme 10.6. 3-step synthesis to a trifluorosulfonimide-containing diester

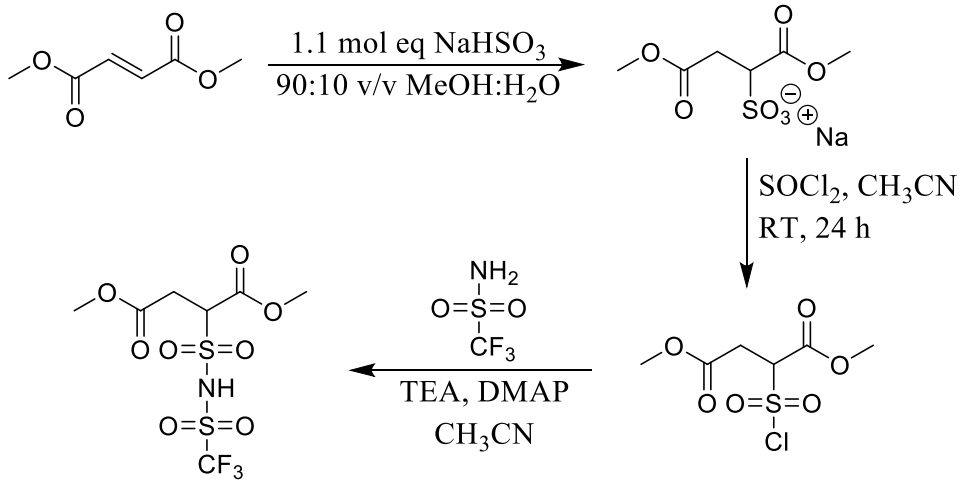

10.4 *Further Improving the Impact and Breadth of the Imidazolium Diol*

Chapter 8 provides an in-depth discussion of possible synthetic strategies to improve the imidazolium-containing copolyesters as non-viral gene delivery vehicles. One strategy was to mimic previously designed chain growth systems which integrated a stabilization block.[7] **Scheme 7** exhibits the synthesis of segmented imidazolium-containing copolyesters. Although still a random copolyester, water soluble poly(ethylene glycol) (PEG) would ideally perform as a stabilization block, decorating the outside of the polyplex and preventing aggregation in serum-containing and serum-free media.[7] Improved stability would hopefully enhance transfection through more polyplexes undergoing successful endocytosis and the stabilization block could also help rupture the endosome for improved release of the nucleic acid. A Pluronic® oligoether could also substitute as the soft segment, or stabilization block, and possibly invoke the reported buffering effect similar to poly(ethylene imine) (PEI).[8, 9] Following a synthetic procedure from Zhang et al.[10] and substituting in the bromomethyl imidazolium diol, **Scheme 8** shows the strategy for obtaining water dispersible polyurethanes with the imidazolium pendant group.

Evaluation of the ion-containing polyurethanes as potential non-viral gene delivery vectors and other applications such as polymer electrolytes could ensue.[11]

Scheme 10.7. Synthesis of segmented imidazolium-containing copolyesters for improved transfection

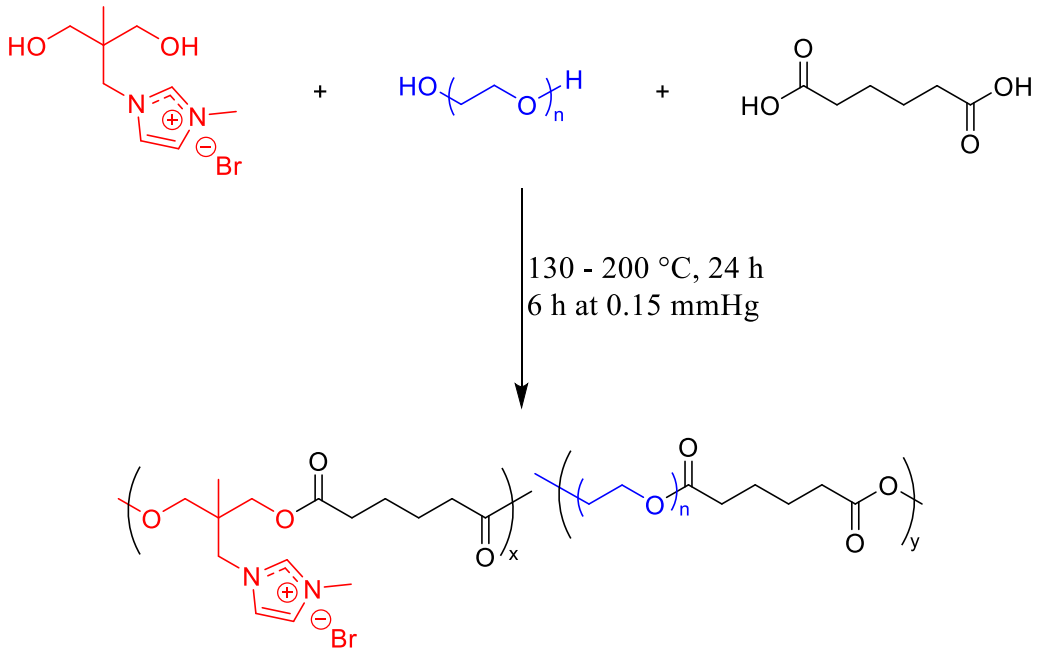

Scheme 10.8. Polyurethanes containing pendant imidazolium groups

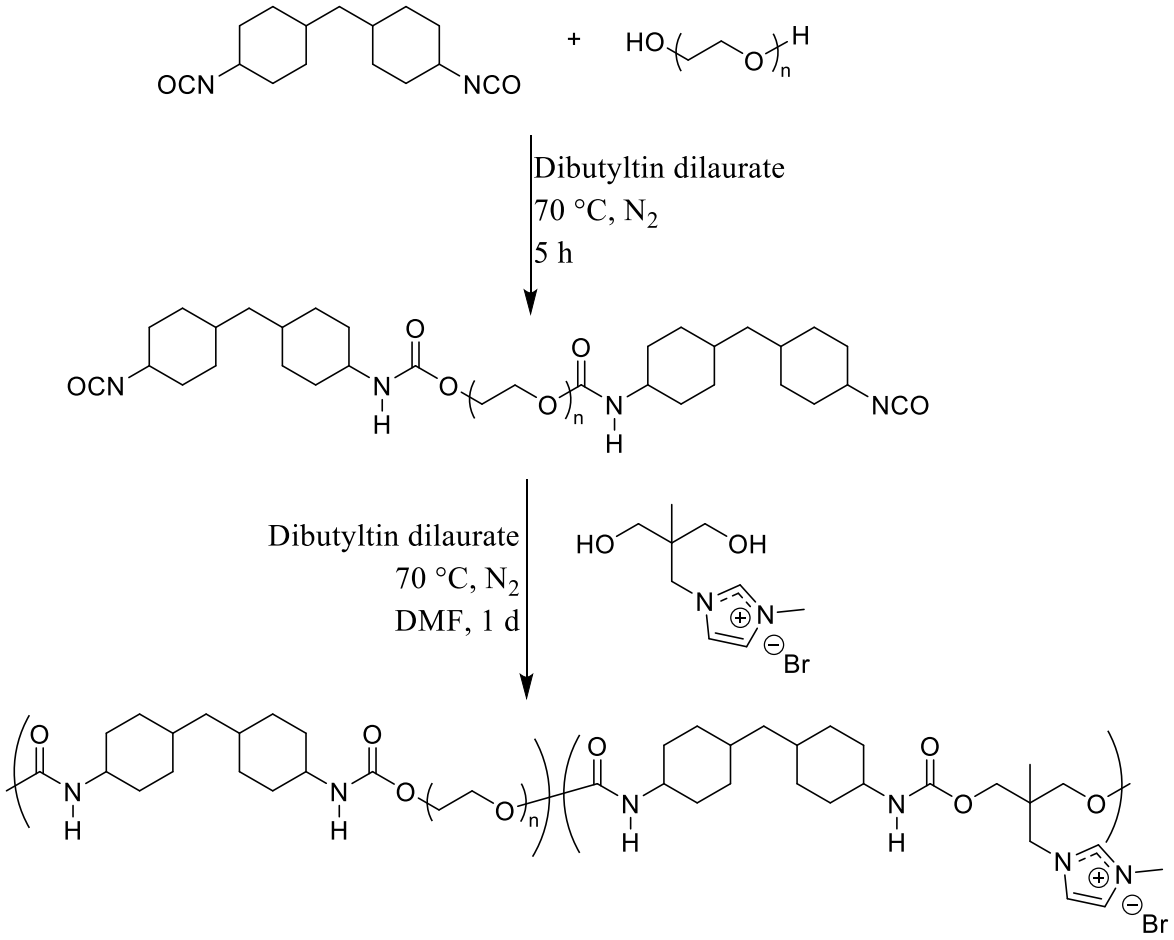

10.5 *Photocrosslinkable Polyesters and Monomers for Additive Manufacturing*

Our research group has recently taken an interest in additive manufacturing, specifically printing using microstereolithography.[12] Copolymerization of the previously mentioned sulfonated dimethyl fumarate with dimethyl fumarate and a diol could afford polyesters with photocrosslinkable sites throughout the backbone.[13] Changing the diol comonomer is a facile approach to influence material properties of both the low molecular weight oligomer and resulting manufactured part. Photoactive comonomers are often copolymerized with photoactive polymers to enhance crosslinking and introduce different chemical functionality/structure.

Figure 2 illustrates two commercially available diacrylates, bisphenol A glycerolate (1 glycerol/phenol) diacrylate **(a)** and glycerol 1,3-diglycerolate diacrylate **(b)**, with hydroxyl functionality which could potentially enhance compatibleness with polyesters and/or act as a handle for further derivitization.

Scheme 10.9. Proposed route to novel photocrosslinkable polyester ionomers

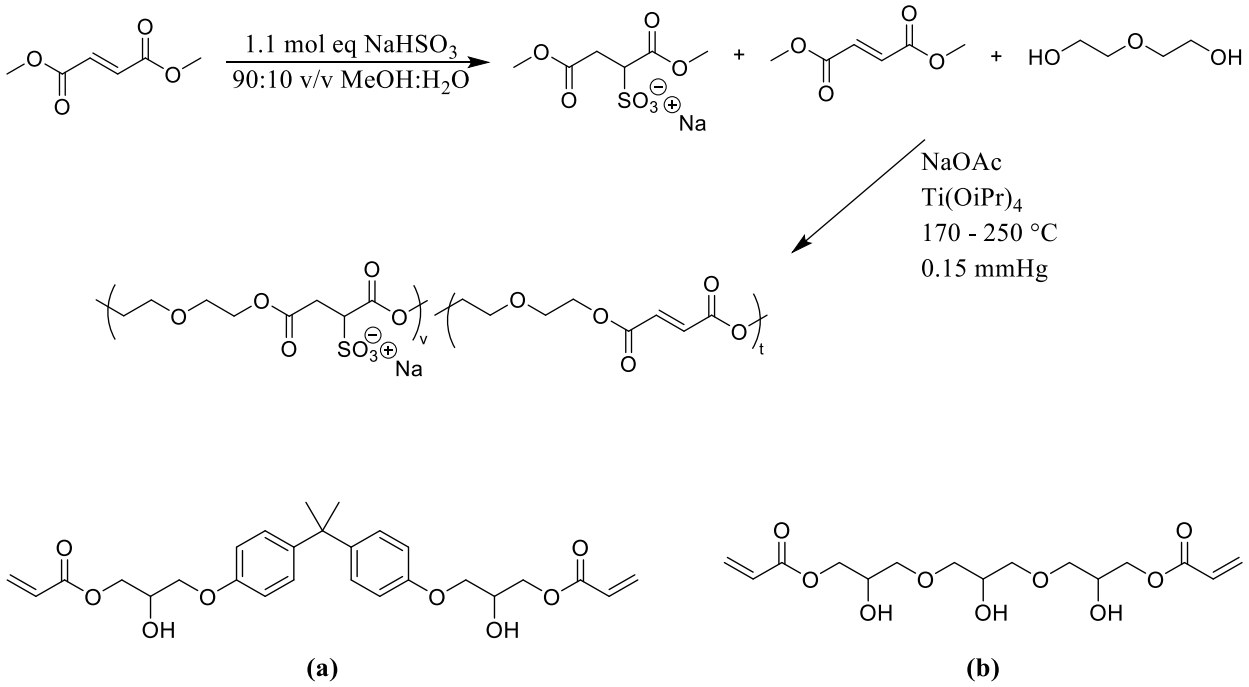

Figure 10.2. Commercially available diacrylates

10.6 *References*

1. Lin Q, Pasatta J, Wang Z-H, Ratta V, Wilkes GL, Long TE, *Polymer International* **51**:540-6 (2002).
2. Kang H, Lin Q, Armentrout RS, Long TE, *Macromolecules* **35**:8738-44 (2002).
3. Engler AC, Chan JMW, Coady DJ, O'Brien JM, Sardon H, Nelson A, et al., *Macromolecules* **46**:1283-90 (2013).
4. Ono RJ, Liu SQ, Venkataraman S, Chin W, Yang YY, Hedrick JL, *Macromolecules* **47**:7725-31 (2014).
5. Zhu W, Tian L, Ren T, Wang X, Tang X, Li G, *Journal of Applied Polymer Science* **84**:67-74 (2002).
6. Srilakshmi GV, Chaudhuri A, *Chemistry – A European Journal* **6**:2847-53 (2000).
7. Hemp ST, Smith AE, Bryson JM, Allen MH, Long TE, *Biomacromolecules* **13**:2439-45 (2012).
8. Astafieva I, Maksimova I, Lukanidin E, Alakhov V, Kabanov A, *FEBS Letters* **389**:278-80 (1996).
9. Kabanov AV, Felgner PL, Seymour LW, Self-Assembling Complexes for Gene Delivery: From Laboratory to Clinical Trial, Wiley, (1998).
10. Zhang M, Hemp ST, Zhang M, Allen MH, Carmean RN, Moore RB, et al., *Polymer Chemistry* **5**:3795-803 (2014).
11. Nelson AM, Long TE, *Macromolecular Chemistry and Physics* **215**:2161-74 (2014).
12. Schultz AR, Lambert PM, Chartrain NA, Ruohoniemi DM, Zhang Z, Jangu C, et al., *ACS Macro Letters* **3**:1205-9 (2014).
13. He S, Timmer MD, Yaszemski MJ, Yasko AW, Engel PS, Mikos AG, *Polymer* **42**:1251-60 (2001).